# Design of smart materials : from primary interactions to supramolecular cyclodextrin-based polymers containing polyoxometalates

Sa Yao

université PARIS-SACLAY

# Design of smart materials: from primary interactions to supramolecular cyclodextrin-based polymers containing polyoxometalates

*Conception de matériaux intelligents : des interactions fondamentales aux polymères supramoléculaires à base de cyclodextrines et polyoxométallates*

**Thèse de doctorat de l'université Paris-Saclay**

École doctorale 571 sciences chimiques : molécules, matériaux, instrumentation et biosystèmes (2MIB)
Spécialité de doctorat : Chimie
Graduate School : Chimie
Référent: Université de Versailles-Saint-Quentin-en-Yvelines

Thèse préparée à l'ILV (Université Paris Saclay, UVSQ, CNRS),
sous la direction d'**Emmanuel CADOT**, Professeur,
la co-direction de **Mohamed HAOUAS**, chargé de recherche,
et le co-encadrement de **Clément FALAISE**, chargé de recherche,

**Thèse soutenue à Versailles, le 10 Mars 2023, par**

YAO SA

## Composition du Jury

### Membres du jury avec voix délibérative

| | |
|---|---|
| **Anne BLEUZEN**<br>Professeure,<br>Université Paris-Saclay | Président |
| **Geoffroy GUILLEMOT**<br>Maitre de conférences,<br>Sorbonne Université | Rapporteur et Examinateur |
| **Laurent RUHLMANN**<br>Professeur,<br>Université de Strasbourg | Rapporteur et Examinateur |
| **Anne PONCHEL**<br>Professeure,<br>Université d'Artois | Examinatrice |

THÈSE DE DOCTORAT
NNT:2023UPASF016

**Titre :** Conception de Matériaux intelligents : des interactions fondamentales aux polymères supramoléculaires à base de cyclodextrines et polyoxométallates

**Mots clés :** chimie supramoléculaire • polyoxométallate • cyclodextrine • polymère • matériaux intelligents • inclusion hôte-invité

L'étude des intéractions supramoléculaires entre une série de polyoxométallates de type Keggin et la cyclodextrine native (γ-CD) en solution aqueuse a été réalisée au moyen d'un ensemble de méthodes complémentaires telles que l'ITC, la RMN, l'électrochimie, et l'analyse par diffraction des rayons X. En variant la charge et la composition des polyoxométalates (W, Mo ou V), l'analyse des résultats met en évidence que le principal facteur qui régit l'interaction hôte-invité entre le POM et le CD est définitivement la charge de l'ion Keggin qui doit être corrélée à un fort effet solvant, appelé l'effet chaotropique. Cet effet a été ensuite mis à profit à partir d'oligomères supramoléculaires à base de POM-CD pour induire une transition gel-fluide en réponse à un stimulus redox ou thermique. Ce comportement physico-chimique est directement lié à l'assemblage hôte-invité qui induit la réticulation supramoleculaire du polymère.

**Title :** Design of smart materials: from primary interactions to supramolecular cyclodextrin-based polymers containing polyoxometalates

**Keywords :** supramolecular chemistry • polyoxometalate • cyclodextrin • polymer • smart materials • host-guest inclusion

In this work, we report on the study of the supramolecular interactions between a series of Keggin-type polyoxometalates and native cyclodextrin (CD) in aqueous solution by using a set of complementary methods such as ITC, NMR, electrochemistry, and X-ray diffraction analysis. Varying the charge and the composition of the polyoxometalates (W, Mo or V), analysis of results evidences that the main factor that governs the host-guest interaction between the POM and the CD is definitively the charge of the Keggin ion, which must be correlated to a strong solvent effect, namely the chaotropic effect. Then, this effect has been exploited in POM-CD based supramolecular oligomers which exhibit a redox or thermal stimuli responsive behavior, inducing a gel-to-fluid transition. Such a physical-chemical responsive behavior is directly related to the host-guest assemblies that act as electro-active crosslinking agents in the polymer.

# Acknowledge

Time is a gift that makes people luckier and luckier, which gives me the courage to move forward. There are too many people and things I want to thank for these four winters in Paris. It all seems like it happened yesterday. First and foremost, I would like to thank the jury members for accepting to evaluate this work Professor Anne PONCHEL and Anne BLEUZEN, both as examinator and Professor Laurent RUHLMANN and Dr. Geoffroy GUILLEMOT as reviewer.

The last three years were full of learning in inorganic chemistry. Thanks to the knowledgeable supervision of Professor Emmanuel CADOT, who gave me a chance to study in Paris. I think he must have given him all the patience he had, thanked him for his guidance throughout the four years project process and the revision of the articles, and thanked him for his friendly personality and selfless help. I thank my co-supervisor, Mohamed HAOUAS, who refuses to waste time. I obtain much knowledge with your patience and those countless discussions. Thanks to Clément Falaise, who was always energetic toward work and offered a lot of help orally and practically. I thank Nathalie LECLERC, who is always ready to help with the synthesis and analysis. I was highly impressed with her cautious attitude during the experiment. Besides, I would like to express my appreciation for my co-worker Soumaya KHLIFI, who offered friendly help when we did the project.

My sincere thanks go to Catherine ROCH, Pierre BAUDUIN, Jerome MARROT, Nathalie GUILLOU, and David LANDY for their invaluable contributions to this thesis's polymer and crystal characterization and ITC testing. Thanks for the contribution work from master students Maxime LAJOYE and Fatma NAGBOU.

I would also like to thank Emmanuel MAGNIER and Anne Dolbecq-BASTIN, director and vice-director of the ILV, to accept me as a member of the lab. Many thanks to Lise MICHELOT, Stephanie GUERET, Sandra JELBI, Bettino DYVRANDE, and the doctoral school for their help in administration and registration each year.

Thanks to all Professors and lecturers of ILV, Olivier OMS, Sebastien FLOQUET, Marc LEPELTIER, and Flavien BOURDREUX, as well as to all my colleagues, Diana CEBOTARI, Maxence LION, Ibrahima Fa BAMBA, Zeinab EL HAJJ, Ali SAAD, Cedric VIRAVAUX, Dang Le Mai VUONG, Srinivasulu PARSHAMONI, Sanchari DASGUPTA, Sergiu CALANCEA, Nour ZEAITER, Gabrielle Mpacko PRISO, Yohan MARTINETTO, Mathis DUGUET, Subharanjan BISWAS, Khaled DASSOUKI, and so on friendly manner, which helps each other keep a good mood and put into work.

Thanks to my eating friends Wei CHEN, Shuyang ZHOU, and Yang Li for saving me from being alone at lunch. Thanks to the accompany of my friends Panpan Ma, Xiaoqing Ye, Huijuan Wang, Clea, Hongwei WAN, Tingting CHEN, Jinwen YANG, Weiyang MA, Yingwei Liu, Liqiao HUANG, Haijuan LIU, Lu LIU, Guangkuo SUN, and Jing XUE helped me through the emotionally difficult times.

Thanks to the funding of the CHARMMMAT project, which helps me participate in many conferences. Thanks to the support of the China Scholarship Council make sure I live well in France. Finally, Thanks to my family's support for me.

Overall, ILV and Paris are great places to learn and provide opportunities to communicate with colleagues from different countries. I'm very proud to have had the chance to be there. Thanks for all the support.

"Si vous avez eu la chance d'avoir vécu à Paris lorsque vous étiez un jeune homme, alors, où que vous alliez pour le reste de votre vie, elle reste avec vous, Paris est une fête"

~ Ernest Hemmingway

# Contents

# Résumé long en français

L'approche supramoléculaire pour la conception de matériaux 'intelligents' permet de développer des stratégies pertinentes et puissantes pour associer et compartimenter des unités fonctionnelles complémentaires et synergiques dans des matrices souples hautement flexibles et accordables.

Parmi cette classe de matériaux, ceux basés sur la reconnaissance supramoléculaire hôte-invité présentent un grand intérêt puisque les interactions à l'origine de ce type de processus sont généralement réversibles et parfaitement spécifiques. Par ailleurs, selon la nature et les propriétés des espèces « hôte-invité », le processus de reconnaissance permet de moduler les propriétés redox, optiques (absorbance et luminescence), magnétiques ou catalytiques. Si l'expérimentateur peut provoquer le processus de reconnaissance « hôte-invité » dans le matériau, alors il dispose d'un système dont il peut commuter les propriétés. Dans le cas de la chimie des polyoxométallates, l'existence de complexes supramoléculaires « hôte-invité » demeurait peu développée et surtout, la nature des forces à l'origine de telles associations assez mal comprise. Récemment, les cyclodextrines (CDs) ont montré une extraordinaire capacité à s'associer à certaines entités inorganiques, comme les polyoxométallates (POMs). Bien que les structures des premiers systèmes supramoléculaires révèlent des complexes d'inclusion partielle entre le POM et la CD, l'analyse structurale ne permet pas de comprendre les valeurs très élevées des constantes de stabilité des adduits POM-CD, montrant encore que les processus fondamentaux régissant la reconnaissance hôte-invité entre la CD et les espèces POMs n'étaient toujours pas compris. Dans ce travail, nous avons entrepris une étude systématique pour comprendre en profondeur la nature des interactions qui régissent l'assemblage d'une cyclodextrine non-chargée avec un polyoxométallate. Nous avons délibérément choisi d'étudier ces interactions à partir d'une série de polyoxométallates dérivés de la structure de Keggin dans lesquels nous avons fait varier la charge, en changeant la nature de l'hétéroatome X dans une série de polyoxotungstates $[XW_{12}O_{40}]^{n-}$. Nous avons également fait varier la composition et l'état redox par électrochimie en utilisant des polyoxométallates de Keggin monosubstitués $[XW_{11}MO_{40}]^{n-}$ (M =

$Mo^{VI}$ ou $Mo^{V}$, $V^{IV}$ ou $V^{V}$ ou W). Enfin, l'étude a nécessité des techniques complémentaires d'analyse comme la titration calorimétrique isothermale (ITC), la RMN $^{1}H$ $^{1}D$ et RMN $^{1}H$ DOSY, les méthodes électrochimiques et la diffusion des rayons X aux petits angles (SAXS). L'analyse structurale par diffraction des rayons X (sur monocristal) a également été utilisée afin d'identifier la nature des interactions à l'état solide, permettant dans une certaine mesure d'utiliser ces résultats pour comprendre le comportement de certaines solutions.

Dans un premier temps, nous nous sommes concentrés sur l'étude des associations « hôte-invité » à partir d'ions de Keggin de la série $[XW_{12}O_{40}]^{n-}$ avec la cyclodextrine (γ-CD). Dans cette série, la charge est modifiée systématiquement de 6- à 3- selon la nature de hétéroatome X (X = $(2H)^{2+}$, $B^{3+}$, $Si^{4+}$ ou $P^{5+}$). Les analyses par diffraction des rayons X sur monocristal ont montré des organisations significativement très différentes avec la γ-CD selon la charge du POM. Alors que l'ion métatungstate $[H_2W_{12}O_{40}]^{6-}$ ne conduit à aucun adduit supramoléculaire, l'ion Keggin $[BW_{12}O_{40}]^{5-}$ interagit plutôt avec la paroi externe de la γ-CD et l'ion $[PW_{12}O_{40}]^{3-}$ pénètre profondément dans la cavité de la γ-CD pour former un véritable complexe « hôte-invité ». De plus, les interactions et les comportements en solution ont été étudiés en détail par ITC, RMN et électrochimie et toutes ces études montrent que l'affinité entre la γ-CD et le POM est directement corrélée à la charge de l'anion Keggin. Ainsi, les constantes d'association $K_{1:1}$ augmentent pratiquement d'un facteur 10 à chaque fois que la charge du POM baisse d'une unité. Pratiquement, la valeur de la constante de stabilité de l'adduit POM@γ-CD croit selon l'ordre $[H_2W_{12}O_{40}]^{6-}$ < $[BW_{12}O_{40}]^{5-}$ < $[SiW_{12}O_{40}]^{4-}$ < $[PW_{12}O_{40}]^{3-}$, d'une valeur négligeable pour l'ion $[H_2W_{12}O_{40}]^{6-}$ à une valeur aussi élevée que $10^5$ pour l'ion $[PW_{12}O_{40}]^{3-}$. Pour compléter cette étude, nous avons ensuite étudié l'influence de la composition dans des POMs monosubstitués en faisant aussi varier leur l'état redox $Mo^{VI/V}$ ou $V^{IV/V}$ dans les systèmes $[XW_{11}MO_{40}]^{n-}$. Là encore, ces études ont révélé que la charge ionique portée par le POM correspondait au facteur prédominant qui gouverne le processus d'agrégation POM@γCD. Les mesures ITC ont montré que pour l'ensemble de ces systèmes, le processus de reconnaissance « hote-invité » est un phénomène

gouverné par l'enthalpie ($\Delta_r H^* < 0$) et toujours associé à un cout entropique ($\Delta_r S^* < 0$). Le signe de ces deux grandeurs thermodynamiques est la marque d'un effet de solvant connu sous le nom d'effet chaotropique. L'origine de cet effet résulte de très faible affinité du solvant (ici les molécules d'eau) pour l'ion inorganique. Cet effet se traduit par une énergie élevée et un état déstructuré pour les molécules d'eau de la couche de solvatation. Ces ions chaotropes sont aussi appelés « briseur de structure de solvant ».

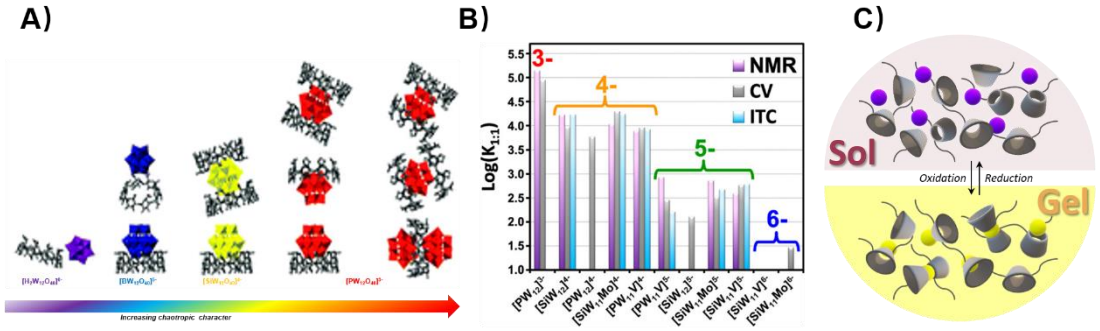


**Résumé graphique**: *A) Diversité des associations POM•γ-CD selon la charge du POM en accord avec les études structurales menées en solution et à l'état solide. B) Graphe montrant l'évolution de la constante $K_{1:1}$ de l'adduit POM@γ-CD en fonction de la charge -3, -4, -5 et -6 dans une série de POMs dérivés de l'ion de Keggin. C) Schéma illustrant l'action du POM comme agent de réticulation électro-actif dans le processus de gélification d'une solution d'oligomères à base de γ-CD.*

Nous avons ensuite cherché à utiliser cet effet chaotrope pour quelques applications comme par exemple l'augmentation de la stabilité hydrolytique des POMs chaotropes en milieu aqueux. Si l'activité biologique de certains POMs est bien connue, leur stabilité dans ces milieux est problématique. A un pH voisin de sept (pH = 7), la plupart d'entre eux se dégradent suite à des processus d'hydrolyse basique. Compte tenu de la très forte affinité des ions de Keggin $[PM_{12}O_{40}]^{3-}$ (M = $W^{VI}$ ou $Mo^{VI}$) pour la cyclodextrine γ, nous nous sommes interrogés sur l'influence d'une telle interaction sur la stabilité hydrolytique de ces POMs en milieu aqueux. Ainsi, nous avons démontré qu'en présence de γ-CD, la stabilité hydrolytique des ions $[PW_{12}O_{40}]^{3-}$ et $[PMo_{12}O_{40}]^{3-}$ s'est élargie jusqu'à 2-3 unités de pH vers les valeurs supérieures.

Enfin, l'effet chaotropique peut aussi être mis à profit pour concevoir des systèmes polymères responsifs permettant par exemple un changement d'état

macroscopique réversible suite à une transition gel-solution fluide. Cette transition peut être opérée au moyen d'un processus élémentaire de reconnaissance supramoléculaire du type hôte-invité en utilisant notre système POM@CD pour lequel il est possible de modifier l'affinité « hôte-invité » en changeant l'état redox du POM. Nous avons alors préparé des oligomères à base de γ-CD en faisant réagir en milieu non-aqueux la γ-CD avec de hexamethylenediisocyanate selon un protocole robuste dont la reproductibilité a été soigneusement vérifiée. Les oligomères formés sont solubles en milieu aqueux et ont été caractérisés principalement par RMN $^{1}$H 1D et DOSY et MALDI-TOF. Les résultats sont en accord avec une distribution centrée sur environ 3-4 γ-CD en moyenne par oligomère. En présence de POMs chaotropes et pour une certaine concentration en oligomères, le système gélifie. Ce système POM-oligomères a été étudié en détails au moyen du protocole méthodologique utilisé précédemment pour l'étude des associations discrètes POM-CD, en incluant en plus les mesures de viscosimétrie et de diffusion des rayons X (SAXS). Les études menées dans des conditions plus diluées montrent que le processus de reconnaissance « hôte-invitée » dans les polymères est maintenu et qu'il est même responsable du processus de gélification. Le gel est alors décrit comme un réseau supramoléculaire dans lequel les polyoxométallates jouent le rôle d'agents de réticulation. Ce processus apparait également corrélé à la charge de l'anion et la réduction ou l'oxydation du POM permet d'opérer une transition macroscopique gel-solution fluide. Dans ce cas de figure, il est même possible de parler d'agent de réticulation électro-actif.

En conclusion, ce travail a permis de révéler un nouvel aspect de la chimie des POMs en solution aqueuse découlant de leurs propriétés de solvatation identifiées comme chaotropiques pour des ions portant une faible densité de charge. Il est certain que cet effet de solvant est promu à un bel avenir puisqu'il ouvre la voie à des associations inédites entre POMs et matière organique en milieu aqueux.

**Title:** Design of smart materials: from primary interactions to supramolecular cyclodextrin-based polymers containing polyoxometalates.

**Keywords:** supramolecular chemistry • polyoxometalate • cyclodextrin • polymer • smart materials • host-guest inclusion

**Abstract:** Supramolecular approaches for designing 'smart' materials prove to be relevant and powerful strategies for accumulating and associating synergistic functions in highly flexible and tuneable soft matrices. Among this class of materials, those based on supramolecular host-guest recognition exhibit surprising potential in redox, luminescence, magnetic or catalytic properties. Cyclodextrins (CDs) have shown an extraordinary ability to associate with inorganic entities, such as polyoxometalates (POMs). However, the fundamental processes governing host-guest recognition between CD or CD-based host and POM species are poorly understood, and to date, only a few studies have been reported on CD-based polymer assemblies using POM as guest species. In this work, we investigate the POM units as molecular effectors of CD or CD-based oligomer receptors to construct functional hybrid polymer assemblies generated through a network of POM-CD junction nodes.

First, we focus on tracking the host-guest supramolecular primary interactions between the CD host and POM functional units. We report the strengths of the host-guest association were analysed within the series of isostructural $[XW_{12}O_{40}]^{n-}$ anions whereby the charge is modified systematically from 6- to 3- depending on the heteroatom, respectively, X = $H_2^{2+}$, $B^{3+}$, $Si^{4+}$ or $P^{5+}$. Single crystal X-ray diffraction analyses showed distinct organizations of POMs with γ-CD in the solid-state, where the modest chaotrope Keggin $[BW_{12}O_{40}]^{5-}$ interacts with the external wall of the γ-CD, while the strongest chaotrope of the series $[PW_{12}O_{40}]^{3-}$ enters deeply in the cavity of the γ-CD through their secondary rim offering maximal contact surface. Furthermore, interactions and behaviours in solution have been studied by ITC, NMR, and electrochemistry, which revealed that the affinity between γ-CD and POM is directly correlated to the charge of the Keggin anion as highlighted by the values of the binding constants $K_{1:1.}$ These constants increase dramatically by decreasing the global POM charge as follows: $[H_2W_{12}O_{40}]^{6-} < [BW_{12}O_{40}]^{5-} < [SiW_{12}O_{40}]^{4-} < [PW_{12}O_{40}]^{3-}$. Then, we extended the study to oxidized and one-electron reduced POMs in a series of molybdenum and vanadium monosubstituted phospho- and silico-tungstate $[XW_{11}MO_{40}]^{n-}$ Keggin-type anions where X = P or Si and M = $Mo^{V/VI}$ or $V^{IV/V}$. Such a study reveals that the host-guest binding constant $K_{1:1}$ increases by more than a magnitude order per charge unit, where $K_{1:1}$ falls down from about $10^5$ to values close to zero as ionic charge varies from 3- to 6-. Furthermore, we demonstrated the encapsulation of the POM within the CD provides an increase of the hydrolytic stability of inorganic guest, like the Keggin-type polyoxometalate $[PM_{12}O_{40}]^{3-}$ anion (M = $W^{VI}$ or $Mo^{VI}$). A shift of up to 2-3 higher pH units is observed for stability domain of $[PM_{12}O_{40}]^{3-}$ species as evidenced by NMR.

Second, we exploit the chaotropic effect to design unconventional reversible polymeric systems exhibiting redox and thermo-responsive sol-gel transition. These supramolecular networks result from the association of CD-based oligomers and Keggin-type POMs acting as electro-active crosslinking agents. The structure and the dynamics of such self-assembly systems have been investigated using a multiscale approach involving MALDI-TOF, viscosity measurements, cyclic voltammetry, $^1$H-NMR (including DOSY), and Small Angle X-ray Scattering.

Overall, numerous techniques were employed in this thesis to explain the interaction mechanisms in the host-guest self-assembly process between CD and Keggin-type POMs, providing new insights into the field of smart material design.

# List of publication and author contribution

Chapter 2 of the thesis was the subject of 3 articles in specialized journals:

1- S. Yao, C. Falaise, A. A. Ivanov, N. Leclerc, M. Hohenschutz, M. Haouas, D. Landy, M. A. Shestopalov, P. Bauduin, E. Cadot “Hofmeister Effect in the Keggin-Type Polyoxotungstate Series” *Inorg. Chem. Front.* (2021), **8**, 12-25.

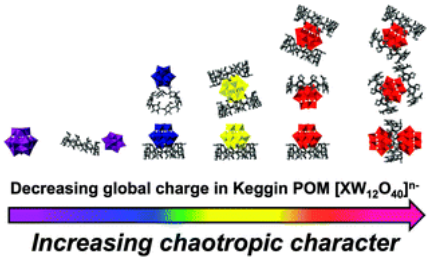


2- S. Yao, C. Falaise, S. Khlifi, N. Leclerc, M. Haouas, D. Landy, E. Cadot “Redox-Responsive Host-Guest Association between γ-Cyclodextrine and Mixed-Metal Keggin-Type Polyoxotungstates” *Inorg. Chem.* (2021), **60**, 7433-7441.

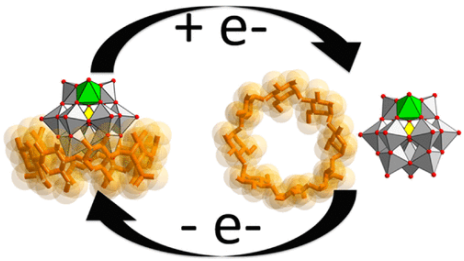


3- S. Yao, C. Falaise, N. Leclerc, C. Roch-Marchal, M. Haouas, E. Cadot “Improvement of the Hydrolytic Stability of the Keggin Molybdo- and Tungsto-Phosphate Anions by Cyclodextrins” *Inorg. Chem.* (2022), **61,** 4193-4203.

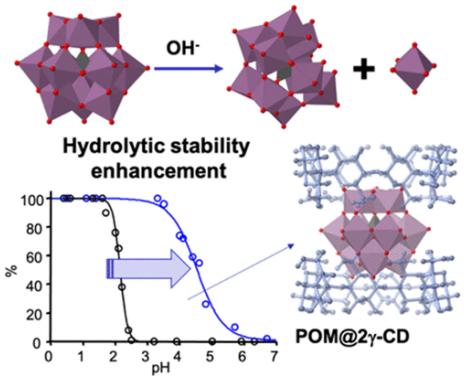

# Abbreviations and Acronyms

**CD** – Cyclodextrin

**CPT** – Cloud Point Temperature

**CP-MAS NMR** – Cross-Polarization Magic Angle Spinning Nuclear Magnetic Resonance

**$C_8E_4$** – Octyl tetraethylene Glycol Ether

**CV** – Cyclic Voltammetry

**DMA** – Dimethylacetamide

**DMF** – Dimethylformamide

**DMSO** – Dimethyl sulfoxide

**EDS** – Energy-dispersive X-ray Spectroscopy

**ESI-MS** – Electrospray Ionization Mass Spectrometry

**EP** – Epichlorohydrin

**HPDec MAS NMR** – High-Power Decoupling with Magic Angle Spinning Nuclear Magnetic Resonance

**HDI** – Hexamethylene Diisocyanate

**IR** – Infrared Spectroscopy

**ITC** – Isothermal Titration Calorimetry

**MB** – Molybdenum Blue

**MALDI-TOF**- Matrix-assisted Laser Desorption/ionization-Time of Flight

**NMR** – Nuclear Magnetic Resonance

**PR** – Propranolol

**POM** – Polyoxometalate

**PEG** – Polyethylene Glycol

**REDOX** – Reduction-oxidation

**SR** – Scan Rate

**SAXS** – Small-angle X-ray Scattering

**TA** – Triamcinolone acetonide

**TGA** – Thermogravimetric Analysis

**XRD** – X-ray Diffraction Analysis

# General Introduction

Polyoxometalates (POMs) represent a class of water-soluble metal-oxo clusters built from group V and VI transition metals in their highest oxidation states, e.g., $V^{V}$, $Mo^{VI}$, and $W^{VI}$.[1,2] This class of compounds exhibits a wide range of structures and chemical compositions, offering various properties that lead to applications in catalysis, energy, biology, and materials science.[3–7] POMs have demonstrated an extraordinary capacity for interacting with organic molecules to create hybrid supramolecular assemblies with particular physicochemical characteristics.[8–11] In this thesis, we discuss the synthesis of a series of compounds derived from classical Keggin polyoxometalates incorporating native cyclodextrins (CDs) as well as the design of novel polymeric hydrogel materials based on CD-polymer molecular fragments and Keggin-type POMs. The text is structured in four distinct sections with two very detailed central chapters (**Chapter 2** and **Chapter 3)**.

The present thesis has four main chapters, as summarized in the scheme below:

1 - Introduction-literature review

2 - Track the primary interactions between cyclodextrin and Keggin-type polyoxometalates

3 - Polymeric materials based on POM-CD supramolecular assembly

4 - Conclusion and perspective

In **Chapter 1,** we briefly overview recent developments in POM and CD research. POM chemistry has made considerable progress with the explosion of new compounds of increasing complexity and nuclearity, ranging from simple to giant structures. Nevertheless, the classical Keggin structure continues to attract growing interest because it could be combined with other chemical entities to produce composites and hybrid materials. As an example, the diverse structures of POM/cyclodextrins host-guest assemblies and their catalytic and medicinal applications are summarized in this chapter. This literature data will constitute the basis of our primary knowledge of host-guest supramolecular interactions in these systems, which is necessary to conduct the studies of **Chapters 2** and **3**. Finally, at the end of this section, we define the goals and the scope of this thesis.

In **Chapter 2**, a series of classical Keggin POMs were synthesized and characterized in solid and solution. We first demonstrate that this intriguing host-

guest association between POMs and CDs is driven by the chaotropic effect, which consists of a solvent impact based on the water structure recovery process resulting from the desolvation of the interacting units. Techniques like ITC, cyclic voltammetry, and NMR were utilized to study the host-guest complexation and to evaluate the binding constants. The ionic charge of POM was found to be a crucial parameter for the strength of the supramolecular assembly. Indeed, by using a series of molybdenum and vanadium monosubstituted anions, controlled reduced species could be readily realized, providing unique redox-responsive host-guest systems. Last but not least, we also investigate the effect of POM encapsulation in CD on the hydrolytic stability of inorganic species, especially the most fragile of them such as phosphomolybdate and phosphotungstate anions $[PM_{12}O_{40}]^{3-}$ (M = $W^{VI}$ or $Mo^{VI}$).

**Chapter 3** is devoted to the design of smart polymers (γPOL) based on γ-cyclodextrin (γ-CD) as a receptive motif for molecular recognition. First, a single crosslinking agent, namely 1,6-hexamethylene diisocyanate (HDI), is used, which leads to soluble polymeric materials when the HDI/CD molar ratio is controlled (< 1.5). Typically, CD-based polymers obtained by reacting γ-CD and HDI in 1:1 were fully characterized in solution by mass spectrometry, and quantitative $^{1}H$ NMR methods, including $^{1}H$ DOSY. Following the same concept from **Chapter 2**, host-guest CD-POM hydrogels were formed by the addition of Keggin-type polyoxometalates, which behave as supramolecular crosslinkers due to their high binding constant with γ-CD. Additionally, a redox process by the presence of a chemical agent leads not only to a color change but also to a phase transition from thick gel to fluid solution in a reversible way. Higher HDI/CD molar ratios (> 1.5) lead to water-insoluble polymers, but do not exhibit adsorption properties towards POMs, even the most chaotropic of them.

Finally, we conclude with **Chapter 4,** which summarizes the main results obtained and conclusions drawn, and proposes some perspectives and directions to further explore the supramolecular properties of POMs. These critical results pave the way for the design of intelligent hybrid systems and highlight their potential nanoscience applications, such as molecular machinery, medicine, adsorption, etc

# Bibliography


1. M.T. Pope. Heteropoly and Isopoly Oxometalates: Inorganic Chemistry Concepts. (1983).
2. Müller, A., Peters, F., Pope, M. T. & Gatteschi, D. Polyoxometalates: Very Large ClustersNanoscale Magnets. *Chem. Rev.* **98**, 239–272 (1998).
3. Bijelic, A., Aureliano, M. & Rompel, A. Polyoxometalates as Potential Next-Generation Metallodrugs in the Combat Against Cancer. *Angew. Chem. Int. Ed.* **58**, 2980–2999 (2019).
4. Bijelic, A., Aureliano, M. & Rompel, A. The antibacterial activity of polyoxometalates: structures, antibiotic effects and future perspectives. *Chem. Commun.* **54**, 1153–1169 (2018).
5. Sadakane, M. & Steckhan, E. Electrochemical Properties of Polyoxometalates as Electrocatalysts. *Chem. Rev.* **98**, 219–238 (1998).
6. Chen, L. *et al.* Polyoxometalates in dye-sensitized solar cells. *Chem. Soc. Rev.* **48**, 260–284 (2019).
7. Fabre, B., Falaise, C. & Cadot, E. Polyoxometalates-Functionalized Electrodes for (Photo)Electrocatalytic Applications: Recent Advances and Prospects. *ACS Catal.* **12**, 12055–12091 (2022).
8. Assaf, K. I., Gabel, D., Zimmermann, W. & Nau, W. M. High-affinity host-guest chemistry of large-ring cyclodextrins. *Org. Biomol. Chem.* **14**, 7702–7706 (2016).
9. Wankar, J. *et al.* Recent Advances in Host–Guest Self-Assembled Cyclodextrin Carriers: Implications for Responsive Drug Delivery and Biomedical Engineering. *Adv. Funct. Mater.* **30**, 1909049 (2020).
10. Ivanov, A. A. *et al.* Host–Guest Binding Hierarchy within Redox- and Luminescence-Responsive Supramolecular Self-Assembly Based on Chalcogenide Clusters and γ-Cyclodextrin. *Chem. – Eur. J.* **24**, 13467–13478 (2018).
11. Falaise, C. *et al.* 'Host in Host' Supramolecular Core-Shell Type Systems Based on Giant Ring-Shaped Polyoxometalates. *Angew. Chem. Int. Ed. Engl.* **60**, 14146–14153 (2021).

# Chapter 1 State of the art: Polyoxometalates as building blocks for the design of supramolecular systems

## 1.1 Polyoxometalates: from fundamental to application

### 1.1.1 Definition and history

Polyoxometalates (POMs) are anionic molecular metal oxides produced primarily from the acidification of tetraoxometalate ions $[MO_4]^{n-}$, where metal M belongs to group 5 or 6 (M = V, Mo, W, Nb, Ta, etc.) of the periodic table in their highest oxidized state +V or +VI (see Figure 1.1).[1] POMs is generally formed by the linking of metal-oxo polyhedral $\{MO_X\}$ through corner-shared or edge-shared junctions which proceed via condensation processes. Then, this class of compounds is characterized by a wide structural diversity as a steady stream of structures has been reported. Furthermore, polyoxometalates can include in their metal-oxo framework almost all the elements leading to highly various compositions. POMs are used for many applications in various domains of science, such as analytical chemistry, catalysis,[2,3] cosmetics,[4] medicine (antitumoral, anti-HIV, antibiotic, anti-melanogenesis, etc.),[4–6] and sensor device.[7]

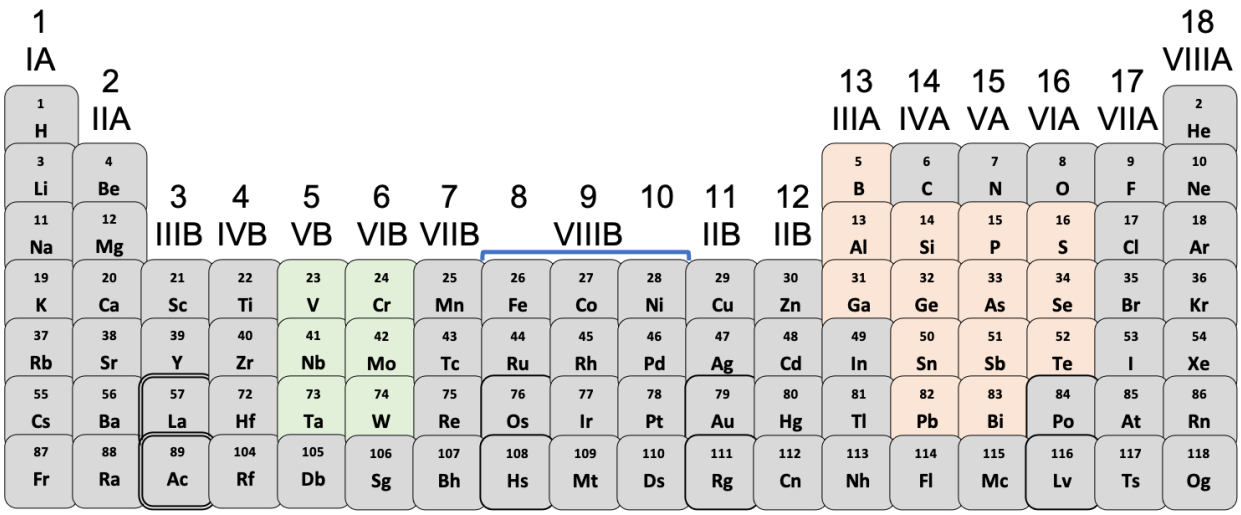


**Figure 1.1** *Periodic table showing the groups 5 and 6 elements (in green), which correspond to the main metals of the POM framework. Besides, POM compounds can contain assembling group (orange cells) belonging to the p block.*

POM research has a long history. POMs were first discovered in 1826 when Berzelius reported on the formation of a yellow solid resulting from the mixing of ammonium molybdate with phosphoric acid. This solid consisted of the ammonium salt of the molybdophosphate anion $[PMo_{12}O_{40}]^{3-}$.[8] In 1862, Marignac determined the chemical composition and reported the exact elemental analysis of the tungstosilicic acid $H_4SiW_{12}O_{40}$ in its crystalline form.[9] Then, in 1903, Rosenheim and Davidsohn established the ionic character of molybdic acid by measuring the conductivity of the acid and corresponding salts.[10] In 1907, Miolati published a review that confirmed the composition and the ionic nature of molybdophosphate ion and derivatives.[11] Later in 1929, Pauling investigated the structure of polyoxometalate and disagreed with the formula and theory used to explain the structure reported in earlier publications. Based on new theoretical assumptions, he proposed a novel structural description of 12-heteropoly acids, where the metal (Mo or W) adopts an octahedral environment $\{MO_6\}$ and the assembling group exhibits a tetrahedral geometry $\{XO_4\}$ with X = Si or P. Accordingly, Pauling suggested that formula may be written as $H_4[SiO_4 \cdot W_{12}O_{18}(OH)_{36}]$ or $H_6[(PO_4)_2 \cdot W_{18}O_{30}(OH)_{48}]$.[12] In 1932, Hoard investigated the cubic crystals of the heteropolyacids such as 12-molybdophosphoric acid, $H_3PMo_{12}O_{40}.30H_2O$, and related compounds by using a modern method called the X-ray diffraction technique. Then Hoard discussed the possible structures according to the results of Pauling.[13] Nevertheless, a year later in 1933, Keggin was the first to establish the emblematic structure of phosphotungstic acid by using powder X-ray diffraction technique. The resulting formula $H_3P(W_3O_{10})_4 \bullet nH_2O$ is related to the structural arrangement of the anion which can be described as a central $P^{5+}$ cation tetrahedrally surrounded by four $\{W_3O_{10}\}^{2-}$ groups. Furthermore, each $\{W_3O_{10}\}^{2-}$ group consists of three edge-shared $\{WO_6\}$ octahedral. Last, these four $\{W_3O_{10}\}^{2-}$ triads are linked together through corner-shared junctions to give the final structure, which corresponds to the so-called *"Keggin structure"* (see Figure 1.2). This important result was the starting point for the fascinating structural chemistry of polyoxometalates that has inspired, stimulated and expanded the field over the past 90 years.[14,15] Furthermore, with the development of X-ray diffraction methodologies and advances in structural chemistry, significant and relevant progresses in this class of compounds have led to the discovery of plethora POM structures.

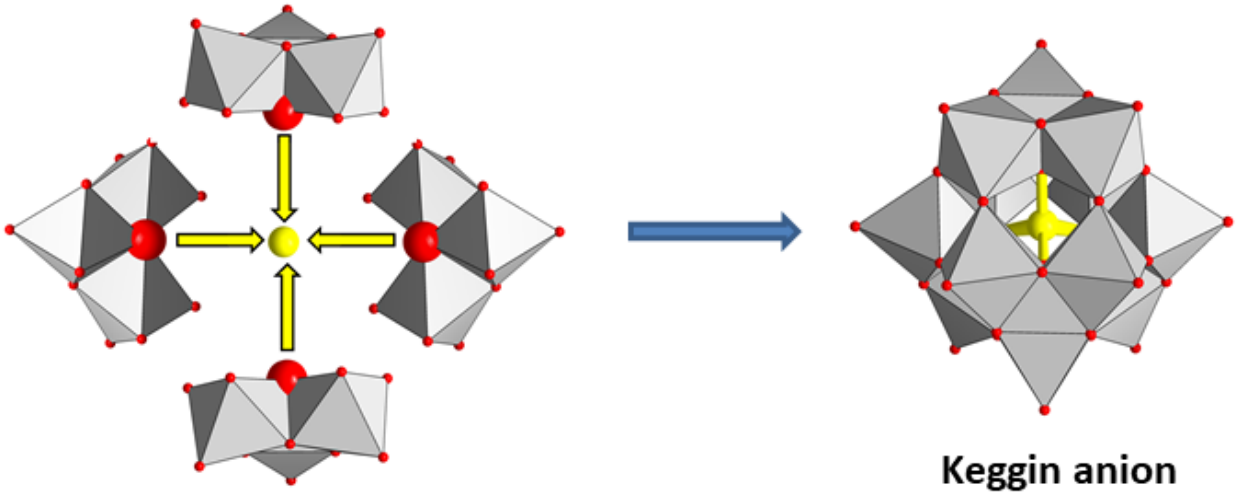


**Figure 1.2** *Polyhedral representation of the Keggin ion built from the coordination of the central $P^{5+}$ ion by four $\{W_3O_{10}\}^{2-}$ triads which are linked together through corner-shared junctions.*

Fifteen years later, Evans reported the second POM structure as ammonium and potassium salts. The structures of the molybdotellurate anion $[TeMo_6O_{24}]^{6-}$ were established by using X-ray diffraction analysis.[16] A large and fruitful body of literature about POM structures has grown from this period. In 1953, Dawson and Lindqvist discovered separately important structural POM arrangements which were named "*Dawson anion"* for the $K_6[P_2W_{18}O_{62}]$ species and *"Lindqvist anion"* for the $[Nb_6O_{19}]^{8-}$ species, respectively.[17,18] Furthermore, the Linqvist-type structures $[Mo_6O_{19}]^{2-}$ and $[W_6O_{19}]^{2-}$ were reported in 1968 by Fuchs and Jahr combining two characterization techniques, i.e., infrared spectroscopy and X-ray diffraction.[19] Also, a new archetypical structure $(NH_4)_2H_6(CeMo_{12}O_{42})$ was reported by Dexter and Silverton in the same year.[20] In 1971, Pettersson described the formation of the pentamolybdodiphosphate anion $[P_2Mo_5O_{23}]^{6-}$ which was structurally characterized by Strandberg two years later.[21-22]

Above all, in 1998, Müller et al. elucidated the mystery of the molybdenum blue solution. Contrary to popular belief at that time according to which this class of material would be made up of ill-defined polymeric substances, it was evidenced that it corresponds rather to highly ordered nanoscopic POM arrangements (see Figure 1.3). These discrete arrangements, resulting from the condensation of molybdate under reducing conditions exhibit large macrocyclic structures which reach over 35 Å in diameter.[23–26] Therefore, the short historical journey along the POM chemistry

development proposed in this section can be schematically summarized in Figure 1.3, showing the most popular structural archetypes. Indeed, there is no doubt that POM chemistry constitutes a constantly expanding disciplinary field given the continuous reports dealing with structures, properties and applications of POMs. Actually, in the following sections, we aim to identify the different classifications, applications, and structure properties of this class of compounds.

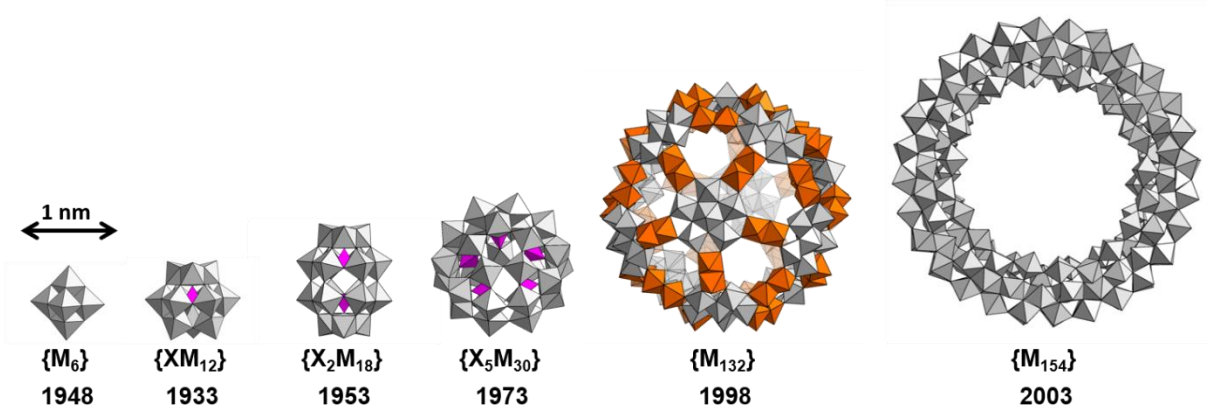


**Figure 1.3** *Polyhedral representation of the most popular historical structures that constitute the wide family of the Polyoxometalate compounds, classified according to their nuclearity or size. From left to right: Lindqvist, Keggin, Dawson, Preyssler, Keplerate-type anion and giant molybdenum blue wheel.*

### 1.1.2 Structures and architectures of POMs

As already written, POMs are well described as discrete anionic soluble metal oxide species with the general formula $[M_yO_X]^{n-}$ for the metal-oxo shell, where M = Mo, W, V, Nb, or Ta (see Figure 1.1). Currently, diverse POM arrangements can be formed in aqueous solution in a controlled manner depending on the experimental conditions, such as pH, ionic strength, temperature, solvent, etc. Conventionally, they are divided into two categories, which may be named isopolyoxometalates $[M_XO_Y]^{n-}$ and heteropolyoxometalates $[X_ZM_XO_Y]^{n-}$ where X is typically an element from the p-block of the periodic table (see Figure 1.1). However, a third category can be included corresponding to the giant-type polyoxometalates (see Figure 1.3). They differ from the conventional POMs in their size and in their constitutional building blocks which contain a striking pentagonal unit $\{M_6O_{21}\}$ as invariant motif.

### 1.1.3 Isopolyoxometalates $[M_XO_Y]^{n-}$

Isopolyanions are built from metal oxide frameworks which contain only metal atoms from group 5 or 6. The archetypical isopolyoxometalate structure is the Lindqvist-type anion, consisting of six $\{MO_6\}$ octahedra connected by edge-shared junctions, to give the general formula $[M_6O_{19}]^{n-}$ (M = Mo, W, Nb, or Ta). The Lindqvist structure which retains the $O_h$ symmetry, is shown in Figure 1.4. So far, isopolyoxomolybdates series includes $[Mo_6O_{19}]^{2-}$, $[Mo_7O_{24}]^{6-}$, and $[Mo_8O_{26}]^{4-}$ species which are built from exclusive edge-shared junctions. Importantly, there is one isomer deriving from the $\alpha$-$[Mo_8O_{26}]$ anion, called the $\beta$-isomer, which can be described as a $\{Mo_6O_{24}\}$ crown symmetrically capped with two $\{MoO_4\}$ tetrahedra.[27,28] Besides, $[W_7O_{24}]^{6-}$ and $[W_{10}O_{32}]^{4-}$ are two isopolyoxotungstates which were formed in aqueous solution, while $[W_6O_{19}]^{2-}$ Linqvist-type anion results from condensation processes carried out in non-aqueous medium (see Figure 1.4). The structure of $[W_{10}O_{32}]^{4-}$ anion derived from that of the Lindqvist-type arrangement and formally corresponds to two $\{W_5O_{18}\}$ units connected by four W-O-W corner edge junctions that have a wide-open angle of ~ 175°. In the same way, vanadates were able to produce Isopolyoxometalates, which correspond to the pyrovanadates and metavanadates, resulting from aqueous solutions of pH > 7. For pH < 7, acidification leads to the formation of the well-known decavadate ion $[V_{10}O_{28}]^{6-}$. This anion consists of $\{VO_6\}$ octahedra self-assembled through edge-shared junctions.

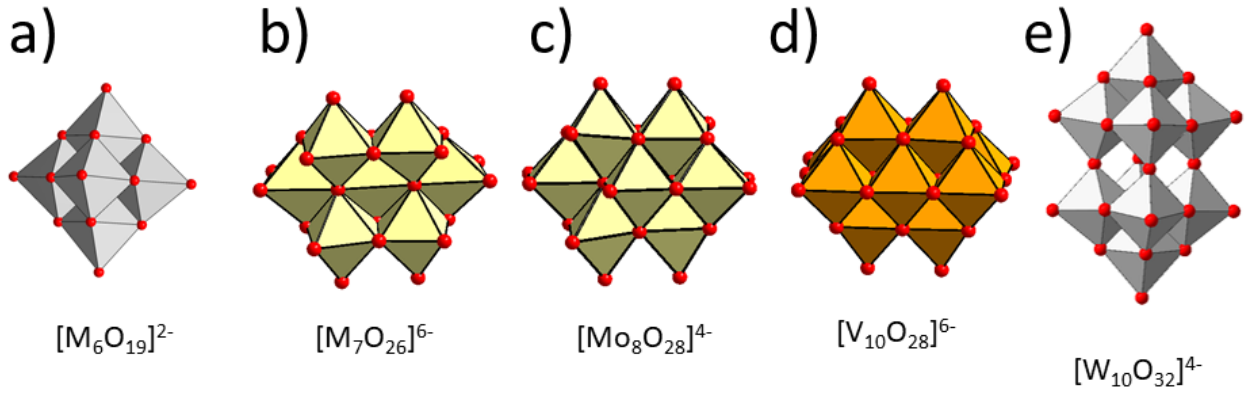


**Figure 1.4** *Five polyhedral representations of archetypical isopolyoxometalate structures: a) $[M_6O_{19}]^{2-}$ (M = Mo, W); b) $[M_7O_{24}]^{6-}$ (M = Mo or W); c) $\beta$-$[Mo_8O_{26}]^{4-}$; d) $[V_{10}O_{28}]^{6-}$; e) $[W_{10}O_{32}]^{4-}$.*

### 1.1.3.1 Heteropolyoxometalates $[X_ZM_XO_Y]^{n-}$

The metal-oxo framework of the POM can include an assembling group $\{XO_p\}^{n-}$ leading to species that have the general formula $[X_ZM_XO_Y]^{n-}$. This assembling group is built from a heteroatom X which generally belongs to the *p* block such as X = B, Al, Ga, Si, Ge, Se, Te, etc. The resulting species, named “heteropolyoxometalates” exhibit structural arrangements closely related to the stereochemical properties of the assembling group which could adopt trigonal $\{XO_3\}$, tetrahedral $\{XO_4\}$ or octahedral $\{XO_6\}$ geometry. Then, the presence of assembling groups enables to direct the self-condensation process of the metalate ions toward the formation of these heteropolyoxometalates. Depending on i) the nature of the heteroatom X (X = B, Al, Ga, Si, Ge, P, As, Sb, Bi, Se, Te, etc.), ii) the geometry of the assembling group, iii) the synthesis conditions (concentration of reactants, pH, ionic strength, temperature, solvent, etc.), numerous species have been isolated and characterized, allowing to expand dramatically the chemical landscape of this class of compounds. The use of tetrahedral group such as phosphate $\{PO_4\}^{3-}$ in the presence of tungstate leads to the formation of popular structural archetypes named Keggin, Dawson or Preyssler ion (see Figure 1.3). The Keggin ion $[XM_{12}O_{40}]^{n-}$ is generally built up from $Mo^{VI}$ or $W^{VI}$ and can contain various tetrahedral assembling groups (see Figure 1.2). For instance, the tungsten-containing Keggin-type anion is known with X = $B^{III}$, $A^{III}$, $Ga^{III}$, $Si^{IV}$, $Ge^{IV}$, $P^{V}$, and $As^{V}$). The Keggin-type tungsten-oxo framework can also contain two protons $H^+$ to give the metatungstate ion $[H_2W_{12}O_{40}]^{6-}$ which ranges in the isopolyoxometalate subclass according to its formula. Besides, five isomers can be formally generated from the formula $[XM_{12}O_{40}]^{n-}$. Actually, the successive 60° rotations of the four trimetallic groups $\{M_3O_{13}\}$ from the most symmetric arrangement leads to the so-called Baker-Figgis isomers $\alpha$, $\beta$, $\gamma$, $\delta$ and $\varepsilon$ (see Figures 1.2 and 1.5). In this series, the Keggin-type ion or $\alpha$ isomer has *T*d symmetry where the four triads are mutually linked through corner-shared M-O-M junctions. The $\beta$ and $\gamma$ isomers adopt $C_{3v}$ and $C_{2v}$ symmetries, respectively, and are mostly encountered with silicotungstate ion $[SiW_{12}O_{40}]^{4-}$. The $\delta$ isomer ($C_{3v}$) is very rare in POM chemistry, but exists with polycations such as the hydroxo(aquo)-aluminium. However, the $\varepsilon$ isomer (*T*d symmetry) can be seen in reduced POMs like the phophosmolybdate derivatives $\{PMo_{12}O_{40}\}$.

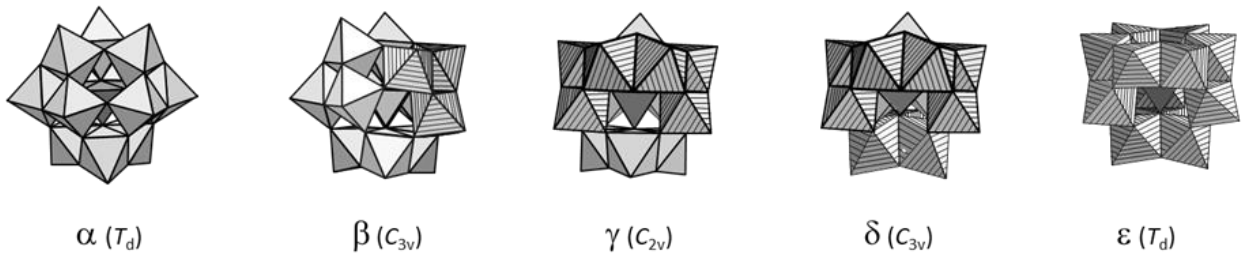


**Figure 1.5** *Polyhedral representations of the five Baker-Figgis isomers of the Keggin structure.*

The Wells-Dawson-type POMs can be also viewed as a Keggin derivative, because the Dawson is formed by the combination of two trivacant Keggin-type units $\{XM_9\}$, leading to the general formula $[X_2M_{18}O_{62}]$ where the central atom X and M can be $P^{5+}$, $S^{6+}$, $As^{5+}$, etc., and Mo or W, respectively. Other heteropolyoxometalates could be cited such as the Silverton-type POMs $[XM_{12}O_{42}]^{8-}$ where the heteroatom X belongs to the f-block (X = $Ce^{4+}$, $Th^{4+}$, etc.) or the Anderson-type anion $[XM_6O_{24}]^{n-}$ (M = Mo or W and X = $Al^{3+}$, $Cr^{3+}$, $Mn^{4+}$, $Pt^{4+}$, $Ni^{4+}$, etc.) which is obtained from aqueous solution in the pH 4-5 range and built from six equivalents metal ion containing terminal cis-dioxo groups. Last, the Waugh-type POMs $[XM_9O_{32}]^{n-}$ (X = $Mn^{4+}$, $Ni^{4+}$, etc.) present a discrete helical structure built from three edge-sharing $\{Mo_3O_{14}\}$ groups, which are arranged around the central heteroatom. It should be worth mentioning that such POM is chiral and give racemic solutions or solids containing both enantiomers. The $[MnMo_9O_{32}]^{6-}$ ion is probably the most reported Waugh-type POM in the literature. Some archetypical representatives are shown in Figure 1.6.

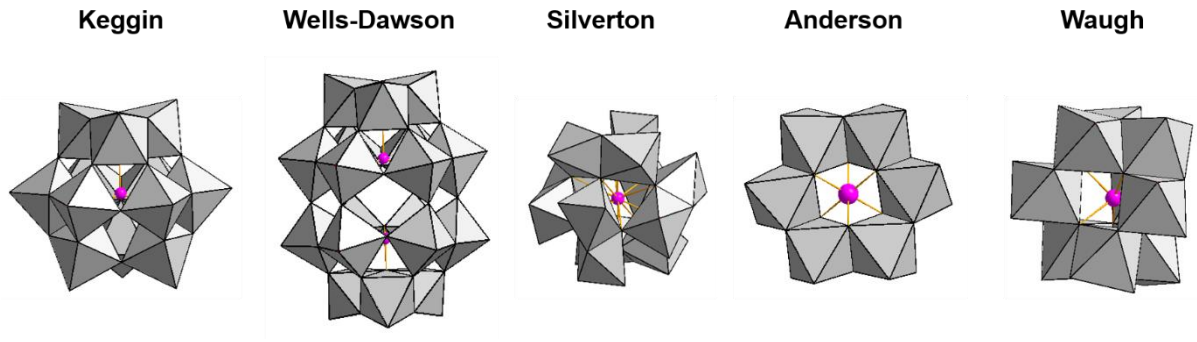


**Figure 1.6** *Polyhedral representations of some popular POM structures.*

### 1.1.3.2 Giant POMs

The condensation of molybdate ions under reducing condition leads to a new class of POMs which find their identity with their large size, reaching the nanoscopic world. In context, the molybdenum blue (MB) solutions described for the first time by Scheele were described for a long time as polymeric and amorphous substances.[29] MB chemical system is obtained almost instantaneously by reducing $Mo^{VI}$ into $Mo^{V}$ type species in acidic solution (pH = 1).[30] The mystery of MB compounds was solved in 1998 by Müller who reported that MB substances correspond to well-defined discrete polyoxometalates, arranged in large torus. This is one of the most important successes over the past three decades in discovering these giant polyoxymolybdates (POMs) that contain several hundreds of Mo centers. Then, depending on the synthesis conditions, these large ring-shaped structure exhibit various nuclearity such as $\{Mo_{154}\}$, $\{Mo_{176}\}$ and $\{Mo_{248}\}$. At last, a lemon-shaped assembly built on 368 Mo atoms $\{Mo_{368}\}$ was isolated and fully characterized by X-ray diffraction method.[23,24,26,31] As shown in Figure 1.7, these MB POMs are built from basic $\{Mo_8\}$, $\{Mo_2\}$, and $\{Mo_1\}$ building blocks, whose the periodic repetition gives rise to the large highly symmetric blue ring. Intensive research in the field allowed the discovery of a second giant POM archetype named Keplerate ion, which is topologically described as well-defined spheroidal hollow capsule (see Figure 1.7b). It is worth mentioning that these large macrocyclic or hollow capsule-type structures exhibit large nanometer-sized cavity which can be used to develop relevant supramolecular host-guest chemistry.[32]

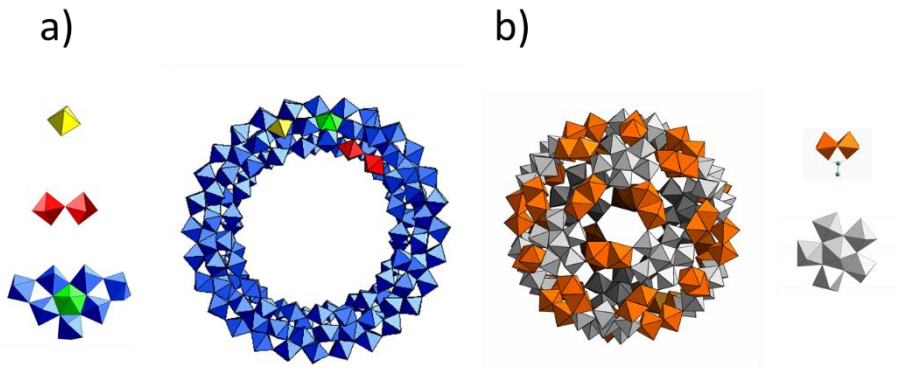


**Figure 1.7** *Two famous nanosized giant polyoxometalates and their constitutive building blocks. a) Ring-shaped molybdenum blue (MB) $[Mo_{154}O_{462}(OH)_{14}(H_2O)_{70}]^{14-}$ (abbreviated $Mo_{154}$) and their elemental building blocks $\{Mo_1\}$ (yellow), $\{Mo_2\}$ (red) and $\{Mo_8\}$ (blue and green). b) The Keplerate anion $[Mo_{132}O_{372}(CH_3COO)_{30}(H_2O)_{72}]^{42-}$ (abbreviated $\{Mo_{132}\}$) built from the linking of 12 pentagonal motifs $\{Mo_6O_{21}\}$ (grey polyhedrons) and 30 linkers $\{Mo_2O_4\text{-}Ac\}$ $CH_3COO\}$ (orange octahedrons).*

### 1.1.4 POMs in aqueous solution

One of the most important properties of POMs lies probably in their solubility in various solvents such as water or organic polar solvents. In context, this large class of anionic polynuclear metal-oxygen clusters exhibits fascinating behavior in aqueous solution allowing many chemical transformations. Identifying the physical-chemical features of POMs is crucial for exploring performance of POMs and their potential applications, while it remains a hard task to determine the specific distribution of the active POM species in aqueous solutions.[1] Commonly used analytical methods such as potentiometry, X-ray absorption, NMR, mass-spectrometry, and electrochemistry are applied to quantify POM distribution present in solution.[33–37] In 1993, Pettersson et al. attempted to establish speciation of polyanionic systems by describing equilibria which take place in aqueous solution. Such a tricky study has been carried out on the five-component system $H^+$-Mo(VI)-V(V)-P(V)-$e^-$ by including the ionic mediator effect, and combining the potentiometry-NMR ($^{31}P$ and $^{51}V$) methods. This methodology was also applied sequentially for the investigation of binary ($H^+$-$MoO_4^{2-}$ and $H^+$-$HVO_4^{2-}$), ternary, and quaternary subsystems.[38,39] Gumerova and Rompel gave a detailed description of the general solution behavior of POMs in a recent review article.[40] Actually, the application of POMs in solutions is ubiquitous and requires conducting in-depth analyses of the structure-property relationship of POM systems.

#### 1.1.4.1 Hydration properties of POMs

In general, stability of POMs in aqueous solution is strongly dependent on pH. As pH decreasing, the electronic charge density of POMs generally decreases, leading to species able to resist to acidic hydrolysis while POM species with high charge density are able to resist against basic attack of hydroxide ions. Further, for species with very low electric charges, hydrolysis can occur even in acidic aqueous solution, revealing that solution studies remain crucial to elucidate in detail the hydrolysis pathway of POMs.[41] Then, pH, POM concentration, buffer type, and nature of counter-ion are able to affect the hydrolysis processes of POMs in solution. The review given by Gumerova and Rompels offered relevant insights about the ion profiles of POMs containing $V^V$, $Nb^V$, $Ta^V$, $Mo^{VI}$ and $W^{VI}$ over the pH scale. For

instance, Murata and Ikeda investigated the formation of molybdophosphate ions in aqueous solution using laser Raman spectroscopy.[42] They observed that the $[MoO_4]^{2-}/[PO_4]^{2-}$ system gives rise to the transformation reaction from 11-molybdophosphate to produce 12-molybdophosphate. Also, the formation product of 12-molybdophosphate (80%) is dramatically fast when the mixture of molybdate and phosphate ions is acidified down to pH 1. However, the hydrolytic degradation of the $[PMo_{12}O_{40}]^{3-}$ is strongly reduced and even cancelled in non-aqueous solutions. Besides, the presence of specific non-ionic compounds can also alter the hydrolytic stability of POMs. Recently, Falaise and co-workers showed how large macrocycles such as γ-CD can be used as trapping agent to capture the elusive Lindqvist anion $[M_6O_{19}]^{2-}$ (M = $Mo^{VI}$, $W^{VI}$) from an aqueous solution, while this ion is completely unstable and has never been observed in pure aqueous solution. The reported results revealed that the presence of γ-CD in aqueous solution alters dramatically the speciation diagrams of molybdate and tungstate over a wide pH range, that is 1 < pH < 6 for tungstate and 1 < pH < 3 for molybdate (see Figure 1.8). This demonstrated that macrocyclic γ-CD can stabilize POMs through host-guest chemistry, acting as a protective shell for the encapsulated guest.[43]

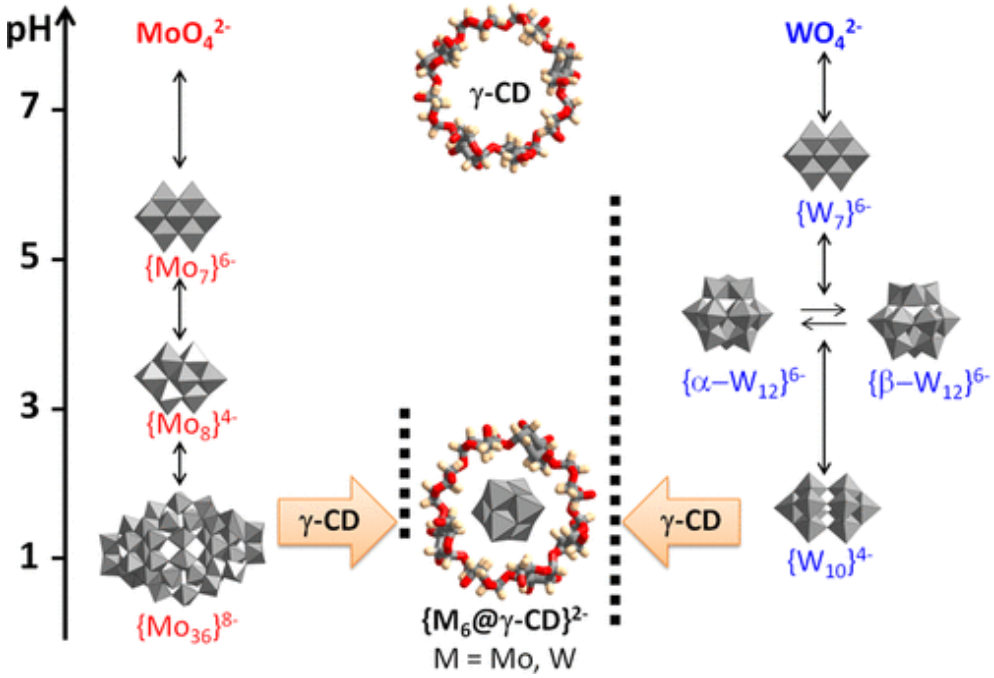


**Figure 1.8** *Interconversion schemes of molybdate and tungstate ions showing the pH domain where γ-CD interferes: pH < 3, for molybdate and pH < 6 for tungstate ions (from reference 43).*

In conclusion, suitable stabilizing agents can be used to expand the hydrolytic stability domain of POMs that is essential to develop applications which require hydrolytic resistance of POMs such as catalysis or medicine.

#### 1.1.4.2 Solvent effect in the aggregation process

The presence of ions affects chemical processes in aqueous solutions. For instance, some salts are known to affect the solubility of proteins in aqueous solutions. In 1888, Hofmeister discovered this widespread phenomenon, showing that depending on their nature, ions exhibit contrasted behavior toward the solubility of egg white (ovalbumin) containing solutions.[44] Such a behavior has been distinguished into two categories, called "salting-in" for ions which increase the solubility of proteins or "salting-out" for ions that lead to the decrease of the proteins solubility. Currently, both effects gave rise to the Hofmeister series which proposed a classification of common anions with respect to their “salting-in” or “salting-out” behaviour (see Figure 1.9). Further, the *“salting”* effect, occurring in aqueous solution was attributed to specific interaction with the water molecules in the hydration shell of the anion. Thus, the anionic species that induce a “salting-out” effect have been identified as *kosmotropic* species while the “salting-in” species have been designed as *chaotropic* substances. The difference between chaotropic and kosmotropic ions is mainly due to the orientation and polarization of the surrounding water molecules which constitute the hydration shell of the ion. Actually, depending on the nature of the anionic species, these water molecules can form assemblies in the hydration shell that differ structurally and energetically from those observed in the bulk. Usually, the kosmotropic ions engage water molecules through strong directed hydrogen bonds within a highly ordered water shell. These ions are characterized by high anionic charge density and low polarizability and they are described as “water-structure maker”. Conversely, the chaotropic ions are weakly bonded to surrounded water molecules which interact mainly through dispersion forces with the ion. Then, the hydration shell around these chaotrope species is characterized by high energy and highly disordered water molecules compared to those of the bulk. These ions exhibit low charge density and high polarizability and they are described as “water structure breaker”.

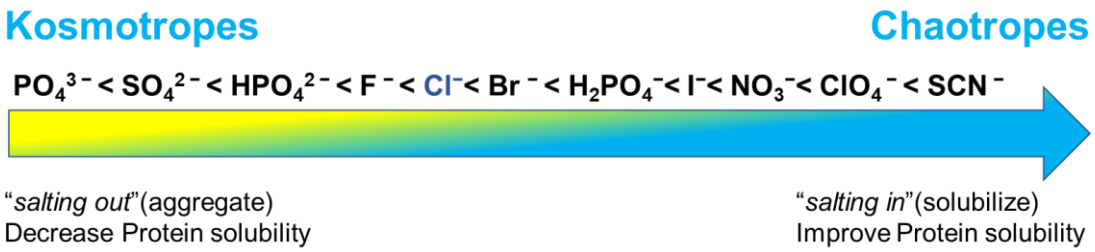


**Figure 1.9** *Hofmeister classification of anions according to their "salting-in"/"salting-out" ability.*

For POMs with nanometer size, high polarizability and low charge density, the solvent-mediated effect arising in water can become predominant, driven by change of the solvent shell around the POM. Such change can be drastic, going from a hydrophilic to a hydrophobic environment around the POM, which allows combinations with organic substrates.[45,46] In context, Naus' group in Germany recently proposed to include POMs to the historical Hofmeister series in the extreme side corresponding to the "superchaotropic ions" (see Figure 1.10).[47]

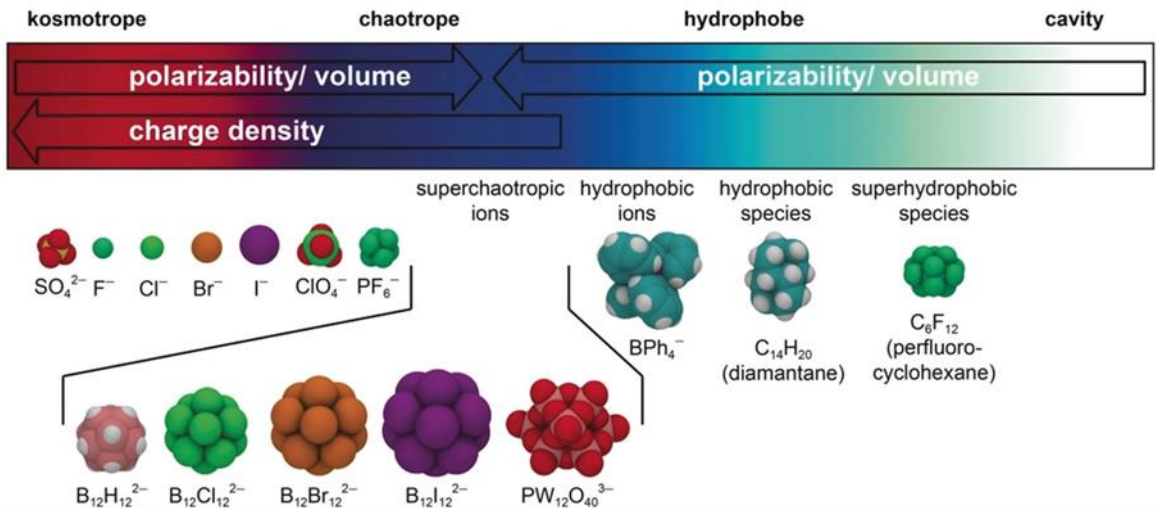


**Figure 1.10** *Extended Hofmeister scale with specification of the superchaotropic, hydrophobic ionic, and superhydrophobic regions (from reference 48).*

### 1.1.5 POMs as components of supramolecular systems

As already shown, POMs are polyanionic clusters with surfaces covered by oxygen atoms providing multiple interaction sites. This makes POMs then useful as functional building blocks for the design of supramolecular hybrid materials for either inorganic or organic subunit. Then, we divide this class of POM-based materials as function of the composition where POMs are assembled with inorganic or with organic molecular architectures.

#### 1.1.5.1 POMs assembled with inorganic molecular architectures

Recent studies have shown that POM-based supramolecular materials not only significantly affect the structural environment of POMs, but may also alter the physicochemical properties, as synergies can arise from the hybrid nature of the materials. In context, one popular strategy for the design of POM-based hybrid materials consists to associate the POM unit with cationic metal complexes. Furthermore, supramolecular aggregates can result from combinations including distinct and complementary POM units.[48]

Okun reported heterogeneous catalysts formed by the sandwich-type POM complex $[(Fe^{III}(OH_2)_2)_3(A\text{-}\alpha\text{-}PW_9O_{34})_2]^{9-}$ and cationic alumina-coated silica nanoparticles $(Si/AlO_2)^{n+}$.[49] This POM/$Si/AlO_2$ combination shows a dramatic increase of the catalytic activity such as the heterogeneous oxidation of the tetrahydrothiophene into tetrahydrothiophene oxide compared to the activity of the POM alone. Besides, Todea and co-workers described one spectacular molecular core-shell structure that consists of the spherical $\{Mo_{72}Fe_{30}\}$ Keplerate-type shell encapsulating the Keggin-type polyoxomolybdates $\{SiMo_{12}O_{40}\}$. The core-shell assembly $\{SiMo_{12}O_{40}\}@\{Mo_{72}Fe_{30}\}$ results of very weak interactions between the two compnents.[50] Furthermore, spectroscopic study reveals that electronic interplay can be induced between the reduced inner POM and the outer shell of the supramolecular system.

### 1.1.5.2 POMs assembled with organic molecular architectures

The synthesis of hybrid multifunctional materials that combine POMs and organic moieties corresponds to an intense research area. Actually, such kind of architectures, based on covalent linkages or non-covalent supramolecular interactions give rise to singular properties that arise from synergy between POM and organic moieties. Many properties could be considered, such as surfactants, light-trapping materials, or backbone materials for applications in drug delivery, photocatalysis or materials science.[51] Usually, organic components consist of polymers, lipid-based derivatives, macrocycles (cyclodextrins, porphyrins or curcubituryls) or chromophore units. For instance, such material types are nicely illustrated by the report of Allain and co-workers showing covalent link between porphyrin and Anderson-type POM or Dawson-type vanadotungstate POM, leading to both hybrids $[N(C_4H_9)_4]_3[MnMo_6O_{18}\{(OCH_2)_3CNHCO(ZnTPP)\}_2]$ and $[N(C_4H_9)_4]_5H[P_2V_3W_{15}O_{59}\{(OCH_2)_3CNHCO(ZnTPP)\}]$, respectively.[52] Such an association revealed photoinduced electron transfer from excited porphyrin units to directly linked POMs, i.e., Anderson or Dawson type.

Furthermore, Wu et al. reported a new strategy to construct flexible ionic organic-inorganic frameworks that behave as a 2D grid based on the precise alternation of anions and supramolecular cations.[53] The reported framework used a mixed metal V-W Keggin type anion $[PVW_{11}O_{40}]^{4-}$ as connecting nodes, and supramolecular host-guest cationic pseudorotaxanes that are obtained from $\alpha$-CD and two cationic azobenzene (Azo) groups connecting with a tri-/tetra-ethylene glycol (Tr/TeEG) spacers. The resulting 2D grid forms a self-assembled single-layer with about 1.4 nm thickness. The stereoselectivity of the supramolecular process appears dynamically dominated by electrostatic interactions guided by steric effects between the spheroidal anions and the bulky cationic linkers. As shown in Figure 1.11, POM anions self-assemble with one CD-shielding cations to give 2D plane that form micron-scale flakes of monolayer assemblies. Using AFM and TEM techniques the authors showed that these 2D nanoscopic materials were highly selective for accurate nano-separation of nanoparticles, such as CdTe quantum dots.[55]

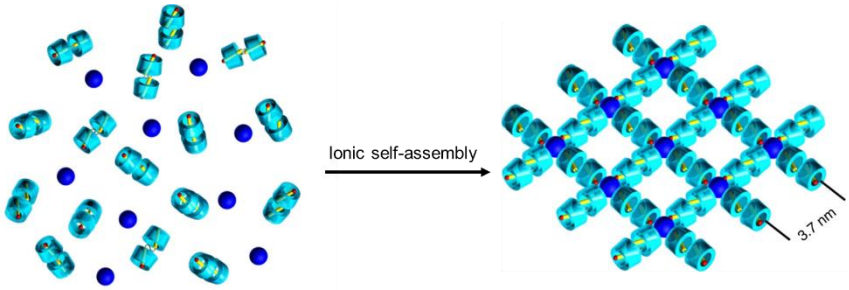


**Figure 1.11** *Schematic representation of the 2D supramolecular framework constructed from an assembly of the Keggin $[PW_{11}VO_{40}]^{4-}$ and the cationic molecules (Azo-Tr/TeEG). Color code: blue, spheres $[PW_{11}VO_{40}]^{4-}$; yellow sticks, $(Azo\text{-}TrEG)^{2+}$; sky blue rings, $\alpha$-CD. (Reproduced from reference 54).*

Furthermore, POMs can also be used as active components within MOF materials (metal-organic-frameworks). Such hybrid-type materials result from non-covalent interaction forces between the guest POM unit and the wall of the MOF cage. Adapted strategies for the design of POM-containing MOF hybrids were successfully developed for the design of materials, catalytically active for relevant reactions such as the photoreduction of $CO_2$.[54]

### 1.1.6 Properties and applications of POM-based materials

As previously illustrated, POMs exhibit wide structural diversity with various physicochemical properties, which lead to their broad applications in photo/electrocatalysis, pharmacology, magnetism, and energy storage/conversion. The main focus here is to introduce their redox and related catalytic properties.

#### 1.1.6.1 Redox properties

POMs are able to undergo reversibly a fast multi-electron redox transfer under mild conditions.[33] Most of them give blue color solution after being reduced, while re-oxidizing process restores their original color, indicating that they exhibit electrochromic behavior.[34] Supriya and co-workers reported a programmable solid-state photochromic switch based on a reversible redox reaction driven by visible light which involves two redox states of a Keggin polyoxometalate $[PW_{12}O_{40}]^{3-}$ interconverted through an one-electron transfer.[55] The dimethylformamide (DMF) molecules present in the POM crystal was used to reversibly control the photochromic change. While hydrogen envisioned as one of the most effective

sustainable fuel, POM compounds are used as active components for electrolysis of water into hydrogen and oxygen.[56] Dong et al. employed the redox properties of POM as electrons and protons reservoir, able to enhance the decoupled electrochemical water splitting process and then efficiently separate hydrogen from oxygen.[57] By adjusting the central heteroatom of the POMs, from Si to Zn, the number of electrons and protons involved in the redox reaction is doubled (from 2 to 4). Then, by contacting the 4e-reduced $H_6ZnW_{12}O_{40}$ aqueous solution with a coated Pt/carbon electrode, a spontaneous release of hydrogen occurred after the reoxidation of the POM. As shown in Figure 1.12, the release amount of hydrogen produced is directly related to the number of stored electrons and protons. In addition, the $H_6ZnW_{12}O_{40}$ species exhibited a high decoupling efficiency of about 95.5% with an electrochemical energy efficiency of 83%, and an excellent cycling behavior (more than 200 cycles without apparent fading).

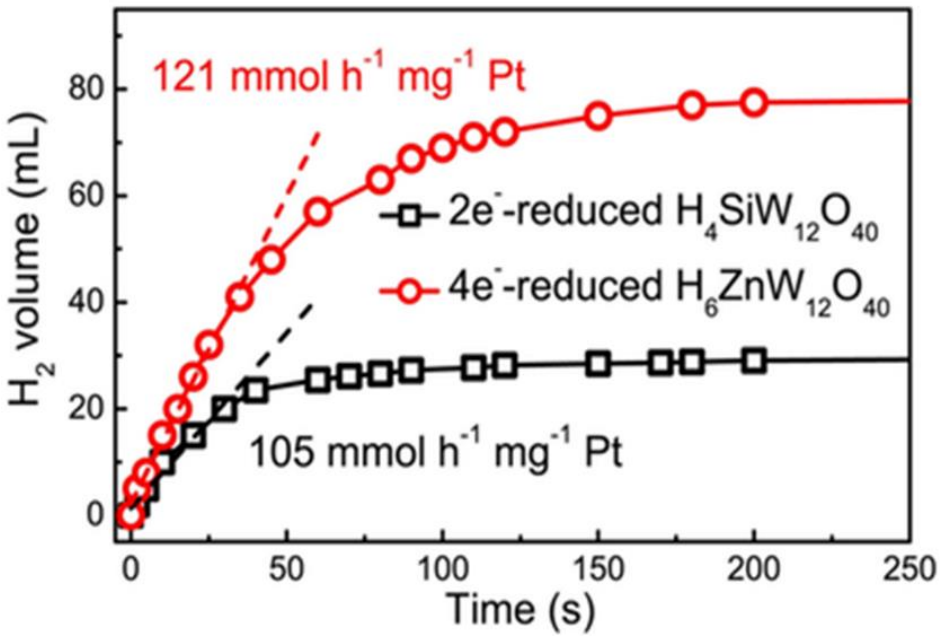


**Figure 1.12** *Spontaneous $H_2$ evolution from a 20 mL sample of 100 mM 4 e−-reduced $H_6ZnW_{12}O_{40}$ or 2 e−-reduced $H_4SiW_{12}O_{40}$ over 5 mg 20% Pt/C (from reference 57).*

### 1.1.6.2 Catalysis

As POMs exhibit fair thermal, hydrolytic and redox stability and offer the possibility to process reversible multi-electron redox exchange without notable change of the

structure, they should have great insights in the field of photo/electrocatalysis.[58] Much research has focused on Keggin-type derivatives due to the wide chemical tunability and reactivity conjugated to exceptional stability. Mizuno and co-workers reported an effective catalyst based on the diiron-substituted silicotungstate γ-$SiW_{10}\{Fe^{3+}(OH_2)\}_2O_{38}^{6-}$ capable to oxygenate alkenes in homogeneous reaction media using very mild catalytic conditions (1 atm $O_2$). Furthermore, they found this catalyst can be recycled multiple times.[59] Since then, Geletii et al. reported an all-inorganic stable and highly active tetraruthenium homogeneous molecular photocatalyst $Rb_8K_2[\{Ru_4O_4(OH)_2(H_2O)_4\}(\gamma\text{-}SiW_{10}O_{36})_2]\cdot 25\,H_2O$. It was found efficient enough for electrocatalytic oxidation of water in aqueous solution at pH = 7 (see Figure1.13A).[60]

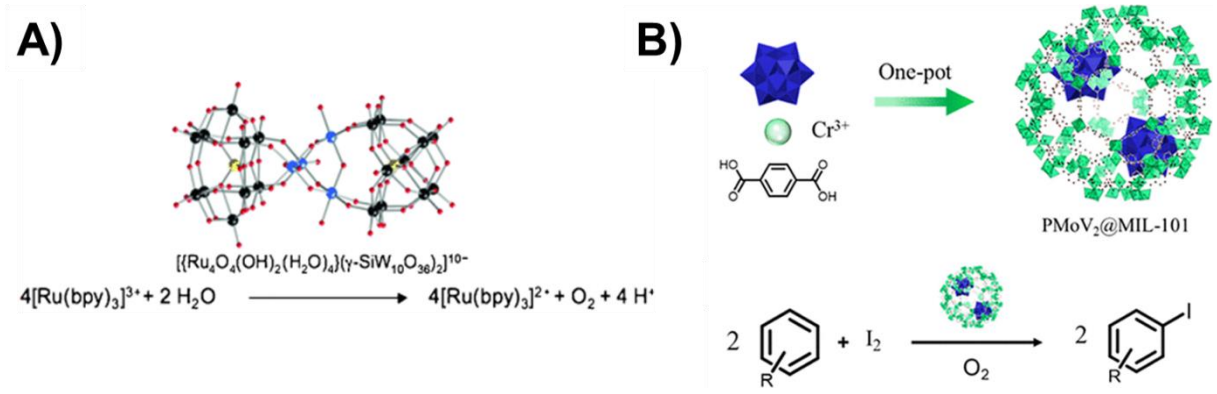


**Figure 1.13** *A) Structure of $[\{Ru_4O_4(OH)_2(H_2O)_4\}(\gamma\text{-}SiW_{10}O_{36})_2]^{10-}$ (ball-and-stick representation: Ru blue, μ-O red, O($H_2$) orange, W gray, and Si yellow; hydrogen atoms omitted for clarity). B) Overview of the one-pot synthesis procedure to prepare $PMoV_2$@MIL-101 in which the MIL-101 grows around the {$PMoV_2$} and encapsulates them in the cage-like pores of the MOF. Direct aerobic iodination of arenes using molecular iodine and $PMoV_2$@MIL-101 as heterogeneous catalyst is shown (from reference 60, 61).*

Recently, the POM@MOF catalyst was also widely studied. Pascal et al. prepared a heterogeneous catalyst $PMoV_2$@MIL-101 through a one-pot procedure.[61] As shown in Figure 1.13B, Molecular iodine was used in the presence of the catalyst to promote the direct aerobic iodination of arene such as mesitylene without additives. The results showed high selectivity of the $PMoV_2$@MIL-101 leading quasi-exclusively to 2-iodomesitylene product after 24 h at 90 °C.

## 1.2 Cyclodextrin (CD)

### 1.2.1 Definition and history

Cyclodextrins (CDs) are a group of macrocyclic oligosaccharides mainly constituted by 6, 7, or 8 D-glucopyranoside units corresponding to α–, β–, or γ-CD with hydrophobic cavity of different diameter sizes. Such macrocycle species can encapsulate many kinds of hydrophobic compounds while the hydrophilic features of the exposed faces lined by hydroxyl groups induce fair solubility in aqueous solution providing a large variety of practical applications in many fields, such as textile,[62–64] food,[65,66] cosmetic industries,[67,68] chromatography,[69–71] catalysis, [72–74] pharmaceutical,[62,75–78] gene therapy,[79,80] tissue engineering,[81,82] soil and wastewater treatment,[83–85] drug delivery,[79,86] and so on.

Cyclodextrins can be described as truncated cone-shaped macrocyclic molecules in which the glucose building block adopts the stable chair conformation shown in Figure 1.14. All primary hydroxyl groups of the methanolic groups (bearing the hydrogen H6) are located on the primary side of the ring, while all secondary hydroxyl groups are located on the second side close to the hydrogen atoms labelled H2 and H3.[87]

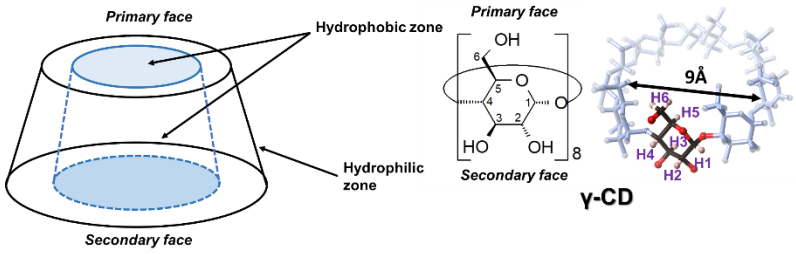


**Figure 1.14** *Molecular structure scheme of γ-cyclodextrin showing the numbering of the six hydrogen atoms of the glucopyranose units (exluding hydroxyl groups).*

As shown in Figure 1.14, the outer wall of cyclodextrin is composed of hydrogen atoms H1, H2 and H4. Furthermore, the lone pair of electrons brought by the oxygen atoms of these glycosidic bonds points toward the interior of the cavity. In consequence, the inner space of CD contains a high density electronic cloud characteristic of Lewis bases.[88] Besides, depending on the number of glucopyranoside which composes the macrocycle, these molecules, i.e., α-, β- or γ-CD, exhibit various solubility and properties which are listed in Table 1-1. [88–90]

**Table 1-1** *Physical and chemical properties of α, β, and γ-CD.*

| Form | Formula | Molecular weight ($g.mol^{-1}$) | Solubility in water at 25 °C ($g.L^{-1}$) | Primary face size (Å) | Secondary face size (Å) | Height of the torus (Å) |
|---|---|---|---|---|---|---|
| α– | $C_{36}H_{60}O_{30}$ | 972 | 145 | 4.3 | 5.3 | 7.9 |
| β– | $C_{42}H_{70}O_{35}$ | 1135 | 18.5 | 6.0 | 6.5 | 7.9 |
| γ– | $C_{48}H_{80}O_{40}$ | 1297 | 232 | 7.5 | 8.3 | 7.9 |

The history of cyclodextrin chemistry can be traced back to the 19th century when Villiers in 1891 reported that potato starch fermented under certain conditions using the action of Bacillus amyloliquefaciens led to the main product, later identified as cyclodextrin.[88,91–93] Twelve years later, this class of natural sugar was named "Schardinger dextrins" in honor of the scientist who was the first to provide a trustworthy description of the products from Bacillus maceration, characteristics of both alpha- and beta-cyclodextrin.[94,95] Pringsheim was likewise interested in the biochemistry and chemistry of CDs from 1912 to 1933. He studied the interaction between dextrins and the amylose/amylopectin macromolecules and discovered that dextrins and their acetate counterparts frequently form complexes with different chemical substances.[93] In 1935, Freudenberg and Jacobi described for the first time the larger γ-CD and suggested that larger cyclodextrins containing nine and ten glucopyranoside units called δ- and ε-CD, respectively, should also exist.[96,97] Furthermore, they proposed that cyclodextrin contains 1,4 glycosidic bond in their framework and reported the method of separating and purifying cyclodextrins. Besides, the ring structure of cyclodextrin was first proposed in 1936.[98] Last, γ-CD was purified and crystalized for structure determination in 1948.[97] French also contributes significantly to the cyclodextrin chemistry, reporting that these cycloamyloses were capable of forming specific adducts from iodine and iodide mixture. French determined accurately the molecular weight of the Schardinger α– and β– dextrins.[95,99–102] The French's strategy to address starch and cyclodextrin research in the 1950s is nicely illustrated by himself in Figure 1.15.

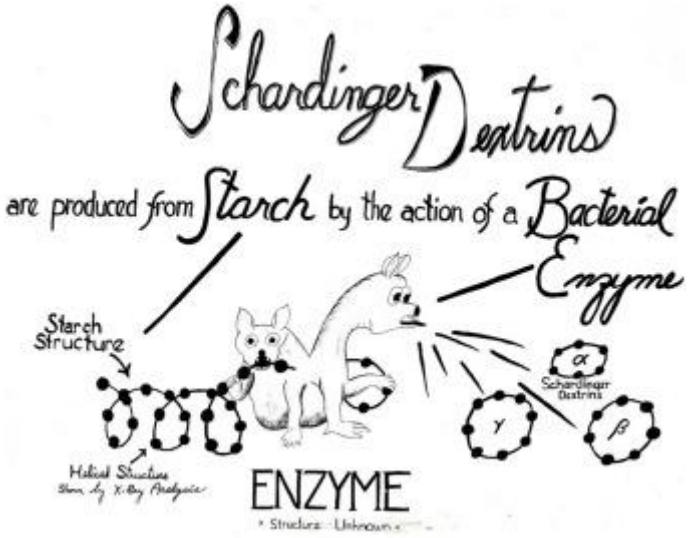


**Figure 1.15** *Artwork of French showing the chain of production of cyclodextrins from starch (from reference 100).*

Freudenberg et al. patented first the use of CDs in medicinal formulations in 1953.[103] In 1976, a report titled:" Cyclodextrin Nephrosis in the Rat" suggested that nephrotoxicity of α- or β-CD is manifested by a series of changes in the vacuolar organelles of the proximal convoluted tubules, eventually leading to cell death.[104] Up to now, the smallest CD members are built from three or four glucopyranose units successfully synthesized by Darki and co-workers.[105] Since then, researchers have engaged intensive and vigorous developments in discovering structural, physical-chemical and biological properties of cyclodextrins leading to industrial production and practical commercial applications.

### 1.2.2 Inclusion complexes with hydrophobic species

Non-covalent interaction forces drive molecular recognition of cyclodextrins through a conglomerate of weak interactions including electrostatic (ionic, ion-dipole, dipole-dipole, dipole-induced dipole), van der Waals (dispersion forces through induced dipoles), hydrophobic effect (solvent effect), hydrogen bonding, π-π stacking and charge transfer. The hydrophobic character of the CDs cavity is favorable to host-guest process leading to inclusion of various hydrophobic molecules. These host-guest adducts can exhibit different modes of inclusion depending on the host-guest stoichiometry and the type of the involved faces, i.e., primary or secondary. These various modes of inclusion and some representative guest molecules are schematically highlighted in Figure 1.16.[88,106]

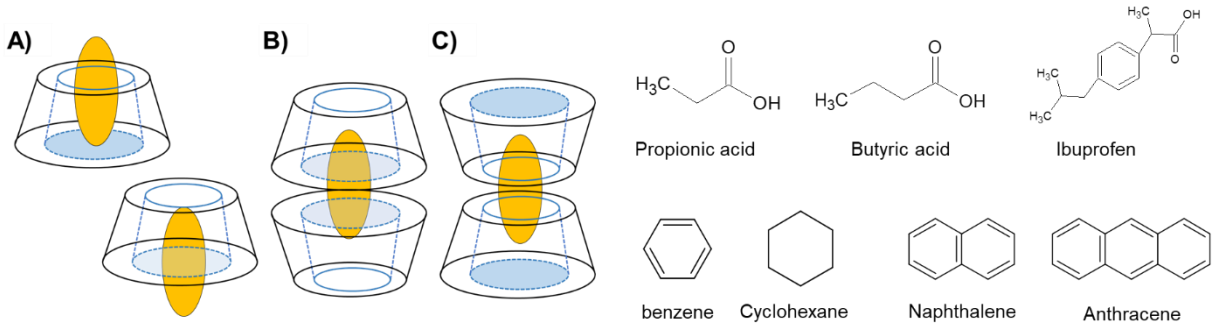


**Figure 1.16** *Schemes of inclusion models between CD and guest molecular species. A) 1:1 CD/guest, the guest molecule enters the cavity of the CD from the primary face or the secondary face. B) 2:1 CD/guest, the guest molecule is bound by the secondary sides of two CDs. C) 2:1 CD/guest, the guest molecule is bound by the primary sides of two CDs. D) Representation of typical hydrophobic molecules interacting with CDs in a host-guest complexation process* (*from reference 88, 106*).

In 1963, Nemethy et al. proposed rational bases to understand the hydrophobic effect at the origin of the solvation process of non-polar compounds in water. The authors proposed that a structurally organized solvation shell of water molecules spreads on the surface of non-polar molecules featured by a large entropy penalty ($\Delta_r S < 0$). To balance such an unfavorable entropy change, non-polar molecules with large hydrophobic area tend to minimize their interface with water through various self-assembly reactions, which are entropy-controlled processes. Actually, the host-guest recognition processes involving cyclodextrins and non-polar molecules range in this category driven by the desolvation processes of the exposed hydrophobic area of the guest and the host components, which lead to a positive entropy change making the process highly favourable.[107]

Then, CDs behave as host unit leading to stable complexes with specific guest molecules. Nevertheless, the host-guest reaction takes place through a thermodynamic equilibrium expressed by the stability constant *K*. *V*arious spectroscopic methods are currently used to study formation of inclusion complexes at the molecular level. For instance, Negi and Singh investigated the complex formation between amisulpride drug (AMI) and γ-CD using UV-vis spectroscopy. Analysis of the UV-vis titration experiments allowed the determination of the stoichiometry and the related binding constant of the AMI/γ-CD chemical system.[108] In the same way, Schneider et al. evaluated the complexation constants of α-, β- and γ-CD with 1-anilino-8-naphthalenesulfonate (ANS) and 2-toluidino-6-

naphthalenesulfonate (TNS) via $^{1}$H NMR titrations, which highlight the host-guest process by the variation of the chemical shits of hydrogen H1-H6 in cyclodextrins (mainly H5, H3, and H6) occurring in the presence of the aromatic guests.[109] Stepniak et al. proposed a complete investigation of an extremely poorly water-soluble inclusion complexes from β-CD and albendazole (ABZ). Using isothermal titration calorimetery (ITC), they determined the enthalpy and entropy parameters related to the ABZ@β-CD complex formation.[110] In addition, other spectroscopic techniques such as circular dichroism, fluorescence spectroscopy, affinity capillary electrophoresis (ACE), capillary electrophoreses (CE), and high-performance liquid chromatography (HPLC) in combination can provide complementary information about the origin of the non-covalent interactions with regard to the formation of the host-guest complexes.[111]

### 1.2.3 Host-guest inclusion with POMs

While CDs interact with various hydrophobic substances, some recent reports showed that CDs were also capable to form host-guest adducts with hydrophilic ionic molecules.[45,46,112] In context, self-assembly involving CDs and amphiphilic macrocyclic molecules are particularly well suited for the development of POM-based supramolecular hybrid systems, envisioned for the creation of smart materials with self-healing properties or multiphasic catalytic systems.[113,114] Associations arising from CDs and POMs interactions can be broadly divided into two classes. The first results from the strong affinity of the CD with a hydrophobic group grafted to the POMs. Such a mode of interaction fits into the classical "*hydrophobic effect*", previously described.[53,113,115,116] The second type involves native inorganic species such as POMs or ionic cluster compounds which were found to form unusually stable host-guest adducts with CDs. In 2015, both Nau's and Stoddart's groups reported that γ- or β-CD strongly interacts with hydrophilic ions such as $[B_{12}X_{12}]^{2-}$ clusters (with X = H, F, Cl, Br or I) and $[PMo_{12}O_{40}]^{3-}$ anions.[45,46] The structure of the host-guest arrangements, shown in Figure 1.17, has been determined by single-crystal X-Ray diffraction technique. These arrangements revealed 2:1 complex where the inorganic ionic species, i.e., either the cluster or the POM, appeared deeply encapsulated between two γ-CDs. Interestingly, depending on the ionic guest, the inclusion

complex is formed by joining the secondary faces of the CD with cluster or the primary faces with POM.

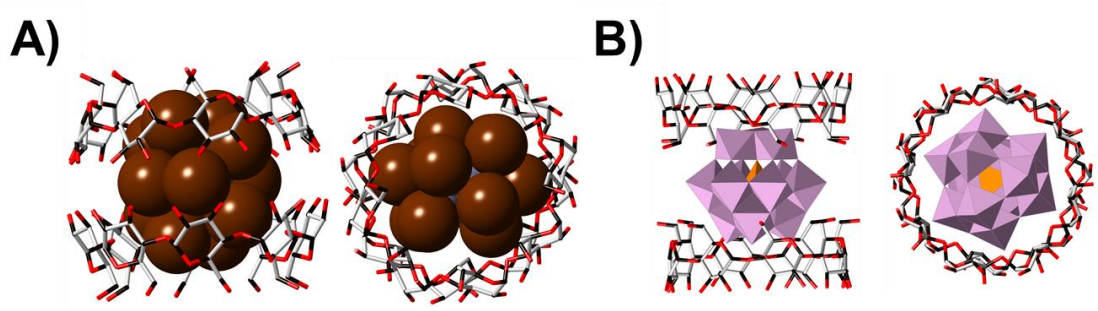


**Figure 1.17** *A) Face (left) and top (right) views of the XRD structure of the inclusion complex of the $[B_{12}X_{12}]^{2-}$ into the γ-CD cavity. B) Face (left) and top (right) views of the XRD structure of the inclusion complex of the $[PMo_{12}O_{40}]^{3-}$ into the γ-CD cavity (from reference 45, 46).*

The inclusion phenomenon involving hydrophilic ionic species has been recently well documented and explained as a solvent effect which arises from the chaotropic nature of the ionic guest. Such chaotropic effect takes place in aqueous solution and gives a characteristic thermochemical fingerprint. As schematically shown in Figure 1.18, low-charge density POM provokes locally the breaking of the water structure, featured by a solvation shell of high enthalpy and high entropy. Along the aggregation process leading to the POM encapsulation (see Figure 1.18), the release of the water from the hydration shell to the bulk is associated to enthalpy and entropy decreases, i.e., $\Delta_r H < 0$ and $\Delta_r S < 0$. Despite the entropy penalty, the aggregation process remains highly favorable and enthalpically driven ($T\Delta_r S > \Delta_r H$ and $\Delta_r G < 0$). Based on these findings, the chemical system have been extended to other POMs with low charge density, including the Lindqvist ions $[M_6O_{19}]^{2-}$,[43] the Preyssler-type $[NaP_5W_{30}O_{110}]^{15-}$ anion,[117] the Dawson-type $[P_2W_{18}O_{62}]^{6-}$ anion, and even, the giant Mo blue wheel $[Mo_{154}O_{462}H_{14}(H_2O)_{70}]^{14-}$, abbreviated $\{Mo_{154}\}$.[32,118] All these anions, varying in their structure, composition, size and shape showed fair ability to form supramolecular aggregates with CDs, due to their low-charge density at the origin of the "chaotropic effect" taking place in aqueous solution.[119] Then, although the chaotropic effect was identified by Hofmeister in 1888 for classical ions, this property has been clearly associated with POM anions very recently and opens

an emerging path in the design of POM-based supramolecular hybrid materials and related applications in the field of smart materials based on POM@CD.

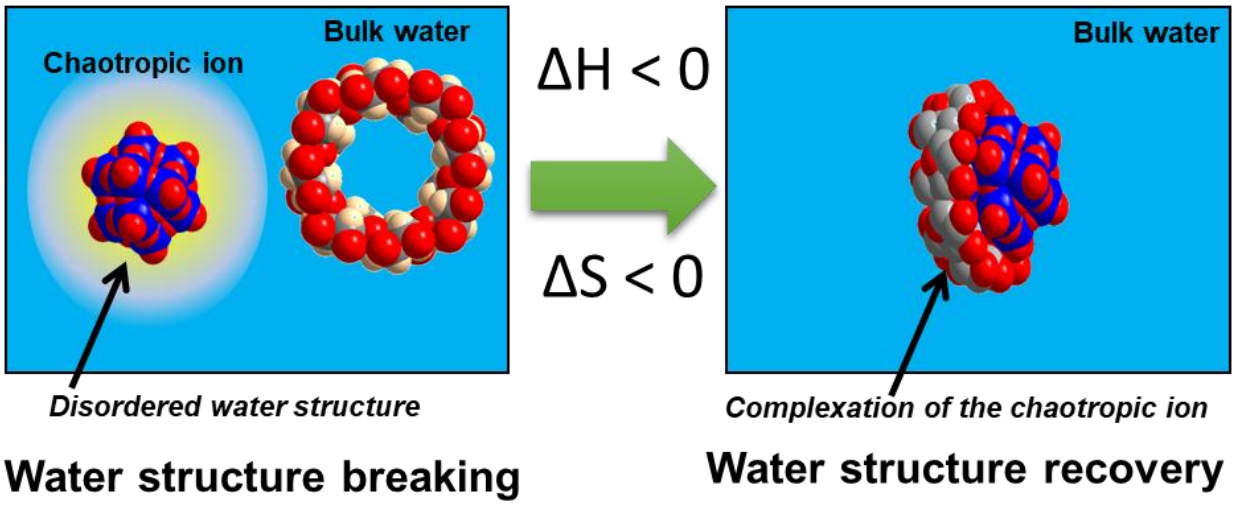


**Figure 1.18** *Schemes of water structure breaking and recovery processes during the inclusion of POM in CD cavity.*

### 1.2.4 CD-based polymers as smart materials

Currently, CDs or functionalized-CD derivatives have also been used as building blocks to develop various polymeric networks or assemblies. The functioning principles of these smart materials lie on the chemical or physical cross-linking of oligomers by using functional guest molecules. The resulting smart materials exhibit unique properties, as for instance self-healing or mechanical responsive to external stimuli. Furthermore, they could appear in various practical physical aspects such as hydrogels or microcapsules.[120]

#### 1.2.4.1 Pharmaceutical engineering

Since the 1970s, a wide variety of pharmaceutically relevant inclusion complexes have appeared on the market due to a better descriptions of cyclodextrin toxicity and fundamental knowledge of the supramolecular encapsulation process.[121] However, due to some limitations of natural cyclodextrins, functionalization of cyclodextrins becomes an important and intensive research area. Modification of CD opens the way to chemical derivatives with increased water solubility or specific physical-

chemical properties. Such derivations of CDs correspond to alkylation, hydroxyalkylation or esterification of the exposed hydroxyl groups.

Siemoneit et al.[122] evaluated the effect of the proportion of acrylamidomethyl-γ-cyclodextrin (γ-CD-NMA) on the loading and release of hydrophobic triamcinolone acetonide (TA) or hydrophilic propranolol (PR) from CD-based hydrogels. The hydrogels were synthesized using *N*,*N*′-methylen(bisacrylamide)(BIS), as a cross-linker for the γ-CD-NMA free radical polymerization and then compared to the γ-CD-NMA-free hydrogels. The resulting hydrogel prepared with 9.4% γ-CD-NMA was able to load 32 mg TA/g gel, which is consistent with a 1:1 stoichiometric ratio between TA and CD while without γ-CD-NMA, the hydrogel performance fall down to 0.6 mg TA/g gel. Furthermore, the release behavior of the two model drugs, i.e., TA and PR, from γ-CD-NMA-containing hydrogels was compared with that of γ-CD-NMA-free hydrogels suspended in 0.1 N HCl (pH 1.2), or phosphate buffer (pH 6.8). As shown in Figure 1.19, the release of hydrophobic drug TA was delayed from 8 to 24 h with the presence of the γ-CD-NMA component. Changing substrate from TA (hydrophobic) to PR (hydrophilic) showed that the release process of the hydrophilic PR was not affected by the loading of γ-CD-NMA in contrast to the hydrophobic TA, demonstrating that the process is mainly controlled by the hydrophobic interaction between the CD-containing hydrogel and the drug.

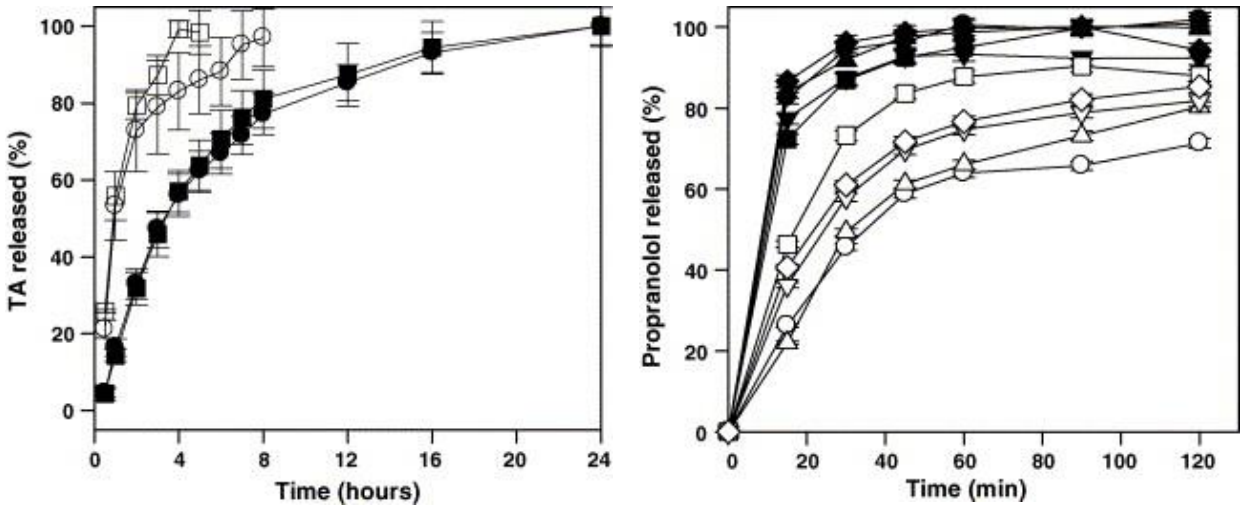


**Figure 1.19** *Left: Triamcinolone (TA) release profiles, in 0.1 N HCl (○, ●) and in pH 6.8 phosphate buffer (□, ■) from hydrogels; Right: Propranolol (PR) release profiles, in 0.1 N HCl (full symbols) and in phosphate buffer pH 6.8 (open symbols) from hydrogels synthesized with 3 M sodium acrylate, 39 mM BIS and different proportions of γ-CD-NMA (1.70% ○, ●; 3.36% □, ■; 4.95%, △, ▲; 6.50% ▽, ▼; 7.99% ◊, ◆) (from reference 122).*

Besides, Brodin and co-workers demonstrated that poly-β-cyclodextrin (pβCD) nanoparticles obtained by cross-linking with epichlorohydrin (EP) exhibit antibacterial properties and behave as effective tuberculosis (anti-TB) drug carriers.[77] They found that after pulmonary administration, pβCD hinders *Mycobacterium tuberculosis*-induced macrophage proliferation by interfering with lipid rafts. Furthermore, these findings demonstrate that pβCD nanoparticles loaded or not loaded with antibiotics remain effective against tuberculosis. Recently, Uyar et al.[123] reported that Ondansetron/hydroxypropyl-beta-cyclodextrins-coated nanofibrous web, abbreviated ODS/HPβCD NW, can be used for potential fast-disintegrating oral antiemetic drug delivery. The preparation of a polymer-free electrospun nanofiber network of ODS/HPβCD inclusion complex (IC) is shown in Figure 1.20A. The decomposition properties of the nanofiber network have been evaluated by simulating the oral environment with filter paper impregnated with artificial saliva. This shows that ODS/HPβCD NW decomposed after 2 seconds of contact with the filter paper as shown in Figure 1.20B. Due to the high absorption properties of the filter paper, ODS readily passed through the fibrous structure during the decomposition process. In contrast, the polyvinyl alcohol (PVA) and PVA NW-based filter papers retain a layer of nanofibrous network even after 50 s as shown in Figure 1.20C. ODS/HPβCD NW releases approximately 80% of active drug within 30 s and reaches ~100 % within 2 min, which is much better than ODS/PVA NW releasing only about 20 % after 10 min (see Figure 1.20C). In conclusion, the ODS/HPβCD NW pharmaceutical composite is very attractive as anti-nausea or anti-vomiting agent, and such a CD-based strategy as drug carrier and delivery has promising applications in pharmaceutical industry.

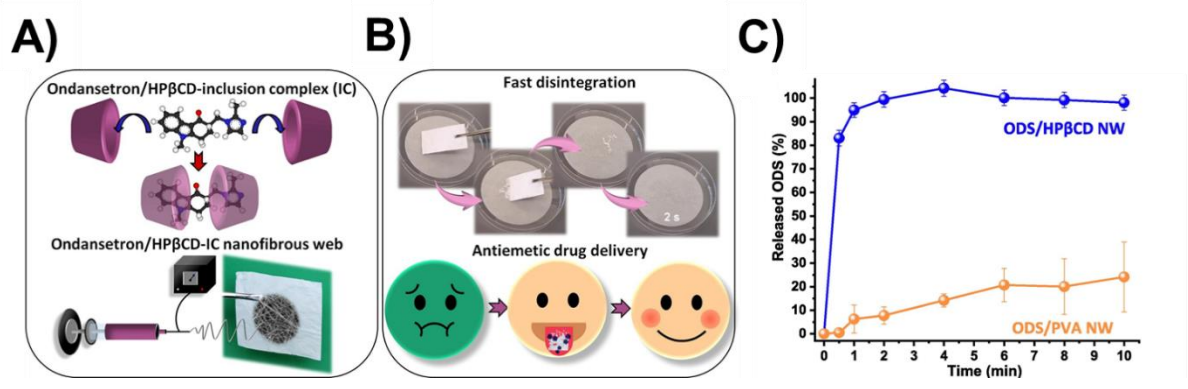


**Figure 1.20** *A) Schematic representation of inclusion complex formation between HPβCD and ODS and the electrospinning of ODS/HPβCD-IC nanofibrous web. B) Disintegration profiles of ODS/HPβCD NW. C) Time-dependent release profile of ODS/HPβCD NW and ODS/PVA NW(from reference 123).*

### 1.2.4.2 Catalysis

For the development of green chemistry and related processes, the need of aqueous-based catalysis is critical. Supramolecular assemblies based on metal nanoparticles consist of macrocyclic compounds and transition metal precursors and can produce a water-dispersible catalytic system with high performance and molecular recognition ability. Interestingly, cyclodextrin-based methods for stabilizing catalytically active metal nanoparticles appear particularly efficient and fill the principles of green chemistry.

Peinemann et al.[124] designed and synthesized a β-cyclodextrin polymer network (CPN)-supported metal nanoparticle as a heterogeneous catalyst. The CPN support works synergistically with the metal nanoparticle, which has high catalytic activity and selectivity and high thermal stability. Per-(6-azido-6-deoxy)-β-cyclodextrin and 1,4-diethynylbenzene were used as monomers, then a 1,2,3-triazolyl bond was formed via a click reaction under mild conditions. This produces the linking of cyclodextrins which behave as effective anchoring groups to facilitate the binding of metal ions to nanoparticles (NPs) and give the composite NPs@CPN. A series of ultra-small noble metal, i.e., palladium (Pd), silver (Ag), platinum (Pt), gold (Au), and rhodium (Rh), NPs were readily stabilized and synthesized by wet chemistry under mild conditions, as shown in Figure 1.21A. To illustrate the potentialities of such NPs-based composites, commercial Pd black (Figure 1.21B) catalyzes the reduction of 4-nitrophenol within 30 min, whereas only 3 min are needed for Pd-NPs@CPN composites operating in similar catalytic conditions (see Figure 1.21C). The authors claimed that the complexation of cyclodextrin with 4-nitrophenol increases the concentration of 4-nitrophenol near the catalytically active surface of the Pd-NPs. In addition, Pd-NPs@CPN maintained 100% 4-nitrophenol conversion after seven cycles, indicating the excellent recyclability of this catalytic composite.

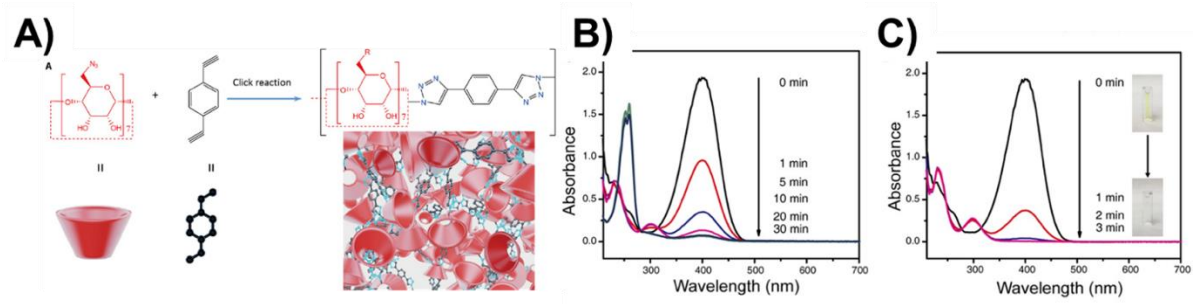


**Figure 1.21** *A) Synthesis of the CPN from per-(6-azido-6-deoxy)-β-cyclodextrins with 1,4-diethynylbenzene. B and C) Time-dependent UV-Vis spectra of the reduction of 4-nitrophenol (0.1 mM) in $NaBH_4$ (10 mM) aqueous solution catalyzed by B) Pd black and C) Pd-NPs@CPN (from reference 124).*

Also, homogeneous catalysts could have great potentialities with high activity and selectivity. The water-soluble supramolecular POM-based catalyst can be used in a biphasic catalytic process, where the organic substrate could be transferred to the aqueous phase through the catalytic material, which can also transport the reaction product back to the organic phase. Diao et al.[125] reported on a one-pot self-assembly procedure to construct a novel 3D supramolecular POM inorganic-organic hybrid framework $(KCl_4)Na_7[(\beta\text{-CD})_3(SiW_{12}O_{40})]\cdot 9H_2O$, abbreviated $\{3CD@SiW_{12}O_{40}\}$, in which β-cyclodextrin (β-CD) acts as a reverse-phase transfer agent for various oxidation catalysts. As shown in Figure 1.22, the β-CD host can effectively increase the solubility of various substrates such as alcohols, alkenes, and thiophene in the aqueous phase by forming inclusion complexes, and then increase significantly the reaction rate. The POM catalyst is strongly attached to the surface of β-CD in the solid state via O-Na-O bonds and hydrogen bonds in the $\{3CD@SiW_{12}\}$ structure. In aqueous solution, the retention of such arrangement is favourable for close contact between the substrate and the catalytic POM. Therefore, the synergistic effect arising from CD as phase transfer agent and POM as oxidation catalyst is realized by molecular recognition to produce the supramolecular system $\{3CD@SiW_{12}\}$ in aqueous solution. Combining the properties of CDs and POMs to create multifunctional catalytic assemblies from CD-POM supramolecular complexes is an attractive strategy for the environment and industry.

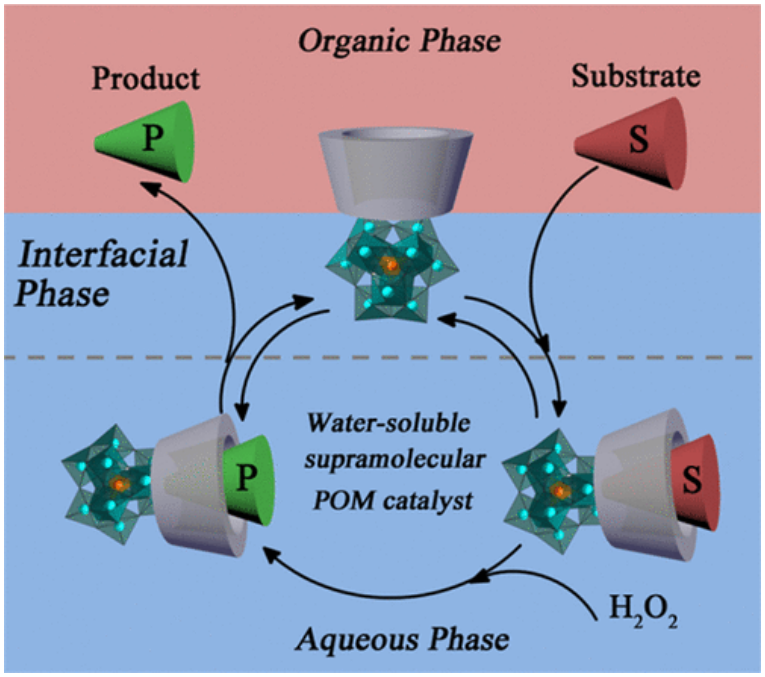


**Figure 1.22** *Proposed catalytic scheme mediated by the supramolecular POM catalyst {3CD@SiW12} in the biphasic system (from reference 125).*

### 1.2.4.3 Adsorption-based wastewater treatment

Chemical pollution of natural water has become a major public concern in almost all regions. Due to increasing surface and groundwater chemical pollution, the long-term effects on aquatic organisms or human health are still unknown today. The role of cyclodextrins in the treatment of industrial pollutant wastewater is now a hot research topic.

Alsbaiee et al.[126] utilized rigid aromatic groups cross-coupled with β-cyclodextrins (see Figure 1.23A) to obtain a 3D mesoporous β-cyclodextrin polymer (abbreviated P-CDP) with a specific surface area of up to 250 $m^2/g$, resulting of rapid adsorption of organic micropollutants. The adsorption rate constants, measured on the P-CDP material was found 15 to 200 times higher than those of other adsorbent materials, i.e., Norit RO 0.8 activated carbon (NAC) and non-porous β-cyclodextrin crosslinked with epichlorohydrin (EPI-CDP). Bisphenol A (BPA) a component of plastics was used as a model pollutant. The results showed that P-CDP removed BPA faster than all other sorbents, reaching 95% of its equilibrium uptake within 10 s, unlike other materials, such as EPI-CDP, which took more than 1 h to reach equivalent equilibrium value. Interestingly, BPA was easily removed by washing the BPA loaded

P-CDP polymer with methanol at room temperature. On this basis, five consecutive cycles of bisphenol A adsorption/desorption were carried out, and it was found that the regenerated P-CDP performance was almost unchanged. Additionally, they also estimated the ability of P-CDP to remove pollutants varying in size, functionality, and hydrophobicity, such as aromatics, pharmaceuticals, or pesticides, as shown in Figure 1.23B. This P-CDP material could be used for various situations such as in household water filtration, but also in industrial wastewater treatment or in natural environment for ecological restoration. Such a type of material will most likely replace activated carbon as the next generation of new water treatment materials.

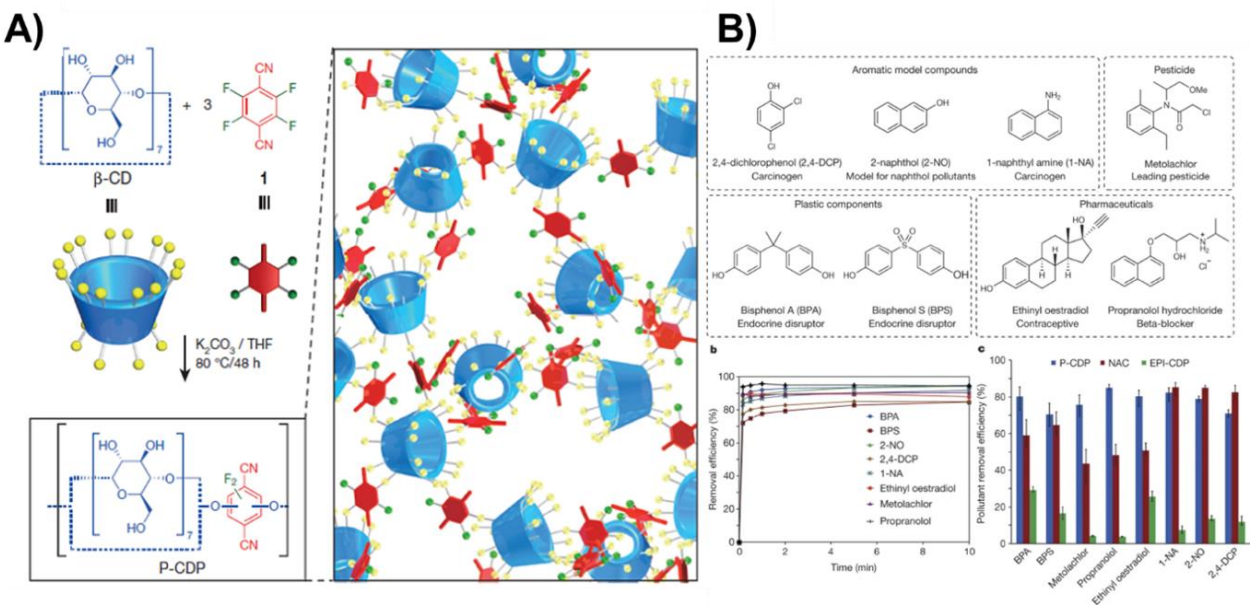


**Figure 1.23** *A) Schematic presentation of the synthesis of the high-surface-area porous P-CDP from β-CD. B) Structures and relevance of each tested emerging organic micropollutant; Time-dependent adsorption of each pollutant (0.1 mM) by P-CDP (1 mg ml$^{-1}$); Percentage removal efficiency of each pollutant obtained by rapidly flowing the adsorbate solution through a thin layer of P-CDP (blue), NAC (red) or EPI-CDP (green) (from reference 126).*

The treatment of pharmaceutical wastewater is also an urgent problem to be solved. Recently, Wang et al.[76] reported nice work about treating pharmaceutical wastewater. A γ-cyclodextrin-modulated thin-film nanofibrous composite (TFNC) as nanofiltration (NF) membrane was designed by interfacial polymerization. γ-CD and piperazine (PIP) were mixed in the aqueous phase to prepare the separation layer, and were expected to react at the interface with trimesoyl chloride (TMC) in the organic phase (see Figure 1.24A). The permeate fluxes of the optimized $PIP_{0.5}γCD_{0.5}$ TFNC

membranes were 23.3 L $m^{-2}$ $h^{-1}$ $bar^{-1}$, much higher than that of the pure polyamide membrane 9.13 L $m^{-2}$ $h^{-1}$ $bar^{-1}$, and the removal rate of $Na_2SO_4$ is still high (> 98.7%) under 0.5 MPa. In addition, as shown in Figure 1.24B, the TFNC membrane exhibited extremely high rejection (> 99%) for several drugs (doxycycline, tetracycline, and amoxicillin). This TFNC membrane showed favorable pressure resistance and long-term operational stability for 24 h, which more usefully indicated that the strategy could be applied in seawater desalination, drug separation, and wastewater treatment.

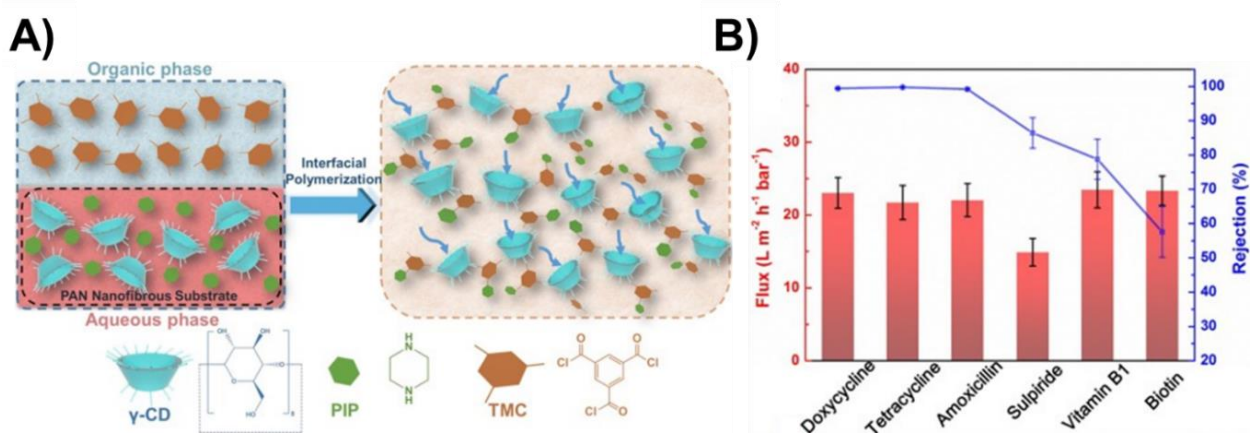


**Figure 1.24** *A) Procedure of γ-CD modulated TFNC NF membranes. B) Separation performances of $PIP_{0.5}\gamma CD_{0.5}$ TFNC membranes under 0.5 MPa with several pharmaceuticals solutions (from reference 76).*

## 1.3 Scope of the thesis

One of the key areas of research in supramolecular chemistry is the development of smart materials based on host-guest interactions. The versatile tunability of supramolecular compounds involving natural cyclodextrins or cyclodextrin-based polymers has always been a research hotspot. Furthermore, POM systems show great potential to act as host or guest depending on targeted supramolecular systems. Chapter 2 contains the investigations and associated results on the fundamental host-guest recognition processes involving CD and polyoxometalate species, highlighting the effect of CD on the solution behavior of POM and an overview of the main driving forces at the origin of interactions. In Chapter 3, we plan to engage POM units as molecular effectors toward CD-based polymers to build

functional hybrid polymeric assemblies arising from the networking through POM-CD connecting nodes. To achieve these objectives, complementary methods, including NMR spectroscopy, electrochemistry, UV-Vis, ESI-mass, Isothermal Titration Calorimetry (ITC), and Small-Angle X-ray Scattering (SAXS) were carried out for multi-scale solution studies. Besides, structural models of CD-POM supramolecular associations have been obtained by X-ray diffraction analysis.

# Bibliography


1. Pope, M. T. & Müller, A. Polyoxometalate Chemistry: An Old Field with New Dimensions in Several Disciplines. *Angew. Chem. Int. Ed. Engl.* **30**, 34–48 (1991).
2. Ni, L. *et al.* Self-Assembled Supramolecular Polyoxometalate Hybrid Architecture as a Multifunctional Oxidation Catalyst. *ACS Appl. Mater. Interfaces* **11**, 38708–38718 (2019).
3. Samaniyan, M., Mirzaei, M., Khajavian, R., Eshtiagh-Hosseini, H. & Streb, C. Heterogeneous Catalysis by Polyoxometalates in Metal–Organic Frameworks. *ACS Catal.* **9**, 10174–10191 (2019).
4. Chen, X. *et al.* Polyoxometalates as Potential Next-Generation Metallodrugs in the Melanogenesis Inhibitor. *Z. Für Anorg. Allg. Chem.* **648**, e202100319 (2022).
5. Gao, N. *et al.* Transition-metal-substituted Polyoxometalate Derivatives as Functional Anti-Amyloid Agents for Alzheimer's Disease. *Nat. Commun.* **5**, 3422 (2014).
6. Bijelic, A., Aureliano, M. & Rompel, A. Polyoxometalates as Potential Next-Generation Metallodrugs in the Combat Against Cancer. *Angew. Chem. Int. Ed.* **58**, 2980–2999 (2019).
7. Herrmann, S., Ritchie, C. & Streb, C. Polyoxometalate – conductive Polymer Composites for Energy Conversion, Energy Storage and Nanostructured Sensors. *Dalton Trans.* **44**, 7092–7104 (2015).
8. Berzelius, J. J. Beitrag zur näheren Kenntniss des Molybdäns. *Ann. Phys.* **82**, 369–392 (1826).
9. Marignac, C. Ueber die Analyse der borsauren Salze und der Fluorbor-Verbindungen. *Z. Für Anal. Chem.* **1**, 405–410 (1862).
10. Rosenheim, A. & Davidsohn, I. Die Hydrate der Molybdänsäure. II. Mitteilung. *Z. Für Anorg. Chem.* **37**, 314–325 (1903).
11. Miolati, A. & Pizzighelli, R. Zur Kenntnis der komplexen Säuren I. 1. Über die Leitfähigkeit von molybdänsäurehaltigen Gemischen. *J. Für Prakt. Chem.* **77**, 417–456 (1908).
12. Pauling, L. The Molecular Structure of the Tungstosilicates and Related Compounds. *J. Am. Chem. Soc.* **51**, 2868–2880 (1929).
13. Hoard, J. L. An X-ray Investigation of the I2-Molybdo-phosphates and Related Compounds. *Z. Für Krist. - Cryst. Mater.* **84**, 217–230 (1933).
14. Keggin, J. F. Structure of the Crystals of 12-Phosphotungstic Acid. *Nature* **132**, 351–351 (1933).
15. Keggin, J. F. Structure of the Molecule of 12-Phosphotungstic Acid. *Nature* **131**, 908–909 (1933).
16. Evans, H. T. The Crystal Structures of Ammonium and Potassium Molybdotellurates. *J. Am. Chem. Soc.* **70**, 1291–1292 (1948).
17. Dawson, B. The Structure of the 9(18)-heteropoly Anion in Potassium 9(18)-tungstophosphate, $K_6(P_2W_{18}O_{62}).14H_2O$. *Acta Crystallogr.* **6**, 113–126 (1953).
18. Lindqvist, I. The Structure of the Hexaniobate Ion in $7Na_2O.\ 6NB_2O_5.\ 32H_2O$. *Ark. Kemi* **5**, 247–250 (1953).
19. Fuchs, J. & Jahr, K. F. Notizen: Über neue Polywolframate und -molybdate. *Z. Für Naturforschung B* **23**, 1380–1380 (1968).
20. Dexter, D. D. & Silverton, J. V. A New Structural Type for Heteropoly Anions. The Crystal Structure of $(NH_4)2H_6(CeMo_{12}O_{42}).12H_2O$. *J. Am. Chem. Soc.* **90**, 3589–3590 (1968).
21. Pettersson, L. Multicomponent Polyanions .1. Yellow and Colourless Molybdophosphates in 3 M $Na(ClO_4)$ - Determination of Formation Constants for 3 Colourless Pentamolybdodiphosphates in pH-Range 3-9. *Acta Chem. Scand.* **25**, 1959-+ (1971).
22. Strandberg, R. The Molecular and Crystal Structure of $Na_6Mo_5P_2O_{23}$ $(H_2O)$ 13, a Compound Containing Sodium-coordinated Pentamolybdodiphosphate Anions. *Acta Chem Scand* **27**, 1004–1018 (1973).
23. Müller, A. *et al.* Archimedean Synthesis and Magic Numbers: "Sizing" Giant Molybdenum-Oxide-Based Molecular Spheres of the Keplerate Type. *Angew. Chem. Int. Ed.* **38**, 3238–3241 (1999).
24. Müller, A., Kögerler, P. & Kuhlmann, C. A Variety of Combinatorially Linkable Units As Disposition: From A Giant Icosahedral Keplerate to Multi-Functional Metal–Oxide Based Network Structures. *Chem. Commun.* **0**, 1347–1358 (1999).
25. Müller, A., Peters, F., Pope, M. T. & Gatteschi, D. Polyoxometalates: Very Large ClustersNanoscale Magnets. *Chem. Rev.* **98**, 239–272 (1998).
26. Müller, A., Beckmann, E., Bögge, H., Schmidtmann, M. & Dress, A. Inorganic Chemistry Goes Protein Size: A Mo368 Nano-Hedgehog Initiating Nanochemistry by Symmetry Breaking. *Angew. Chem. Int. Ed.* **41**, 1162–1167 (2002).
27. Bridgeman, A. J. The Electronic Structure and Stability of the Isomers of Octamolybdate. *J. Phys. Chem. A* **106**, 12151–12160 (2002).
28. Fuchs, J. & Hartl, H. Anion Structure of Tetrabutylammonium Octamolybdate [N(C4H9)4]4Mo8O26. *Angew. Chem. Int. Ed. Engl.* **15**, 375–376 (1976).
29. Müller, A., Meyer, J., Krickemeyer, E. & Diemann, E. Molybdenum Blue: A 200 Year Old Mystery Unveiled. *Angew. Chem. Int. Ed. Engl.* **35**, 1206–1208 (1996).
30. Müller, A. & Serain, C. Soluble Molybdenum Blues"des Pudels Kern". *Acc. Chem. Res.* **33**, 2–10 (2000).
31. Al-Sayed, E. & Rompel, A. Lanthanides Singing the Blues: Their Fascinating Role in the Assembly of Gigantic Molybdenum Blue Wheels. *ACS Nanosci. Au* **2**, 179–197 (2022).
32. Moussawi, M. A. *et al.* Nonconventional Three-Component Hierarchical Host–Guest Assembly Based on Mo-Blue Ring-Shaped Giant Anion, γ-Cyclodextrin, and Dawson-type Polyoxometalate. *J. Am. Chem. Soc.* **139**, 14376–14379 (2017).

33. M.T. Pope. Heteropoly and Isopoly Oxometalates: Inorganic Chemistry Concepts. Berlin: Springer-Verlag **8**, (1983).
34. Yamase, T. Photo- and Electrochromism of Polyoxometalates and Related Materials. *Chem. Rev.* **98**, 307–326 (1998).
35. Fedotov, M. A. & Maksimovskaya, R. I. NMR Structural Aspects of the Chemistry of V, Mo, W Polyoxometalates. *J. Struct. Chem.* **47**, 952–978 (2006).
36. Miras, H. N., Wilson, E. F. & Cronin, L. Unravelling the Complexities of Inorganic and Supramolecular Self-Assembly in Solution with Electrospray and Cryospray Mass Spectrometry. *Chem. Commun.* **11**, 1297–1311 (2009).
37. Nyman, M. Small-angle X-ray Scattering to Determine Solution Speciation of Metal-oxo Clusters. *Coord. Chem. Rev.* **352**, 461–472 (2017).
38. Pettersson, L. Equilibria of Polyoxometalates in Aqueous Solution. *Mol. Eng.* **3**, 29–42 (1993).
39. Dumoulin, C. L. & Levy, G. C. Spectroscopic Data Processing. NMRI Software and Its Applications in Chemistry and Biophysics. *J. Mol. Struct.* **113**, 299–310 (1984).
40. Gumerova, N. I. & Rompel, A. Polyoxometalates in Solution: Speciation Under Spotlight. *Chem. Soc. Rev.* **49**, 7568–7601 (2020).
41. McGarvey, G. B. & Moffat, J. B. A Study of Solution Species Generated During the Formation of 12-heteropoly Oxometalate Catalysts. *J. Mol. Catal.* **69**, 137–155 (1991).
42. Murata, K. & Ikeda, S. A Mechanistic Investigation on the Formation of Molybdophosphate Complexes in Aqueous Solution by the Use of Laser Raman Spectroscopy. *Polyhedron* **6**, 1681–1685 (1987).
43. Falaise, C. *et al.* Probing Dynamic Library of Metal-Oxo Building Blocks with γ-Cyclodextrin. *J. Am. Chem. Soc.* **140**, 11198–11201 (2018).
44. Kunz, W., Henle, J. & Ninham, B. W. 'Zur Lehre von der Wirkung der Salze' (about the science of the effect of salts): Franz Hofmeister's historical papers. *Curr. Opin. Colloid Interface Sci.* **9**, 19–37 (2004).
45. Assaf, K. I. *et al.* Water Structure Recovery in Chaotropic Anion Recognition: High-Affinity Binding of Dodecaborate Clusters to γ-Cyclodextrin. *Angew. Chem. Int. Ed.* **54**, 6852–6856 (2015).
46. Wu, Y. *et al.* Complexation of Polyoxometalates with Cyclodextrins. *J. Am. Chem. Soc.* **137**, 4111–4118 (2015).
47. Assaf, K. I. & Nau, W. M. The Chaotropic Effect as an Assembly Motif in Chemistry. *Angew. Chem. Int. Ed.* **57**, 13968–13981 (2018).
48. Stuckart, M. & Monakhov, K. Y. Polyoxometalates as Components of Supramolecular Assemblies. *Chem. Sci.* **10**, 4364–4376 (2019).
49. Okun, N. M., Ritorto, M. D., Anderson, T. M., Apkarian, R. P. & Hill, C. L. Polyoxometalates on Cationic Silica Nanoparticles. Physicochemical Properties of an Electrostatically Bound Multi-Iron Catalyst. *Chem. Mater.* **16**, 2551–2558 (2004).
50. Todea, A. M. *et al.* Reduced Molybenum-Oxide-Based Core–Shell Hybrids: "Blue" Electrons are Delocalized on the Shell. *Chem. – Eur. J.* **17**, 6635–6642 (2011).
51. Anyushin, A. V., Kondinski, A. & Parac-Vogt, T. N. Hybrid Polyoxometalates as Post-Functionalization Platforms: From Fundamentals to Emerging Applications. *Chem. Soc. Rev.* **49**, 382–432 (2020).
52. Allain, C. *et al.* Synthesis, Electrochemical and Photophysical Properties of Covalently Linked Porphyrin–Polyoxometalates. *Dalton Trans.* **42**, 2745–2754 (2013).
53. Yue, L. *et al.* Flexible Single-Layer Ionic Organic–Inorganic Frameworks Towards Precise Nano-Size Separation. *Nat. Commun.* **7**, 10742 (2016).
54. Du, Z.-Y. *et al.* Polyoxometalate-induced 'cage-within-cage' Metal–Organic Frameworks with High Efficiency Towards $CO_2$ Photoreduction. *Sustain. Energy Fuels* **5**, 3876–3883 (2021).
55. Tandekar, K., Garai, S. & Supriya, S. A Reversible Redox Reaction in a Keggin Polyoxometalate Crystal Driven by Visible Light: A Programmable Solid-State Photochromic Switch. *Chem. – Eur. J.* **24**, 9747–9753 (2018).
56. McHugh, P. J., Stergiou, A. D. & Symes, M. D. Decoupled Electrochemical Water Splitting: From Fundamentals to Applications. *Adv. Energy Mater.* **10**, 2002453 (2020).
57. Lei, J. *et al.* Tuning Redox Active Polyoxometalates for Efficient Electron-Coupled Proton-Buffer-Mediated Water Splitting. *Chem. – Eur. J.* **25**, 11432–11436 (2019).
58. Li, N., Liu, J., Dong, B.-X. & Lan, Y.-Q. Polyoxometalate-Based Compounds for Photo- and Electrocatalytic Applications. *Angew. Chem. Int. Ed.* **59**, 20779–20793 (2020).
59. Nishiyama, Y., Nakagawa, Y. & Mizuno, N. High Turnover Numbers for the Catalytic Selective Epoxidation of Alkenes with 1 atm of Molecular Oxygen. *Angew. Chem. Int. Ed.* **40**, 3639–3641 (2001).
60. Geletii, Y. V. *et al.* An All-Inorganic, Stable, and Highly Active Tetraruthenium Homogeneous Catalyst for Water Oxidation. *Angew. Chem.* **120**, 3960–3963 (2008).
61. Sun, J. *et al.* A Green Alternative for the Direct Aerobic Iodination of Arenes Using Molecular Iodine and a POM@MOF Catalyst. *ACS Appl. Mater. Interfaces* **12**,1297-1311 (2022).
62. Massella, D. *et al.* Bio-Functional Textiles: Combining Pharmaceutical Nanocarriers with Fibrous Materials for Innovative Dermatological Therapies. *Pharmaceutics* **11**, 403 (2019).
63. Semeraro, P. *et al.* Interaction Between Industrial Textile Dyes and Cyclodextrins. *Dyes Pigments* **119**, 84–94 (2015).
64. Radu, C.-D., Parteni, O. & Ochiuz, L. Applications of Cyclodextrins in Medical Textiles — review. *J. Controlled Release* **224**, 146–157 (2016).

65. Liu, Y., Chen, Y., Gao, X., Fu, J. & Hu, L. Application of Cyclodextrin in Food Industry. *Crit. Rev. Food Sci. Nutr.* **62**, 2627–2640 (2022).
66. Astray, G., Gonzalez-Barreiro, C., Mejuto, J. C., Rial-Otero, R. & Simal-Gándara, J. A Review on the Use of Cyclodextrins in Foods. *Food Hydrocoll.* **23**, 1631–1640 (2009).
67. Chisvert, A., Tarazona, I. & Salvador, A. A reliable and Environmentally-Friendly Liquid-Chromatographic Method for Multi-Class Determination of Fat-Soluble UV Filters In Cosmetic Products. *Anal. Chim. Acta* **790**, 61–67 (2013).
68. Giovannelli, L., Milanesi, A., Ugazio, E., Fracchia, L. & Segale, L. Effect of Methyl–β–Cyclodextrin and Trehalose on the Freeze–Drying and Spray–Drying of Sericin for Cosmetic Purposes. *Pharmaceuticals* **14**, 262 (2021).
69. Xiao, Y., Ng, S.-C., Tan, T. T. Y. & Wang, Y. Recent Development of Cyclodextrin Chiral Stationary Phases and Their Applications in Chromatography. *J. Chromatogr. A* **1269**, 52–68 (2012).
70. Wang, R.-Q., Ong, T.-T. & Ng, S.-C. Synthesis of Cationic β-cyclodextrin Derivatives and Their Applications as Chiral Stationary Phases for High-performance Liquid Chromatography and Supercritical Fluid Chromatography. *J. Chromatogr. A* **1203**, 185–192 (2008).
71. Qiu, X., Sun, W., Wang, C., Yan, J. & Tong, S. Enantioseparation of Acetyltropic Acid by Countercurrent Chromatography with Sulfobutyl Ether-β-cyclodextrin as Chiral Selector. *J. Sep. Sci.* **43**, 681–688 (2020).
72. Zhang, Y. *et al.* Three-Dimensional Anionic Cyclodextrin-Based Covalent Organic Frameworks. *Angew. Chem. Int. Ed.* **56**, 16313–16317 (2017).
73. Tu, X. *et al.* Mxene/carbon Nanohorn/B-Cyclodextrin-Metal-Organic Frameworks as High-Performance Electrochemical Sensing Platform for Sensitive Detection of Carbendazim Pesticide. *J. Hazard. Mater.* **396**, 122776 (2020).
74. Zhao, Y., Huang, Y., Zhu, H., Zhu, Q. & Xia, Y. Three-in-One: Sensing, Self-Assembly, and Cascade Catalysis of Cyclodextrin Modified Gold Nanoparticles. *J. Am. Chem. Soc.* **138**, 16645–16654 (2016).
75. van de Manakker, F., Vermonden, T., van Nostrum, C. F. & Hennink, W. E. Cyclodextrin-Based Polymeric Materials: Synthesis, Properties, and Pharmaceutical/Biomedical Applications. *Biomacromolecules* **10**, 3157–3175 (2009).
76. Zhang, T., Zhang, H., Li, P., Ding, S. & Wang, X. Highly Permeable Composite Nanofiltration Membrane via γ-Cyclodextrin Modulation for Multiple Applications. *Sep. Purif. Technol.* **297**, 121541 (2022).
77. Machelart, A. *et al.* Intrinsic Antibacterial Activity of Nanoparticles Made of β-Cyclodextrins Potentiates Their Effect as Drug Nanocarriers against Tuberculosis. *ACS Nano* **13**, 3992–4007 (2019).
78. Wankar, J. *et al.* Recent Advances in Host–Guest Self-Assembled Cyclodextrin Carriers: Implications for Responsive Drug Delivery and Biomedical Engineering. *Adv. Funct. Mater.* **30**, 1909049 (2020).
79. Haley, R. M., Gottardi, R., Langer, R. & Mitchell, M. J. Cyclodextrins in drug delivery: applications in gene and combination therapy. *Drug Deliv. Transl. Res.* **10**, 661–677 (2020).
80. Wang, J. *et al.* Supramolecular Nanoplatforms via Cyclodextrin Host-guest Recognition for Synergistic Gene-Photodynamic Therapy. *Eur. Polym. J.* **118**, 222–230 (2019).
81. Saekhor, K., Udomsinprasert, W., Honsawek, S. & Tachaboonyakiat, W. Preparation of an Injectable Modified Chitosan-based Hydrogel Approaching for Bone Tissue Engineering. *Int. J. Biol. Macromol.* **123**, 167–173 (2019).
82. Lukášek, J. *et al.* Cyclodextrin-Polypyrrole Coatings of Scaffolds for Tissue Engineering. *Polymers* **11**, 459 (2019).
83. Topuz, F., Holtzl, T. & Szekely, G. Scavenging Organic Micropollutants from Water with Nanofibrous Hypercrosslinked Cyclodextrin Membranes Derived From Green Resources. *Chem. Eng. J.* **419**, 129443 (2021).
84. Berset, J. D., Kupper, T., Etter, R. & Tarradellas, J. Considerations About The Enantioselective Transformation of Polycyclic Musks in Wastewater, Treated Wastewater and Sewage Sludge and Analysis of Their Fate in a Sequencing Batch Reactor Plant. *Chemosphere* **57**, 987–996 (2004).
85. Shabtai, I. A. & Mishael, Y. G. Polycyclodextrin–Clay Composites: Regenerable Dual-Site Sorbents for Bisphenol A Removal from Treated Wastewater. *ACS Appl. Mater. Interfaces* **10**, 27088–27097 (2018).
86. Pinho, E., Grootveld, M., Soares, G. & Henriques, M. Cyclodextrins as Encapsulation Agents for Plant Bioactive Compounds. *Carbohydr. Polym.* **101**, 121–135 (2014).
87. Schneider, H.-J., Hacket, F., Rüdiger, V. & Ikeda, H. NMR Studies of Cyclodextrins and Cyclodextrin Complexes. *Chem. Rev.* **98**, 1755–1786 (1998).
88. Szejtli, J. Introduction and General Overview of Cyclodextrin Chemistry. *Chem. Rev.* **98**, 1743–1754 (1998).
89. Harata, K. Crystal Structure of γ-cyclodextrin at Room Temperature. *Chem. Lett.* **13**, 641–644 (1984).
90. Saenger, W. Cyclodextrin Inclusion Compounds in Research and Industry. *Angew. Chem. Int. Ed. Engl.* **19**, 344–362 (1980).
91. Villiers, A. Sur la fermentation de la fécule par l'action du ferment butyrique. *Compt Rend Acad Sci* **112**, 536–538 (1891).
92. Loftsson, T. & Duchêne, D. Cyclodextrins and their Pharmaceutical Applications. *Int. J. Pharm.* **329**, 1–11 (2007).
93. Crini, G. Twenty years of Dextrin Research: a Tribute to Professor Hans Pringsheim (1876–1940). *J. Incl. Phenom. Macrocycl. Chem.* **98**, 11–27 (2020).
94. Schradinger, F. Uber thermophile Bakterien aus verschiedenen Speisen und Milch sowie uber einige Umsetzungsprodukte derselben in kohlenhydrathaltigen Nahrlosungen, darunter kristallisierte Polysaccharide Dextrin aus Starke. *Z Unters Nahr.-Genubmittel Gebrauchsgegenstande* **6**, 865 (1903).

95. French, D. The Schardinger Dextrins. *Advances in Carbohydrate Chemistry* **12**, 189–260 (, 1957).
96. Freudenberg, K. & Jacobi, R. Über Schardingers Dextrine aus Stärke. *Justus Liebigs Ann. Chem.* **518**, 102–108 (1935).
97. Freudenberg, K. & Cramer, F. Notizen: Die Konstitution der Schardinger-Dextrine α, β und γ. *Z. Für Naturforschung B* **3**, 464–466 (1948).
98. Freudenberg, K., Blomqvist, G., Ewald, L. & Soff, K. Hydrolyse und Acetolyse der Stärke und der Schardinger-Dextrine. *Berichte Dtsch. Chem. Ges. B Ser.* **69**, 1258–1266 (1936).
99. French, D. & Rundle, R. E. The Molecular Weights of the Schardinger Alpha and Beta Dextrins1. *J. Am. Chem. Soc.* **64**, 1651–1653 (1942).
100. Crini, G., French, A. D., Kainuma, K., Jane, J. & Szente, L. Contributions of Dexter French (1918–1981) to cycloamylose/cyclodextrin and starch science. *Carbohydr. Polym.* **257**, 117620 (2021).
101. French, Dexter., Levine, M. L., Pazur, J. H. & Norberg, Ethelda. Studies on the Schardinger Dextrins. The Preparation and Solubility Characteristics of Alpha, Beta and Gamma Dextrins. *J. Am. Chem. Soc.* **71**, 353–356 (1949).
102. French, Dexter. An Investigation of the Configuration of Starch and Its Crystalline Degradation Products. lowa State University (1942).
103. Freudenberg, K., Cramer, F. & Plieninger, H. Verfahren zur Herstellung von Einschlussverbindungen physiologisch wirksamer organischer Verbindungen. *Ger. Pat* **895**, 769 (1953).
104. Frank, D. W., Gray, J. E. & Weaver, R. N. Cyclodextrin Nephrosis in the Rat. *Am. J. Pathol.* **83**, 367–382 (1976).
105. Ikuta, D. *et al.* Conformationally Supple Glucose Monomers Enable Synthesis of The Smallest Cyclodextrins. *Science* **364**, 674–677 (2019).
106. Szejtli, J. Cyclodextrin Inclusion Complexes. *Cyclodextrin Technology* 79–185 (1988).
107. Némethy, G., Steinberg, I. Z. & Scheraga, H. A. Influence of Water Structure and of Hydrophobic Interactions on the Strength of Side-Chain Hydrogen Bonds in Proteins. *Biopolymers* **1**, 43–69 (1963).
108. Negi, J. S. & Singh, S. Spectroscopic Investigation on the Inclusion Complex Formation Between Amisulpride and γ-cyclodextrin. *Carbohydr. Polym.* **92**, 1835–1843 (2013).
109. Schneider, H. J., Blatter, T. & Simova, S. NMR and Fluorescence Studies of Cyclodextrin Complexes with Guest Molecules Containing Both Phenyl and Naphthyl Units. *J. Am. Chem. Soc.* **113**, 1996–2000 (1991).
110. Stepniak, A., Buczkowski, A., Zavodnik, L., Belica-Pacha, S. & Palecz, B. Study of the Interaction of β-Cyclodextrin with Albendazole in Aqueous Solutions. *J. Mol. Liq.* **248**, 19–23 (2017).
111. Parker, K. M. & Stalcup, A. M. Affinity Capillary Electrophoresis and Isothermal Titration Calorimetry for the Determination of Fatty Acid Binding with Beta-cyclodextrin. *J. Chromatogr. A* **1204**, 171–182 (2008).
112. Leclercq, L. *et al.* Versatile Eco-friendly Pickering Emulsions Based on Substrate/Native Cyclodextrin Complexes: A Winning Approach for Solvent-Free Oxidations. *ChemSusChem* **6**, 1533–1540 (2013).
113. Izzet, G. *et al.* Cyclodextrin-Induced Auto-Healing of Hybrid Polyoxometalates. *Angew. Chem. Int. Ed.* **51**, 487–490 (2012).
114. Ivanov, A. A. *et al.* Size-Exclusion Mechanism Driving Host–Guest Interactions between Octahedral Rhenium Clusters and Cyclodextrins. *Inorg. Chem.* **58**, 13184–13194 (2019).
115. Zhang, B., Guan, W., Zhang, S., Li, B. & Wu, L. Controlled Chiral Electrochromism of Polyoxometalates Incorporated in Supramolecular Complexes. *Chem. Commun.* **52**, 5308–5311 (2016).
116. Guan, W., Wang, G., Ding, J., Li, B. & Wu, L. A Supramolecular Approach of Modified Polyoxometalate Polymerization And Visualization of a Single Polymer Chain. *Chem. Commun.* **55**, 10788–10791 (2019).
117. Leclerc, N. *et al.* Supramolecular Association between gamma-Cyclodextrin and Preyssler-Type Polyoxotungstate. *Molecules* **26**, (2021).
118. Falaise, C. *et al.* 'Host in Host' Supramolecular Core-Shell Type Systems Based on Giant Ring-Shaped Polyoxometalates. *Angew. Chem. Int. Ed. Engl.* **60**, 14146–14153 (2021).
119. Ivanov, A. A. *et al.* Cyclodextrin-Assisted Hierarchical Aggregation of Dawson-type Polyoxometalate in the Presence of {Re6Se8} Based Clusters. *Inorg. Chem.* **59**, 11396–11406 (2020).
120. Deng, Z., Guo, Y., Zhao, X., Ma, P. X. & Guo, B. Multifunctional Stimuli-Responsive Hydrogels with Self-Healing, High Conductivity, and Rapid Recovery through Host–Guest Interactions. *Chem. Mater.* **30**, 1729–1742 (2018).
121. Davis, M. E. & Brewster, M. E. Cyclodextrin-based Pharmaceutics: Past, Present and Future. *Nat. Rev. Drug Discov.* **3**, 1023–1035 (2004).
122. Siemoneit, U. *et al.* Acrylic/cyclodextrin Hydrogels with Enhanced Drug Loading and Sustained Release Capability. *Int. J. Pharm.* **312**, 66–74 (2006).
123. Hsiung, E., Celebioglu, A., Emin Kilic, M., Durgun, E. & Uyar, T. Ondansetron/Cyclodextrin inclusion Complex Nanofibrous Webs for Potential Orally Fast-disintegrating Antiemetic Drug Delivery. *Int. J. Pharm.* **623**, 121921 (2022).
124. Huang, T. *et al.* Cyclodextrin Polymer Networks Decorated with Subnanometer Metal Nanoparticles for High-Performance Low-Temperature Catalysis. *Sci. Adv.* **5**, eaax6976 (2019).
125. Ni, L. *et al.* Self-Assembled Supramolecular Polyoxometalate Hybrid Architecture as a Multifunctional Oxidation Catalyst. *ACS Appl. Mater. Interfaces* **11**, 38708–38718 (2019).
126. Alsbaiee, A. *et al.* Rapid Removal of Organic Micropollutants From Water by a Porous Beta-Cyclodextrin Polymer. *Nature* **529**, 190–4 (2016).

# Chapter 2 Primary interactions between cyclodextrin and Keggin-type polyoxometalates. Synthesis, Characterizations, and Applications

## 2.1 Introduction

Smart materials change their properties according to external stimuli (temperature, pressure, pH, light, etc.) and respond in a controllable and reversible manner.[1,2] Designing smart materials using supramolecular approaches is an efficient strategy to accumulate and associate synergistic functions in highly flexible and tunable soft matrices. In the subfield of supramolecular chemistry driven by non-covalent bonds (molecular self-assembly, molecular recognition, mechanically interlocking molecular structures, etc.), supramolecular materials based on host-guest interactions and supramolecular polymer materials are currently widely studied.[3] Supramolecular host-guest recognition exhibits exciting properties such as synergistic redox, catalytic, and magnetic properties.[4,5] Among this class of materials, CD-containing supramolecular hydrogels have shown great potential applications in self-healing materials, artificial muscles, drug delivery, etc.[6]

Due to the particularity of the outer hydrophilic and inner hydrophobic cavities, CDs have been widely used in nanomaterials, pharmacy, adsorption, and other fields.[3,7–11] Historically, CD is known for its affinity for hydrophobic organic molecules, and much less for hydrophilic inorganic species. It is only recently that CDs are known to exhibit interesting properties as host molecules for a wide variety of inorganic species, including POMs.[12] The host–guest assembly of the toroidal CDs and spherical POM clusters has attracted much attention and is a fast-growing topic. In 2015, Stoddart and co-workers published the first examples of host–guest complexes between β- and γ-CD and phosphomolybdate $[PMo_{12}O_{40}]^{3-}$.[13] Since then, several hybrid (organic/inorganic) adducts or materials have also been reported with various archetypal polyoxotungstates, including the Lindqvist-type $[W_6O_{19}]^{2-}$,[14,15] the Keggin-type ions $[PW_{12}O_{40}]^{3-}$ and $[SiW_{12}O_{40}]^{4-}$,[16–20] and the Dawson-type $[P_2W_{18}O_{62}]^{6-}$.[21,22] Some of these hybrid CD/POM materials are promising for application in catalysis[18,20] and energy storage,[23] where surface effects and hybrid structures would play a crucial role. However, there is a lack of fundamental

knowledge about the host-guest recognition process in these systems. Therefore, detailed characterization of the interactions between CDs and POMs and a better understanding of the phenomena occurring at their interfaces are essential for further innovative development of redox-responsive systems and related applications.

In this context, we will track the primary interactions between cyclodextrin and Keggin-type polyoxometalates. To this end, the formation of host-guest inclusion complexes between γ-CD and Keggin-type POM anions will be systematically investigated by varying the anionic charge from 3- to 6- while keeping constant the shape and size of both host and guest. This can be achieved in two different ways, either by changing the nature of the heteroelement X along the $[XW_{12}O_{40}]^{n-}$ series, where X = P, Si, B, or $H_2$ (**section 2.3**), or by modifying the redox state of the POM $[XW_{11}MO_{40}]^{n-}$ using molybdenum and vanadium (M = Mo or V) monosubstituted anions (**section 2.4**). Figure 2.1 shows the structure of such Keggin POMs studied in this chapter. We will demonstrate that such POM-CD complexation is essentially driven by the chaotropic effect offering the possibility of fine-tune the strength of the host−guest association, and thus opening a new avenue for the design of smart materials through redox stimuli. In the last **section 2.5**, we will study the hydrolytic stabilization of POM $[PM_{12}O_{40}]^{3-}$ (M = $W^{VI}$ or $Mo^{VI}$) induced by CD.

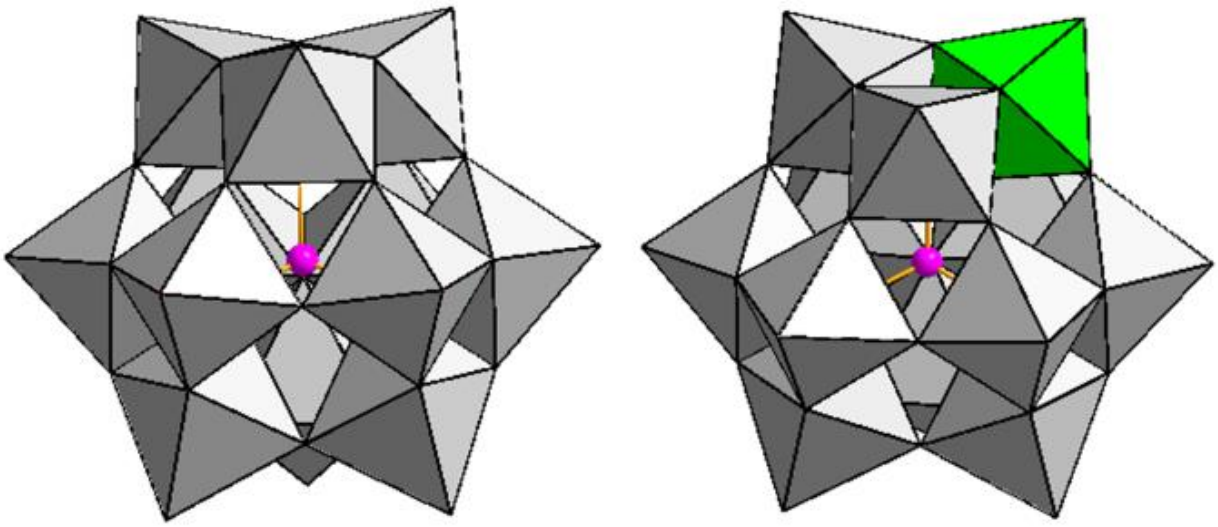

**Figure 2.1** *Polyhedral representation of Keggin-type POM $[XM_{12}O_{40}]^{n-}$ (left) and mixed-metal-Keggin POM $[XW_{11}MO_{40}]^{y-}$(right) studied in this chapter. The magenta sphere represents the heteroatom X = P, Si, B, or $H_2$, the grey polyhedron, $Mo^{VI}$ or $W^{VI}$, the green polyhedron: metal addenda M = $Mo^{VI/V}$ or $V^{V/IV}$.*

## 2.2 Experimental Part

### 2.2.1 Synthesis

All reagents were purchased from commercial sources and used without further purification. Solutions were prepared in Milli-Q water. We synthesized the classical POMs, $Na_3[PW_{12}O_{40}]\cdot 14H_2O$, $H_3[PW_{12}O_{40}]\cdot 9H_2O$, $H_3[PMo_{12}O_{40}]\cdot 29H_2O$, $Na_4[SiW_{12}O_{40}]\cdot 12H_2O$, $H_4[SiW_{12}O_{40}]\cdot 17H_2O$, $K_5[BW_{12}O_{40}]\cdot 12H_2O$, $H_5[BW_{12}O_{40}]\cdot 9H_2O$, and $Rb_{4.5}Na_{1.5}[H_2W_{12}O_{40}]\cdot 11H_2O$ according to the reported procedures.[24–27] $K_7[PW_{11}O_{39}]\cdot 12H_2O$, $K_8[SiW_{11}O_{39}]\cdot 14H_2O$, $Na_1K_3[PW_{11}V^{V}O_{40}]\bullet 7H_2O$, $K_5[PW_{11}V^{IV}O_{40}]\bullet 14H_2O$, $K_4[SiW_{11}Mo^{VI}O_{40}]\bullet 5H_2O$, $K_5[SiW_{11}Mo^{V}O_{40}]\bullet 12H_2O$, $K_5[SiW_{11}V^{V}O_{40}]\bullet 7H_2O$, and $Rb_5K_1[SiW_{11}V^{IV}O_{40}]\bullet 7H_2O$ were synthesized and purified according to published procedures.[28–34] Here are the details of the experimental protocols.

**$Na_3[PW_{12}O_{40}]\cdot 14H_2O$.** $Na_2WO_4\bullet 2H_2O$ (50 g, 151 mmol) is dissolved in 50 mL $H_2O$ with magnetic stirring at room temperature (RT). Then 38.5 mL hydrogen chloride (HCl, 37 wt%) and 4.8 mL phosphoric acid ($H_3PO_4$, 85 wt%) are added dropwise. The solution is kept boiling for 1 h. After cooling to room temperature, the solution is filtered (crude product: 37.63 g). The solid obtained is dissolved in 30 mL 1 M HCl and 30 mL $H_2O$, and allowed to crystalize in air to obtain $Na_3PW_{12}O_{40}\bullet 14H_2O$. (Yield: 17.0 g, 5.3 mmol, 42 %). EDX, obs. W/P: 12/1.1. TGA showed a weight loss of 8.2 % in the 30-600 °C temperature range, corresponding to 14 hydration water molecules (calculated 7.9 %). $^{31}P$ and $^{183}W$ NMR (100 mM in $D_2O$), $\delta_{31P}$ -14.5 ppm, $\delta_{183W}$ -97.4 ppm, $^{2}J_{W\text{-}P}$ 1.1 Hz. FT-IR (Diamond ATR, ATR correction applied) $\nu$ ($cm^{-1}$) 1075 (P-$O_a$), 977 (W=$O_t$), 906 (W-$O_b$-W), 800 (W-$O_c$-W).

**$H_3[PW_{12}O_{40}]\cdot 9H_2O$**. $Na_2WO_4\bullet 2H_2O$ (20 g, 60 mmol) is dissolved in 30 mL $H_2O$ with magnetic stirring at room temperature. Then 30 mL ether and 10 mL HCl (37 wt%) have been added for extraction by using a separatory funnel. The mixture provided 3 phases. The lowest layer was collected and evaporated with a rotary evaporator to remove ether. Then, the crude product is dissolved in 10 mL $H_2O$ with stirring to obtain a clear solution and left to crystalize (Yield: 15.0 g, 4.8 mmol, 96 %). EDX, obs. W/P: 12/1.4. TGA showed a weight loss of 5.3 % in the 30-600 °C temperature range, corresponding to 9 hydration water molecules (calculated 5.3 %). $^{31}P$ and

$^{183}$W NMR (90 mM in $D_2O$), $\delta_{31P}$ -14.3 ppm, $\delta_{183W}$ -97.4 ppm, $^2J_{W-P}$ 1.1 Hz. FT-IR (Diamond ATR, ATR correction applied) $\nu$ ($cm^{-1}$) 1074 (P-$O_a$), 974 (W=$O_t$), 899 (W-$O_b$-W), 779 (W-$O_c$-W).

**$H_3[PMo_{12}O_{40}]\cdot 29H_2O$.** $Na_2MoO_4\bullet 2H_2O$ (14.52 g, 60 mmol) is dissolved in mixed-solution 21 mL $H_2O$ and 0.34 mL $H_3PO_4$ (85 wt%) with magnetic stirring at room temperature. Then 14.2 mL $HClO_4$ (65 wt%) was added dropwise. The precipitate appears when the reaction is almost complete. The crude product was obtained by filtration (7.5 g), which is then dissolved in 19 mL $H_2O$ and added to 4.75 mL concentrated HCl and 24 mL ether for the exaction. Finally, the lowest layer was collected and evaporated with a rotary evaporator to remove ether. The resulting solution was again dissolved in $H_2O$ and allowed to crystalize. (Yield: 7.5 g, 3.2 mmol, 64%) EDX, obs. Mo/P: 12/1.1. TGA showed a weight loss of 22 % in the 30-600 °C temperature range, corresponding to 29 hydration water molecules (calculated 22 %). $^{31}$P NMR (80 mM in 50:50 $D_2O$:1,4-dioxane + HCl), $\delta_{31P}$ -2.9 ppm. FT-IR (Diamond ATR, ATR correction applied) $\nu$ ($cm^{-1}$) 1076 (P-$O_a$), 958 (Mo=$O_t$), 875 (Mo-$O_b$-Mo), 784 (Mo-$O_c$-Mo).

**$Na_4[SiW_{12}O_{40}]\cdot 12H_2O$.** $Na_2WO_4.2H_2O$ (45.5 g, 138 mmol) was dissolved in 75 mL $H_2O$, then the solution is heated to boiling. The boiling solution was acidified by adding 41.25 mL 4 M HCl dropwise. Then, an aqueous solution of sodium metasilicate ($Na_2SiO_3.5H_2O$, 2.75 g; 13 mmol, in 25 mL $H_2O$) was added under stirring. Finally, the resulting solution was acidified by adding 12.5 mL 4 M HCl to quickly adjust the pH to 5- 6. The solution was kept boiling for 1.5 h. After cooling to room temperature, 90 mL solution is collected. Then 16.0 g NaCl is added and the solution is allowed to crystalize in air. The crystals obtained are left to dry in air (Yield: 35.33 g, 11 mmol, 95%). TGA showed a weight loss of 6.8 % in the 30-600 °C temperature range corresponding to 12 hydration water molecules (calculated 6.8 %). $^{29}$Si and $^{183}$W NMR (100 mM in $D_2O$), $\delta_{29Si}$ -84.78 ppm, $\delta_{183W}$ -103.8 ppm. FT-IR (Diamond ATR, ATR correction applied) $\nu$ ($cm^{-1}$) 1017 (Si-$O_a$), 980 (W=$O_t$), 926 (W-$O_b$-W), 789 (W-$O_c$-W).

**$H_4[SiW_{12}O_{40}]\cdot 17H_2O$.** $Na_2WO_4.2H_2O$ (45.5 g, 137.9 mmol) was dissolved in 75 mL $H_2O$, then the solution is heated to boiling. The hot solution was acidified by adding 41.25 mL 4 M HCl dropwise. Then, an aqueous solution of sodium metasilicate

($Na_2SiO_3.5H_2O$, 2.75 g; 13 mmol, in 25 mL $H_2O$) was added under stirring. Finally, the resulting solution was acidified by adding 12.5 mL 4 M HCl to quickly adjust the pH to 5- 6. The solution was kept boiling for 1.5 h. After cooling to room temperature, 90 mL of the solution is collected and transferred to a 500 mL extraction funnel, to which 90 mL of ether and 30 mL of HCl (37 wt%) are added. The mixture provided 3 distinct phases after vigorous shaking. The 3rd layer (the organic phase) is collected and the solvent ether evaporated. The solution is diluted with 10 mL $H_2O$ under stirring to produce a clear solution. The crystals were obtained by slow evaporation (Yield: 14 g, 4.5 mmol, 39 %). TGA showed a weight loss of 9.7 % in the 30-600 °C temperature range corresponding to 17 hydration water molecules (calculated 9.6 %). $^{29}Si$ and $^{183}W$ NMR (100 mM in $D_2O$), $\delta_{29Si}$ -85.09 ppm, $\delta_{183W}$ -103.8 ppm. FT-IR (Diamond ATR, ATR correction applied) $\nu$ ($cm^{-1}$) 1017 (Si-$O_a$), 979 (W=$O_t$), 919 (W-$O_b$-W), 780 (W-$O_c$-W).

**$K_5[BW_{12}O_{40}]\cdot 12H_2O$.** $Na_2WO_4\bullet 2H_2O$ (50 g, 151 mmol) is dissolved in 50 mL $H_2O$ with magnetic stirring at room temperature. 2.5 g of boric acid ($H_3BO_3$, 40 mmol) was first added, followed by 30 mL of aqueous 6 M HCl. The solution (pH ~6) was transferred to a 250 mL flask and allowed to boil for 24 h (water was added from time to time). After cooling to room temperature, the insoluble solid, i.e., paratungstate ($Na_{10}W_{12}O_{41}\bullet xH_2O$), was filtered off. Then, the 88 mL filtrate was acidified by aqueous 6 M HCl to pH ~2 and allowed to boil for 30 min. A precipitation is observed after adding 10 g of solid KCl. After filtration and washing with ethanol, 28.3 g of crude product was obtained. Then the crude product is dissolved in 40 mL $H_2O$ at ca. 70 °C with continuous stirring, the pH is adjusted to 6 with 6 M HCl in the meantime. The clear solution was left to crystalize in the air (Yield: 13.6 g, 4.4 mmol, 35 %). TGA showed a weight loss of 5.7 % in the 30-600 °C temperature range, corresponding to 9 hydration water molecules (calculated 6.6 %). FT-IR (Diamond ATR, ATR correction applied) $\nu$ ($cm^{-1}$) 1001 (B-$O_a$), 956 (W=$O_t$), 903 (W-$O_b$-W), 798 (W-$O_c$-W).

**$H_5[BW_{12}O_{40}]\cdot 9H_2O$**. $K_5BW_{12}O_{40}$ (9 g, 2.7 mmol) is dissolved in 20 mL $H_2O$, which used for K/H cationic exchange by Dower@(R)50 WX2 Hydrogen form. After filtration and washing the resin with plenty of water and 6 M HCl, the filtrate is collected (125 mL). The solution was freeze-dried for 24 h to obtain a white powder

(Yield: 6.8 g, 2.3 mmol, 85 %). TGA showed a weight loss of 5.7 % in the 30-600 °C temperature range, corresponding to 9 hydration water molecules (calculated 5.4 %). $^{11}B$ and $^{183}W$ NMR (100 mM in $D_2O$), $\delta_{11B}$ -2.17 ppm, $\delta_{183W}$ -130.2 ppm. FT-IR (Diamond ATR, ATR correction applied) $\nu$ ($cm^{-1}$) 1002 (B-$O_a$), 959 (W=$O_t$), 899 (W-$O_b$-W), 805 (W-$O_c$-W).

**$Rb_{4.5}Na_{1.5}[H_2W_{12}O_{40}]\cdot 11H_2O$.** An aqueous solution of sodium tungstate ($Na_2WO_4\bullet 2H_2O$, 20.0 g, 138 mmol, 60 mL $H_2O$) was boiled for 24 h after adjusting the pH to ca. 3 with 6 M HCl (15-20 mL). After cooling to RT, the mixture was filtrated to obtain 88 mL of clear solution. RbCl (10.89 g) was added to obtain a precipitate, isolated by filtration and air-dried (Yield: 7.74 g, 2.3 mmol, 20 %). IR ($cm^{-1}$): 956 (sh), 935 (s), 896 (s), 878 (s), 766 (vs), $^{183}W$ NMR: −117.6 ppm; $^{1}H$ NMR: 5.99 ppm. ICP-OES Anal. Calcd for $H_{24}Na_{1.5}O_{51}Rb_{4.5}W_{12}$: Na, 1.00; Rb, 11.10; W, 63.66. Found: Na, 0.9; Rb, 10.5; W, 58.0. TGA showed a weight loss of 5.5 % in the 20-220 °C temperature range corresponding to the eleven hydration water molecules (calculated 5.7 %).

**$K_7[PW_{11}O_{39}]\cdot 12H_2O$.** $Na_2WO_4\bullet 2H_2O$ (33 g, 100 mmol) is dissolved in 60 mL $H_2O$ with magnetic stirring at room temperature. Then 10 mL $H_3PO_4$ (1M) and 17.6 mL acetic acid (90 %) are added with vigorous stirring. The solution is boiled for 1 h and then cooled in a water bath at room temperature. A white precipitation is obtained after addition of KCl (12.0 g, 161 mmol) to the solution. The crude product obtained after filtration is washed with ethanol and ether (Yield: 23.5 g, 7.3 mmol, 80 %). $^{31}P$ NMR: -10.76 ppm, $^{183}W$ NMR, $\delta$ (ppm)/ $^{2}J_{W\text{-}P}$ (Hz): -96.9/1.1 (2W), -102.0/1.7 (2W), -110.2/2.1 (2W), -116.6/1.8 (1W), -131.6/1.3 (2W), -152.9/1.3 (2W). FT-IR ($cm^{-1}$): 1084–1037 (P–O), 949 (W O), 899–727 (W–O–W).

**$K_5[PW_{11}V^{IV}O_{40}]\cdot 14H_2O$**. First, a solution A is prepared by dissolving 30 g (9.92 mmol) $\alpha$-$K_7PW_{11}O_{39}$ in 390 mL $H_2O$. A second solution B is obtained by dissolving 2.51 g $VOSO_4$ in 30 mL $H_2O$. Solution B was added to solution A and heated 15-30 min at 60-80 °C. After cooling to room temperature, 105 g KCl was added to the solution which resulted of a precipitate. The product was obtained after filtration and washing with ethanol and ether (Yield: 20.3 g, 6.3 mmol, 64 %). EDX: calc. W/V/P/K: 11/1/1/5; obs. W/V/P/K: 11/1.1/1.5/5.4. $^{31}P$ NMR, $\delta$ (ppm)/ $\Delta\nu_{1/2}$ (Hz): -4.1/1200. $^{183}W$ NMR, $\delta$

(ppm)/ $\Delta\nu_{1/2}$ (Hz): -141.2/190, -169/200. FT-IR ($cm^{-1}$): 1088 (m), 1062 (m), 963 (s), 886 (m), 797 (s).

**$Na_1K_3[PW_{11}V^{V}O_{40}]\cdot 7H_2O$**. α-$K_5PW_{11}V^{IV}O_{40}$ was oxidated by electrochemistry, scan rate 100 mV/s. α-$K_5PW_{11}V^{IV}O_{40}$ (8 g, 2.5 mmol) was dissolved in 70 mL buffer solution 50:50 v:v 0.1 M HCl:0.9 M NaCl. To fully reduce the compound a potential of 1 V was imposed for 1 h (until the full color change from blue-violet to yellow). The addition of 7.5 g NaCl and 1.43 g KCl after electroreduction provoked a yellow precipitate. The product was filtered off and dried with ethanol and ether (Yield: 4.3 g, 1.3 mmol, 52 %). EDX: calc. W/V/P/K/Na: 11/1/1/3/1; obs. W/V/P/K/Na: 11/1.2/1.3/3.1/0.5. $^{31}$P NMR, $\delta$ (ppm)/ $\Delta\nu_{1/2}$ (Hz): -13.8/1. $^{51}$V NMR, $\delta$ (ppm)/ $\Delta\nu_{1/2}$ (Hz): -555.5/30. $^{183}$W NMR, $\delta$ (ppm)/ $\Delta\nu_{1/2}$ (Hz): -72.2/70, -98.5/1, -101.1/1, -103.5/1, -108.5/1, -108.6/50. FT-IR ($cm^{-1}$): 1099 (m), 1076 (m), 982 (s), 881 (m), 784 (s).

**$K_8[SiW_{11}O_{39}]\cdot 14H_2O$.** Sodium metasilicate ($Na_2SiO_3$, 11 g, 50 mmol) is dissolved with magnetic stirring at room temperature in 100 mL of distilled water to produce solution A (if the solution is not completely clear, it is filtered). In a 1-L beaker, containing a magnetic stirring bar, sodium tungstate ($Na_2WO_4 \bullet 2\ H_2O$, 182 g, 550 mol) is dissolved in 300 mL of boiling distilled water (solution B). To the boiling solution B, a solution of 4 M HCl (165 mL) is added dropwise in ~30 min, with vigorous stirring to dissolve the local precipitate of tungstic acid. Solution A is then added and, quickly, 50 mL of 4 M HCl is also added. The pH is about 5 to 6. The solution is kept boiling for 1 h. After cooling to room temperature, the solution is filtered if it is not completely clear. Potassium chloride (KCl,150 g) is added to the solution, which is stirred magnetically. The white solid product is washed with plenty of ethanol (2 or 3 times to remove residual mother solution), and finally dried in air (Yield: 140 g, 43.2 mmol, 94 %). FT-IR ($cm^{-1}$): at 995 (w), 958 (m), 889 (vs), 870 (sh), 796 (m), 725 (m).

**$K_4[SiW_{11}Mo^{VI}O_{40}]\cdot 5H_2O$**. $Na_2MoO_4.2H_2O$ (12.0 g, 50 mmol) was dissolved in 50 mL $H_2O$, followed by the dropwise addition of 35.0 mL 12 M $HNO_3$ (420 mmol). α-$K_8SiW_{11}O_{39}$ (50.0 g, 16.5 mmol) was added and stirred overnight. The precipitate obtained was washed with ethanol and ether, then redissolved in 5 mL hot $H_2O$ to recrystallize in the refrigerator at 5 °C (Yield: 10 g, 3.3 mmol, 73 %). EDX: calc. W/Mo/Si/K: 11/1/1/4; obs. W/Mo/Si/K: 11/1.1/1.0/3.8. $^{29}$Si NMR, $\delta$ (ppm)/ $\Delta\nu_{1/2}$ (Hz): -

84.1/0.4. $^{183}$W NMR, $\delta$ (ppm)/ $\Delta\nu_{1/2}$ (Hz): -100.8/1, -101.1/1, -103.2/1, -104.1/1, -104.3/1, -108.3/1. $^{95}$Mo NMR, $\delta$ (ppm)/ $\Delta\nu_{1/2}$ (Hz): 13.2/1100. FT-IR (cm$^{-1}$): 1016 (w), 973 (s), 920 (s), 877 (sh), 773 (s).

**$K_5[SiW_{11}Mo^{V}O_{40}]\cdot 12H_2O$**. α-$K_5SiW_{11}Mo^{VI}O_{40}$ was reduced by electrochemistry using a rotating carbon glassy electrode, scan rate 100 mV/s. α-$K_4SiW_{11}Mo^{VI}O_{40}$ (4 g, 1.3 mmol) was dissolved in 70 mL buffer solution 50:50 v:v 0.1 M HCl:0.9 M NaCl. To fully reduce the compound a potential of 0 V was imposed for 1 h, until the full color change from light-green to deep purple. The solution was filtered to remove eventual carbon particulates from electrodes, then 15.0 g KCl were added. The purple precipitate was filtered off and washed with ethanol and ether (Yield: 2 g, 0.6 mmol, 46 %). EDX: calc. W/Mo/Si/K: 11/1/1/5; obs. W/Mo/Si/K: 11/0.9/0.3/4.9. $^{29}$Si NMR, $\delta$ (ppm)/ $\Delta\nu_{1/2}$ (Hz): -80.0/60. $^{183}$W NMR, $\delta$ (ppm)/ $\Delta\nu_{1/2}$ (Hz): -155/80, -201/160. FT-IR (cm$^{-1}$): 1009 (w), 966 (s), 913 (s), 860 (w), 770 (s).

**$K_5[SiW_{11}V^{V}O_{40}]\cdot 7H_2O$.** To a solution of $NaVO_3$ (0.5 g in 10 mL $H_2O$), 4.5 mL 4 M HCl was added. The orange solution turned yellow, then diluted with 100 mL $H_2O$ and kept under stirring for 30 min after the addition α-$K_8SiW_{11}O_{39}$ (12 g, 3.7 mmol) and KCl (40.0 g, 536 mmol). The solution gradually became turbid. Finally, the product was obtained after filtration and dried with ethanol and ether (Yield: 10.5 g, 3.2 mmol, 86 %). EDX : calc. W/V/Si/K : 11/1/1/5 ; obs. W/V/Si/K : 11/0.9/1.0/4.9. $^{29}$Si NMR, $\delta$ (ppm)/ $\Delta\nu_{1/2}$ (Hz) : -84.5/0.5. $^{51}$V NMR, $\delta$ (ppm)/ $\Delta\nu_{1/2}$ (Hz) : -549.1/40. $^{183}$W NMR, $\delta$ (ppm)/ $\Delta\nu_{1/2}$ (Hz) : -78.4/70, -102.1/1, -112.1/1, -112.6/1, -118.7/1, -124.8/160. FT-IR (cm$^{-1}$): 1013 (w), 965 (s), 920 (vs), 880 (sh), 773 (s).

**$Rb_5K_1[SiW_{11}V^{IV}O_{40}]\cdot 7H_2O$.** Two solutions were prepared at first. Solution A was obtained by dissolving 10.0 g of α-$K_8SiW_{11}O_{39}$ (3.09 mmol) in 50 mL $H_2O$. Solution B was prepared by dissolving 0.78 g $VOSO_4\bullet 5H_2O$ (3.09 mmol) in 5 mL of hot water. Solution B was added to solution A and kept under heating 15 min until the solution turned purple. Finally, 10.0 g KCl and 0.5 g RbCl were added to the solution, and left to stir for 30 min in an ice bath. The product was obtained after filtration of the precipitate and drying with ethanol and ether (Yield: 5.4 g, 1.7 mmol, 55 %). EDX: calc. W/V/Si/Rb/K: 11/1/1/5/1; obs. W/V/Si/Rb/K: 11/0.9/1.0/5.3/0.7. $^{29}$Si NMR, $\delta$ (ppm)/ $\Delta\nu_{1/2}$ (Hz): -76.1/230. FT-IR (cm$^{-1}$): 1007 (w), 955 (s), 912 (vs), 798 (w), 698 (s).

**$CsK_2H_2\{[BW_{12}O_{40}]\cdot 2(C_{48}H_{80}O_{40})\}\cdot 29H_2O$ ($BW_{12}$·2CD).** A mixture of $K_{4.3}Na_{0.7}[BW_{12}O_{40}]\cdot 17H_2O$ (68 mg, 0.02 mmol) and γ-CD (85 mg, 0.06 mmol) in 3.5 mL of aqueous solution of CsCl (0.05 mol $L^{-1}$) and KCl (0.1 mol $L^{-1}$) was stirred until a clear solution was obtained. The solution was then allowed to stand for crystallization in air. Colorless crystals of $BW_{12}$·2CD were obtained by slow ethanol vapor diffusion into water solution (10 mL vessel containing 2 mL of water solution was placed into a 250 mL vessel with a tight-fitting lid containing 50 mL of ethanol) after 3 days, and were collected, washed with a water/ethanol mixture and dried in air. Yield 37 mg, 30 %. ICP-OES Anal. Calcd for $BC_{1.5}CsH_{220}K_2O_{149}W_{12}$: B, 0.17; C, 18.64; K, 1.26; W, 35.66. Found: B, 0.2; C, 18.5; K, 1.2; W, 32.5. EDX showed Cs:K:W ratio = 1.7:2.1:12. TGA showed a weight loss of 8.4 % in the 20–220 °C temperature range corresponding to the twenty-nine hydration water molecules (calculated 8.4 %) and a weight loss of 42 % in the 220–700 °C range assigned to the loss of 2 CDs (calculated 41.1 %).

**$Na_3\{[PW_{12}O_{40}]\cdot(C_{48}H_{80}O_{40})\}\cdot 10H_2O$ ($PW_{12}$@CD).** $Na_{1.4}H_{1.6}[PW_{12}O_{40}]\cdot 12H_2O$ (0.3 g, 0.096 mmol) was dissolved in 10 mL aqueous solution of NaCl (0.2 mol $L^{-1}$) and γ-CD (0.138 g, 0.096 mmol) was added. The clear solution was stirred for 15 min. The solution was then allowed to stand for crystallization in air. Needle-like colorless crystals of $PW_{12}$@CD suitable for single crystal X-ray diffraction appeared within 5 days. They were isolated by filtration and washed with cold water. Yield 0.35 g, 76 %. ICP-OES Anal. Calcd for $C_{48}H_{100}Na_3O_{90}PW_{12}$: C, 13.03; Na, 1.56; P, 0.70; W, 49.87. Found: C, 12.8; Na, 1.6; P, 0.7; W, 48.9. EDX showed Na:P:W ratio = 2.7:1.1:12. TGA showed a weight loss of 3.9 % in the 20–220 °C temperature range corresponding to the ten hydration water molecules (calculated 4.1 %) and a weight loss of 26.8 % in the 220–700 °C range assigned to the loss of 1.3 CDs (calculated 27 %).

### 2.2.2 Characterization Methods

**Single-Crystal X-ray diffraction analysis (XRD).** Intensity data collections were carried out at T = 200(2) K with a Bruker D8 VENTURE diffractometer equipped with a PHOTON 100 CMOS bidimensional detector using a high brilliance IμS microfocus X-ray Mo Kα monochromatized radiation (λ = 0.71073 Å). Crystals were glued in

paratone oil to prevent any loss of crystallization water. Data reduction was accomplished using SAINT V7.53a. The substantial redundancy in data allowed a semi-empirical absorption correction (SADABS V2.10) to be applied, on the basis of multiple measurements of equivalent reflections.

**Fourier Transform Infrared (FT-IR).** Fourier transform infrared (FT-IR) spectra were recorded on a 6700 FT-IR Nicolet spectrophotometer, using the diamond ATR technique. The spectra were recorded on non-diluted compounds and ATR correction was applied.

**Elemental analyses (ICP).** Quantitative analyses of C, H, and metal contents were carried out by ICP analysis performed in CREALINS laboratory in Vernaison, France.

**Energy-dispersive X-ray spectroscopy (EDX).** Energy-dispersive X-ray spectroscopy (EDX) measurements were performed using a SEM-FEG (scanning electron microscope enhanced by a field emission gun) equipment (JSM 7001-F, Jeol). The measures were acquired with a SDD XMax 50 $mm^2$ detector and the Aztec (Oxford) system working at 15 kV and 10 mm working distance. The quantification is realized with the standard library provided by the constructor using Lα lines.

**Thermal gravimetric analysis (TGA).** Thermal gravimetric analysis (TGA) measurements were performed to determine water contents, using a Mettler Toledo TGA/DSC 1, STAR$^e$ System apparatus under oxygen flow (50 mL $min^{-1}$) at a heating rate of 5 °C $min^{-1}$ up to 700 °C.

**Isothermal Titration Calorimetry (ITC).** Formation constants and inclusion enthalpies were simultaneously determined for each γ-CD/POM system by the use of an isothermal calorimeter (ITC200, MicroCal Inc., USA). Degassed deionized water solutions were used in both cell ($V_0$ = 202.8 µL) and syringe (40 µL). After the addition of an initial aliquot of 2 µL, 10 aliquots of 3.5 µL of the syringe solution were delivered over 7 s for each injection. The time interval between two consecutive injections was 70 s, which proved to be sufficient for a systematic and complete return to the baseline. The agitation speed was set to 1000 rpm. The resulting heat flow was recorded as a function of time. ITC titrations were realized at three temperatures (288, 298 and 308 K), with 5 mM γ-CD solution in the syringe and 0.25 mM POM solution in the cell. Values and uncertainties of formation constants and

inclusion enthalpies were determined by global analysis of the binding isotherms, by means of a dedicated homemade program, implementing 1:1 and 1:1 + 1:2 binding polynomials.

**Electrochemistry.** Purified water was used throughout. It was obtained by passing water through a RiOs 8 unit followed by a Millipore-Q Academic purification set. All reagents were of high-purity grade and were used as purchased without further purification. Cyclic voltammetry (CV) experiments were carried out with an Methrohm Autolab PGSTAT12 potentiostat/galvanostat associated with a GPES electrochemical analysis system (EcoChemie). Measurements were performed at room temperature in a conventional single compartment cell. A glassy carbon (GC) electrode with a diameter of 3 mm was used as the working electrode. The auxiliary electrode was a Pt plate placed within a fritted-glass isolation chamber and potentials are quoted against a saturated calomel electrode (SCE). The solutions were deaerated thoroughly for at least 30 min with pure argon and kept under a positive pressure of this gas during the experiments.

**Nuclear Magnetic Resonance (NMR)**. All solution NMR spectra were measured in $D_2O$ at 21 °C. $^{1}H$, $^{29}Si$, $^{31}P$, $^{51}V$, and $^{95}Mo$ NMR spectra were recorded on a Bruker Avance 400 spectrometer at Larmor frequencies of 400.1, 162.0, 105.2, 79.5, and 26.1 MHz, respectively, using 5 mm standard NMR tubes. The $^{183}W$ NMR spectra were obtained with 10 mm NMR tubes and a Bruker Avance 500 spectrometer operating at a Larmor frequency of 20.8 MHz. The $^{1}H$ NMR spectra were recorded with one pulse sequence at 30° flip angle (pulse duration 2.7 µs), using 0.1 s recycle delay, 3 s acquisition time, and 8 number of scans. Chemical shifts are scaled with respect to standards ($\delta$ = 0 ppm): $Me_4Si$ (1% $CDCl_3$) for $^{1}H$ and $^{29}Si$, $H_3PO_4$ for $^{31}P$, $VOCl_3$ for $^{51}V$, $Na_2MoO_4$ ($D_2O$, 2 M) for $^{95}Mo$, and $Na_2WO_4$ ($D_2O$, 1 M) for $^{183}W$.

**Cloud points measurements.** Aqueous solutions containing 60 mM tetra-ethylene glycol mono-octyl ether ($C_8E_4$) and a given amount of POM were prepared in 1 mL glass vials. The vials were placed in a temperature-controlled water bath. The heating rate was constant at 1 K $min^{-1}$ and the CP was detected by visual inspection after the occurrence of turbidity. The choice of the counter-ion has negligible effects on the cloud point evolution.

### 2.2.3 Hydrolytic stability study

The solutions were prepared in $D_2O$. Each sample was prepared from stock solutions of POM ($H_3PW_{12}O_{40}$ or $H_3PMo_{12}O_{40,}$ 64-100 mmol/l) and each CD ($\alpha$-, $\beta$-, or $\gamma$-CD) which are mixed in known proportions to make 1- or 3-mL final solutions. The volume was adjusted with $D_2O$ to achieve the desired concentrations of POM and CD. Usually, the POM solution was added to cyclodextrin solution to ensure its integrity before its use. The pH of the solutions is measured systematically and adjusted with concentrated solutions of NaOH (6 M or 12 M). The samples were then transferred into 5 mm (600 $\mu$l) NMR tubes for the $^{1}H$ and $^{31}P$ analyzes, or 10 mm (2.5 mL) tubes for the $^{183}W$ analyzes. The pH can change over time (especially for tungstate samples). pH measurements were thus taken at each start and end of an NMR experiment, which can last 24 h. Similar series were also prepared in pure $D_2O$ or in a 50:50 v:v $D_2O$:1,4-dioxane mixture for comparison.

## 2.3 Interaction of $\gamma$-CD with Keggin-type $[XW_{12}O_{40}]^{n-}$ ions

One of the most striking supramolecular properties of POMs arises from their ability to form in solution resilient non-bonding contacts with non-ionic compounds such as organic macrocycles, micelles, proteins, or polymers.[35–37] Electrostatic and hydrophobic interactions contribute to the affinity and activity of POM anions towards biomolecules, suggesting that POMs can integrate the Hofmeister family.[38] This classification of ions aims to evaluate their lyotropic properties, which are the ability to salt out or salt in proteins. Recently, Nau's group in Germany suggested POMs can be used as representative models for superchaotropic anions, located between chaotropic and hydrophobic ions in an expanded Hofmeister scale.[39] Common chaotropic ions are characterized by a large size and weak charge density. Therefore, these parameters can be useful descriptors to assess the strength of the chaotropic character of a given ion. The chaotropic property of POMs even widely discussed in the literature remains to be proven.[38,40]

In this section, we study the charge effect on host guest association between $\gamma$-CD and a series of Keggin POMs $[XW_{12}O_{40}]^{n-}$ (X can be P, Si, B, or $H_2$) of the same shape and size. As shown in Figure 2.2, the structure of Keggin-type POMs (~1nm) $[XW_{12}O_{40}]^{n-}$ with its tetrahedral symmetry and spherical shape perfectly fits with the

size of the central cavity of the host γ-CD. However, the nature of the heteroatom X located in the central cavity of the 12 octahedral $WO_6$ units of the POM, imposes a different ionic charge density on its surface, which could influence its solvation properties and then its ability to interact with the host molecule.

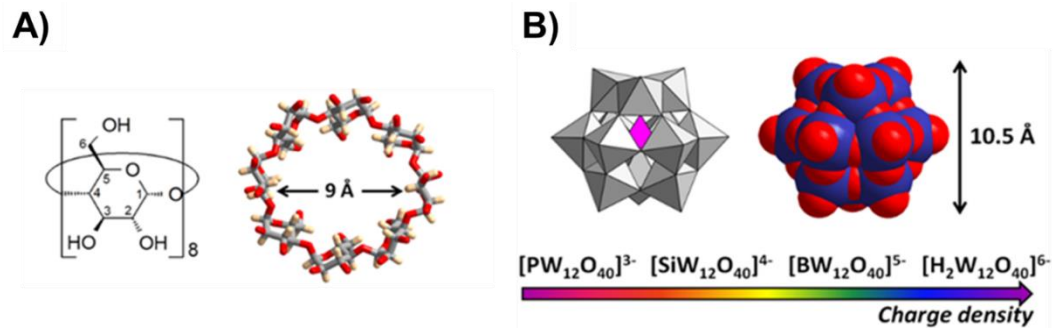


**Figure 2.2** *Structural representations of the molecular entities used as building blocks. (a) γ-cyclodextrin $C_{48}H_{80}O_{40}$ (γ-CD), the toroidal macrocycle delimits a hydrophobic cavity of 9 Å in diameter. (b) The Keggin-type POM, $[XW_{12}O_{40}]^{n-}$, the nature of X allows the control of the charge density of the nano-sized inorganic unit.*

### 2.3.1 Single-crystal structures of $PW_{12}$@CD and $BW_{12}$@2CD

Based on single crystal X-ray diffraction data, we obtained the crystallographic structures of two composite compounds: $Na_3\{[PW_{12}O_{40}]\cdot(C_{48}H_{80}O_{40})\}\cdot 10H_2O$ ($PW_{12}$@CD), and $CsK_2H_2\{[BW_{12}O_{40}]\cdot 2(C_{48}H_{80}O_{40})\}\cdot 29H_2O$ ($BW_{12}\cdot$2CD). Although the two Keggin POMs have the same shape and size, they display different types of interactions and organization with γ-CD in their crystal lattices. Actually, these structures are significantly different from the previously published crystal structure obtained with the Keggin phosphomolybdate $[PMo_{12}O_{40}]^{3-}$ exhibiting a sandwich complex with γ-CD, ($PMo_{12}$@2CD).[13] The local arrangement between POM and CD in these three compounds is depicted and compared in Figure 2.3. Selected crystallographic parameters are included in Table 2-1.

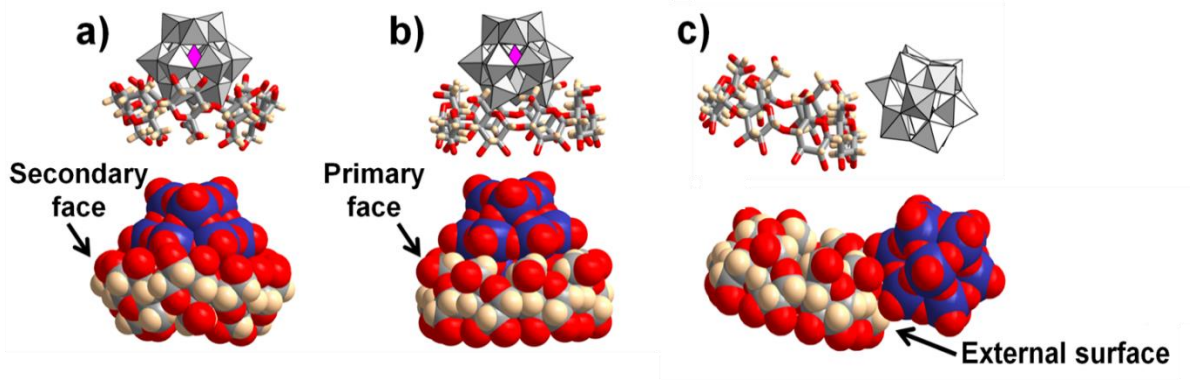


**Figure 2.3** *Illustration of the different supramolecular assemblies observed in the solid-state involving γ-CD and the Keggin anions (a) $[PW_{12}O_{40}]^{3-}$ in **$PW_{12}$@CD**, (b) $[PMo_{12}O_{40}]^{3-}$ in **$PMo_{12}$@2CD** from reference,[30] and (c) $[BW_{12}O_{40}]^{5-}$ in **$BW_{12}$•2CD.***

**Table 2-1** Selected crystallographic parameters of the single-crystal X-ray diffraction structural analysis.

| Identification code | $PW_{12}$@CD | $BW_{12}$•2CD |
|---|---|---|
| **CCDC number** | 2015681 | 2015682 |
| **Empirical formula** | $C_{48}H_{54}Na_{0.67}O_{87}PW_{12}$ | $C_{96}H_{108}BCsO_{120}W_{12}$ |
| **Formula weight** | 4275.39 | 5531.74 |
| **Temperature/K** | 210 | 210 |
| **Crystal system** | cubic | tetragonal |
| **Space group** | *I*23 | $P42_12$ |
| ***a*/Å** | 41.7867(14) | 23.199(2) |
| ***b*/Å** | 41.7867(14) | 23.199(2) |
| ***c*/Å** | 41.7867(14) | 17.304(2) |
| ***α*/°** | 90 | 90 |
| ***β*/°** | 90 | 90 |
| ***γ*/°** | 90 | 90 |
| **Volume/Å$^3$** | 72965(7) | 9313(2) |

**$PW_{12}$@CD arrangement.** **$PW_{12}$@CD** consists of a supramolecular 1:1 adduct containing one $[PW_{12}O_{40}]^{3-}$ motif incorporated into the central cavity of one γ-CD through its secondary rim (Figure 2.3a). Such a configuration is unique among the known polyoxometalate/γ-CD composites which exhibit host-guest adducts usually through primary face.[13,22] Of particular interest, the comparison with the isostructural Keggin phosphomolybdate $[PMo_{12}O_{40}]^{3-}$ ion reveals a different complexation mode with γ-CD which is bound through its opposite face, namely, the primary rim (Figure 2.3b).[13] Furthermore, the stoichiometry of the adduct is 1:2 with $[PMo_{12}O_{40}]^{3-}$, while it is 1:1 with $[PW_{12}O_{40}]^{3-}$ although higher stoichiometry numbers should be expected as observed with other systems for higher guest/host molar ratio introduced in the aqueous solution. Indeed, while **$PW_{12}$@CD** crystallized in a solution with an initial

ratio of 1:1, other crystalline products were obtained with higher γ-CD contents (2 γ-CDs per POM unit), but we were unable, despite repeated attempts, to solve the solid-state X-ray diffraction structures due to severe disorder in these crystals. Nevertheless, the unit cell parameters (*a* = 23.94 and *c* = 18.54 Å) in a tetragonal system were determined, indicating a different organization. The 1:1 adduct observed in **$PW_{12}$@CD** exhibits several supramolecular interactions involving terminal $O^t$ and bridging $O^b$ atoms of the POM and H3 and H5 protons of the inner cavity of the γ-CD (see Figure 2.2a for H labeling). The short interatomic distances H3•••$O^t$=W ( ~2.7 Å), H3•••$O^b$-W (~2.5 Å) and H5•••$O^t$=W (~2.3 Å), are consistent with a strong and deep host-guest inclusion (see Figure 2.4a). As **$PW_{12}$@CD** crystallizes in a cubic crystallographic system, the 1:1 host-guest adduct is surrounded by four other γ-CDs of other host-guest units from the non-complexed half of the POM. This latter interacts with the external surface of each of the γ-CD of the four neighboring 1:1 adducts (see Figure 2.4b).

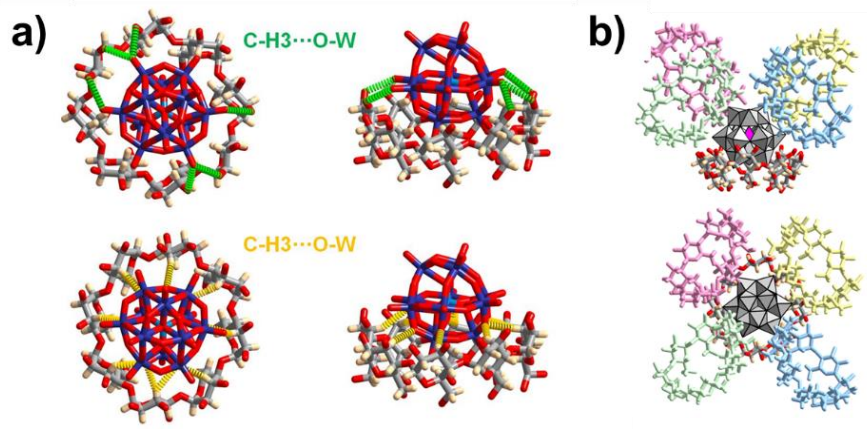


**Figure 2.4** *Structural views of **$PW_{12}$@CD**. a) Illustration of the different supramolecular interactions involved in the 1:1 host-guest complex $\{PW_{12}O_{40}@CD\}^{3-}$ in **$PW_{12}$@CD**. The oxygen atoms of the $PW_{12}O_{40}^{3-}$ entity interact with H3 CD through numerous H-bonds with their terminal $O^t$ (green) and bridging $O^b$ (yellow). b) Illustration of the structural arrangement between the 1:1 host-guest complex $\{PW_{12}O_{40}@CD\}^{3-}$ and the four CDs of other inclusion complexes.*

**$BW_{12}$@CD arrangement.** In the solid-state, the organization of the $[BW_{12}O_{40}]^{5-}$ and γ-CD is completely different since the crystalline structure of **$BW_{12}$•2CD** reveals that the two components co-crystallize together side by side without forming inclusion complex. Indeed, the $[BW_{12}O_{40}]^{5-}$ is located next to the γ-CD, in close contact with its outer wall (Figure 2.3c). Each $[BW_{12}O_{40}]^{5-}$ POM unit interacts with eight CD hosts

through the three extern protons H1, H2, and H4 as well as the H6 of the methoxy arm (see Figure 2.5). This leads to a global stoichiometry of 2(γ-CD):1POM. Two neighboring γ-CDs are face-to-face connected through a hydrogen bonding network from their secondary rims blocking their accessibility. The $[BW_{12}O_{40}]^{5-}$ is thus positioned near the primary face with short H6•••$O^t$=W and H6•••$O^b$-W distances in the range 2.7–2.8 Å. Finally, it is highly intriguing to understand how γ-CD interacts so differently with isostructural nano-sized objects, namely $[PW_{12}O_{40}]^{3-}$, $[PMo_{12}O_{40}]^{3-}$, and $[BW_{12}O_{40}]^{5-}$. By keeping the charge constant, the basicity of Keggin molybdates are known to be higher compared to their tungstate analogues that makes charge density more localized on surface oxygen of molybdates.[41,42] Furthermore, the ionic charge should also play a crucial role on the supramolecular association.[43] Both these aspects would affect considerably polar solvent structuration around the POM, and therefore solvation phenomenon is expected to play a major role to the supramolecular arrangement around the POMs. To verify such assumption, we had undertaken systematic studies in solution by using complementary techniques (ITC, electrochemistry, and NMR spectroscopy) on the four archetypical anions ($[XW_{12}O_{40}]^{n-}$, X = P, Si, B, or $H_2$) belonging to this well-known Keggin series.

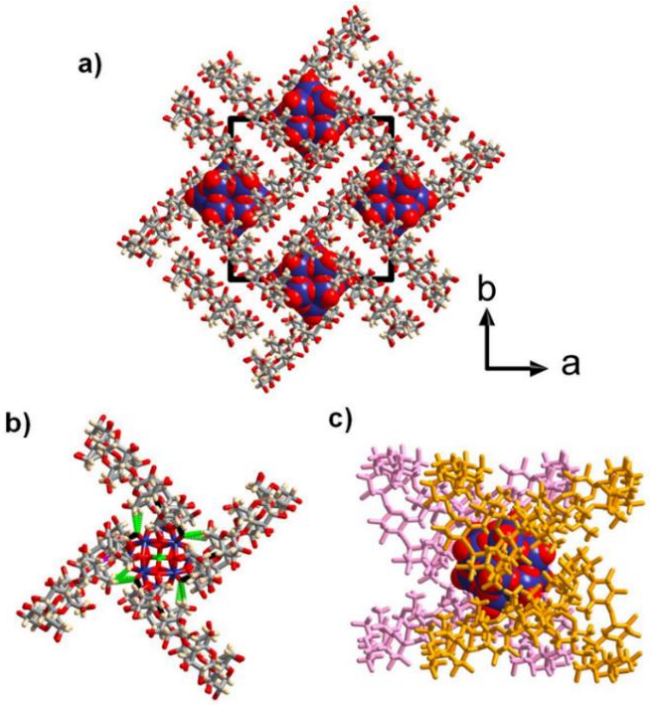


**Figure 2.5** *a) View of the tetragonal unit cell of the compound* ***$BW_{12}$•2CD*** *along c axis. Free water molecules and counter cations are omitted for clarity. b) and c) Illustrations of the CD around $\{BW_{12}O_{40}\}^{5-}$. Each POM unit interacts with eight CD hosts through their external surface (H1, H2 H4 and H6).*

### 2.3.2 Isothermal titration calorimetry

Isothermal titration calorimetry (ITC) experiments were carried out to give thermodynamic insights about interactions between the γ-CD and the four types of Keggin heteropolytungstates. Table 2-2 gives a summary of binding constants, enthalpy $\Delta_rH^*$ and entropy $\Delta_rS^*$ changes at 298 K from ITC thermograms and isotherms. Besides the 1:1 complexation, a second consecutive step leading to the 1:2 complex is systematically considered, according to equations (2.1) and (2.2) shown below.

$$POM^{n-} + CD \rightarrow [POM@CD]^{n-} \quad (2.1)$$

$$[POM@CD]^{n-} + CD \rightarrow [POM@2CD]^{n-} \quad (2.2)$$

Nonetheless, only ITC data for silicotungstate/γ-CD system was found relevant with such a two-sites binding model involved in a sequential process. No significant heat release was observed in the case of $[H_2W_{12}O_{40}]^{6-}$ meaning that the interaction with γ-CD is too weak to be reliably measured with this POM. For all other complexes, supramolecular binding revealed to be an enthalpically driven process according to negative enthalpy changes $\Delta_rH^* < 0$ and to the entropy penalty $\Delta_rS^* < 0$. The enthalpic change appears correlated to entropic penalty according to the usual enthalpy-entropy compensation observed with CD-based encapsulation process.[42] Such a thermodynamic fingerprint together with negative values of both enthalpic and entropic changes suggests that Keggin POMs behave as chaotropic species (water structure breakers).[39] In such a case, the magnitude of the chaotropic character is expected to increase with decreasing the global charge. However, the highest enthalpic and entropic changes, which are signature of chaotropic effect, were observed for $[SiW_{12}O_{40}]^{4-}$ and the lowest values were found for $[PW_{12}O_{40}]^{3-}$. This latter POM with the lowest charge in the series represents therefore an anomaly within the series, probably due to two reasons: i) the partial hydrolysis of the $[PW_{12}O_{40}]^{3-}$ anion under the ITC conditions (non-buffered and dilute solutions) and ii) the two-step consecutive complexation model used do not fit with the experimental data. Formation of numerous complexes with various stoichiometries, e.g., 1:1,1:2,

2:1, etc., is not excluded with this highly reactive POM. Such a hypothesis will be verified in part by the $^{1}$H NMR DOSY analysis, presented below.

**Table 2-2** *ITC binding constants K involving γ-CD with the Keggin POM anions and associated thermodynamic parameters at T = 298 K.*

| POM | POM:CD | *K* ($M^{-1}$) | $\Delta_r H^*$ ($kJ.mol^{-1}$) | $-T\Delta_r S^*$ ($kJ.mol^{-1}$) | $\Delta_r G^*$ ($kJ.mol^{-1}$) |
|---|---|---|---|---|---|
| $[H_2W_{12}O_{40}]^{6-}$ | — | — | — | — | — |
| $[BW_{12}O_{40}]^{5-}$ | 1:1 | 1032 | -53.5 | +36.3 | -17.2 |
| $[SiW_{12}O_{40}]^{4-}$ | 1:1 | 17209 | -56.4 | +32.3 | -24.2 |
| | 1:2 | 459 | -55.0 | +39.8 | -15.2 |
| $[PW_{12}O_{40}]^{3-}$ | 1:1 | 2919 | -35.1 | +15.3 | -19.8 |

### 2.3.3 Cyclic voltammetry

Interactions of the Keggin-type ions with γ-CD have been studied further using cyclic voltammetry (CV). Figure 2.6 shows the CVs of the four POMs in the presence of different amounts of γ-CD. It clearly appears that the effect of CD is strongly dependent on the nature of the Keggin anion. Figure 2.7 displays the variation of the first half-wave potential recorded for the four POMs as a function of the amount of CD introduced CD, highlighting the differences in behavior in the Keggin series. The presence of γ-CD significantly alters the redox properties of POMs as a direct result of POM-CD complexation, where the binding process is expected to impact the redox potentials of the POM.

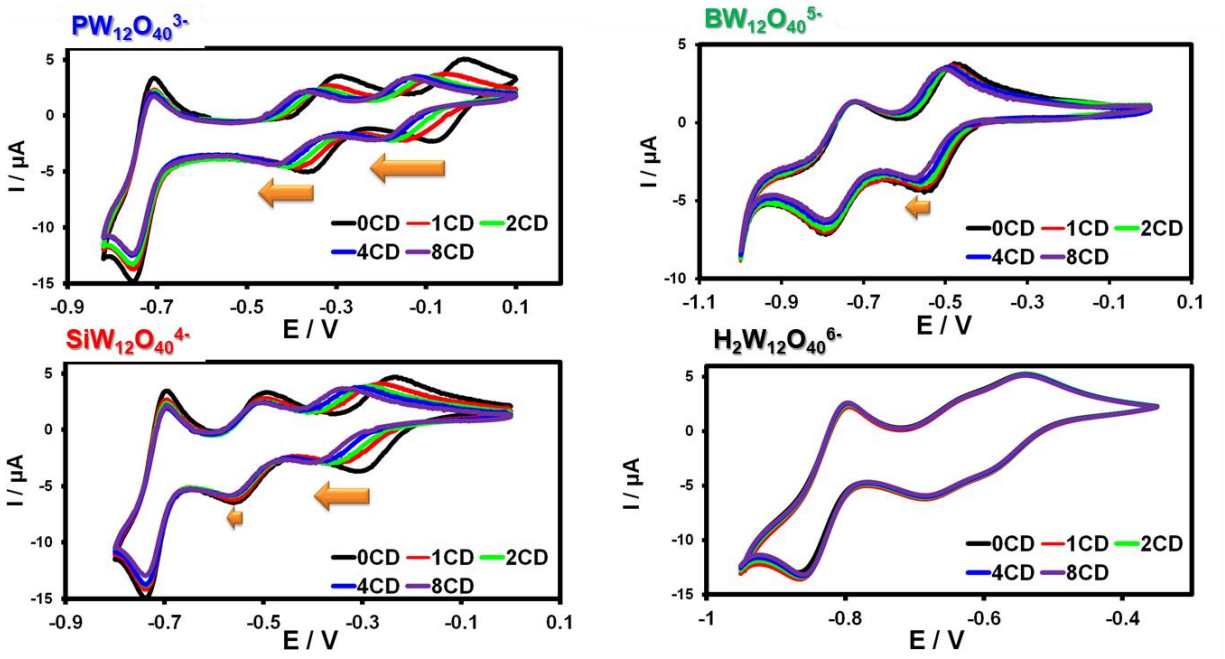


**Figure 2.6** *Cyclic voltammetry curves of $[PW_{12}O_{40}]^{3-}$, $[SiW_{12}O_{40}]^{4-}$, $[BW_{12}O_{40}]^{5-}$ and $[H_2W_{12}O_{40}]^{6-}$ anions (0.5 mmol $L^{-1}$, glassy carbon working electrode, scan rate 50 mV $s^{-1}$) in the presence of increasing amounts of γ-CD (from 0 to 8 equivalents). The experiments involving $[PW_{12}O_{40}]^{3-}$, $[SiW_{12}O_{40}]^{4-}$ and $[BW_{12}O_{40}]^{5-}$ have been performed in 25 mmol $L^{-1}$ $HClO_4$ aqueous solution, while acetate buffer solution (0.5 M $CH_3COONa$; 0.5 M $CH_3COOH$) has been used for the electrochemical measurements of $[H_2W_{12}O_{40}]^{6-}$.*

For instance, as the amount of γ-CD increases up to 8 equivalents, the half-wave potential related to the two first monoelectronic transfers of the $[PW_{12}O_{40}]^{3-}$ ion decreases continuously. Actually, the electrochemical behavior of the $[PW_{12}O_{40}]^{3-}$ ion gives the most representative effect reflected by a rough dependency of about −60 mV/pCD where pCD = −Log [CD]. This variation indicates that γ-CD is involved in the predominant redox process written in equations (2.3 and 2.4), with two consecutive monoelectronic transfers, n = 3 or 4 for the first and the second redox processes, respectively. Furthermore, the complexation behavior of γ-CD should be rather consistent with x = 2 or 1 corresponding to a 1:2 or 1:1 POM:CD supramolecular adduct, respectively. Along the Keggin series, the variation of the redox properties becomes less pronounced as the ionic charge of the Keggin ion increases as illustrated in Figure 2.7. Thus, in the case of $[SiW_{12}O_{40}]^{4-}$, the first mono-electronic redox wave appears strongly affected, whereas the second one varies weakly. For the boron derivative, only the first redox wave is moderately shifted and finally, the redox features of $[H_2W_{12}O_{40}]^{6-}$ remain nearly unchanged in

the presence of γ-CD (see Figure 2.6). With the exception of $[PW_{12}O_{40}]^{3-}$, the redox behavior reflects the trend highlighted by the ITC analysis.

$$[POM@CD_x]^{n-} + 1e^- \rightarrow [POM@CD_{x-1}]^{(n+1)-} + 1\ CD \qquad (2.3)$$

$$E_{1/2}^{obs} = E_{1/2}^{POM} - 0.059\, pCD \qquad (2.4)$$

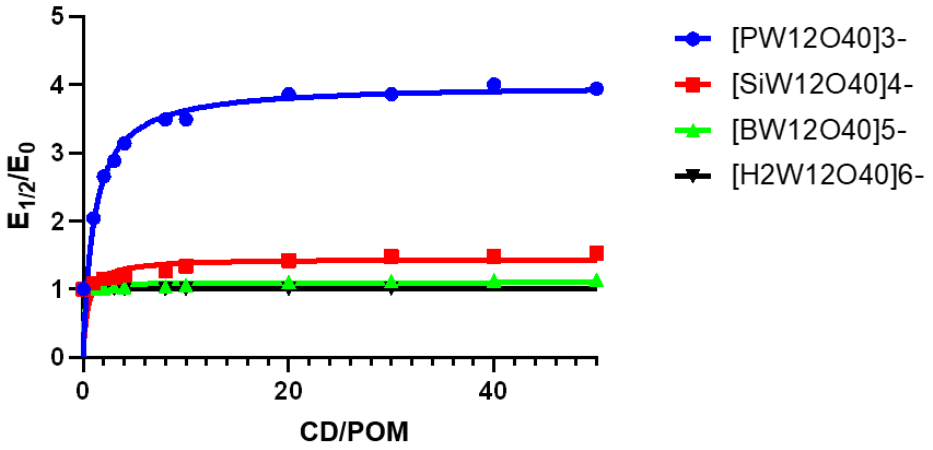


**Figure 2.7** *Variation of the first half-wave potential of the $[XW_{12}O_{40}]^{n-}$ anions with X = $P^{5+}$, $Si^{4+}$, $B^{3+}$ or $H_2^{2+}$ as a function of introduced fraction of CD.*

Quantitative analysis of these electrochemical data can yield the equilibrium constants ($K_{1:1}$ and $K_{1:2}$) regarding the binding of the Keggin anions at various redox states by the γ-CD. Considering the three available oxidation states of $POM^{n-}$ (ox), $POM^{(n+1)-}$ ($red_1$), $POM^{(n+2)-}$ ($red_2$), associated with the three related complexed forms POM@xCD with x = 0, 1 or 2, the 3X3 matrix diagram can be drawn (see scheme 2.1). Including the three components involved for each redox process, the Nernst equations are given in Equations (2.5) and (2.6).

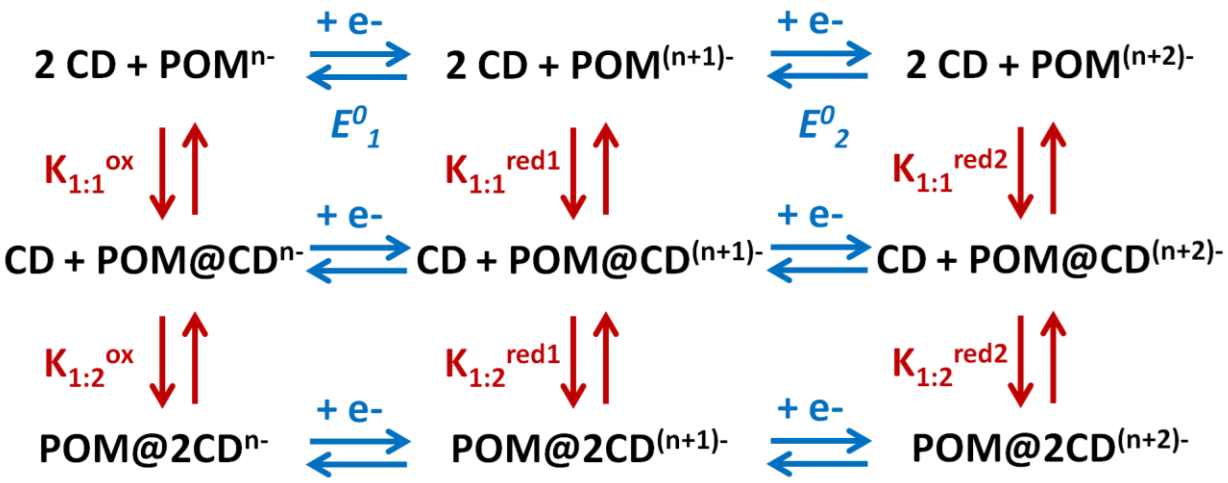


**Scheme 2.1** *Equilibriums involved in redox-dependent supramolecular associations of γ-cyclodextrin (CD) and Keggin type anions (POM) at various charges.*

$$E_{peak,1} = E_1^0 + \frac{RT}{F} ln \frac{(1+K_{1:1}^{ox}\,[CD]_{eq}+K_{1:1}^{ox}\,K_{1:2}^{ox}\,[CD]_{eq}^2)}{(1+K_{1:1}^{red1}\,[CD]_{eq}+K_{1:1}^{red1}\,K_{1:2}^{red1}\,[CD]_{eq}^2)} \qquad (2.5)$$

$$E_{peak,2} = E_2^0 + \frac{RT}{F} ln \frac{(1+K_{1:1}^{red1}\,[CD]_{eq}+K_{1:1}^{red1}\,K_{1:2}^{red1}\,[CD]_{eq}^2)}{(1+K_{1:1}^{red2}\,[CD]_{eq}+K_{1:1}^{red2}\,K_{1:2}^{red2}\,[CD]_{eq}^2)} \qquad (2.6)$$

where $E_1^0$ and $E_2^0$ are the standard potentials of each redox process and $[CD]_{eq}$ is the concentration in free γ-CD at the equilibrium. The values $K_{1:1}$ and $K_{1:2}$ for the three redox states of each $[XW_{12}O_{40}]^{n-}$ anion have been determined through the fitting of the shift of the half-wave potentials of the two first redox waves upon addition of γ-CD (see Table 2-3).[†] The binding constants determined for the $[BW_{12}O_{40}]^{5-}$ and $[SiW_{12}O_{40}]^{4-}$ are in good agreement with those determined by ITC given in Table 2-2. The POM can exhibit three successive redox states, oxidized (ox), one-electron reduced ($red_1$) or two-electron reduced ($red_2$) (see scheme 2.1). The binding constants of the reduced $POM^{(n+1)-}$ retain lower values compared to those determined for the oxidized parents ($POM^{n-}$), evidencing again the preponderant

[†] The fitting of the curves of the experimental half-wave potentials as a function of CD concentration (example shown in Figure 2.8) is performed using Microsoft Excel software. Both curves were fitted simultaneously to use the same set of binding constants K1:1 and K1:2 for the (ox), (red1) and (red2) POM species. For a given CD concentration, the redox potentials are calculated with optimal binding constants that give minimal deviation from the experimental values over the entire CD concentration range. The Excel macro "Solver", a script incorporated in the program, was used to perform automatic iteration until convergence.

effect of the charge on the association process with the macrocyclic host. For instance, variation of standard potential of the two one-electron exchanges undergone by the $[PW_{12}O_{40}]^{3-}$ ion with the concentration of γ-CD is given in Figure 2.8 ($[PW_{12}O_{40}]^{3-}$, $K_{1:1}$ = 90000). According to the best fit, the binding constant with the one-electron reduced anion $[PW_{12}O_{40}]^{4-}$ ($K_{1:1}$ = 6000 $M^{-1}$) is in a similar order of magnitude to that found for the oxidized silicotungstate $[SiW_{12}O_{40}]^{4-}$ ($K_{1:1}$ = 9500 $M^{-1}$) carrying the same charge (see Table 2-3). A similar observation also holds for the one electron-reduced silicotungstate $[SiW_{12}O_{40}]^{5-}$ and the oxidized borotungstate $[BW_{12}O_{40}]^{5-}$, which both exhibit comparable affinity toward γ-cyclodextrin.

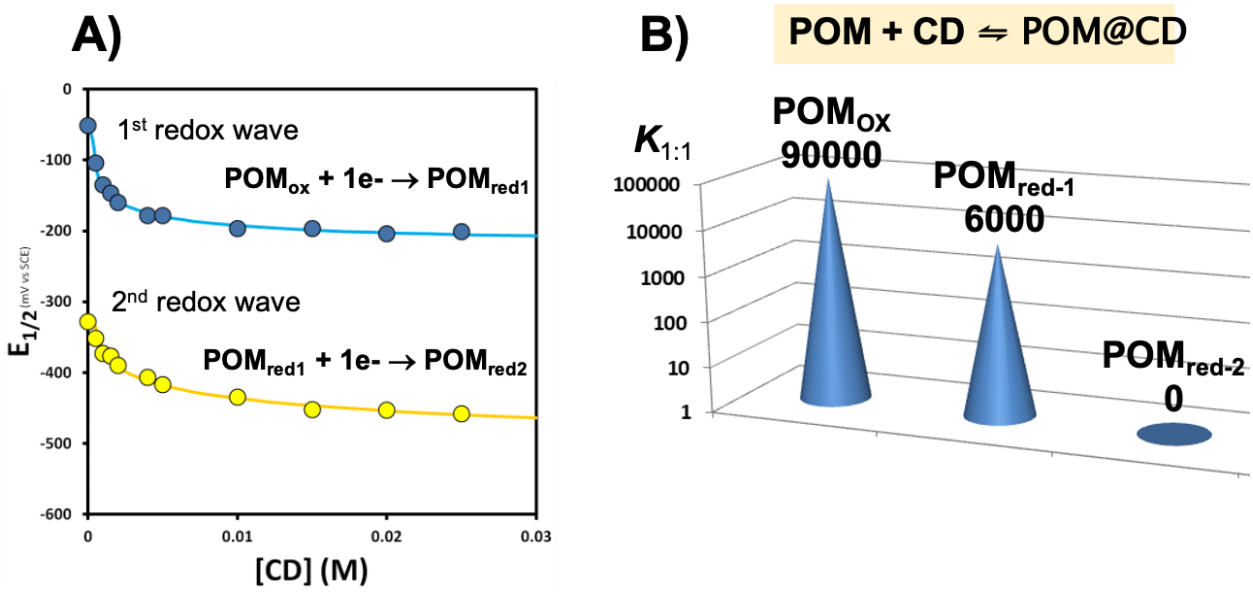


**Figure 2.8** *A) Variation of potential of the first (blue) and second (yellow) waves observed in CV of 0.5 mM $[PW_{12}O_{40}]^{3-}$ as a function of [CD], using Equations (2.5) and (2.6). B) Binding constants $K_{1:1}$ involving γ-CD with $[PW_{12}O_{40}]^{3-}$ at different oxidation states as determined from electrochemistry.*

**Table 2-3** *Binding constants $K_{1:1}$ and $K_{1:2}$ involving γ-CD with the Keggin POM anions at different oxidation states as determined from electrochemistry.*

| X | POM:CD | $[XW_{12}O_{40}]^{3-}$ | $[XW_{12}O_{40}]^{4-}$ | $[XW_{12}O_{40}]^{5-}$ |
|---|---|---|---|---|
| **P** | 1:1 | 90 000 | 6000 | 0 |
| | 1:2 | 1 500 | 30 | 0 |
| **Si** | 1:1 | - | 9 500 | 130 |
| | 1:2 | - | 150 | 10 |
| **B** | 1:1 | - | - | 600 |
| | 1:2 | - | - | 0 |

In context, proton-coupled electron transfer (PCET) involving POM species is a well-known pH dependent process featured by an increase of the standard potential as pH decreases. Such an effect can even be extended to the POM-lithium aggregation process under reducing conditions in non-aqueous solvents.[44] In the presence of γ-CD, the origin of the redox potential variation upon γ-CD interaction should arise mostly from a change in the solvation shell of the POM corresponding to a loss of surrounding water molecules upon binding to γ-CD resulting in a more hydrophobic environment around the POMs.

To sum up, the electrochemistry investigations demonstrate that both binding constants $K_{1:1}$ and $K_{1:2}$ increase by at least one order of magnitude along the Keggin-type series $[XW_{12}O_{40}]^{n-}$ with increasing *n*. According to this observation, the Keggin/γ-CD association appears as an interesting redox switch that could be integrated within stimuli-responsive supramolecular systems controlled by the redox state of POM, which can be easily tuned and achieved chemically.

### 2.3.4 $^1$H and DOSY NMR studies in solution

***$^1$H NMR.*** The formation and stability of Keggin POM-(γ-CD) complexes in aqueous solution were further probed by $^1$H NMR spectroscopy in $D_2O$. NMR is a popular technique to study cyclodextrins and their supramolecular complexes because such flexible macrocycles offer local NMR probes highly sensitive to through-space contact with guest molecules.[45] Cyclodextrins have six magnetically different protons, labelled H1-6, and their typical $^1$H NMR spectrum is shown in Figure 2.9.

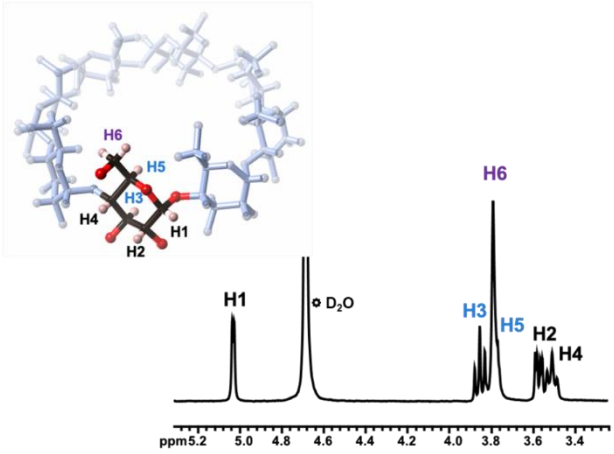


**Figure 2.9** *$^1$H NMR spectrum of 2 mmol L$^{-1}$ aqueous solution of γ-CD showing the 6 different proton signals: The outer protons H1, H2 and H4, the inner protons H3 and H5, and the methoxy arm protons H6.*

Here, we conducted a comparative study of titration of 2 mM aqueous solution of γ-CD by the four types of Keggin POMs. Figure 2.10 shows the resulting spectra in the range 3.7-4.5 ppm corresponding to the resonance domain of the protons of interest to probe the short contact interaction. Exposed protons namely H3 and H5 are located inside the cavity while the H6 proton belong to the methoxy group on the top of the secondary rim. These protons (H3, H5 and H6) are the most sensitive toward host-guest complexation and are usually used as a probe of inclusion phenomenon. Depending on Keggin anion, the spectra underwent more or less important alteration evidencing different host-guest reactivity. Table 2-4 summarizes the extent of shift variations observed for H3, H5, and H6 after adding 8 equivalents of each POM.

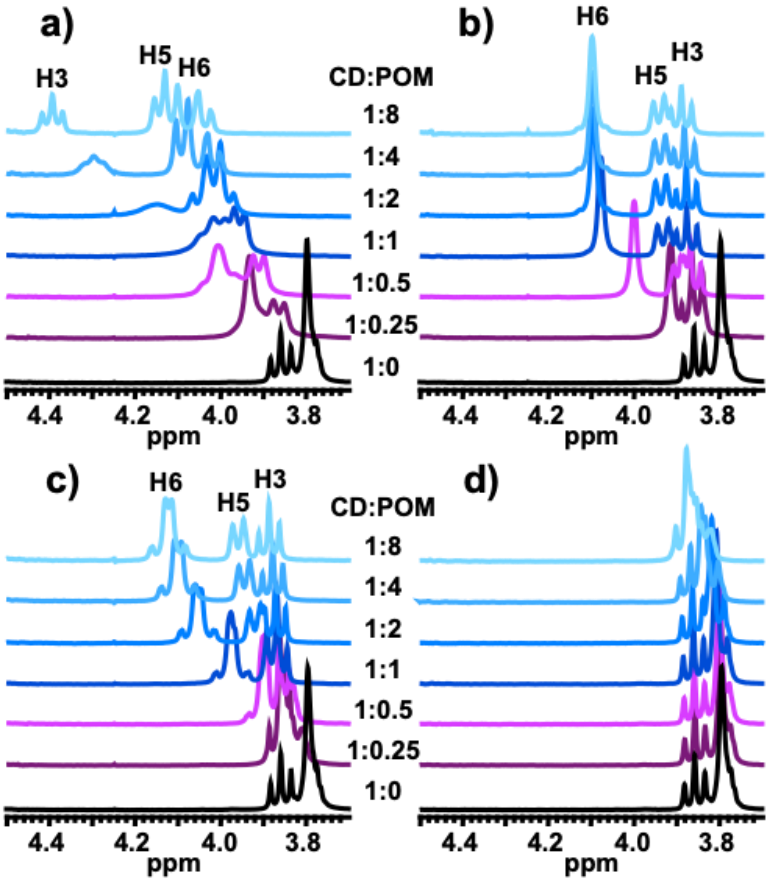


**Figure 2.10** *$^{1}$H NMR spectra in the chemical shift range for H3, H5, and H6 resulting of the titration of 2 mmol L$^{-1}$ aqueous solution of γ-CD by $[XW_{12}O_{40}]^{n-}$ POMs: (a) $[PW_{12}O_{40}]^{3-}$; (b) $[SiW_{12}O_{40}]^{4-}$; (c) $[BW_{12}O_{40}]^{5-}$ and (d) $[H_2W_{12}O_{40}]^{6-}$.*

**Table 2-4** *Largest magnitude in chemical shifts of protons H3, H5, and H6 of γ-CD measured for 8 equivalents of POM.*

| POM | ΔδH3 (ppm) | ΔδH5 (ppm) | ΔδH6 (ppm) |
|---|---|---|---|
| $[H_2W_{12}O_{40}]^{6-}$ | 0.02 | 0.06 | 0.07 |
| $[BW_{12}O_{40}]^{5-}$ | 0.03 | 0.18 | 0.33 |
| $[SiW_{12}O_{40}]^{4-}$ | 0.03 | 0.16 | 0.30 |
| $[PW_{12}O_{40}]^{3-}$ | 0.53 | 0.36 | 0.28 |

The spectrum of macrocyclic host did not alter much when $[H_2W_{12}O_{40}]^{6-}$ was added in the γ-CD solution with the increasing equivalent POM, and the maximum shifts observed were ca. 0.07 ppm for both H5 and H6 as an indication of very weak interaction. Notably, much bigger effects were observed in cases of $[BW_{12}O_{40}]^{5-}$ and $[SiW_{12}O_{40}]^{4-}$, where shifts up to 0.33 and 0.18 ppm were observed for H6 and H5, respectively. These changes in the spectra are similar, suggesting comparable behavior in solution for $[BW_{12}O_{40}]^{5-}$ and $[SiW_{12}O_{40}]^{4-}$. Nevertheless, close inspection revealed some few differences. First, the H6 (and also H5) signal evolves faster with increasing the $[SiW_{12}O_{40}]^{4-}$ amount compared to $[BW_{12}O_{40}]^{5-}$ although the final chemical shift at the plateau is the same. As the observed chemical shift corresponds to a weighted average of free and complexed γ-CD species, this means the affinity constant for POM-CD complexation should be higher with $[SiW_{12}O_{40}]^{4-}$ than with $[BW_{12}O_{40}]^{5-}$. The second observation is the splitting of the initial singlet of the H6 protons into two unresolved doublets in solution containing $[BW_{12}O_{40}]^{5-}$. This may be due to restriction in dynamic rotation of the methoxy arms leading to quasi-resolved signals for the two methylenic diastereotopic H6 protons. Such steric hindrance would result from the interaction of the POM specifically with the primary rim of the γ-CD since H3 protons present in the secondary rim did not show any significant perturbation. The situation is totally different with the $[PW_{12}O_{40}]^{3-}$ ion where in addition to the significant shift of H6, we can also see strong effects on both H5 and H3 resonances with up to 0.53 ppm downfield shifts. Such an observation would be consistent with the involvement of the secondary face of the γ-CD as well as the primary one in the host-guest process with $[PW_{12}O_{40}]^{3-}$.

All these observations (continuous change in chemical shifts) are rather consistent with a fast exchange regime with respect to the NMR time scale. The observed

chemical shift of CD corresponds therefore to a weighted average of the chemical shift of the individual species, i.e., the free CD ($\delta_1$), the 1:1 POM:CD complex ($\delta_2$), and the 1:2 POM:CD complex ($\delta_3$):

$$\delta_{obs} = X_1\delta_1 + X_2\delta_2 + X_3\delta_3 \qquad (2.7)$$

In the simplest case of single step complexation, the 1:2 species is negligible and the observed chemical shifts can be written as a function of free CD fraction $X_1$ alone:

$$\delta_{obs} = X_1\delta_1 + X_2\delta_2 = X_1\delta_1 + (1\text{-}X_1)\delta_2 \qquad (2.8)$$

As the molar fraction $X_1$ is a function of equilibrium constant $K$ and initial CD concentration $C_{CD}$, Equation (2.8) can be expressed as a function of molar ratio $R$ = POM/CD:

$$d_{obs} = d_1\frac{\left(KC_{CD} - KC_{CD}R - 1\right) + \sqrt{\left(KC_{CD}R - KC_{CD} + 1\right)^2 + 4KC_{CD}}}{2KC_{CD}} + d_2\left(\frac{\left(KC_{CD} + KC_{CD}R + 1\right) - \sqrt{\left(KC_{CD}R - KC_{CD} + 1\right)^2 + 4KC_{CD}}}{2KC_{CD}}\right)$$

*(2.9)*

This quantitative treatment allows determination of affinity constants for single step 1:1 POM:γ-CD complexation (see Equation (2.9) and Figure 2.11). The values obtained for $K_{1:1}$ are 23 and 1100 $M^{-1}$ for $[H_2W_{12}O_{40}]^{6-}$:CD and $[BW_{12}O_{40}]^{5-}$:CD, respectively. For the other POMs with lower charge, $[SiW_{12}O_{40}]^{4-}$ and $[PW_{12}O_{40}]^{3-}$, we note the line broadening of H3 signal in moderate POM:γ-CD (< 4) which is a signature of strong 1:2 POM:γ-CD sandwich adduct.[46] A two-step complexation model should then be applied in this case, using Equations (2.7) and (2.12-15), to determine individual fractions $X_1$, $X_2$, and $X_3$ (see below).

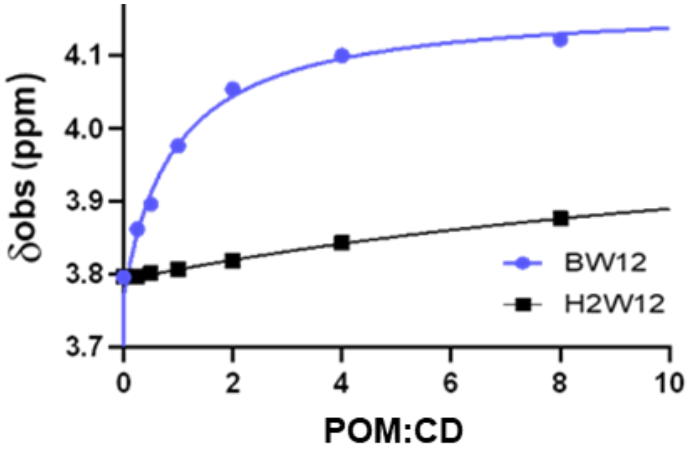


**Figure 2.11** *Quantitative analysis of observed $^1$H NMR chemical shifts of most affected γ-CD proton (H6) as a function of the molar ratio R = POM/CD during the titration of 2 mM γ-CD by $[H_2W_{12}O_{40}]^{6-}$ and $[BW_{12}O_{40}]^{5-}$ using Equation (2.9).*

***$^1$H DOSY.*** Further quantitative investigation was also carried out using DOSY NMR. This technique is a valuable tool to study dynamic equilibriums, and similarly to chemical shift, the observed diffusion coefficient *D* in the extreme narrowing regime (fast exchange) can be described as a weighted average of a given species exchanging between different states.[47]

Similarly to chemical shift, the observed diffusion coefficient $D_{obs}$ of a species exchanging its environment between solvated and different binding states could be written as a weighted average of diffusion constants of each situation. Such an analysis holds for fast process in the NMR time scale. For these POM/CD systems, the CD could be present as free species ($D_1$) or either as 1:1 POM:CD complex ($D_2$) or 1:2 POM:CD complex ($D_3$). In the simple case restricted to a one-step complexation, the observed diffusion coefficient is given by Equation (2.10) or (2.11).

$$D_{obs} = X_1 D_1 + X_2 D_2 \qquad (2.10)$$

$$D_{obs} = D_1 \frac{(KC_{CD} - KC_{CD}R - 1) + \sqrt{(KC_{CD}R - KC_{CD} + 1)^2 + 4KC_{CD}}}{2KC_{CD}} + D_2 \frac{(KC_{CD} + KC_{CD}R + 1) - \sqrt{(KC_{CD}R - KC_{CD} + 1)^2 + 4KC_{CD}}}{2KC_{CD}} \qquad (2.11)$$

In the case of two-step complexation, the expression becomes:

$$D_{obs} = X_1 D_1 + X_2 D_2 + X_3 D_3 \qquad (2.12)$$

The fraction of free CD $X_1$ can be obtained from the following relation:

$$abX_1^3 + (2abR - ab + a)X_1^2 + (aR - a + 1)X_1 = 1 \qquad (2.13)$$

with a = $K_{11}C_{CD}$ and b = $K_{12}C_{CD,}$ where $K_{11}$ and $K_{12}$ are equilibrium constants for step 1 and step 2 processes (see Equations (2.1) and (2.2)). The fractions of 1:1 and 1:2 POM:CD complexes, respectively $X_2$ and $X_3$ are calculated as follows:

$$X_2 = \frac{1-X_1}{1+2bX_1} \qquad (2.14)$$

$$X_3 = 1 - X_1 - X_2 \qquad (2.15)$$

In our case, $^1$H NMR of γ-CD in presence of POM should correspond to an average situation taking into account the various configurations of γ-CD, as free or bound in 1:1 or 1:2 complexes. The observed diffusion coefficients *D* as a function of POM:γ-CD molar ratio is plotted in Figure 2.12 for the four studied Keggin anions. The curves can be modeled using one-step complexation Equation (2.11) for $[BW_{12}O_{40}]^{5-}$ and $[H_2W_{12}O_{40}]^{6-}$, or two-step complexation Equations (2.12-15) for $[PW_{12}O_{40}]^{3-}$ and $[SiW_{12}O_{40}]^{4-}$. Table 2-5 gathers the parameters used, either optimized or fixed. It can be seen that the initial value of *D* for free γ-CD measured at 254 μm$^2$/s drops more or less quickly upon addition of POM. It reaches a plateau at large excess of POM at 226 μm$^2$/s in the case of $[SiW_{12}O_{40}]^{4-}$ and $[BW_{12}O_{40}]^{5-}$, while with the $[H_2W_{12}O_{40}]^{6-}$ ion, the diffusion coefficient decreases much more slowly without reaching any limit value consistently with a weaker host-guest interaction. For the P containing Keggin, the drop of *D* is the fastest and reaching even a lower limit value at *D* = 219 μm$^2$/s. We note also a minima value for the curves of both $[SiW_{12}O_{40}]^{4-}$ and $[PW_{12}O_{40}]^{3-}$ at ca. POM:γ-CD = 0.5 suggesting presence of larger intermediate species in these POM:γ-CD molar ratio. Such curve profiles can be modeled using two consecutive complexation steps with 1:1 and 1:2 POM:γ-CD stoichiometries, and in such conditions, the 1:2 sandwich complex corresponds to the first intermediate, whose formation could be favored at that POM:γ-CD molar ratio of 0.5. We estimate the volume/size of the $[XW_{12}O_{40}]$@γ-CD adduct does not change much with varying the nature of the hetero-element X. The observed lower limit value with $[PW_{12}O_{40}]^{3-}$ at high POM content (219 vs 226 μm$^2$/s) may result from some further aggregation

phenomenon due to its pronounced chaotropic character, which manifests with high ability to interact with both primary and secondary faces of the γ-CD.

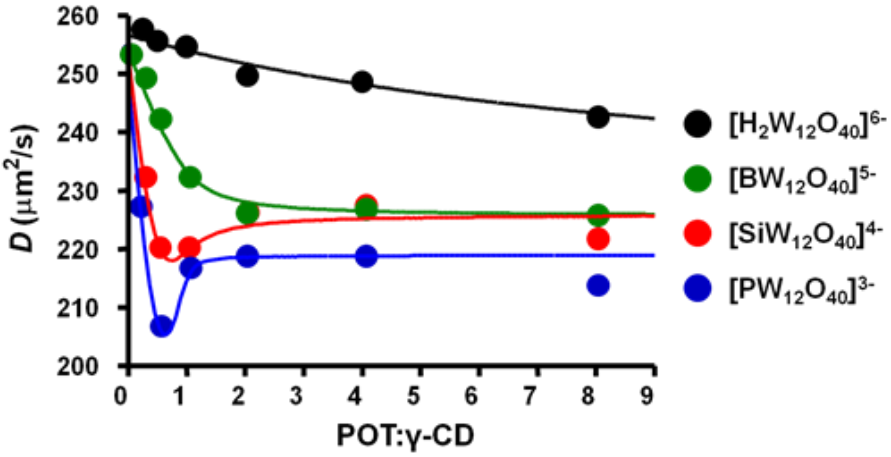


**Figure 2.12** *Diffusion coefficients of γ-CD as a function of POM:γ-CD molar ratio, measured from $^1$H DOSY NMR of a solution of 2 mM of γ-CD with various POM content. Lines correspond to calculated curves with one-step 1:1 POM:CD complexation for $[H_2W_{12}O_{40}]^{6-}$ and $[BW_{12}O_{40}]^{5-}$ using Equation (2.11), and with two-step 1:2 POM:CD complexation for $[SiW_{12}O_{40}]^{4-}$ and $[PW_{12}O_{40}]^{3-}$ using Equations (2.12-15).*

**Table 2-5** *Diffusion coefficients of CD as free ($D_1$), 1:1 POM:CD ($D_2$), and 1:2 POM:CD ($D_3$) complexes and $K_{1:1}$ and $K_{1:2}$ binding constants in 1:1 and 1:2 POM/CD complexes used for modeling observed D curves of Figure 2.12.*

| POM | $D_1$ (μm² s$^{-1}$) | $D_2$ (μm² s$^{-1}$) | $D_3$ (μm² s$^{-1}$) | $K_{1:1}$ (M$^{-1}$) | $K_{1:2}$ (M$^{-2}$) |
|---|---|---|---|---|---|
| $[H_2W_{12}O_{40}]^{6-}$ | 254 | 226 | - | 50 | - |
| $[BW_{12}O_{40}]^{5-}$ | 254 | 226 | - | 3000 | - |
| $[SiW_{12}O_{40}]^{4-}$ | 254 | 226 | 163 | 17000 | 460 |
| $[PW_{12}O_{40}]^{3-}$ | 254 | 219 | 163 | 160000 | 1500 |

Furthermore, $^1$H NMR can also evidence the resonance of the two protons embedded within the metatungstate $[H_2W_{12}O_{40}]^{6-}$ ion at ca. 6.0 ppm, allowing to give a direct measure of the diffusion coefficient of the POM species. Very small changes in either chemical shift or diffusion coefficient *D* (260-245 μm$^2$/s) were observed with increasing amount of POM in solution, in agreement with very weak interaction with this POM.

In summary, $^{1}$H NMR results including DOSY are fully consistent with electrochemistry showing that the strength of the host-guest interaction increases following this order: $[H_2W_{12}O_{40}]^{6-} < [BW_{12}O_{40}]^{5-} < [SiW_{12}O_{40}]^{4-} < [PW_{12}O_{40}]^{3-}$.

### 2.3.5 Cloud point temperature measurements and SAXS study

The monotonous trend observed along the native derivatives of the Keggin-type series could be understood by thermodynamic features of the hydration shell around the POM, which is directly related to its chaotropic nature. Actually, it would be important to find a property and develop a method to classify the chaotropic nature of these inorganic species. It is worth noting that it exists a method described by Hofmeister in the 19$^{th}$ century, based on the visual observation of the “salting in” or “salting out” effect resulting of the presence of various ions within aqueous solution of proteins.[48] Inspired by these works, Bauduin et al. developed the Cloud Point Temperature (CPT) measurement, which revealed an excellent method to establish a classification of the chaotropic nature of various POMs.[38]

The evolution of the CPT of a non-ionic surfactant, tetra-ethylene glycol mono-octyl ether ($C_8E_4$), upon addition of POMs was proposed as a tool to evaluate their chaotropic behavior.[38] The $C_8E_4$ surfactant exhibits weak solubility in water which increases in the presence of chaotropic salt. Such an observation can be viewed as the “salting in” effect, previously reported by Hofmeister. However, the temperature increases of the homogenous mixture {POM + $C_8E_4$ + water} leads to the de-mixing of the solution into two distinct phases corresponding mostly to {POM + water} and {$C_8E_4$}. At the de-mixing temperature, the solution becomes turbid and the measured temperature corresponds to the CPT. Then, the experiment consists in measuring the CPT of 60 mM $C_8E_4$ aqueous solutions containing various concentrations of POMs (see Figure 2.13). The corresponding curves obtained for various POM species allow establishing a clear classification of their chaotropic character (see Figure 2.13). For a given POM concentration, higher CPT value results from stronger interaction with the non-ionic surfactant that should be understood as a stronger chaotropic nature of the tested ion. Such a protocol was applied to the four Keggin-type anions investigated here. The results presented in Figure 2.13 are compared to some representative classical chaotropic ions. These results revealed that respective

CPT increase with POM concentration and the magnitude of these variations increase monotonously from $[H_2W_{12}O_{40}]^{6-}$ to $[PW_{12}O_{40}]^{3-}$, *i.e.* from high to low charge density. Even more, these results revealed the superchaotropic behavior of the P-, Si- and B-Keggin POMs which produce much stronger increases of the CPT compared to the classical chaotrope $SCN^-$. The resulting ordering of POMs according to their chaotropic behavior is in full agreement with the series obtained by electrochemistry and NMR measurements.

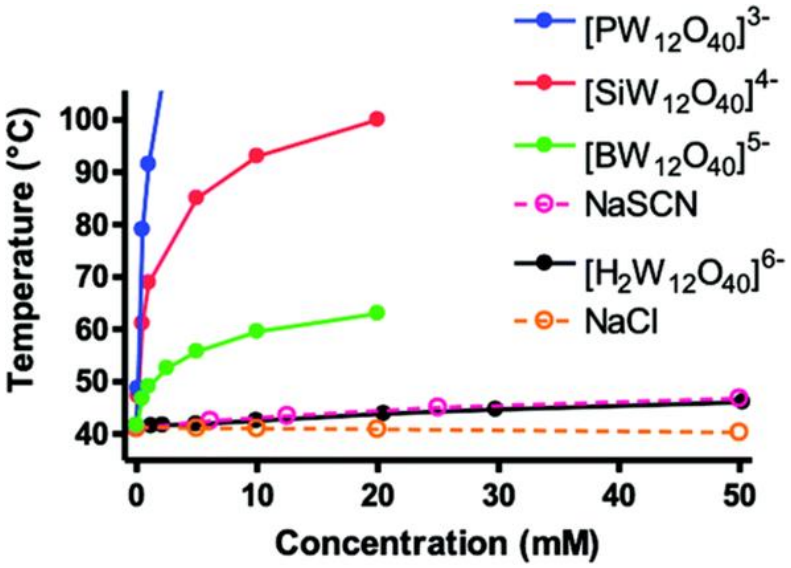


**Figure 2.13** *Cloud point temperature evolution of 60 mM $C_8E_4$ as a function of salt concentration for the four isostructural Keggin-ions. The classical salts NaCl (neutral salt) and NaSCN (classical chaotropic salt) are included as references.*

**SAXS study.** SAXS measurements provided further insight into aggregation behavior and repulsive interaction of the Keggin POMs, and thus their the superchaotropic character (see Figure 2.14). The SAXS spectra have been measured at room temperature from homogeneous aqueous solutions containing $C_8E_4$ (60 mM) and POMs (10 mM). The SAXS spectrum of $[H_2W_{12}O_{40}]^{6-}$ / $C_8E_4$ solution shows the same scattering pattern as that observed for bare $[H_2W_{12}O_{40}]^{6-}$ aqueous solution. On the contrary, SAXS spectrum of $[BW_{12}O_{40}]^{5-}$ / $C_8E_4$ solution exhibits a well-defined oscillation at about $q$ = 1 $nm^{-1}$, which is even more pronounced with $[SiW_{12}O_{40}]^{4-}$. According to the literature, this oscillation is characteristic of core–shell structuration which should be described as POM-decorated $C_8E_4$-based micelles.[38,49]

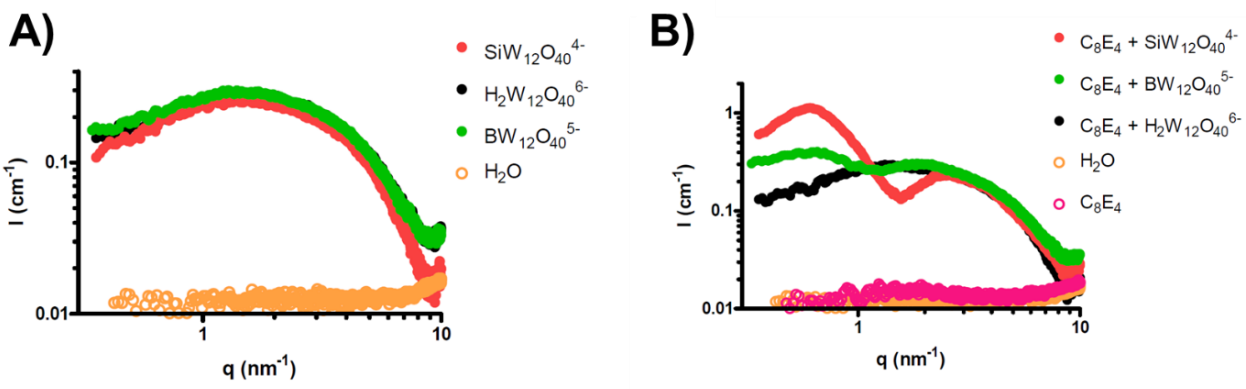


**Figure 2.14** *SAXS-spectra of 10 mM Keggin-POM in water A) without or B) with 60 mM $C_8E_4$. The background scatterings of water and solution of $C_8E_4$ are additionally shown.*

Furthermore, the scattering intensity at low *q* values (q ~ 0,2 $nm^{-1}$) increases also in the series $[H_2W_{12}O_{40}]^{6-}$ < $[BW_{12}O_{40}]^{5-}$ < $[SiW_{12}O_{40}]^{4-}$, in accordance with the formation of larger aggregates, which pinpoint stronger interaction. Then, increase of the oscillation magnitude and the scattering intensity in the Keggin-ion series is a direct indicator of the extent of POM adsorption onto the $C_8E_4$-micelles resulting in the same ordering as in other experiments: $[SiW_{12}O_{40}]^{4-}$ > $[BW_{12}O_{40}]^{5-}$ > $[H_2W_{12}O_{40}]^{6-}$. It is worth noting that in the case of $[PW_{12}O_{40}]^{3-}$, precipitation occurs in the presence of $C_8E_4$ micelles, preventing SAXS measurement. Nevertheless, precipitate formation suggests a particularly strong interaction of the $[PW_{12}O_{40}]^{3-}$ ion with the surfactant.

### 2.3.6 Conclusion

Complementary experimental measurements (ITC, NMR, electrochemistry, CPT, and SAXS) had shown that the interaction of the γ-CD with $[H_2W_{12}O_{40}]^{6-}$ is weak ($K_{1:1}$ ≈ 2.3 x $10^1$ $M^{-1}$), while it is very strong with $[PW_{12}O_{40}]^{3-}$ ($K_{1:1}$ ≈ 1.6 x $10^5$ and $K_{1:2}$ ≈ 1.8 x $10^3$ $M^{-1}$). The plot of Log$K_{1:1}$ versus the ionic charge of the Keggin-type anion yields a linear decreasing relationship illustrating the decreasing effect of charge in CD-POM complexation (see Figure 2.15A). When the charge of the POM is reduced systematically keeping the same size and shape ($[XW_{12}O_{40}]^{n-}$; X = 2H, $B^{III}$, $Si^{IV}$, or $P^{V}$, and n = 6, 5, 4, or 3, respectively), the ability to form host-guest complexes increases continuously. The effects governing such supramolecular assemblies are suggested to be directly related to the solvation properties of the POM and depend on their ability of desolvation resulting of adsorption of POM on neutral surfaces such as CD.

While the most charged POMs such as the $[H_2W_{12}O_{40}]^{6-}$ ion showed no affinity to bind CD, the $[BW_{12}O_{40}]^{5-}$ species interacts moderately showing structural model where the POM-CD contact occurs mainly through exterior wall of the macrocycle. Last, the less charged $[SiW_{12}O_{40}]^{4-}$ or $[PW_{12}O_{40}]^{3-}$ ions are able to form host-guest sandwich-type complexes involving either the primary face or the secondary face of the CD as decreasing further the global charge of the POM (see Figure 2.15B). Besides, POM/CD association has dramatic consequences on the redox properties of POM consisting of a significant decrease in the standard redox potential. This effect can be understood as a partial removal of the hydration shell of the redox active ions arising from the presence of bulky γ-CD in the close vicinity of the POM. It is worth noting that opposite effects corresponding to a redox potential increase were commonly observed for interaction of the reduced derivatives with cations such as protonation or ion-pairing with lithium cation. Finally, the propensity of the Keggin-type anions to bind to γ-CD can be dramatically tuned by reversible electron transfer as it will be further demonstrated in next section.

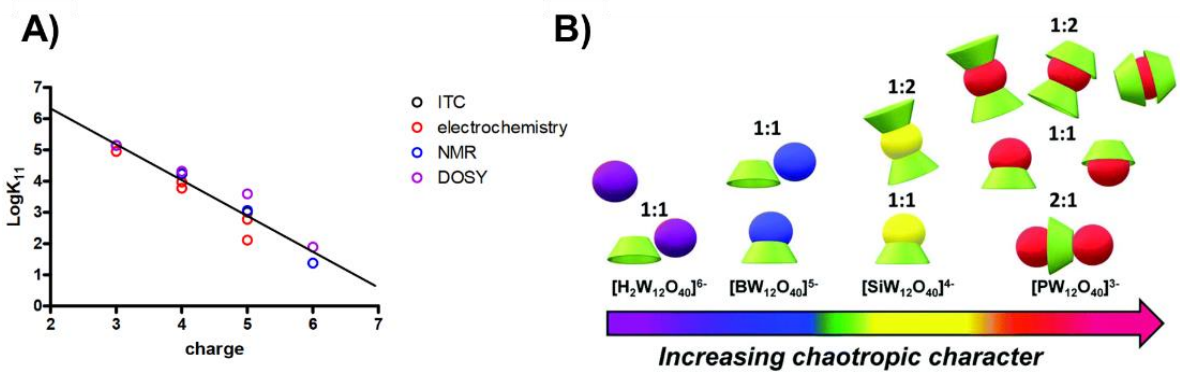


**Figure 2.15** *A) Variation of binding constants in 1:1 adduct between $[XW_{12}O_{40}]^{n-}$ ions and γ-CD as a function of ionic charge of the Keggin-type anion as measured by ITC, electrochemistry and NMR ($^1$H chemical shift and DOSY). B) Illustration of the most representative binding modes involved in the supramolecular assemblies of γ-CD (green torus) and the Keggin anions (spheres).*

Besides, POM/CD association has dramatic consequences on the redox properties of POM consisting of a significant decrease in the standard redox potential. This effect can be understood as a partial removal of the hydration shell of the redox active ions arising from the presence of bulky γ-CD in the close vicinity of the POM. It is worth noting that opposite effects corresponding to a redox potential increase were commonly observed for interaction of the reduced derivatives with cations such

as protonation or ion-pairing with lithium cation. Finally, the propensity of the Keggin-type anions to bind to γ-CD can be dramatically tuned by reversible electron transfer as it will be further demonstrated in next section.

## 2.4 Toward redox molecular switch supramolecular system

POMs have ability to reversibly exchange electrons, and redox activity of POMs is probably the most intriguing and remarkable property of this class of materials. Utilization of POMs in redox processes is now generalized and commonly employed.[50,51] In the previous section, we have demonstrated that the strength of the supramolecular host-guest association between $[XW_{12}O_{40}]^{n-}$ and γ-CD mainly depends on the charge density carried by POM. The charge of POMs can be modified either by varying the nature of the heteroatom X (as demonstrated in **section 2.3**), or by introducing electrons via redox processes, or by substituting metal center by another metallic addenda with different oxidation state. Mixed-metal Keggin anions $[XW_{11}MO_{40}]^{n-}$ can be easily prepared from addition of metal addenda (M = $Mo^{V/VI}$ or $V^{IV/V}$) on monolacunary heteropolyoxotungstates such as $[PW_{11}O_{39}]^{7-}$ or $[SiW_{11}O_{39}]^{8-}$(see Figure 2.16 and experiment part). The oxidized and the one-electron reduced forms of mixed-metal polyanions are highly stable in solution contrary to reduced heteropolytungstates which are easily oxidized in air. This approach therefore offers a very convenient system for tuning the strength of host-guest association through redox stimuli.

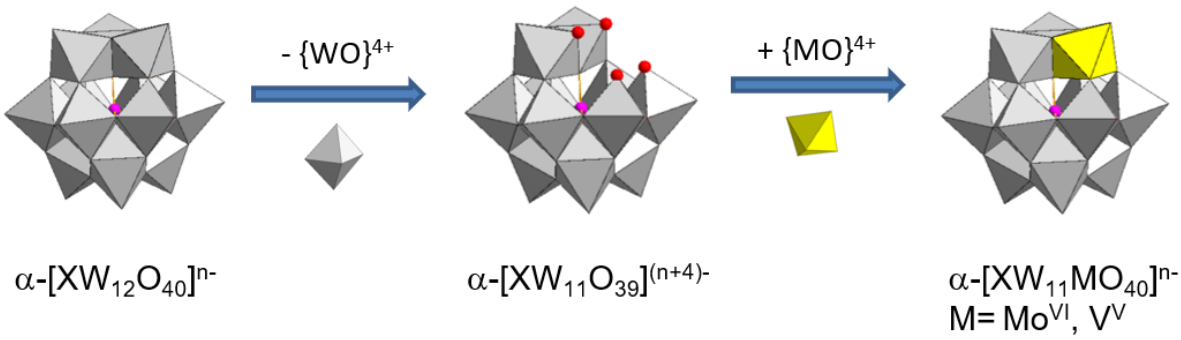


**Figure 2.16** *Schematic representation of formation of mixed-metal Keggin $\{XW_{11}MO_{40}\}^{n-}$ from Keggin-ions to monolacunary Keggin. The POMs used in this study correspond to X = P or Si, and M = $Mo^{VI/V}$ or $V^{V/IV}$.*

In this section, we studied the interaction of γ-CD with mixed-metal Keggin anions $[XW_{11}MO_{40}]^{n-}$, where X = $P^{V}$ or $Si^{IV}$ and M = $Mo^{VI/V}$ or $V^{V/IV}$. Then, varying the redox state of the Mo or the V atoms chemically or electrochemically, complexation was observed in all cases as probed by NMR spectroscopy, ITC, and cyclic voltammetry. As expected, binding affinity was found to depend mostly upon the global charge of the POM, but not on the composition related to the nature of the addenda atoms Mo or V. Actually, host-guest stability increases significantly with decreasing the global ionic charge of the Keggin POM in a similar way to previous study on Keggin-type polyoxotungstates $[XW_{12}O_{40}]^{n-}$. Thus, superchaotropic nature of low charged Keggin POMs was confirmed but can be easily canceled by simple one electron transfer within the POM unit. The current study represents basic fundamental knowledge for the development of smart supramolecular devices with responsive behavior based on change of the redox state of the POM unit.

### 2.4.1 Cyclic voltammetry

POMs exhibit rich electrochemical behavior in solutions with redox response sensitive enough to their local environment (nature of the solvent, ion-pairing, protonation, etc.).[52] The interaction of $[XW_{11}MO_{40}]^{n-}$ anions with γ-CD can be monitored through the variation of the redox potentials of the POM in presence of the tori host. A solution of 1 mM of POM in acidic aqueous solution was then titrated with γ-CD up to 50 equivalents. The resulting CVs obtained for the three oxidized forms of the mixed-metal Keggin anions $[PW_{11}V^{V}O_{40}]^{4-}$, $[SiW_{11}Mo^{VI}O_{40}]^{4-}$, and $[SiW_{11}V^{V}O_{40}]^{5-}$ are shown in Figure 2.17. It should be mentioned that similar CV profiles were also obtained using the reduced forms $[PW_{11}V^{IV}O_{40}]^{5-}$, $[SiW_{11}Mo^{V}O_{40}]^{5-}$, and $[SiW_{11}V^{IV}O_{40}]^{6-}$. As shown in Figure 2.17, presence of γ-CD leads to significant negative shifts of the redox potentials of the Keggin ion as an indication of host-guest complexes formation according to the previous **section 2.3**. Effect of γ-CD has been investigated on the first two quasi-reversible monoelectronic waves in the case of $[SiW_{11}Mo]^{4/5-}$ anions and only for the first exchange of V-containing mixed derivatives because the second transfer in these POMs is not fully reversible and involve more than one electron. The negative shift of potentials indicates that the Keggin anions become more difficult to reduce in presence of γ-CD, meaning the γ-CDs interact much stronger with the oxidized species. Such an effect on redox properties of POMs is opposite to the ion-pairing effect observed in non-aqueous solvents with

lithium or to the protonation in aqueous solution, which both result of stabilizing the reduced POM units.[44]

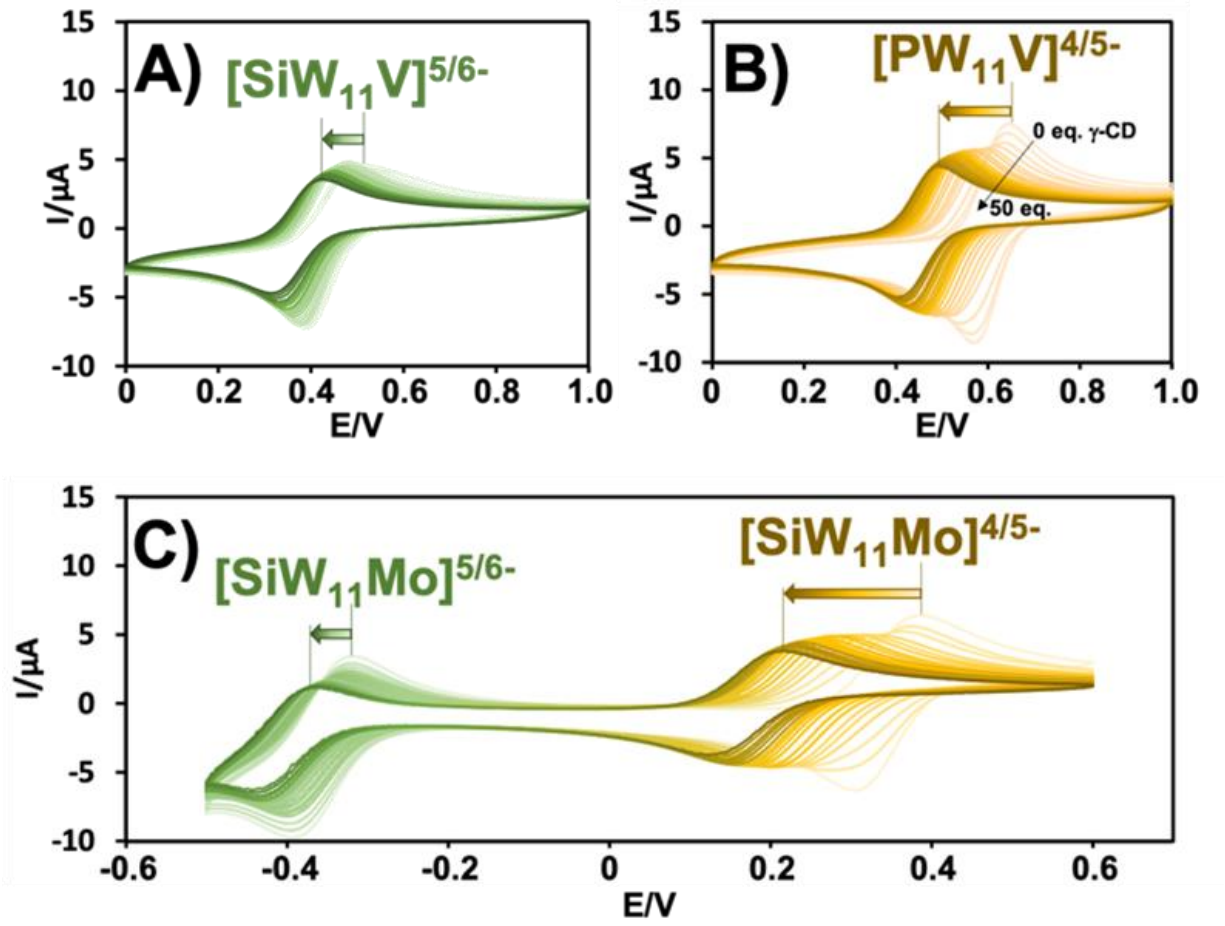


**Figure 2.17** *Cyclic voltammetry of A) $[SiW_{11}V]^{5-}$, B) $[PW_{11}V]^{4-}$, and C) $[SiW_{11}Mo]^{4-}$ anions (1 mmol $L^{-1}$, glassy carbon working electrode, Ag/AgCl reference electrode, scan rate 50 $mV.s^{-1}$) in the presence of increasing amounts of γ-CD (from 0 to 50 equivalents). The experiments have been performed in 50:50 (v:v) HCl (100 mmol $L^{-1}$):NaCl (900 mmol $L^{-1}$) aqueous solution for $[SiW_{11}V]^{5-}$ and $[PW_{11}V]^{4-}$, and 50:50 (v:v) $H_2SO_4$ (500 mmol $L^{-1}$):$Na_2SO_4$ (500 mmol $L^{-1}$) aqueous solution for $[SiW_{11}Mo]^{4-}$.*

Interaction of POMs with neutral hydrophobic surfaces such as CD cavity or alkyl chains of bulky organic cations, is driven by the chaotropic character of POMs that is more effective in their oxidized forms. Indeed, the variation of the redox potential appears less pronounced as the ionic charge of the Keggin ion increases. As shown in Figure 2.18, the variation of the potential upon 50 equivalents addition of γ-CD appears larger for the redox couples $POM^{4-/5-}$ (about -150 mV for $[PW_{11}VO_{40}]^{4/5-}$ and $[SiW_{11}MoO_{40}]^{4/5-}$) than for $POM^{5-/6-}$ couples (about -50 mV for $[SiW_{11}MoO_{40}]^{5/6-}$ and $[SiW_{11}VO_{40}]^{5/6-}$). Such results reflect the influence of global charge density of the guest on the strength of the host-guest interaction. Concomitantly to the shift of the

redox potentials, substantial decrease of the peak currents is also observed upon addition of supramolecular host. This is direct evidence of the formation of inclusion complexes POM@*n*CD which diffuse with a slower rate in the aqueous electrolyte than γ-CD-free Keggin anions. Variation of the observed half-wave potentials can be analyzed quantitatively to estimate the equilibrium constants ($K_{1:1}$ and $K_{1:2}$) of host-guest complexes formation involving the Keggin anions in its both oxidized and reduced states. Such an analysis considers the two consecutive steps of host-guest complexation given in Scheme 2.1 and the resulting Nernst equation (Equations (2.5) and (2.6)).

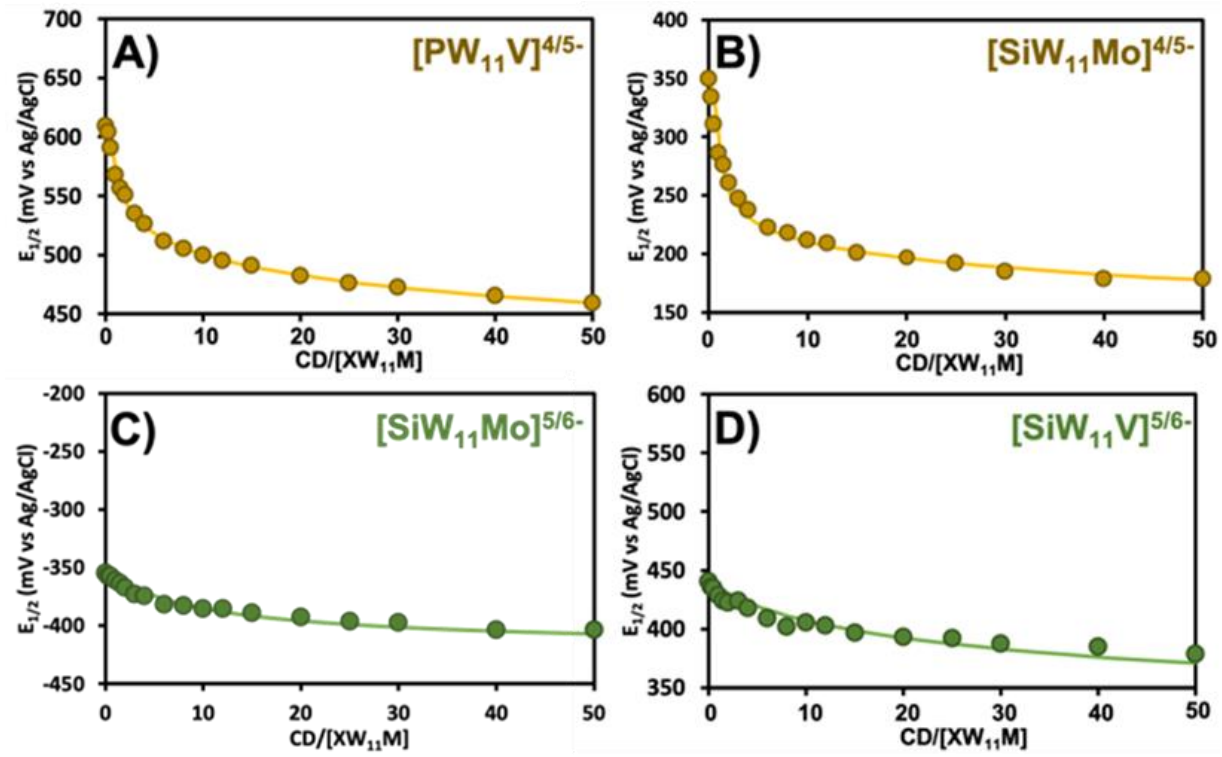


**Figure 2.18** *Variation of half-wave potentials of the couple $[XW_{11}M]^{n/(n+1)-}$ observed in CVs of 1 mM A) $[PW_{11}V]^{4-}$, B) $[SiW_{11}Mo]^{4-}$, C) $[SiW_{11}Mo]^{5-}$, and D) $[SiW_{11}V]^{5-}$ as a function of molar ratio CD/$[XW_{11}M]$. The curves correspond to the best fits of experimental measurements (circles), calculated with Equations (2.5) and (2.6).*

The binding constants $K_{1:1}$ and $K_{1:2}$ are then obtained by fitting the experimental shifts of the apparent potentials shown in Figure 2.18A-C. Analysis of the electrochemical data allows extracting general features which still appear mainly directed by the global ionic charge of the involved species. Then, the redox behavior of the $POM^{4-}/POM^{5-}$ couples is fairly modelled considering the three $K_{1:1}^{ox}$, $K_{1:2}^{ox}$ and $K_{1:1}^{red}$ stability constants associated to the

consecutives processes presented in Scheme 2.1, while the fourth $K_{1:2}^{red}$ stability constant can be neglected in the Equations (2.5) and (2.6). Therefore, applying such a treatment for the $[PW_{11}V^{V}O_{40}]^{4-}$/$[PW_{11}V^{IV}O_{40}]^{5-}$ and $[SiW_{11}Mo^{VI}O_{40}]^{4-}$/$[SiW_{11}Mo^{V}O_{40}]^{5-}$ systems gave satisfactory fits shown in Figure 2.18A-B, using stability constant values for $K_{1:1}^{ox}$, $K_{1:2}^{ox}$ and $K_{1:1}^{red}$ of 9200, 220, and 290 $M^{-1}$ for the former, and 20000, 400, and 340 $M^{-1}$ for the second, respectively. Moreover, calculations of the $[POM]^{5-}$/$[POM]^{6-}$ redox system requires only the single $K_{1:1}^{ox}$ stability constant while the three others remain close to zero ($K_{1:2}^{ox} = K_{1:1}^{red} = K_{1:2}^{red} \approx 0$) and have been then neglected in the Nernst equation, i.e., Equation (2.6). In this way, the behavior of the second one-electron transfer involving the $[SiW_{11}Mo^{V}]^{5-}$/$[SiW_{10}W^{V}Mo^{V}]^{6-}$ system (see Figure 2.17C) has been modeled using $K_{1:1}^{ox} = 340\ M^{-1}$ while similar analysis for the $[SiW_{11}V^{V}O_{40}]^{5-}$/$[SiW_{11}V^{IV}O_{40}]^{6-}$ system leads to $K_{1:1}^{ox} = 590\ M^{-1}$ (see Figure 2.18D). Thus, the behavior of the less charged ionic species $POM^{4-}$ must be analyzed by taking into account the two consecutive complexation steps, while for the other anions $POM^{5-}$ with larger ionic charge, only the 1:1 complex formation is significant. Furthermore, the $K_{1:1}$ stability constant exhibits the highest values (ca. 20000-9200) for the $POM^{4-}$ anions and falls down of two orders of magnitude (ca. 600-300) as the ionic charge increases to give the $POM^{5-}$ ion. At last, $POM^{6-}$ species exhibit only negligible affinity for γ-CD as shown by corresponding $K_{1:1}$ and $K_{1:2}$ constant values close to zero (see Table 2-7 below).

### 2.4.2 $^{1}$H NMR and DOSY studies in solution

Like in **section 2.3**, we also investigate the formation and stability of mixed metal Keggin POM complexes with γ-CD by $^{1}$H NMR spectroscopy in similar way. For such a study, in contrast to the electrochemical study, we observe the supramolecular behavior by probing the effect of the guest on the host. Therefore, a 2 mM aqueous solution of γ-CD is systematically titrated with the six different Keggin anions to monitor changes in CD NMR. The $^{1}$H NMR spectra obtained in the range of 3.7 to 4.5 ppm corresponding to the protons of internal cavity are depicted in Figure 2.19.

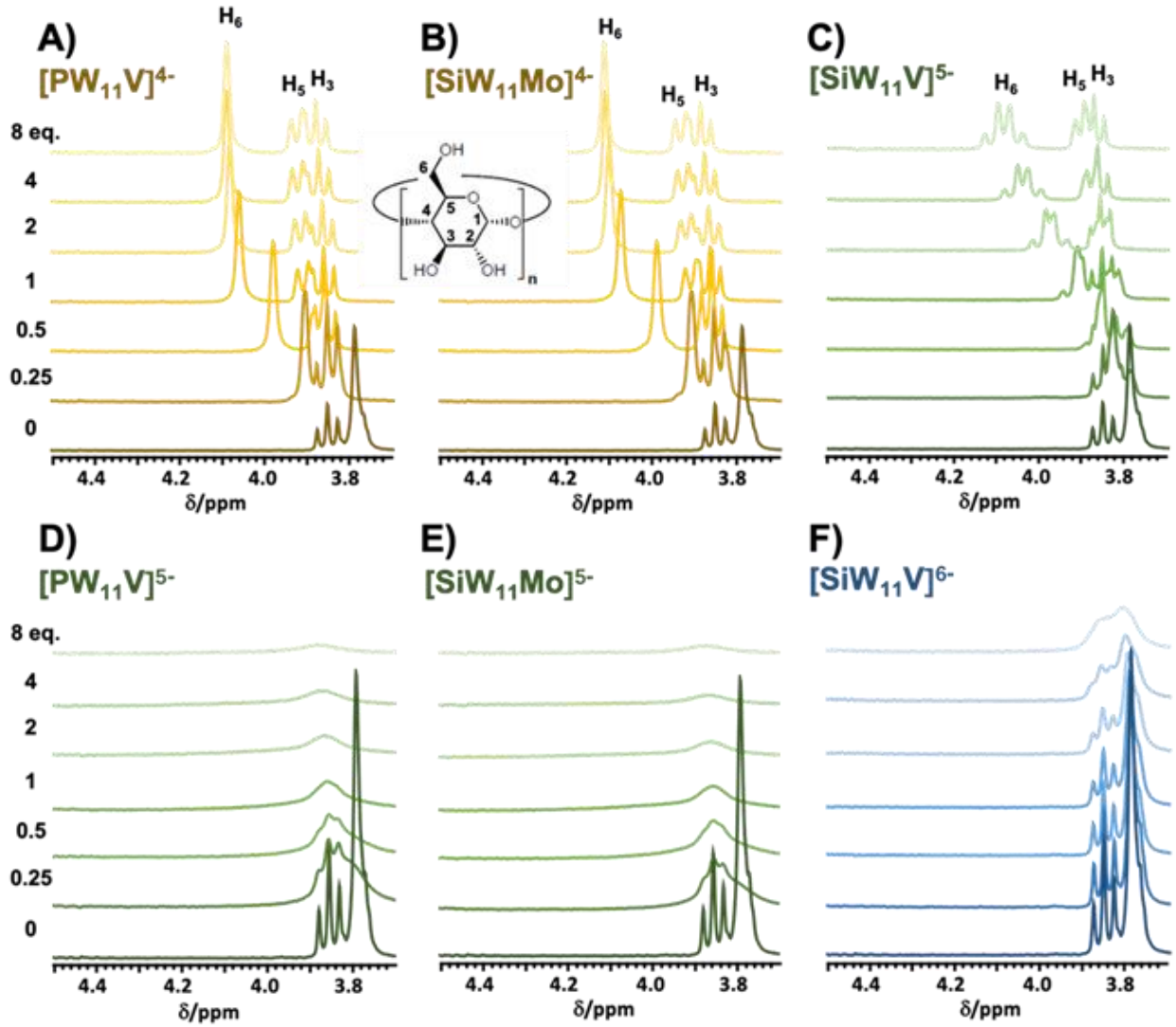


**Figure 2.19** *$^1$H NMR spectra of γ-CD in the chemical shift range for H3, H5, and H6 protons resulting from the titration of 2 mM γ -CD aqueous solution with mixed metal Keggin anions A) $[PW_{11}V]^{4-}$, B) $[SiW_{11}Mo]^{4-}$, C) $[SiW_{11}V]^{5-}$, D) $[PW_{11}V]^{5-}$, E) $[SiW_{11}Mo]^{5-}$, and F) $[SiW_{11}V]^{6-}$.*

The diamagnetic or paramagnetic nature of POM gives rise to different effects on the $^1$H NMR spectrum profile through the supramolecular POM-CD interactions. Titrations with paramagnetic POMs containing the paramagnetic ions $V^{4+}$ or $Mo^{5+}$, in $[PW_{11}VO_{40}]^{5-}$, $[SiW_{11}MoO_{40}]^{5-}$, and $[SiW_{11}VO_{40}]^{6-}$ induce gradual line broadening as a result of nuclear spin–electronic spin dipolar interactions while interaction with diamagnetic POMs $[PW_{11}VO_{40}]^{4-}$, $[SiW_{11}MoO_{40}]^{4-}$, and $[SiW_{11}VO_{40}]^{5-}$ results in continuous variation in the chemical shift of the hydrogen nuclei in contact with the guest. Then, among the six γ-CD resonances, essentially the H3, H5 and H6 resonances undergo significant alterations consistent with the partial inclusion of the

Keggin anion within the γ-CD torus. Moreover, the H6 signal exhibits the strongest effect observed as a low-field shift in the presence of diamagnetic POMs (see Figure 2.19A-C), or as a linebroadening in the presence of paramagnetic POMs (see Figure 2.19D-F). The observed results, in both diamagnetic and paramagnetic cases, should be consistent with through-space magnetic interactions that involves the γ-CD primary rim in a labile complexation mode. As shown in Figure 2.19A-B, the evolution of $^{1}$H NMR spectra upon titration with $[PW_{11}V^{V}O_{40}]^{4-}$ ion appears very similar to that observed with $[SiW_{11}Mo^{VI}O_{40}]^{4-}$, indicating that the host-guest interaction is mainly directed by the overall ionic charge rather than by the POM composition.

Furthermore, H6 resonance gives a single line in the presence of $POM^{4-}$ ion (see Figure 2.19A-B), consistent with a fast exchange process with respect to the NMR time scale. Surprisingly, upon the $[SiW_{11}V^{V}O_{40}]^{5-}$ addition, the shape of the H6 signal splits gradually from single line into two doublets (see Figure 2.19C). Such an evolution is related to a decrease of the dynamic involving the two H6 diastereotopic hydrogen nuclei and then suggests partial hindrance in the vicinity of the primary rim due to supramolecular $POM^{5-}$-CD interactions. Then, the H6 dynamics appear faster in the presence of the $POM^{4-}$ ions, while the corresponding stability constants exhibit the highest values. Interestingly, similar features have been already observed with the two Keggin-types polyoxotungstates $[SiW_{12}O_{40}]^{4-}$ and $[BW_{11}O_{40}]^{5-}$ ions (see Figure 2.10B-C), showing that ionic charge dictates both the thermodynamic stability and the lability of the POM•••γ-CD supramolecular aggregates. At first glance, these apparent contradictory results could be explained by considering the contributors to the ionic recognition process. In one hand, the solvent effects are predominant for low charge density species, identified as superchaotropes. Such a “pushing effect” leads to highly stable aggregates with γ-CD featured by very weak local attractive interactions. These latter, such as ion-dipole interactions or hydrogen bonding, can be considered as “pulling effects”, which favor the frozen configuration as opposed to the pushing effect leading to labile associations. As the ionic charge increases, the chaotropic nature of POM decreases and consequently, the solvent effect (or pushing effect) becomes less predominant, leading to fragile aggregates. However, due to their higher ionic charge, the local “pulling effect” contributes to effective ion-dipole interactions or hydrogen bonding involving the methanolic groups of the

primary ring that become quasi-frozen on the NMR time scale. Such results and related explanations highlight the preponderant role of the solvent within the aggregation process involving POM anions and non-ionic substrate such as γ-CD. In such systems, local attractive intermolecular forces have a minor influence within the thermodynamic stability which appears mainly governed by the chaotropic effect, but have a major effect on the dynamics.

Figure 2.20 shows the calculated curves fitting the experimental data that allow extraction of the binding constants $K_{1:1}$ and $K_{1:2}$. The calculated values, summarized in Table 2-7 (see below), appear in fair agreement with those determined by electrochemistry, although the NMR values are systematically larger than those found by electrochemistry. Such differences could be attributed to the presence of electrolytes required for the electrochemical measurements, which changes the ionic strength or could even compete to some extent within the POM-CD association process.

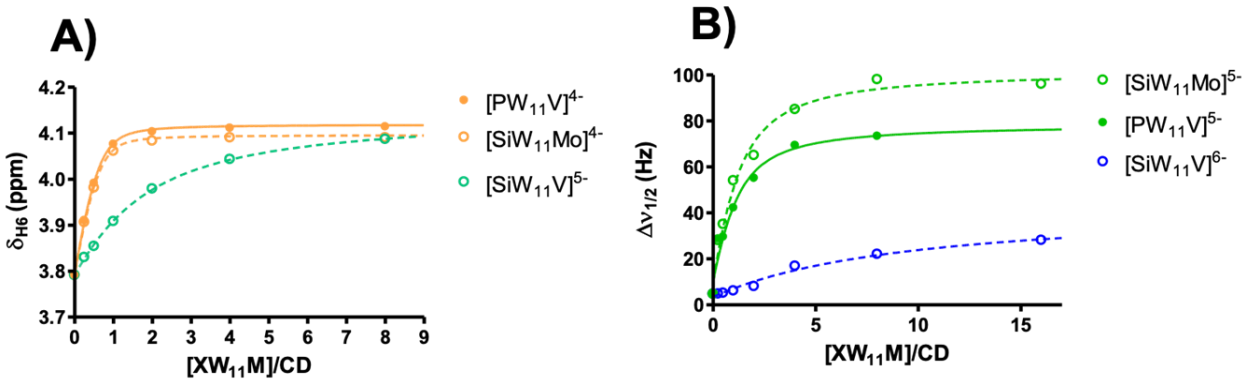


**Figure 2.20** *A) Chemical shifts for H6 and B) Average half-height line width $\Delta\nu_{1/2}$ of resonances H3, H5, and H6, as a function of the POM/CD molar ratio. The curves correspond to the best fit of experimental measurements (circles), calculated with Equations (2.7) and (2.13-15).*

Consistent with the moderate effect of the paramagnetic species $[SiW_{11}V^{IV}O_{40}]^{6-}$ on line-broadening of the γ-CD resonances, the data could be satisfactory modeled with a modest binding constant $K_{1:1}$ of 55 $M^{-1}$ (Figure 2.20B) but long-range paramagnetic effect could not be ruled out. To verify such a hypothesis similar NMR and CV titration experiments were carried out with α-CD and $[SiW_{11}V^{IV}O_{40}]^{6-}$. As expected, no inclusion could occur with this

smaller host molecule as evidenced by electrochemical study where CV patterns were not altered at all with increasing amounts of α-CD. However, similar NMR line broadening effect to that observed with γ-CD was also noticed, which allows to conclude that the broadening in this case would be due to long range contact with paramagnetic POM species rather than to short range complexation. Thus, we could reasonably admit that no significant interaction would take place between this highly charged POM and γ-CD in agreement with previous electrochemical data and as it will be confirmed by ITC (see below). Then, the $K_{1:1}$ stability constant of the $[SiW_{11}V^{IV}O_{40}]^{6-}$/γ-CD adduct should be better considered close to zero.

### 2.4.3 Isothermal titration calorimetry (ITC)

Thermodynamic parameters at 298 K ($\Delta_r H^*$ and $\Delta_r S^*$) from ITC measurements, are given in Table 2-6. Related stability constants at 298 K are provided in Table 2-7 for comparison with those determined by NMR and electrochemistry. As observed with previous chaotropic systems, host-guest supramolecular complexation of mixed Keggin anions with γ-CD is enthalpically driven, partially counterbalanced by entropy penalty. The enthalpy changes range from ca. -30 to -40 kJ $mol^{-1}$ with $POM^{5-}$ Keggin anions while they are slightly higher from ca. -40 to -45 kJ $mol^{-1}$ for complexation involving lower charged POMs $[XW_{11}MO_{40}]^{4-}$. The entropy contribution given by the product $-T\Delta_r S^*$ varies however independently of the charge of the Keggin POM from ca. +15 to +30 kJ.$mol^{-1}$ at 298 K. Consequently, complexes with less charged POMs $[XW_{11}MO_{40}]^{4-}$ showed higher stability than those with higher charged POMs $[XW_{11}MO_{40}]^{5-}$. This trend reflects nicely the results previously obtained by NMR and electrochemistry studies.

**Table 2-6** *Thermodynamic parameters (kJ mol$^{-1}$) at 298 K of 1:1 and 1:2 complexation in mixed metal Keggin. [$XW_{11}M$]:γ-CD systems measured by ITC.*

| [$XW_{11}M$] | [$XW_{11}M$]:CD | $\Delta_r H$* | $-T\Delta_r S$* | $\Delta_r G$* |
|---|---|---|---|---|
| $[PW_{11}VO_{40}]^{4-}$ | 1:1 | -45.3 ± 0.7 | +23.6 ± 0.8 | -21.7 ± 0.1 |
| | 1:2 | -39.7 ± 9.4 | +26.3 ± 10.2 | -13.4 ± 0.7 |
| $[SiW_{11}MoO_{40}]^{4-}$ | 1:1 | -40.2 ± 0.7 | +16.8 ± 0.8 | -23.4 ± 0.1 |
| | 1:2 | -42.7 ± 4.4 | +28.1 ± 4.8 | -14.7 ± 0.3 |
| $[SiW_{11}VO_{40}]^{5-}$ | 1:1 | -31.3 ± 1.6 | +15.9 ± 1.6 | -15.4 ± 0.1 |
| | 1:2 | - | - | - |
| $[PW_{11}VO_{40}]^{5-}$ | 1:1 | -39.9 ± 11.2 | +27.7 ± 11.3 | -12.2 ± 0.1 |
| | 1:2 | - | - | - |
| $[SiW_{11}MoO_{40}]^{5-}$ | 1:1 | -34.0 ± 2.0 | +19.3 ± 2.1 | -14.8 ± 0.1 |
| | 1:2 | - | - | - |
| $[SiW_{11}VO_{40}]^{6-}$ | 1:1 | - | - | - |
| | 1:2 | - | - | - |

**Table 2-7** *Binding constants (M$^{-1}$) of γ-CD with the Keggin-type POMs measured by NMR, CV, and ITC.*

| [$XW_{11}M$] | [$XW_{11}M$]:CD | NMR | Electrochemistry | ITC |
|---|---|---|---|---|
| $[PW_{12}O_{40}]^{3-}$ | 1:1 | 140000 | 90000 | |
| | 1:2 | 800 | 1500 | |
| $[SiW_{12}O_{40}]^{4-}$ | 1:1 | 17000 | 9500 | 17200 |
| | 1:2 | 470 | 150 | 459 |
| $[SiW_{11}MoO_{40}]^{4-}$ | 1:1 | 11000 | 20000 | 17700 |
| | 1:2 | 330 | 400 | 371 |
| $[PW_{11}VO_{40}]^{4-}$ | 1:1 | 7800 | 9200 | 8490 |
| | 1:2 | 320 | 220 | 222 |
| $[PW_{12}O_{40}]^{4-}$ | 1:1 | | 6000 | |
| | 1:2 | | 30 | |
| $[PW_{11}VO_{40}]^{5-}$ | 1:1 | 860 | 290 | 164 |
| | 1:2 | 0 | 0 | 0 |
| $[SiW_{11}MoO_{40}]^{5-}$ | 1:1 | 730 | 340 | 478 |
| | 1:2 | 0 | 0 | 0 |
| $[SiW_{11}VO_{40}]^{5-}$ | 1:1 | 390 | 590 | 618 |
| | 1:2 | 0 | 0 | 0 |
| $[SiW_{12}O_{40}]^{5-}$ | 1:1 | | 130 | |
| | 1:2 | | 0 | |
| $[SiW_{11}VO_{40}]^{6-}$ | 1:1 | 0 | 0 | 0 |
| | 1:2 | | 0 | 0 |
| $[SiW_{11}MoO_{40}]^{6-}$ | 1:1 | | <30 | |
| | 1:2 | | 0 | |

The ITC data were found consistent with the 1:2 binding model involving a sequential process for only $[PW_{11}V^{V}O_{40}]^{4-}$ and $[SiW_{11}Mo^{VI}O_{40}]^{4-}$ POMs, whereas $POM^{5-}$based systems ($[PW_{11}V^{IV}O_{40}]^{5-}$, $[SiW_{11}V^{IV}O_{40}]^{5-}$, and $[SiW_{11}Mo^{V}O_{40}]^{5-}$) were analyzed considering only 1:1 stoichiometry. No significant heat exchange was observed in the case of the most charged $[SiW_{11}V^{IV}O_{40}]^{6-}$ ion consistent with negligible interactions with γ-CD. The overall results confirm the NMR and electrochemistry conclusions. ITC also revealed that the binding process is enthalpically driven, but systematically accompanied by an entropic penalty as often observed in inclusion phenomenon with CD involving encapsulation of polynuclear chaotrope entities, such

as dodecaborates or metal-atom clusters.[53,54] These thermochemical fingerprints are consistent with the chaotropic character of Keggin POMs.

### 2.4.4 Conclusion

In summary, electrochemistry, NMR and ITC studies allowed to produce a convergent compiled set of data, showing the close relationship between the supramolecular behavior of mixed metal Keggin-type derivatives toward γ-CD binding and the global ionic charge of the polyanion. Host-guest association strength is directly correlated with POM ionic charge. The $K_{1:1}$ stability constant for the first complexation step was found in the range of ca. $10^5$ $M^{-1}$ for the Keggin $[PW_{12}O_{40}]^{3-}$ ion and drops down to ca. $10^4$ $M^{-1}$ for $POM^{4-}$ ions and until ca. $10^2$-$10^3$ $M^{-1}$ for $POM^{5-}$ species. Besides, the highest charged Keggin $[SiW_{11}VO_{40}]^{6-}$ exhibited negligible values of $K_{1:1}$. Actually, such a variation corresponds to the decrease of the stability constant by one order of magnitude in average per increasing the global charge by one unit in similar way to previous study with native Keggin anions $[XW_{12}O_{40}]^{n-}$. This follows nicely the classification of the chaotropic character of the Keggin POM previously established by its ability to adsorb on neutral micelle surfaces (CPT measurements). Driven by the chaotropic effect, the affinity between Keggin-type POMs and γ-CD can be tuned finely over a wide range of stability constants up to three orders of magnitude of variation. It was shown that such a motif of assembly can be described as a “pushing effect” mainly orchestrated by the water molecules of the hydration sphere while we evidence by NMR that the “pulling factor”, such as ion-dipole interaction or hydrogen bonding do not contribute significantly within the host-guest stability but have a significant influence upon the local dynamics. Consistently, the global charge of the polyanion appears as the key factor affecting the strength of the host-guest association. Monosubstituted Keggin-type phospho- or silico-tungstates containing $Mo^{V/VI}$ or $V^{IV/V}$ as addenda offer a wide choice of redox active species $[XW_{11}MO_{40}]^{n-}$ with standard potential varying in the [+0.6 ; -0.2] V *vs* Ag/AgCl. Then, one-electron transfer is easily achievable and controllable either chemically or electrochemically resulting in significant change of the stability constants of the host-guest CD-POM complexes highlighted in Figure 2.21. This interesting property could be exploited in future application in the field of redox-responsive smart materials.

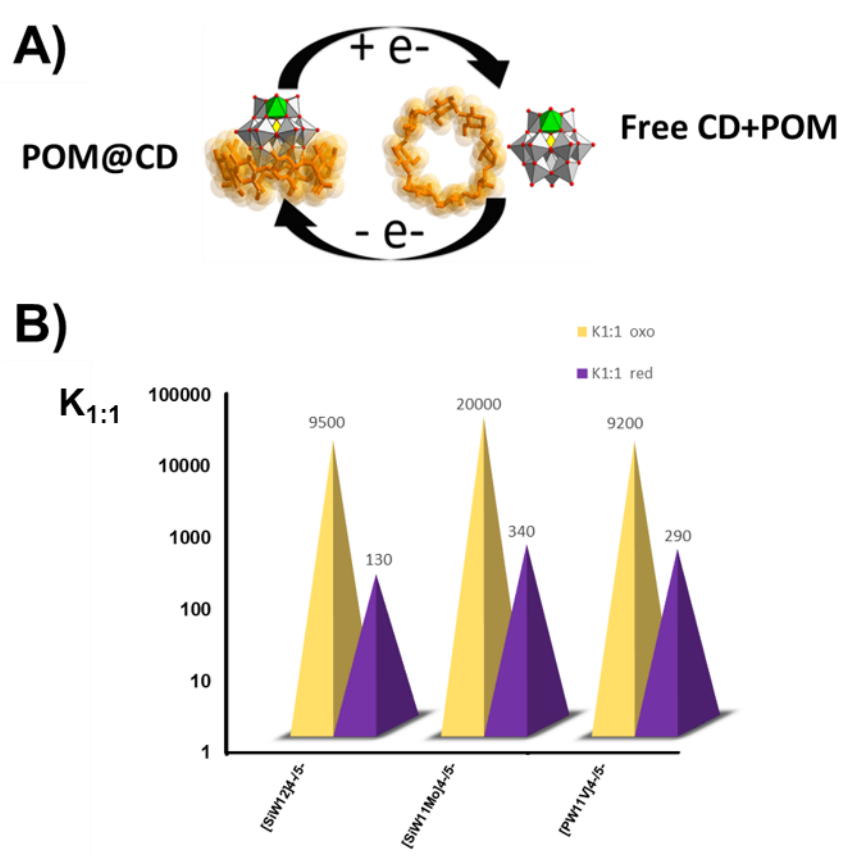


**Figure 2.21** *A) Redox responsive host-guest POM@γ-CD complexation. B) Variation of binding constants in 1:1 adduct between $[XW_{11}MO_{40}]^{5/4-}$ POM and γ-CD upon one-electron oxidation/reduction.*

## 2.5 Hydrolytic stability improvement of $[PM_{12}O_{40}]^{3-}$ (M = W or Mo)

The POMs of interest in this section are the Keggin-type phospho-molybdate or tungstate, the least stable in aqueous solution but also the most chaotropic. The question then arises: can CD improve their stability and to what extent? The heteropolyanion is composed of a metal-oxo shell containing twelve $MO_6$ polyhedral (M = $Mo^{VI}$ or $W^{VI}$) connected together that defined a central cavity in which a phosphorus atom $P^V$ is located (Figure 2.1), leading to a general chemical formula $[PM_{12}O_{40}]^{3-}$, hereafter abbreviated $\{PM_{12}\}$. Due to their low global ionic charge, their stability in aqueous solution is weak and they only exist in strong acidic medium (generally for pH < 1), which greatly limits their use at pH close to neutral or physiological medium.[57,58]

Hydrolysis of these anions leads to highly charged lacunary Keggin-type POMs like $[PM_{11}O_{39}]^{7-}$ (M = W or Mo) or $[PMo_9O_{34}]^{9-}$ which dominate the phospho-tungstate or -

molybdate speciation, respectively. Although such a degradation process can be avoided in organic solvents, their utilization in biological systems remains hampered. Therefore, finding chemical additives to stabilize the phosphorus-based Keggin structure in aqueous solution is strongly demanding for basic and application purposes.

Now, we have highlighted in previous sections the driving force of the chaotropic effect is able to produce highly stable host-guest supramolecular association between Keggin-type POMs and CDs in solution. Furthermore, the magnitude of effect is more effective for low-charged POMs which are the most hydrolytically fragile. Thus, we can wonder at what extent this supramolecular complexation can increase the hydrolytic stability of these species. In this section, we evaluate the effect of the CD interactions upon the stability at various pH. Indeed, the acidic polycondensation and basic hydrolysis of metal oxides are both processes mainly governed by the pH. Herein, we provide a detailed $^{31}P$ NMR study on the CDs stabilizing effect of Keggin phospho-tungstate and -molybdate POMs over a wide range of pH. The POM speciation and the related formation constants are modeled demonstrating the influence of CDs for expanding the pH stability domain of both $[PW_{12}O_{40}]^{3-}$ and $[PMo_{12}O_{40}]^{3-}$ anions.

### 2.5.1 Mutual interaction of CDs with POMs

Before studying the stabilizing role of CDs on $H_3PW_{12}O_{40}$ and $H_3PMo_{12}O_{40}$, we first need to understand the mutual interaction between POM and the different types of CD. As we discussed above, the main factor directing the strength of the attractive association of CDs for a given POM of comparable size and shape is its overall charge which is directly related to its solvation properties and its chaotropic character. However the size of the cavitand should also be taken under consideration, as this has been reported in similar host-guest systems.[59] In their pioneer work, Stoddart et al. had also shown significant differences in the behavior of $[PMo_{12}O_{40}]^{3-}$ when it reacted with $\gamma$- or $\beta$-CD.[13] Here, we reinvestigate the behavior of these two POMs in the presence of the three types of native CD ($\alpha$, $\beta$ or $\gamma$) in a systematic methodology.

The study of the interaction of Keggin-type POMs with cyclodextrins was carried out by proton NMR through the variation of the chemical shifts of the six types of protons in the molecule, labelled from H1 to H6 (see Figure 2.9). These experiments involved the preparation of 4 mM aqueous solutions of CD to which a variable number of equivalents of the acid form of the $[PW_{12}O_{40}]^{3-}$ or $[PMo_{12}O_{40}]^{3-}$ anions were added. The pH in these solutions was not controlled and varied from ca. 0.5 to 2 depending on the proportion of the POM. The purpose of this titration is to identify the protons that will be most affected and to assess its magnitude as a result of the interaction between the POM and the CD. Protons pointing towards the cavity (H3 and H5) and those of the methoxy group (H6) are generally the most subject to interactions with guest molecules. The profile of the spectra and the effects of the presence of POM are different depending on the size of the CD. However, similar results were obtained with both POMs, i.e., $[PW_{12}O_{40}]^{3-}$ and $[PMo_{12}O_{40}]^{3-}$, confirming that the nature of the metal content does not affect the interaction with the CD. As an example, the spectra of Mo-based systems are shown in Figure 2.22.

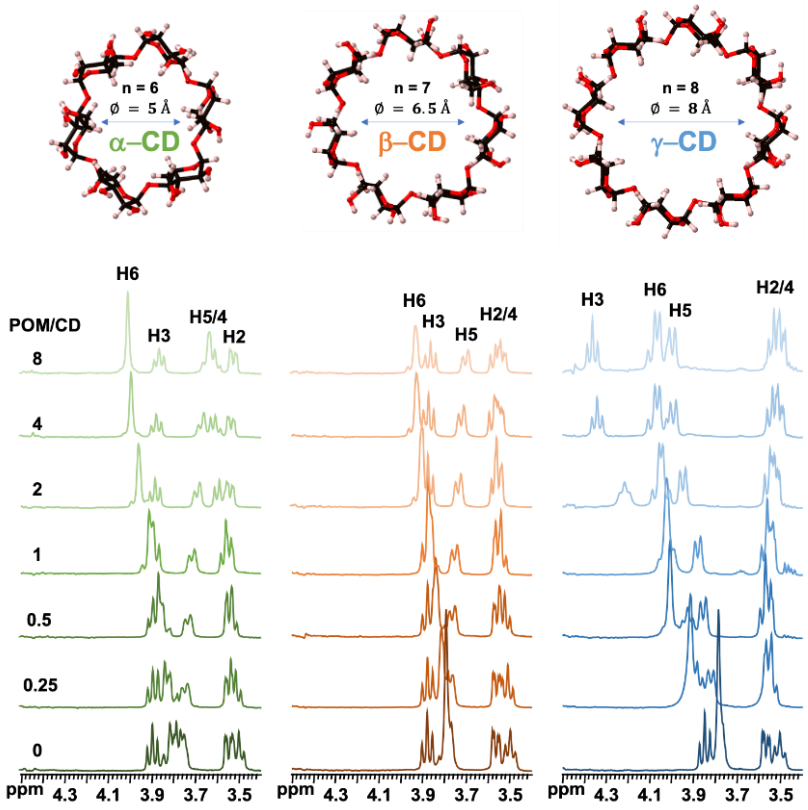


**Figure 2.22** *Partial $^1$H NMR spectra of 4 mM left) α-CD, middle) β-CD, and right) γ-CD after adding increasing amounts of $PMo_{12}O_{40}^{3-}$ up to 8 equivalents.*

The interaction of γ-CD with $\{PW_{12}\}$ species has been extensively studied in **section 2.3**. It has been shown very strong interaction leading to inclusion complexes with association constants of the order of $10^5$ $M^{-1}$. Figure 2.22 shows the evolution of the $^1H$ NMR spectra of a 4 mM γ-CD solution with gradual addition of increasing amount of $\{PMo_{12}\}$ up to 8 equivalents. The evolution of the spectra is very similar to that observed with $\{PW_{12}\}$ (see Figure 2.10a), but different from that reported by Stoddard et al.,[13] probably because of the difference in experimental conditions (our solutions being 4 times more concentrated). As expected, H2 and H4 show negligible effect with only a slight chemical shift variation for H4. However, strong interactions are observed with H5 and H6, undergoing a clear deshielding with a slightly less effect on H5 in the case of $\{PMo_{12}\}$ compared to $\{PW_{12}\}$. Nevertheless, H3 is the most interacting hydrogen, as shown by about 0.7 ppm variation for large POM/CD ratio. Thus, γ-CD appears to interact with POM preferentially through H3 and H5 hydrogens when encapsulated in its cavity. The interaction with the primary face of γ-CD is then privileged as shown by the variations observed on H6. This confirms the mode of POM insertion into the γ-CD cavity from the primary rim. As it has been demonstrated in previous studies, the driving force behind such an association arises from the chaotropic nature of POM which facilitates its desolvation and thus promotes inclusion complexation.

The titration of 4 mM β–CD solution by $\{PMo_{12}\}$ is shown in Figure 2.22. The six types of protons (H1-H6) of the glucopyranose unit show the same NMR signature as their counterpart in the γ–CD molecule. The six signals are resolved with the exception of those attributed to H5 and H6 which overlap mutually. The introduction of the POM in aqueous solution makes it possible to distinguish perfectly the two signals moving each in the opposite direction of the other. No significant effect can be seen for H2 and H3, while H4 and H5 undergo a slight chemical shift of about 0.1 ppm. The hydrogen which interacts the most is H6 shifting of more than 0.15 ppm from the first POM additions and reaches a plateau for 4 equivalents of POM. These results indicate that interactions occur mainly with the primary face of the CD, but no deep inclusion within the organic macrocycle was evidenced since the chemical shift of the internal H3 proton appears quite unaffected. Actually, the supramolecular recognition process involving β-CD and Keggin-type anion

exhibits weak selectivity because the host-guest pairing does not allow the desolvation of the POM unit as observed in inclusion complexes built with γ-CD. In a similar way, a 4 mM solution of α–CD is titrated with the $\{PW_{12}\}$ or $\{PMo_{12}\}$ Keggin-type POMs, and the resulting NMR spectra are shown in Figure 2.22 for $\{PMo_{12}\}$. The six proton types of α-CD are observed as before with a difference in the shape of the H6 signal which changes from a multiplet to a singlet during the titration. All confirms that like β-CD, α–CD is too small to entirely accommodate POM in its cavity.

In summary, the $\{PMo_{12}\}$ or $\{PW_{12}\}$ Keggin-type anions behave similarly toward CD. However, the three CDs interact with the Keggin POM in different ways. The α- and β-CD interact mostly with their outer surface, while γ-CD leads to the usual host-guest inclusion, involving internal cavity. It then becomes interesting to know whether such contrasted supramolecular behavior could have consequences in the particular context of the hydrolytic stability of POMs in aqueous solution.

### 2.5.2 Monitoring hydrolytic stability by $^{31}$P NMR

**$[H_3PW_{12}O_{40}]$.** The stability of $H_3PW_{12}O_{40}$ in pure water and in presence of 2 equivalents of the three forms of CD (α-, β-, and γ-CD) was studied over a pH range from 0 to 8.5 by $^{31}$P NMR. The concentration of the POM was kept constant and the pH was adjusted using concentrated NaOH solutions. Representative $^{31}$P NMR spectra obtained for the pure water system, compared to those contained two equivalents of α- and γ-CD are shown in Figure 2.23. The hydrolytic conversions of $\{PW_{12}\}$ anion have been extensively studied by Maksimovskaya using $^{31}$P NMR, and more recently the previously published work in the field, including her research, has been carefully reviewed, providing the most comprehensive hydrolysis scheme, currently existing.[57,60] The present study allows identifying at least 4 main signals in addition to the signal of the parent Keggin POM $\{PW_{12}\}$, labelled A, B, C, H and F according to the notation of Maksimovskaya and Maksimov.[57] The assignment of these $^{31}$P NMR resonances is reported in Table 2-8 based on this review, although the authors did not provide a clear assignment for the H and F signals. At very low pH, the -14.3 ppm resonance is attributed to $\{PW_{12}\}$. As shown in Fig. 2.23, the hydrolytic degradation of the $\{PW_{12}\}$ occurs as soon as pH > 1.5. From a pH 1.8

solution, many new signals in the [-10.5; -13.5 ppm] range arise from the hydrolytic degradation of the $\{PW_{12}\}$ anion. These species (labelled A, B, C, H, and F) grow as the pH increases to the detriment of the $\{PW_{12}\}$ anion which disappears at pH 2.5. It is also possible that the monovacant $[PW_{11}O_{39}]^{7-}$ species, labelled B and abbreviated $\{PW_{11}\}$ hereafter, begins to form in this pH range but remains as minor product. From pH = 3.9, the $\{PW_{11}\}$ anion becomes predominant, while the other intermediates have almost entirely disappeared. Furthermore, the signal attributed to $\{PW_{11}\}$ is very pH dependent and stabilizes around -9.7 ppm in the 4-8 pH range. Because the resulting transient cationic species $[WO_2(H_2O)_4]^{2+}$ and $[WO(H_2O)_5]^{4+}$ arising from the $\{PW_{12}\}$ hydrolysis would be stabilized in acidic medium, they should be trapped by vacant POMs forming various complexes such as $[PW_{11}O_{39}{\cdot}WO_2]^{5-}$ (species A), $[(PW_{11}O_{39})_2WO_2]^{12-}$ (species C), $[P_2W_{20}O_{70}(H_2O)_2]^{10-}$ (species H), and $[P_2W_{21}O_{71}(H_2O)_3]^{6-}$ (species F). These two latter correspond to sandwich-like POMs resulting from assemblies of two trilacunary Keggin $PW_9O_{34}^{9-}$ linked by two or three W centers, have been isolated by Tourné et al.,[61,62] and their $^{31}P$ NMR spectrum is consistent with such assignments.

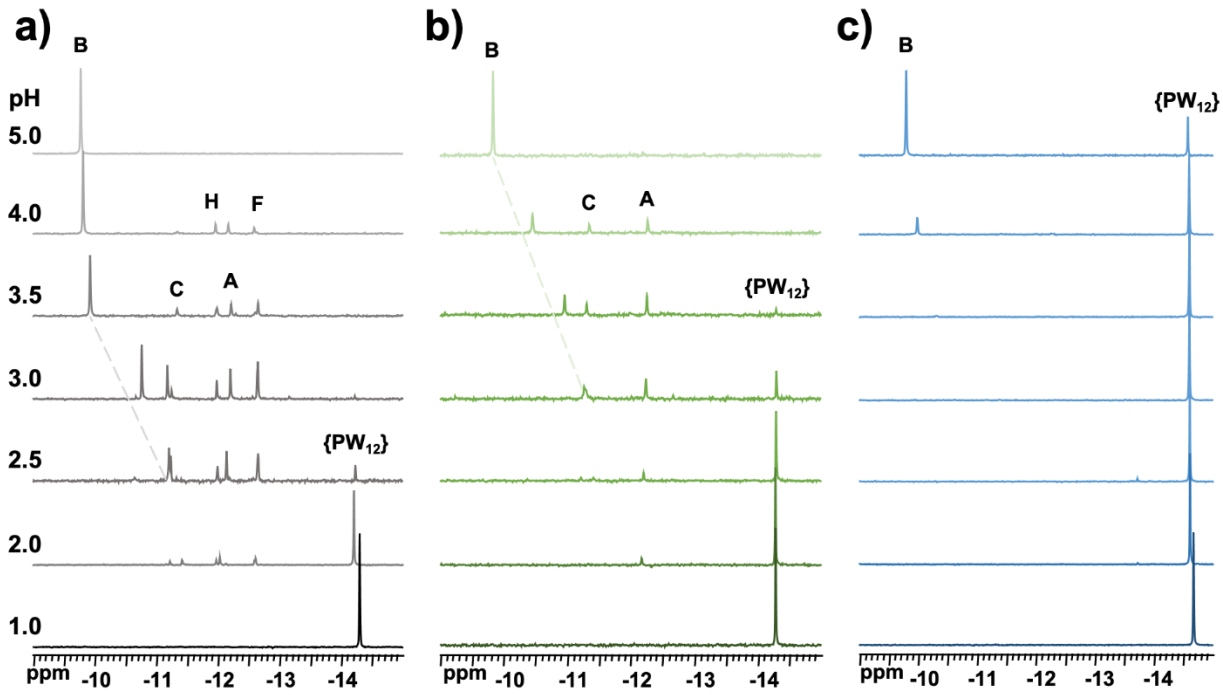


**Figure 2.23** *Representative $^{31}P$ NMR spectra of a) 95 mM $H_3PW_{12}O_{40}$ in $D_2O$, b) 7.5 mM $H_3PW_{12}O_{40}$ in presence of 15 mM $\alpha$-CD in $D_2O$, and c) 60 mM $H_3PW_{12}O_{40}$ in presence of 120 mM $\gamma$-CD in $D_2O$, at various pH, adjusted with concentrated NaOH. All samples were equilibrated for 24 h before NMR measurements.*

**Table 2-8** *Assignment of the main $^{31}P$ NMR signals from degradation of $H_3PW_{12}O_{40}$.*

| Label | Species | $^{31}P$ shift (ppm) | Reference |
|---|---|---|---|
| **{$PW_{12}$}** | $PW_{12}O_{40}^{3-}$ | -14.3 to -14.2 | 60 |
| **A** | $PW_{11}O_{39}{\cdot}WO_2^{5-}$ | -12.3 to -12.0 | 60 |
| **B** | $PW_{11}O_{39}^{7-}$ | -11.4 to -9.8 | 60 |
| **C** | $(PW_{11}O_{39})_2WO_2^{12-}$ | -11.3 to -11.2 | 57 |
| **H** | $P_2W_{20}O_{70}(H_2O)_2^{10-}$ | -12.6 to -12.5 | 61 |
| **F** | $P_2W_{21}O_{71}(H_2O)_3^{6-}$ | -12.0 | 62 |

Similar studies were performed in presence of 2 equivalents α- and β-CDs. The $^{31}P$ NMR spectra corresponding to the α-CD system (see Figure 2.23), reveal that the first intermediate, species A $[PW_{11}O_{39}{\cdot}WO_2]^{5-}$, appears at pH 2. This species continues to form accompanied by a second intermediate, the species C $[(PW_{11})_2WO_2]^{12-}$. Nevertheless, the most abundant species formed corresponds to the monocavant {$PW_{11}$} anion. Furthermore, it can be worth noting that the presence of α- or β-CD reduces the number of intermediates generated form the {$PW_{12}$} degradation. Indeed, the species H $[P_2W_{20}O_{70}(H_2O)_2]^{10-}$ and F $[P_2W_{21}O_{71}(H_2O)_3]^{6-}$ do not appear here, while the species C $[(PW_{11})_2WO_2]^{12-}$ and A $[PW_{11}O_{39}{\cdot}WO_2]^{5-}$ persist over an extended pH range. α- and β-CD produce the same effects upon the hydrolytic behavior of the {$PW_{12}$} anion. In the presence of 2 equivalents **γ-CD**, the chemical system becomes remarkably simple and restricted to the {$PW_{12}$} anion and its hydrolysis product {$PW_{11}$} (see Figure 2.23). For pH < 3.5, only {$PW_{12}$} is present while for pH 4, its intensity ratio decreases in favor of that of the resonance attributed to {$PW_{11}$} (labelled B). The pH must be increased up to 6.7 to observe the complete disappearance of the {$PW_{12}$} in favor of {$PW_{11}$}. Then, no intermediates were observed in this system, and the stability of {$PW_{12}$} was found to be extended at much higher pH. Therefore, the {$PW_{12}$} anion appears very sensitive to pH and hydrolysis equilibria take place as soon as pH = 1.7. Decomposition leads to numerous degradation products but the monovacant POM {$PW_{11}$} becomes predominant from pH 3.5. In the presence of α- or β-CD, much fewer intermediate species were observed and only those based on the {$PW_{11}$} fragment persist. However, the most dramatic effect is observed with γ-CD which suppresses all intermediate species and improves the stability of {$PW_{12}$} at significantly higher pH.

**[$H_3PMo_{12}O_{40}$].** The stability of $H_3PMo_{12}O_{40}$ in pure $D_2O$ and in the presence of 2 equivalents of γ-CD as well as in a 50:50 *v:v* $D_2O$:1,4-dioxane mixture, was studied over a pH range of 0 to 7 by $^{31}P$ NMR. The concentration of POM was kept constant at 60 mM in all three systems and the pH was adjusted using concentrated NaOH solutions. Figure 2.24 shows representative $^{31}P$ NMR spectra obtained from these three systems. The four main identified POM species resulting from the {$PMo_{12}$} decomposition in the pH range 0-7 are $[PMo_{11}O_{39}]^{7-}$ ({$PMo_{11}$}), A-$[PMo_9O_{31}(H_2O)_3]^{3-}$ (A-{$PMo_9$}), B-$[H_2PMo_9O_{34}]^{7-}$ (B-{$PMo_9$}), and $[P_2Mo_5O_{23}]^{6-}$ ({$P_2Mo_5$}).[63,64]

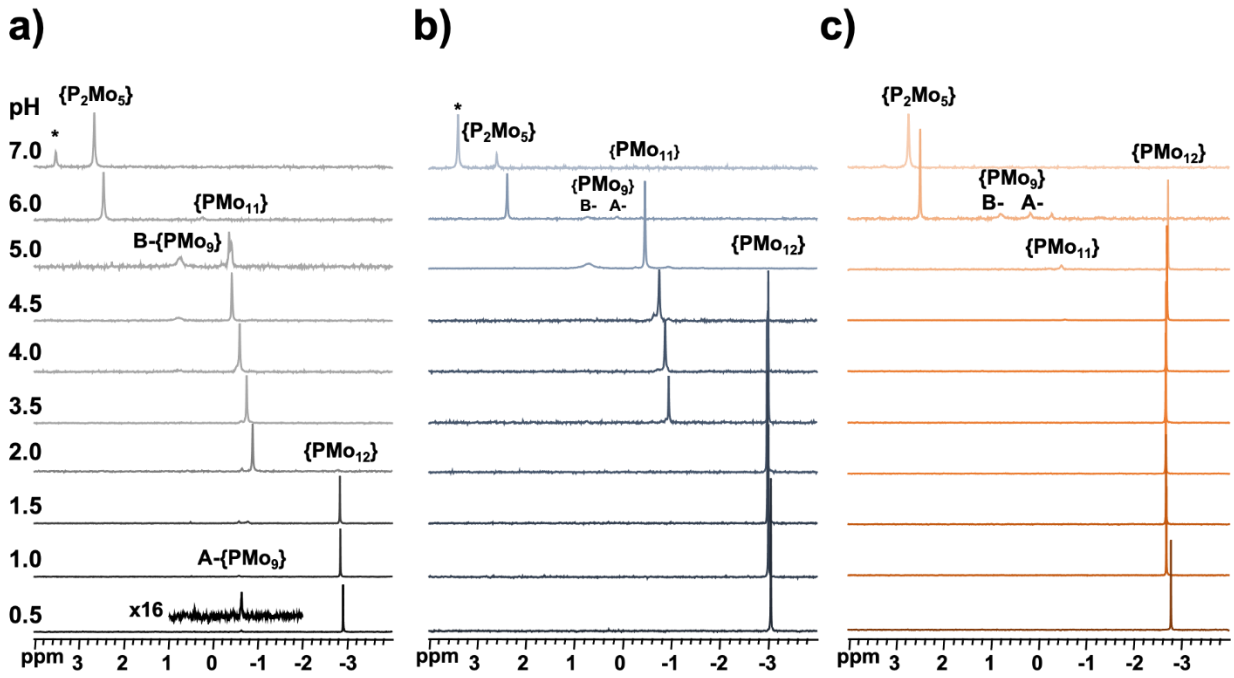


**Figure 2.24** *Representative $^{31}P$ NMR spectra of 60 mM $H_3PMo_{12}O_{40}$ in a) $D_2O$, b) presence of 120 mM γ-CD in $D_2O$, and c) 50:50 v:v $D_2O$:1,4-dioxane, at various pH, adjusted with concentrated NaOH. Asterisk indicates free phosphate $H_2PO4^-$.*

In pure water system (see Figure 2.24), the ca. -3 ppm resonance is attributed to {$PMo_{12}$} and the two other minor signals at -0.6 and 0.4 ppm are assigned to the A-{$PMo_9$} species and to free phosphates $H_3PO_4/H_2PO_4^-$, respectively. From pH = 1.6, many new signals appear between -1 and +3.4 ppm due to the decomposition species of {$PMo_{12}$}. The {$PMo_{11}$} anion is formed from pH = 1.6 and becomes predominant until pH = 4.5. For pH = 5, we observe the formation of the trivacant Keggin-type anion B-{$PMo_9$} identified by the

resonance at +0.6 ppm. Above pH = 6, the solution is dominated by the presence of the $\{P_2Mo_5\}$ species and solvated phosphates $H_2PO_4^-/HPO_4^{2-}$ observed respectively at +2.4

ppm and +3.4 ppm. In the presence of 2 equivalents γ-CD, the $^{31}P$ NMR spectra (Figure 2.24) show the presence of only $\{PMo_{12}\}$ for pH < 2.8, but its signal decreases in intensity to the detriment of the signal of $\{PMo_{11}\}$ when pH increases. The complete disappearance of $\{PMo_{12}\}$ occurs at approximately pH = 4.2. The formation of the $\{PMo_{11}\}$ anion occurs until pH = 6 associated with the presence of the A- and B-forms of the lacunar $\{PMo_9\}$, as minor species. The stabilizing effect of γ-CD on $\{PMo_{12}\}$ is evidenced by two observations. The first one lies on the fact that $\{PMo_{12}\}$ can be dissolved in water without any decomposition as in a mixed hydro-organic medium. The second observation arises from the pH domain of the $\{PMo_{12}\}$ presence, which is extended to more than 2 pH units. However, no significant change in phosphate speciation could be observed for pH above 5, where highly charged $\{PMo_{11}\}$ converts into $\{P_2Mo_5\}$ and free phosphates as observed in pure water. There is almost no action of the γ-CD in this pH range from 5 to 7.

Finally, we also carried out the same experiments in a mixture 50:50 *v:v* $D_2O$:1,4-dioxane, known to stabilize the $\{PMo_{12}\}$ POM, in order to compare the influence of the CD to that of this specific environment (Figure 2.24). Only the $^{31}P$ NMR $\{PMo_{12}\}$ signal is visible over a wide pH range from 0.5 to 4.5. It is remarkable to note the presence of the monovacant $\{PMo_{11}\}$ and trivacant $\{PMo_9\}$ anions only as minor products. However, the fraction of $\{PMo_{12}\}$ decreases until disappearance at pH ca. 7 in favor of $\{P_2Mo_5\}$ as the major end-product. The comparison clearly showed that γ-CD acts as a very good specific stabilizer for the $\{PMo_{12}\}$ anion in aqueous solution. Even if the hydro-organic mixture makes possible to expand the hydrolytic stability of the $\{PMo_{12}\}$ species until pH = 5-6, it should be worth noting that such a comparison requires activity corrections which were not taken into account in this study.

**Quantitative analysis of phosphate speciation.** The previous results showed that distribution of the P-containing species is dependent on the nature of the medium, which can shift the thermodynamic equilibria. From these experimental

measurements, the fraction of the phosphate species can be plotted as a function of the pH for the different media such as pure water ($D_2O$), in the presence of 2 equivalents CD ($\alpha$-, $\beta$-, or $\gamma$-form), and in 50:50 *v:v* $D_2O$:1,4-dioxane, hydro-organic mixture (Figures 2.25 and 2.26). The curves are calculated to best fit our experimental data, making it possible to estimate the formation constants of the various POMs identified during the degradation process of the Keggin-type anions. To this end, we use the individual formation equilibria associated to the formation of each species (see Table 2-9). The formation constants of phosphates, isopolyoxomolybdates, and isopolyoxotungstates should also be taken into account and can be found in the literature.[14] For phosphomolybdates and phosphotungstates, their constants were optimized as a function of the medium to fit the experimental data (see Tables 2-10 and 2-11).

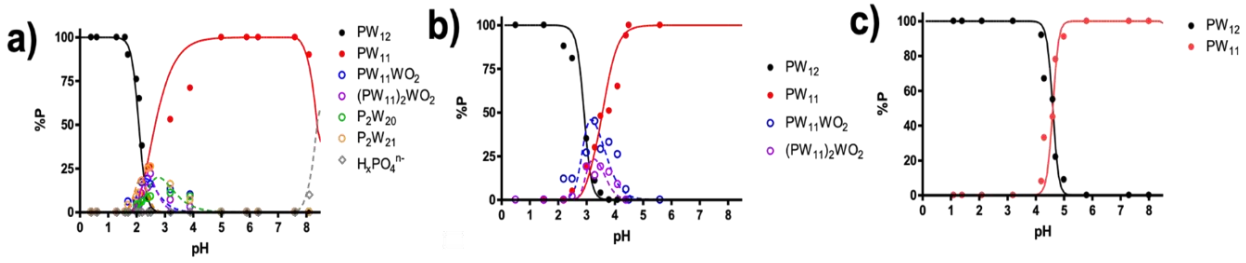


**Figure 2.25** *Phosphate species distributions in a) 95 mM $H_3PW_{12}O_{40}$ in $D_2O$, b) 7.5 mM $H_3PW_{12}O_{40}$ in presence of 15 mM $\alpha$-CD in $D_2O$, and c) 60 mM $H_3PW_{12}O_{40}$ in presence of 120 mM $\gamma$-CD in $D_2O$, from $^{31}P$ NMR spectra. The computed curves correspond to the best fits of experimental data using formation constants reported in* ***Table 2-10****.*

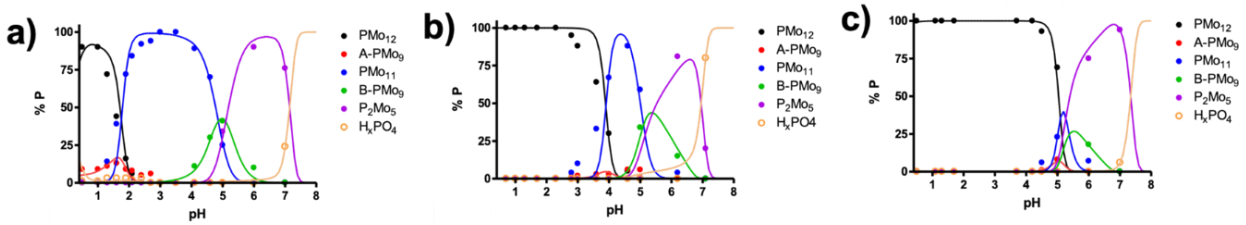


**Figure 2.26** *Phosphate species distributions in 60 mM $H_3PMo_{12}O_{40}$ in a) $D_2O$, b) presence of 120 mM $\gamma$-CD in $D_2O$, and c) 50:50 v/v $D_2O$:1,4-dioxane, from $^{31}P$ NMR spectra. The computed curves correspond to the best fits of experimental data using formation constants reported in* ***Table 2-11****.*

**Table 2-9** *Equilibria used to compute phosphate speciations.*

| Species | Equilibium | Log*K* |
|---|---|---|
| | Free phosphates | |
| $HPO_4^{2-}$ | $PO_4^{3-} + 1\ H^+ \rightleftharpoons HPO_4^{2-}$ | 12.4 |
| $H_2PO_4^-$ | $PO_4^{3-} + 2\ H^+ \rightleftharpoons H_2PO_4^-$ | 19.6 |
| $H_3PO_4$ | $PO_4^{3-} + 3\ H^+ \rightleftharpoons H_3PO_4$ | 21.7 |
| | Isotungstates | |
| $W_7O_{24}^{6-}$ | $7\ WO_4^{2-} + 8\ H^+ \rightleftharpoons W_7O_{24}^{6-} + 4\ H_2O$ | 68.5[a] |
| $W_{10}O_{32}^{4-}$ | $10\ WO_4^{2-} + 16\ H^+ \rightleftharpoons W_{10}O_{32}^{4-} + 8\ H_2O$ | 120.1[a] |
| $H_2W_{12}O_{40}^{6-}$ | $12\ WO_4^{2-} + 18\ H^+ \rightleftharpoons H_2W_{12}O_{40}^{6-} + 8\ H_2O$ | 144.7[a] |
| | Phosphotungstates | |
| $\{PW_{12}\}$ | $1\ PO_4^{3-} + 12\ WO_4^{2-} + 24\ H^+ \rightleftharpoons PW_{12}O_{40}^{3-} + 12\ H_2O$ | 183.1[b] |
| $\{PW_{11}\}$ | $1\ PO_4^{3-} + 11\ WO_4^{2-} + 18\ H^+ \rightleftharpoons PW_{11}O_{39}^{7-} + 9\ H_2O$ | 160.2[b] |
| $\{(PW_{11})W\}$ | $1\ PO_4^{3-} + 12\ WO_4^{2-} + 21\ H^+ \rightleftharpoons PW_{11}O_{39}WO_2(OH)^{6-} + 10\ H_2O$ | 176.0[b] |
| $\{(PW_{11})_2W\}$ | $2\ PO_4^{3-} + 23\ WO_4^{2-} + 40\ H^+ \rightleftharpoons (PW_{11}O_{39})_2WO_2O^{12-} + 20\ H_2O$ | 340.0[b] |
| $\{P_2W_{20}\}$ | $2\ PO_4^{3-} + 20\ WO_4^{2-} + 34\ H^+ \rightleftharpoons P_2W_{20}O_{70}(OH)_2^{12-} + 16\ H_2O$ | 299.3[b] |
| $\{P_2W_{21}\}$ | $2\ PO_4^{3-} + 21\ WO_4^{2-} + 39\ H^+ \rightleftharpoons P_2W_{21}O_{71}(OH)_3^{9-} + 18\ H_2O$ | 320.2[b] |
| | Isomolybdates | |
| $Mo_7O_{24}^{6-}$ | $7\ MoO_4^{2-} + 8\ H^+ \rightleftharpoons Mo_7O_{24}^{6-} + 4\ H_2O$ | 53.5[a] |
| $Mo_8O_{26}^{4-}$ | $8\ MoO_4^{2-} + 12\ H^+ \rightleftharpoons Mo_8O_{26}^{4-} + 6\ H_2O$ | 73.5[a] |
| $Mo_{36}O_{112}^{8-}$ | $36\ MoO_4^{2-} + 64\ H^+ \rightleftharpoons Mo_{36}O_{112}^{8-} + 32\ H_2O$ | 356.2[a] |
| $MoO_2^{2+}$ | $1\ MoO_4^{2-} + 4\ H^+ \rightleftharpoons MoO_2^{2+} + 2\ H_2O$ | 9.8[a] |
| | Phosphomolybdates | |
| $\{PMo_{12}\}$ | $1\ PO_4^{3-} + 12\ MoO_4^{2-} + 24\ H^+ \rightleftharpoons PMo_{12}O_{40}^{3-} + 12\ H_2O$ | 139.7[c] |
| $\{PMo_{11}\}$ | $1\ PO_4^{3-} + 11\ MoO_4^{2-} + 18\ H^+ \rightleftharpoons PMo_{11}O_{39}^{7-} + 9\ H_2O$ | 118.7[c] |
| A-$\{PMo_9\}$ | $1\ PO_4^{3-} + 9\ MoO_4^{2-} + 18\ H^+ \rightleftharpoons A\text{-}PMo_9O_{31}(H_2O)_3^{3-} + 6\ H_2O$ | 107.2[c] |
| A-$\{PMo_9\}$ | $1\ PO_4^{3-} + 9\ MoO_4^{2-} + 17\ H^+ \rightleftharpoons A\text{-}PMo_9O_{31}(OH)(H_2O)_2^{4-} + 6\ H_2O$ | 104.7[c] |
| B-$\{PMo_9\}$ | $1\ PO_4^{3-} + 9\ MoO_4^{2-} + 14\ H^+ \rightleftharpoons B\text{-}H_2PMo_9O_{34}^{7-} + 6\ H_2O$ | 104.9[c] |
| B-$\{PMo_9\}$ | $1\ PO_4^{3-} + 9\ MoO_4^{2-} + 13\ H^+ \rightleftharpoons B\text{-}HPMo_9O_{34}^{8-} + 6\ H_2O$ | 102.0[c] |
| $\{P_2Mo_5\}$ | $2\ PO_4^{3-} + 5\ MoO_4^{2-} + 10\ H^+ \rightleftharpoons P_2Mo_5O_{23}^{6-} + 5\ H_2O$ | 62.0[c] |

[a] : from[14], [b] : values for $D_2O$ and see Table 2-10 for other media, [c] : values for $D_2O$ and see Table 2-11 for other media .

**Table 2-10** *Formation constants (LogK) at 28 °C of phosphotungstate species calculated from degradation of $H_3PW_{12}O_{40}$, in pure Water ($D_2O$), and in presence of 2 equivalents α-, β-, and γ-CD.*

| species | Protonation state | 2 eq. γ-CD in $D_2O$ | 2 eq. β-CD in $D_2O$ | 2 eq. α-CD in $D_2O$ | $D_2O$ |
|---|---|---|---|---|---|
| **{$PW_{12}$}** | $PW_{12}O_{40}^{3-}$ | 208.0 | 196.6 | 196.6 | 183.1 |
| **{$PW_{11}$}** | $PW_{11}O_{39}^{7-}$ | 175.0 | 170.2 | 170.5 | 160.2 |
| **{($PW_{11}$)$WO_2$}** | $PW_{11}O_{39}WO_2(OH)^{6-}$ | | 187.7 | 187.7 | 176.0 |
| **{($PW_{11}$)$_2WO_2$}** | $(PW_{11}O_{39})_2WO_2^{12-}$ | | 363.3 | 363.5 | 340.0 |
| **{$P_2W_{20}$}** | $P_2W_{20}O_{70}(OH)_2^{12-}$ | | | | 299.3 |
| **{$P_2W_{21}$}** | $P_2W_{21}O_{71}(OH)_3^{9-}$ | | | | 320.2 |

**Table 2-11** *Formation constants (LogK) at 28 °C of phosphomolybdate species calculated from the degradation of $H_3PMo_{12}O_{40}$, in water ($D_2O$), with 2 equivalents γ-CD or in 50:50 v:v $D_2O$:1,4-dioxane mixture.*

| Species | Protonation state | 50:50 $D_2O$:Dioxane | 2 eq. γ-CD in $D_2O$ | $D_2O$ | Literature[a] |
|---|---|---|---|---|---|
| **{$PMo_{12}$}** | $PMo_{12}O_{40}^{3-}$ | 159.7 | 152.3 | 142.7 | 139.7 |
| **{$PMo_{11}$}** | $PMo_{11}O_{39}^{7-}$ | 127.0 | 125.2 | 125.3 | 118.7 |
| **A-{$PMo_9$}** | A-$PMo_9O_{31}(H_2O)_3^{3-}$ | | | 111.1 | 107.2 |
| **A-{$PMo_9$}** | A-$PMo_9O_{31}(OH)(H_2O)_2^{4-}$ | 116.9 | 112.9 | | 104.7 |
| **B-{$PMo_9$}** | B-$H_2PMo_9O_{34}^{7-}$ | | | 101.1 | 104.9 |
| **B-{$PMo_9$}** | B-$HPMo_9O_{34}^{8-}$ | 96.6 | 95.5 | | 102.0 |
| **{$P_2Mo_5$}** | $P_2Mo_5O_{23}^{6-}$ | 86.1 | 83.4 | 84.7 | 62.0 |

a) At 25 °C, ionic strength μ = 3 M (NaCl), from reference[64].

We did not find in the literature any formation constants related to the formation of phosphotungstates species. Nevertheless, the constant values corresponding to the formation of {$PW_{12}$} and {$PW_{11}$} are 40 orders of magnitude higher than their molybdenum analogues (Tables 2-10 and 2-11), confirming that phosphotungstate POMs are thermodynamically more stable than their molybdenum equivalents. The presence of CDs led to a significant increase in the formation constant of {$PW_{12}$} by 14 orders of magnitude with α- and β-CD, but by 25 orders of magnitude with γ-CD. Such a stabilizing effect of the {$PW_{12}$} anion takes place at the expense of other less stable POMs such as {$P_2W_{20}$} and {$P_2W_{21}$} anions. For phosphomolybdate speciation, our calculations compare well with published data (Table 2-11). The stability constant of the {$PMo_{12}$} anion increases by 10 orders of magnitudes in the presence of γ-CD, but also remains ca. 10 orders of magnitude lower than the value observed in the mixture 50:50 *v/v* $D_2O$:1,4-dioxane. The equilibrium shifts affect mainly the

stability domain of {$PMo_{11}$}, which disappears almost completely in hydro-organic medium but still persists in water with the presence of γ-CD although considerably reduced (see Figure 2.26). These results confirm quantitatively the stabilizing influence of CDs.

**Stability domain enhancement of phosphorus-Keggin POMs.** Supramolecular associations between Keggin-type POMs and CDs alter significantly the properties of the POM in aqueous solution. Depending on the nature of these interactions, the stability domains of POM can be shifted to a large extent as shown in Figure 2.27. The stability of POM in the presence of α- or β-CD is only slightly improved by about one pH unit (Figure 2.27). These two CDs have shown to behave similarly with the Keggin anion. In fact, the interactions have been identified as non-specific, involving mainly the outer surface of the CDs, leading to very similar and comparable effects. However, γ-CD, acting as a true host molecule for inclusion complexation, its stabilizing effect is much larger. This CD is able to maintain the {$PW_{12}$} anion intact up to near pH = 4, and to expand its existence in aqueous solution up to pH = 6, a value close to that of the physiological pH. In addition, no intermediate decomposition products are observed during the transformation of {$PW_{12}$} into {$PW_{11}$}. Similar behavior was also observed with the less stable {$PMo_{12}$}, but with one pH unit lower, i.e., maintaining its structure intact up to pH = 3, and its existence up to pH = 5 (Figure 2.27).

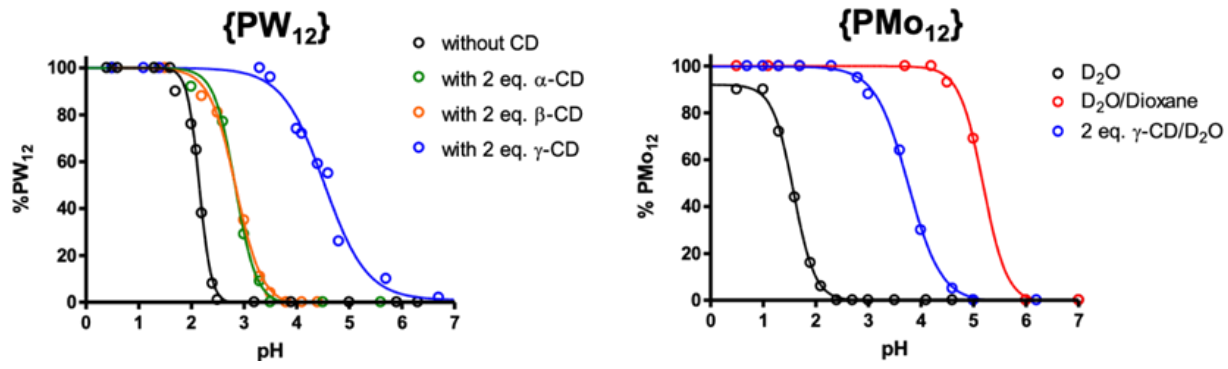


**Figure 2.27** *Effect of medium on stability domains of Keggin POM {$PW_{12}$} and {$PMo_{12}$} as measured by $^{31}P$ NMR (see Figures 2.25 and 2.26).*

### 2.5.3 Conclusion

The stabilizing role of cyclodextrins on $[PW_{12}O_{40}]^{3-}$ and $[PMo_{12}O_{40}]^{3-}$ has been studied by NMR spectroscopy. While degradation of POMs occurs at pH ca. 1.5 and becomes complete until pH = 3, we show that specific supramolecular interactions are able to expand the pH stability scale. The α- and β-CD showed similar interactions in solution, which were identified as non-specific due to small size of the cavities compared to the size of the Keggin anion. Conversely, the larger γ-CD exhibits specific recognitions with the POM, leading to a stable host-guest inclusion complex involving two γ-CDs and a POM. As a result, α- and β-CD have a limited stabilizing effect on POMs by expanding their pH stability domain by only about 1 pH unit. Due to the formation of close host-guest assembly, γ-CD acts as a protecting shell for the POM against hydrolytic attack of hydroxide ions. Significant stability improvement has been demonstrated, up to pH = 5 for $[PMo_{12}O_{40}]^{3-}$ and pH = 6 for $[PW_{12}O_{40}]^{3-}$. We highlight that these POM@CD supramolecular interactions, driven by the chaotropic effect were strong enough to modify the speciation diagram of metalate ions or increase significantly the rate of the polycondensation processes.[14,65] Moreover, such an interaction-type, directed by the chaotropic effect reveals important consequences about the solution properties of POMs, that could be one of the important keys for a rational understanding of the POM behavior in complex matrices, such as biological media or aqueous wastes.

## 2.6 Summary and general conclusions

We demonstrated that this intriguing host-guest association between POMs and CDs is driven by the chaotropic effect which consists of solvent effect based on water structure recovery process resulting from the desolvation of the interacting units, i.e., POM and cavitand. As a consequence, the binding constant between γ-CD and Keggin $[XW_{12}O_{40}]^{n-}$ anions can be controlled by the global charge density of the POM from $n$ = 3 to 6, an tuned finely from K ~$10^5$ to ~$10^1$ (see Figure 2.28). This can be achieved by changing the heteroelement X, where X = P, Si, B, or 2H, but also by changing the redox state of the POM. Then, by using a series of molybdenum and vanadium monosubstituted anions, controlled reduced species could be performed delivering unique redox-responsive host guest systems. At last but not least, the

encapsulation of the POM within the CD provides an increase of the hydrolytic stability of inorganic guest, herein the Keggin-type polyoxometalate $[PM_{12}O_{40}]^{3-}$ anion (M = $W^{VI}$ or $Mo^{VI}$). While degradation of POMs occurs at pH ca. 1.5 and becomes complete until pH = 3, we show that specific supramolecular interactions are able to expand the pH stability domain. Moreover, these preliminary studies on such an interaction type, directed by the chaotropic effect, reveal important consequences about the solution properties of POMs, which should open up new avenues for exciting, extensive and challenging physical chemistry or physics of smart materials.

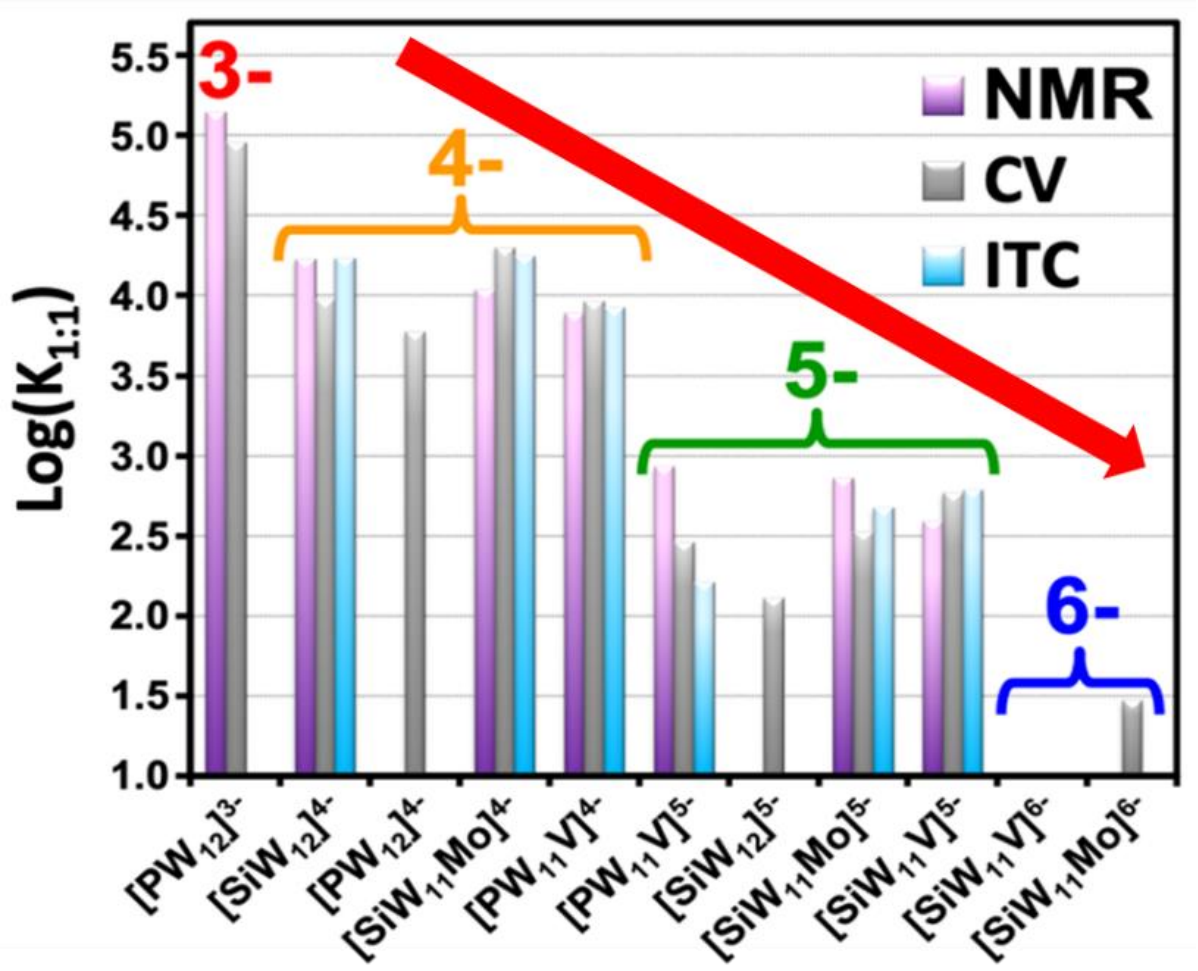


**Figure 2.28** *Summary of affinity constants of Keggin type POMs* $[XM_{12}]^{n-}$ *toward binding to γ-CD to form 1:1 supramolecular complex as obtained from different techniques, showing the general decreasing trend of association strength with increasing the global charge of the POM.*

The current fundamental research sheds light on the remarkable chaotropic behavior of POMs in solution and provides important basic knowledge about supramolecular

association involving POM species that could be used for the rational design of advanced functional hybrid materials. Indeed, hybrid organic−inorganic hydrogels and polymers that exhibit changes in physical and chemical properties triggered by external stimuli are appealing functional materials with intricate features such as self-healing and shape-memory functions.[66] In context, the unique behavior of CD-POM systems opens new perspectives for the design of redox-responsive smart materials.[67] For instance, the redox-active ferrocene group is frequently utilized in the fabrication of CD-based responsive supramolecular systems due to its ability to be encapsulated in or expelled from the β-CD cavity through a single-electron exchange process.[68,69] Keggin-type POMs, like ferrocene, are ideal molecular redox-switching units that possess good size/shape matching with the larger macrocyclic receptor γ-CD. However, in the case of ionic species in aqueous medium, the driving forces are based mostly on the chaotropic character property rather than the hydrophobic effect. Thus, using a hierarchical supramolecular recognition approach from preformed nano-objects constitutes a straightforward synthetic strategy to compartmentalize the complementary units embedded within hybrid supramolecular polymers, such as coacervate, hydrogel, xerogel, or aerogel derivatives.[70] The next chapter will focus on this strategy, using the basic knowledge gained in this chapter.

# Bibliography


1. Stuart, M. A. C. *et al.* Emerging Applications of Stimuli-Responsive Polymer Materials. *Nat. Mater.* **9**, 101–113 (2010).
2. Lendlein, A. & Kelch, S. Shape-Memory Polymers. *Angew. Chem. Int. Ed.* **41**, 2034–2057 (2002).
3. Musarurwa, H. & Tavengwa, N. T. Recyclable Polysaccharide/Stimuli-Responsive Polymer Composites and Their Applications in Water Remediation. *Carbohydr. Polym.* **298**, 120083 (2022).
4. Holliday, B. J. & Mirkin, C. A. Strategies for the Construction of Supramolecular Compounds through Coordination Chemistry. *Angew. Chem. Int. Ed.* **40**, 2022–2043 (2001).
5. Lehn, J.-M. Perspectives in Supramolecular Chemistry—From Molecular Recognition towards Molecular Information Processing and Self-Organization. *Angew. Chem. Int. Ed. Engl.* **29**, 1304–1319 (1990).
6. Nakahata, M., Takashima, Y. & Harada, A. Supramolecular Polymeric Materials Containing Cyclodextrins. *Chem. Pharm. Bull.* **65**, 330–335 (2017).
7. Stasiłowicz-Krzemień, A. *et al.* Cyclodextrin Derivatives as Promising Solubilizers to Enhance the Biological Activity of Rosmarinic Acid. *Pharmaceutics* **14**, 2098 (2022).
8. Saenger, W. Cyclodextrin Inclusion Compounds in Research and Industry. *Angew. Chem. Int. Ed. Engl.* **19**, 344–362 (1980).
9. Lukášek, J. *et al.* Cyclodextrin-Polypyrrole Coatings of Scaffolds for Tissue Engineering. *Polymers* **11**, 459 (2019).
10. Haley, R. M., Gottardi, R., Langer, R. & Mitchell, M. J. Cyclodextrins in Drug Delivery: Applications in Gene and Combination Therapy. *Drug Deliv. Transl. Res.* **10**, 661–677 (2020).
11. Morin-Crini, N. *et al.* 130 Years of Cyclodextrin Discovery for Health, Food, Agriculture, and the Industry: a Review. *Environ. Chem. Lett.* **19**, 2581–2617 (2021).
12. Prochowicz, D., Kornowicz, A. & Lewiński, J. Interactions of Native Cyclodextrins with Metal Ions and Inorganic Nanoparticles: Fertile Landscape for Chemistry and Materials Science. *Chem. Rev.* **117**, 13461–13501 (2017).
13. Wu, Y. *et al.* Complexation of Polyoxometalates with Cyclodextrins. *J. Am. Chem. Soc.* **137**, 4111–4118 (2015).
14. Falaise, C. *et al.* Probing Dynamic Library of Metal-Oxo Building Blocks with γ-Cyclodextrin. *J. Am. Chem. Soc.* **140**, 11198–11201 (2018).
15. Su, P., Smith, A. J., Warneke, J. & Laskin, J. Gas-Phase Fragmentation of Host-Guest Complexes of Cyclodextrins and Polyoxometalates. *J. Am. Soc. Mass Spectrom.* **30**, 1934–1945 (2019).
16. Pacaud, B., Leclercq, L., Dechézelles, J.-F. & Nardello-Rataj, V. Hybrid Core–Shell Nanoparticles by “Plug and Play” Self-Assembly. *Chem. – Eur. J.* **24**, 17672–17676 (2018).
17. Zhang, B. *et al.* Induced Chirality and Reversal of Phosphomolybdate Cluster via Modulating Its Interaction with Cyclodextrins. *Dalton Trans.* **47**, 1388–1392 (2018).
18. Fan, Y., Lu, S. & Cao, J. A Novel Inorganic-Organic Hybrid Complex Between Polyoxometalate and Cyclodextrin: Synthesis, Structure and Catalytic Activity. *Int. J. Mass Spectrom.* **435**, 163–167 (2019).
19. YanXuan, F., Yan, Z., QiaoDi, J., Jie, C. & WenJie, W. The Stabilizing Role of Cyclodextrins on Keggin Phosphotungstic Acid by Complexation Unveiled by Electrospray Mass Spectrometry. *Mass Spectrom. Lett.* **6**, 13–16 (2015).
20. Ni, L. *et al.* Self-Assembled Supramolecular Polyoxometalate Hybrid Architecture as a Multifunctional Oxidation Catalyst. *ACS Appl. Mater. Interfaces* **11**, 38708–38718 (2019).
21. Moussawi, M. A. *et al.* Nonconventional Three-Component Hierarchical Host–Guest Assembly Based on Mo-Blue Ring-Shaped Giant Anion, γ-Cyclodextrin, and Dawson-type Polyoxometalate. *J. Am. Chem. Soc.* **139**, 14376–14379 (2017).
22. Moussawi, M. A. *et al.* Polyoxometalate, Cationic Cluster, and γ-Cyclodextrin: From Primary Interactions to Supramolecular Hybrid Materials. *J. Am. Chem. Soc.* **139**, 12793–12803 (2017).
23. Yang, P. *et al.* Polyoxometalate–Cyclodextrin Metal–Organic Frameworks: From Tunable Structure to Customized Storage Functionality. *J. Am. Chem. Soc.* **141**, 1847–1851 (2019).
24. Rocchiccioli-Deltcheff, C., Fournier, M., Franck, R. & Thouvenot, R. Vibrational Investigations of Polyoxometalates. 2. Evidence for Anion-anion Interactions in Molybdenum(VI) and Tungsten(VI) Compounds Related to the Keggin Structure. *Inorg. Chem.* **22**, 207–216 (1983).
25. Fletcher, H., Allen, C. C., Burns, R. C. & Craig, D. C. Pentapotassium Dodecatungsto-borate(III) Hexadecahydrate. *Acta Crystallogr. C* **57**, 505–507 (2001).
26. Hervé, G. & A, T. Study of Alpha - and Beta -Enneatungstosilicates and -germanates. *Inorg. Chem.* **16**, 2115-2117 (1977).
27. Wu, H. Contribution to the Chemistry of Phosphomolybdic Acids, Phosphotungstic Acids, and Allied Substances. *J. Biol. Chem.* **43**, 189–220 (1920).
28. Assessment, U. E. N. C. for E. Synthesis and Characterization of the Potassium 11-Tungstovanado (IV) Phosphate. Revue Roumaine De Chimie **55**, 843-+ (2009).
29. Grigoriev, V. A., Cheng, D., Hill, C. L. & Weinstock, I. A. Role of Alkali Metal Cation Size in the Energy and Rate of Electron Transfer to Solvent-Separated 1:1 [(M+)(Acceptor)] (M+ = Li+, Na+, K+) Ion Pairs. *J. Am. Chem. Soc.* **123**, 5292–5307 (2001).

30. de Paiva Floro Bonfim, R. *et al.* Synthesis and Structural Characterization of a New Nanoporous-like Keggin Heteropolyanion Salt: $K_3(H_2O)_4[H_2SiVW_{11}O_{40}](H_2O)_8$+x. *Inorg. Chem.* **46**, 7371–7377 (2007).
31. Li, C., Sun, M., Xu, L., Wang, Y. & Huang, J. The First Heteropoly Blue-Embedded Metal–Organic Framework: Crystal Structure, Magnetic Property and Proton Conductivity. *Cryst.Eng.Comm.* **18**, 596–600 (2016).
32. Sanchez, C., Livage, J., Launay, J. P., Fournier, M. & Jeannin, Y. Electron Delocalization in Mixed-Valence Molybdenum Polyanions. *J. Am. Chem. Soc.* **104**, 3194–3202 (1982).
33. Leparulo-Loftus, M. A. & Pope, M. T. Vanadium-51 NMR Spectroscopy of Tungstovanadate Polyanions. Chemical Shift and Line-Width Patterns for The Identification of Stereoisomers. *Inorg. Chem.* **26**, 2112–2120 (1987).
34. Domaille, P. J. The 1- and 2-dimensional Tungsten-183 and Vanadium-51 NMR Characterization of Isopolymetalates and Heteropolymetalates. *J. Am. Chem. Soc.* **106**, 7677–7687 (1984).
35. Kobayashi, D., Nakahara, H., Shibata, O., Unoura, K. & Nabika, H. Interplay of Hydrophobic and Electrostatic Interactions between Polyoxometalates and Lipid Molecules. *J. Phys. Chem. C* **121**, 12895–12902 (2017).
36. Paul, T. J., Parac-Vogt, T. N., Quiñonero, D. & Prabhakar, R. Investigating Polyoxometalate–Protein Interactions at Chemically Distinct Binding Sites. *J. Phys. Chem. B* **122**, 7219–7232 (2018).
37. Solé-Daura, A., Poblet, J. M. & Carbó, J. J. Structure–Activity Relationships for the Affinity of Chaotropic Polyoxometalate Anions towards Proteins. *Chem. – Eur. J.* **26**, 5799–5809 (2020).
38. Buchecker, T. *et al.* Polyoxometalates in the Hofmeister Series. *Chem. Commun.* **54**, 1833–1836 (2018).
39. Assaf, K. I. & Nau, W. M. The Chaotropic Effect as an Assembly Motif in Chemistry. *Angew. Chem. Int. Ed.* **57**, 13968–13981 (2018).
40. Drummond, C., Pérez-Fuentes, L. & Bastos-González, D. Can Polyoxometalates Be Considered as Superchaotropic Ions? *J. Phys. Chem. C* **123**, 28744–28752 (2019).
41. HimenoSadayuki, TakamotoMasayo, SantoRyoko & IchimuraAkio. Redox Properties and Basicity of Keggin-Type Polyoxometalate Complexes. *Bull. Chem. Soc. Jpn.* **78**, 95-100 (2005).
42. Kamata, K. & Sugahara, K. Base Catalysis by Mono- and Polyoxometalates. *Catalysts* **7**, 345 (2017).
43. Buchecker, T. *et al.* Self-Assembly of Short Chain Poly-N-isopropylacrylamid Induced by Superchaotropic Keggin Polyoxometalates: From Globules to Sheets. *J. Am. Chem. Soc.* **141**, 6890–6899 (2019).
44. Konishi, T. *et al.* Impact of the Lithium Cation on the Voltammetry and Spectroscopy of [XVM11O40]n− (X = P, As (n = 4), S (n = 3); M = Mo, W): Influence of Charge and Addenda and Hetero Atoms. *Inorg. Chem.* **59**, 10522–10531 (2020).
45. Schneider, H.-J., Hacket, F., Rüdiger, V. & Ikeda, H. NMR Studies of Cyclodextrins and Cyclodextrin Complexes. *Chem. Rev.* **98**, 1755–1786 (1998).
46. Ivanov, A. A. *et al.* Front Cover: Host–Guest Binding Hierarchy within Redox- and Luminescence-Responsive Supramolecular Self-Assembly Based on Chalcogenide Clusters and γ-Cyclodextrin (Chem. Eur. J. 51/2018). *Chem. – Eur. J.* **24**, 13378–13378 (2018).
47. Schalley, C. A. *Analytical Methods in Supramolecular Chemistry*. (John Wiley & Sons, 2012).
48. Hofmeister, F. About the Science of the Effects of Salts: About the Water Withdrawing Effect of the Salts. *Arch Exp Pathol Pharmacol* **24**, 247–260 (1888).
49. Naskar, B., Diat, O., Nardello-Rataj, V. & Bauduin, P. Nanometer-Size Polyoxometalate Anions Adsorb Strongly on Neutral Soft Surfaces. *J. Phys. Chem. C* **119**, 20985–20992 (2015).
50. Huang, B., Yang, D.-H. & Han, B.-H. Application of Polyoxometalate Derivatives in Rechargeable Batteries. *J. Mater. Chem. A* **8**, 4593–4628 (2020).
51. Sun, J., Abednatanzi, S., Van Der Voort, P., Liu, Y.-Y. & Leus, K. POM@MOF Hybrids: Synthesis and Applications. *Catalysts* **10**, 578 (2020).
52. Sadakane, M. & Steckhan, E. Electrochemical Properties of Polyoxometalates as Electrocatalysts. *Chem. Rev.* **98**, 219–238 (1998).
53. Ivanov, A. A. *et al.* Host–Guest Binding Hierarchy within Redox- and Luminescence-Responsive Supramolecular Self-Assembly Based on Chalcogenide Clusters and γ-Cyclodextrin. *Chem. – Eur. J.* **24**, 13467–13478 (2018).
54. Assaf, K. I. *et al.* Water Structure Recovery in Chaotropic Anion Recognition: High-Affinity Binding of Dodecaborate Clusters to γ-Cyclodextrin. *Angew. Chem. Int. Ed.* **54**, 6852–6856 (2015).
55. Maksimovskaya, R. I. & Maksimov, G. M. P-31 NMR Studies of Hydrolytic Conversions of 12-tungstophosphoric Heteropolyacid. *Coord. Chem. Rev.* **385**, 81–99 (2019).
56. Gumerova, N. I. & Rompel, A. Polyoxometalates in Solution: Speciation Under Spotlight. *Chem. Soc. Rev.* **49**, 7568–7601 (2020).
57. Maksimovskaya, R. I. & Maksimov, G. M. 31P NMR studies of Hydrolytic Conversions of 12-tungstophosphoric Heteropolyacid. *Coord. Chem. Rev.* **385**, 81–99 (2019).
58. Gumerova, N. I. & Rompel, A. Polyoxometalates in Solution: Speciation UnderSpotlight. *Chem. Soc. Rev.* **49**, 7568–7601 (2020).
59. Ivanov, A. A. *et al.* Size-Exclusion Mechanism Driving Host–Guest Interactions between Octahedral Rhenium Clusters and Cyclodextrins. *Inorg. Chem.* **58**, 13184–13194 (2019).
60. Maksimovskaya, R. I. Hydrolysis of Heteropoly Acid $H_3PW_{12}O_{40}$ by $^{31}P$ NMR. *Russ. J. Inorg. Chem.* **43**, (1998).
61. M. Tourné, C. & F. Tourné, G. Aquanonadecatungstodiphosphate(14–) polyanion, [P 2 W 19 O 69 (OH 2 )] 14–: X -ray Crystallographic Structure of Its Potassium Salt, Chemical Relationships in the

Tungstophosphate System, and Conversion into The Diaquaicosatungstodiphosphate $[P_2W_{20}O_{70}(OH_2)_2]^{10-}$. *J. Chem. Soc. Dalton Trans.* **0**, 2411–2420 (1988).
62. M. Tourné, C., F. Tourné, G. & R. Weakley, T. J. Triaquahenicosatungstodiphosphate(6–) Heteropolyanion, $[P_2W_{21}O_{71}(OH_2)_3]^{6-}$: X -ray Crystallographic and 183 W Nuclear Magnetic Resonance Structural Studies. *J. Chem. Soc. Dalton Trans.* **0**, 2237–2242 (1986).
63. Pettersson, L., Andersson, I. & Ohman, L.-O. Multicomponent Polyanions. XXXV: A 31P NMR Study of Aqueous Molybdophosphates. *Multicomponent Polyanions XXXV 31P NMR Study Aqueous Molybdophosphates* **39**, 53–58 (1985).
64. Pettersson, L., Andersson, I. & Oehman, L. O. Multicomponent Polyanions. 39. Speciation in the Aqueous Hydrogen ion-molybdate(MoO42-)-hydrogenphosphate(HPO42-) System as Deduced from a Combined Emf-phosphorus-31 NMR Study. *Inorg. Chem.* **25**, 4726–4733 (1986).
65. Falaise, C. *et al.* 'Host in Host' Supramolecular Core-Shell Type Systems Based on Giant Ring-Shaped Polyoxometalates. *Angew. Chem. Int. Ed. Engl.* **60**, 14146–14153 (2021).
66. Sinawang, G., Osaki, M., Takashima, Y., Yamaguchi, H. & Harada, A. Supramolecular Self-healing Materials from Non-covalent Cross-linking Host–guest Interactions. *Chem. Commun.* **56**, 4381–4395 (2020).
67. Liu, X., Zhao, L., Liu, F., Astruc, D. & Gu, H. Supramolecular Redox-responsive Ferrocene Hydrogels and Microgels. *Coord. Chem. Rev.* **419**, 213406 (2020).
68. Aramoto, H. *et al.* Redox-responsive Supramolecular Polymeric Networks Having Double-threaded Inclusion Complexes. *Chem. Sci.* **11**, 4322–4331 (2020).
69. Sinawang, G., Osaki, M., Takashima, Y., Yamaguchi, H. & Harada, A. Biofunctional Hydrogels Based on Host–guest Interactions. *Polym. J.* **52**, 839–859 (2020).
70. Baroudi, I. *et al.* Supramolecular Assembly of Gelatin and Inorganic Polyanions: Fine-Tuning the Mechanical Properties of Nanocomposites by Varying Their Composition and Microstructure. *Chem. Mater.* **27**, 1452–1464 (2015).

# Chapter 3 Polymeric materials based on POM-CD supramolecular assembly

## 3.1 Introduction

Supramolecular polymers are a class of polymeric materials based on fundamental principles of supramolecular chemistry that deal with molecular recognition processes through a conglomerate of non-covalent interactions.[1] The supramolecular approach for developing smart materials emerged as an appropriate and effective method for assembling and connecting synergistic properties in flexible, tunable and responsive soft matrices.[2] Supramolecular polymers consist of aggregates of molecular chains linked together by non-covalent contacts. Furthermore, some of them exhibit fair solubility in solution and therefore they are characterized by solution and bulk polymer properties.[3] Typically, supramolecular polymer hydrogels are soft materials composed of physically or chemically cross-linked polymer networks embedding large amounts of water.[4,5] Furthermore, they possess unique properties such as temperature responsiveness, photoelectric/chemical reactivity, chemical self-healing, physical adaptability, etc., in relationship with the nature of non-covalent bonds which ensure the polymer cohesion.[6–8] These relevant properties have attracted extensive attention of researchers to the study of supramolecular polymers.[9] In context, supramolecular host-guest polymers based on cyclodextrin (CD) and small organic molecules as guest molecules have been widely reported in many applications, such as self-healing electronic devices, sewage treatment, drug delivery vehicles, wound dressings, and artificial muscles. In addition, this kind of systems show huge potential applications in the field of artificial skin.[10–14] Surprisingly, few polynuclear metal ions or clusters are used as guest components in CD-containing polymers,[15] while this type of inorganic material is expected to exhibit cumulative physicochemical properties that can be used to design smart supramolecular networks.[15–17] Recently, supramolecular host-guest systems based on polyoxometalates (POMs) and cyclodextrins (CDs) have been reported,[15–27] and such a discrete supramolecular POM-CD adduct could be transposed within polymeric matrices. The unique features of POM compounds, which are well-known as electron reservoir units,[30] redox active ions,[31] efficient catalysts,[32] electrochromic

and biologically active species,[33–35] provide relevant prospects in materials science.[36] POMs can exchange electrons reversibly and massively without significant structural changes. Furthermore, in previous chapter of this thesis, the chaotropic or superchaotropic character of the Keggin-type POM anions was evidenced allowing to extend the Hofmeister classification.[18,37] Such a solvation properties occurring in aqueous solution has been identified as the main driving forces in recognition processes with γ-cyclodextrin, leading to unusual very high stability constant. Consistently, it has been demonstrated that the supramolecular host-guest stability strongly dependent on the global charge density.[19,38] Such a feature is relevant for the design of supramolecular polymeric architectures with the ability to modify their physicochemical properties by external stimuli. Nevertheless, only a few studies were reported so far on CD-based polymeric assemblies using POMs as guest species.[39–41] In Chapter 2, we showed that stability constant $K_{1:1}$ of the {POM@γ-CD} supramolecular adduct is directly related to the global charge of Keggin POM. Dissociation process occurs gradually as the ionic charge increases. Furthermore, this spontaneous process resulting from the formation of the {POM@γ-CD} adduct is accompanied by an entropy penalty ($\Delta_r S° < 0$) and a favorable enthalpy change ($\Delta_r H° < 0$) consistent with the decrease of the binding constant with increasing temperature. Accordingly, it seems interesting to develop stimuli-responsive polymers through reversible host-guest interactions between CDs and POMs.

This Chapter describes an efficient and reproducible synthetic method to prepare CD-based polymer precursors abbreviated (γPOL) by condensation of γ-cyclodextrin (γ-CD) with 1,6-hexamethylene diisocyanate (abbreviated HDI). Subsequent crosslinking of the precursor chains with $[XW_{11}MO_{40}]^{n-}$ Keggin type POMs (where X can be $P^{5+}$ or $Si^{4+}$, and M = $W^{VI}$, $V^{V/IV}$ or $Mo^{V/VI}$) via host-guest interactions should be able to produce polymeric materials with improved chemical structure and physical properties. Moreover, these CD-POM polymers are expected to exhibit similar host-guest properties to those observed for the discrete units. Therefore, association-dissociation processes induced by redox or thermal stimulation could give rise to switchable sol-gel phase transitions in supramolecular hydrogels, paving the way for the design of smart functional materials.

## 3.2 CD-based polymeric precursors

### 3.2.1 Synthesis

γ-cyclodextrin (γCD, >99 %) was purchased from TCI. 1,6-diisocyanatohexane (HDI, 98+ %) and *N*,*N*-dimethylacetamide (DMA, 99 %) were purchased from Alfa Aesar. The DMA was dried over 4 Å (8-12 mesh) molecular sieves prior to use. Maleic acid (MA, ≥98 %) was purchased from Honeywell-Fluka. All products were used without any further purification.

Native cyclodextrins are decorated by several exposed hydroxyl groups which offer numerous possibilities for further functionalization (see Figure 3.1A). The synthetic strategy chosen to produce CD-based polymeric precursors consists of condensing γ-CD with HDI (see Figure 3.1B). These precursors will be named *a*POL$_{HDI/CD=m}$, with *a* corresponds to the type of used cyclodextrin (α, β, or γ), and HDI/CD = m is the introduced ratio in the initial synthesis mixture. The same sample could also be named *a*POL$_n$, where *n* correspond to the final molar ratio HDI:CD found in the product.

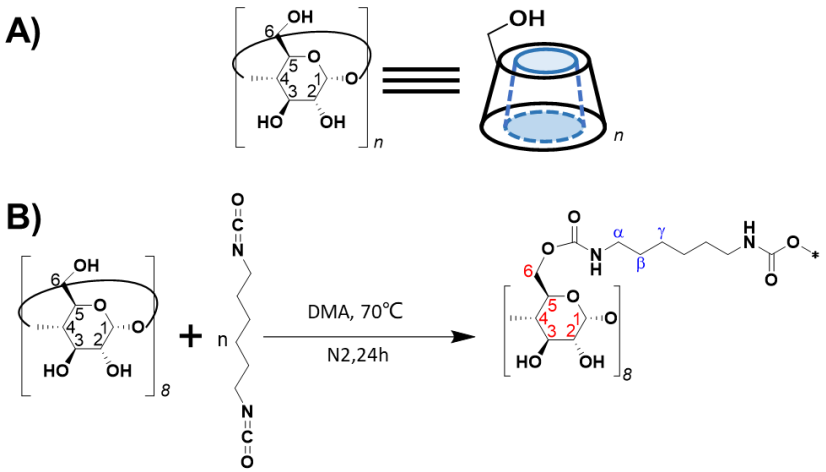


**Figure 3.1** *A) Structure of cyclodextrin. B) Schematic diagram of the synthetic route of γPOL$_n$.*

Then, *a*POL$_n$ materials were synthesized according to previously reported procedures with minor changes.[7,8] All reagents and solvents were carefully dried before use: CD was oven-dried at 110 °C overnight (~1.5-2.5% adsorbed

water according to TGA), while dimethylacetamide (DMA) and HDI were dried over 4 Å (8−12 mesh) molecular sieves. Two synthesis procedures were considered depending on the addition rate of the reagents.

#### 3.2.1.1 Slow drip procedure

Several syntheses were performed with α-, β-, and γ-CD using this slow drip procedure. The initial HDI/CD molar ratios in the synthesis were fixed to 1 for α- and β-CD, while for γ-CD this ratio was varied from 0.4 to 4. Here we give examples of detailed protocols for the synthesis of these oligomers.

**αPOL$_{1,86}$ (or αPOL$_{HDI/CD=1}$).** α-CD (4.86 g, 5 mmol) was dissolved in 50 mL of dried DMA, and then heated to 70 °C under nitrogen atmosphere until all cyclodextrin dissolved. Then a HDI (0.84 g, 5 mmol) solution in 30 mL of dried DMA was added dropwise (1 drop per 10 s) to the previous solution under vigorous stirring. The reactional medium was kept under a nitrogen atmosphere at 70 °C for 24 h (see Figure 3.1B). The solution was then concentrated to ~10 mL by solvent evaporation using a rotary evaporator. The crude product was precipitated by adding dropwise the concentrated solution in 600 mL methanol. After filtration, the solid was washed three times with ~1.8 L methanol to remove traces of DMA and soluble materials. The resulting solid was dried under vacuum and kept in an oven at 100 °C overnight. The mass of the product was 0.9 g.

**βPOL$_{1.41}$ (or βPOL$_{HDI/CD=1}$).** The same procedure as for **αPOL$_{HDI/CD=1}$** was used, except that β-CD (11.35 g, 10 mmol) was dissolved in 100 mL of dried DMA, and a HDI (1.7 g, 10 mmol) solution in 10 mL of dried DMA was added dropwise (1 drop per 10 s) to the previous solution. The mass of the product recovered was 3.9 g.

**γPOL$_{0.35}$ (or γPOL$_{HDI/CD=0.4}$).** The same procedure as for **αPOL$_{HDI/CD=1}$** was used, except that γ-CD (6.5 g, 5 mmol) was dissolved in 30 mL of dried DMA, and a HDI (0.34 g, 2 mmol) solution in 20 mL of dried DMA was added dropwise (1 drop per 10 s) to the previous solution. Here, the crude product was precipitated by adding dropwise the concentrated solution in 600 mL diethyl ether. After filtration, the solid was washed three times with ~1.3 L diethyl ether to remove traces of ethanol and

soluble materials. The resulting solid was dried under vacuum and kept in an oven at 100 °C overnight. The mass of the product was 6.76 g.

**γPOL$_{1.16}$ (or γPOL$_{HDI/CD=1}$).** The same procedure as for **αPOL$_{HDI/CD=1}$** was used, except that γ-CD (13 g, 10 mmol) was dissolved in 100 mL of dried DMA, and a HDI (1.7 g, 10 mmol) solution in 10 mL of dried DMA was added dropwise (1 drop per 10 s) to the previous solution. The mass of the product was 6.26 g.

**γPOL$_{HDI/CD=2}$.** The same procedure as for **αPOL$_{HDI/CD=1}$** was used, except that γ-CD (6.5 g, 5 mmol) was dissolved in 30 mL of dried DMA, and a HDI (1.7 g, 10 mmol) solution in 30 mL of dried DMA was added dropwise (1 drop per 10 s) to the previous solution. The mass of the product was 4.96 g.

**γPOL$_{HDI/CD=3}$.** The same procedure as for **αPOL$_{HDI/CD=1}$** was used, except that γ-CD (6.5 g, 5 mmol) was dissolved in 30 mL of dried DMA, and a HDI (2.52 g, 15 mmol) solution in 50 mL of dried DMA was added dropwise (1 drop per 10 s) to the previous solution. The mass of the product was 6.39 g.

**γPOL$_{HDI/CD=4}$.** The same procedure as for **αPOL$_{HDI/CD=1}$** was used, except that γ-CD (6.5 g, 5 mmol) was dissolved in 30 mL of dried DMA, and a HDI (3.4 g, 20 mmol) solution in 70 mL of dried DMA was added dropwise (1 drop per 10 s) to the previous solution. The mass of the product was 8.3 g.

All soluble samples, when HDI/CD < 2, were fully characterized by solution ($D_2O$) NMR and ESI-mass spectrometry. Here an example of **γPOL$_{HDI/CD=1}$**:

**γPOL$_{1.16}$**. $^1$H-NMR (400 MHz, $D_2O$): 5.60-4.95 (m, 8H, H1), 4.35-3.70 (m, 24H, H3/H5/H6), 3.70-3.35 (m, 16H, H2/H4), 3.25-2.60 (m, 4H, α-$CH_2$), 1.80-1.0 (m, 8H, β/γ-$CH_2$). $^{13}$C{$^1$H}-NMR (100.6 MHz, $D_2O$): 158.0 (C=O), 102.6 (C1), 81.5 (C4), 73.8 (C2), 73.1 (C3), 72.6 (C5), 61.0 (C6), 41.4 (α-$CH_2$), 29.5 (β-$CH_2$), 26.4 (γ-$CH_2$). Mass spectrometry (ESI-): $(C_{48}H_{80}O_{40})_4(C_8H_{12}N_2O_2)_7$, *M,* 6360; $(C_{48}H_{80}O_{40})_3(C_8H_{12}N_2O_2)_6$, *M,* 4896; $(C_{48}H_{80}O_{40})_2(C_8H_{12}N_2O_2)_4$, *M,* 3264 and 3261.

#### 3.2.1.2 Fast drip procedure

The same procedure as before is used, except that the HDI addition rate is changed from 1 drop per 10 s to 1 drop per 1s.

**γPOL$_{0.8}$(or γPOL$_{HDI/CD=0.625}$).** The same procedure as for **αPOL$_{HDI/CD=1}$** was used, except that γ-CD (13 g, 10 mmol) was dissolved in 100 mL of dried DMA, and a HDI (1.06 g, 6.25 mmol) solution in 10 mL of dried DMA was added dropwise (1 drop per 1 s) to the previous solution. The mass of the product was 10.97 g.

**γPOL$_{1.0}$(or γPOL$_{HDI/CD=1}$).** The same procedure as for **αPOL$_{HDI/CD=1}$** was used, except that γ-CD (13 g, 10 mmol) was dissolved in 100 mL of dried DMA, and a HDI (1.7 g, 10 mmol) solution in 10 mL of dried DMA was added dropwise (1 drop per 1 s) to the previous solution. The mass of the product was 10.29 g.

**γPOL$_{1.33}$(or γPOL$_{HDI/CD=1.5}$).** The same procedure as for **αPOL$_{HDI/CD=1}$** was used, except that γ-CD (13 g, 10 mmol) was dissolved in 100 mL of dried DMA, and a HDI (2.55 g, 15 mmol) solution in 10 mL of dried DMA was added dropwise (1 drop per 1 s) to the previous solution. The mass of the product was 7.77 g.

**γPOL$_{1.36}$(or γPOL$_{HDI/CD=2}$).** The same procedure as for **αPOL$_{HDI/CD=1}$** was used, except that γ-CD (6.5 g, 5 mmol) was dissolved in 30 mL of dried DMA, and a HDI (1.7 g, 10 mmol) solution in 30 mL of dried DMA was added dropwise (1 drop per 1 s) to the previous solution. The mass of the product was 3.44 g.

### 3.2.2 Characterization of polymeric precursors

#### 3.2.2.1 Thermal gravimetric analysis

Thermal gravimetric analysis (TGA) measurements were performed to determine the thermal decomposition process of chemical. TGA curve of the representative precursor γPOL$_{1.16}$ is given in Figure 3.2 and compared with those of native γ-CD and HDI. Like the pristine CD, the first mass loss around 110 °C is due to the loss of moisture. Decomposition of the sample at a higher temperature (from 310 to 350 °C) indicates that CD-containing oligomers is produced by HDI reaction with γ-CD. Three thermal events, corresponding to loss of weight can be observed for γPOL$_{1.16}$. The first weight loss that ends at 100 °C is due to adsorbed water. The second weight loss starts at 300 °C and corresponds to the beginning of the combustion of the glucopyranoside macrocycles as also observed for the native γ-CD species in the same temperature range. The third and last decomposition step starts at ca. 350 °C

and ends at 530 °C. A similar behavior is also observed for native γ-CD but this third weight loss occurs and ends in a lower temperature range (about 20 °C). This difference could be due to the presence of HDI linker and generates a weight difference of 13% at 350 °C.

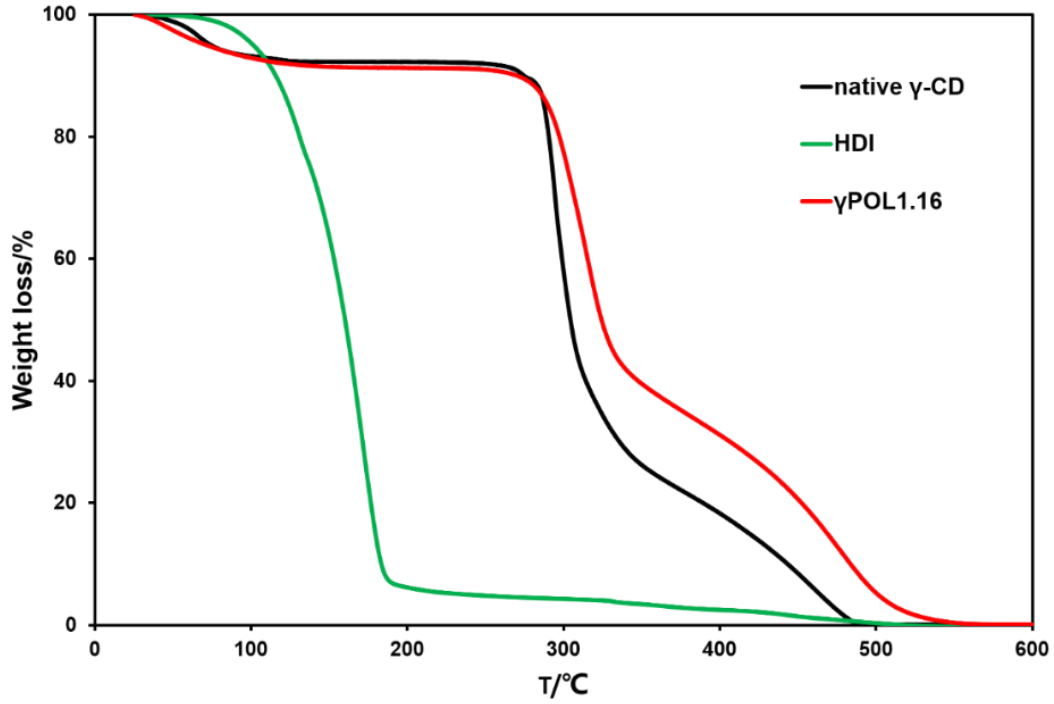


**Figure 3.2** *TGA curves of native γ-CD, HDI and γPOL$_{1.16}$.*

### 3.2.2.2 Optimizing the experimental synthesis by NMR study

The composition and the properties of the resulting CD-based polymeric precursors *a*POL$_n$ are found to be highly dependent upon some parameters of synthesis such as the mixing time. Therefore, two experiments were realized for the synthesis of γ-POL$_n$ precursors, differing by fast dropwise addition of HDI (1 drop per 1 second) and the slow addition (1 drop per 10 seconds). Under same conditions, HDI:γCD synthesis ratios ranging from 0.4 to 4 were tested, and water solubility also checked. The final ratio between HDI and γCD was estimated using $^1$H NMR employing maleic acid (MA) as internal standard (see Equations (3.1)-(3.6) for further details). The experimental methodology consists to add various aliquot of maleic acid to a solution of γ-POL. The resulting $^1$H NMR spectra contains the resonances of the CD, the linker and those of the reference maleic acid. Integrations and quantitative analysis

allow to determine relevant parameters of the *a*POL$_n$, such as *n* which is the HDI/CD ratio and also the number of mole of CD per mg of *a*POL$_n$.

Liquid state $^1$H NMR NMR is a quantitative technique of choice to determine the precursor composition (CD units and hexamethyl linkers per mg) as it is fully soluble in water in the applied conditions. The γCD concentration within the synthesized POL is determined from the integration (*I*) of the $^1$H-NMR signal since it is directly proportional to the number of magnetically active nuclei $N$ per unit responsible for this signal and the concentration $[C]$ of the observed unit:

$$I \propto A^{NMR}.[C].N \qquad (3.1)$$

where $A^{NMR}$ is the response factor of the system to NMR interactions depending on the NMR spectroscopic parameters such as relaxation times $T_1$ & $T_2$, scalar couplings *J*, detection scale calibrations, etc.). Quantitative NMR based on the internal reference method consists of adding an internal standard whose concentration $[C]_{ref}$ is known in the sample. The integration of the resonances of precursor components such as CD and HDI linker, noted $I_i$, with that of the reference $I_{ref}$ allows the calculation of their concentration $[C]_i$ in the sample. From the expression for the integration (*I*):

$$I_i \propto A_i^{NMR}.[C]_i.N_i \qquad (3.2)$$

$$I_{ref} \propto A_{ref}^{NMR}.[C]_{ref}.N_{ref} \qquad (3.3)$$

with, $A_i^{NMR} \sim A_{ref}^{NMR}$, then:

$$\frac{I_i}{I_{ref}} \approx \frac{[C]_i.N_i}{[C]_{ref}.N_{ref}} \qquad (3.4)$$

Finally, we obtain:

$$[C]_i = \frac{I_i.N_{ref}}{I_{ref}.N_i}[C]_{ref} \qquad (3.5)$$

In this work, maleic acid was selected as standard internal reference due to its high purity, stability and solubility in water. Most importantly, this weak diacid (p$K_{a1}$ = 1.9, p$K_{a2}$ = 6.07) is chemically inert toward γCD, and its $^1$H NMR signal is well separated from $^1$H-POL signals (singlet for two protons at + 6.30 ppm in $D_2O$). Besides, the γCD signal selected for integration corresponds to H1 (5.60-4.95 ppm) and accounts for 8 protons. Then, the γCD concentration is calculated with the following established expression:

$$[C]_{\gamma CD} = \frac{I_{H1}.N_{MA}}{I_{MA}.N_{H1}}[C]_{MA} \qquad (3.6)$$

with: $N_{MA}$ = 2, $N_{H1}$ = 8, and $[C]_{MA}$ varied from 8 to 33 mM (see Table 3-1).

In a similar way, the concentration of hexamethyl linker corresponding to reacted HDI is calculated from the integration of the β/γ-$CH_2$ signal observed in the 1-2 ppm range with $N_{CH2}$ = 8. Experimentally, the NMR samples were prepared by mixing the three specific volumes of i) POL solution (Solution A), ii) reference solution of MA (Solution B), iii) and $D_2O$. The sampling carried out for the NMR analysis is detailed in Table 3.1 and typical NMR spectra are presented in Figure 3.3.

**Table 3-1** *NMR experimental titration plan of γPOL$_{HDI/CD=1}$ in aqueous solution (20 mg/mL $D_2O$) using maleic acid as internal standard.*

| POL + Maleic acid (internal standard reference) | | | | | | |
|---|---|---|---|---|---|---|
| γPOL$_{HDI/CD=1}$ Volume Sol. A (µL)[a] | [γCD]$_{POL}$ (mg/mL)[b] | *Maleic acid* Volume Sol. B (µL) | [MA] (mM) | $D_2O$ (µL) | Calculated [γCD]$_{POL}$ (mM) | Calculated [HDI]$_{POL}$ (mM) |
| 200 | 20 | 100 | 8.33 | 300 | 14.7 | 17.0 |
| | | 200 | 16.7 | 200 | 15.1 | 17.6 |
| | | 250 | 20.8 | 150 | 15.4 | 17.6 |
| | | 300 | 25.0 | 100 | 15.1 | 17.5 |
| | | 400 | 33.3 | 0 | 15.1 | 17.8 |
| Averaged [γCD]$_{POL}$ for 20 mg/mL (mM) = | | | | | **15.1 ± 0.2** | **17.5 ± 0.3** |
| Final HDI/γ-CD= | | | | | **1.16± 0.01** | |

*a) Mother solution A of POL used: 60 mg/mL (300 mg in 5 mL of $D_2O$). b) Final POL concentration titrated*

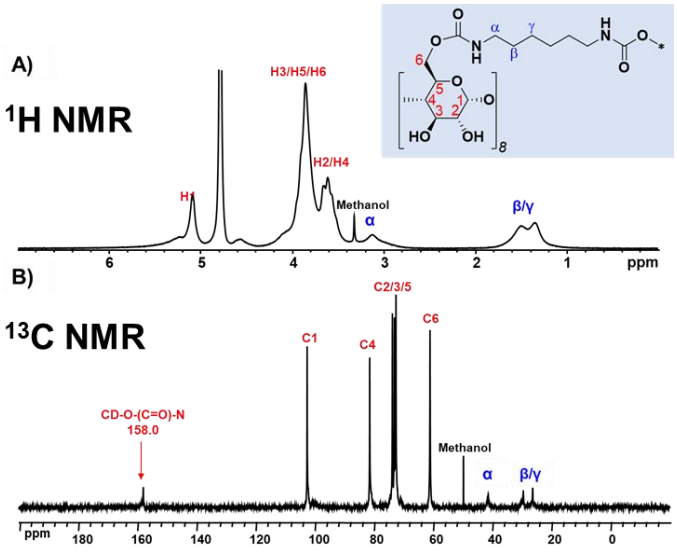


**Figure 3.3** *A) $^1H$ and B) $^{13}C\{^1H\}$ NMR spectra of γPOL$_{1.16}$ in $D_2O$.*

In comparison with the $^{13}C\{^1H\}$-NMR spectrum of the precursor reagent HDI (measured in $CDCl_3$), we note the disappearance of the signal at 122.8 ppm of the isocyanate function (-N=C=O) and the appearance of a new signal at 158 ppm due

to the formation of the carbamate group (-NHCOO-). We therefore can conclude that the HDI reactant has been fully converted during the reaction.

The main properties of the different resulting precursors are given in Table 3-2. Then, the yield of the synthesis, water solubility, and composition were found closely dependent on the synthetic conditions. It can be seen that the HDI:γCD ratio in the final product is generally higher than the initial one of the synthesis medium. However, we note an exception for the rapid drip addition synthesis with high HDI:γCD ratio (> 1) in the synthesis medium (see Figure 3.4 black curve). The possible explanation can be found in the linear propagation favored by rapid dropwise addition leading to a low final ratio HDI:γCD, while slow HDI addition promotes mostly reticulation featured by a high final ratio HDI:γCD. As the condensation reaction is expected kinetically fast and CD offers many reactive exposed and available hydroxyl groups, linear propagation prevents the formation of condensed and compact aggregates, leading preferentially to the formation of smaller oligomeric products obtained in high yield. Interestingly, we observed that the HDI:CD ratios in the polymeric products were always higher than the initial HDI/CD ratios in the synthesis medium with slow HDI addition procedure (see Figure 3.4 blue curve). Therefore, we conclude that the “slow addition” procedure allows a better control of the polymeric precursor formation and better molecular mass weight.

**Table 3-2** *Yield, solubility in water and final HDI:γCD ratio for aPOLn synthesized from “slow or fast additions” of HDI protocol.*

| **Slow drip polymeric precursors (1 drop per 10 s)** | | |
|---|---|---|
| Sample | Initial introduced HDI:γCD ratio | Solubility in water for 500 g.L$^{-1}$ |
| **αPOL$_{1.86}$** | 1 | partial |
| **βPOL$_{1.41}$** | 1 | yes |
| **γPOL$_{1.16}$** | 1 | yes |
| **γPOL$_{0.41}$** | 0.4 | yes |
| **γPOL$_{HDI/CD=2}$** | 2 | no |
| **γPOL$_{HDI/CD=3}$** | 3 | no |
| **γPOL$_{HDI/CD=4}$** | 4 | no |
| **Fast drip polymeric precursors (1 drop per 1 s)** | | |
| Sample | Initial introduced HDI:γCD ratio | Solubility in water for 500 g.L$^{-1}$ |
| **γPOL$_{0.8}$** | 0.625 | yes |
| **γPOL$_{1.01}$** | 1 | yes |
| **γPOL$_{1.33}$** | 1.5 | yes |
| **γPOL$_{1.36}$** | 2 | partial |

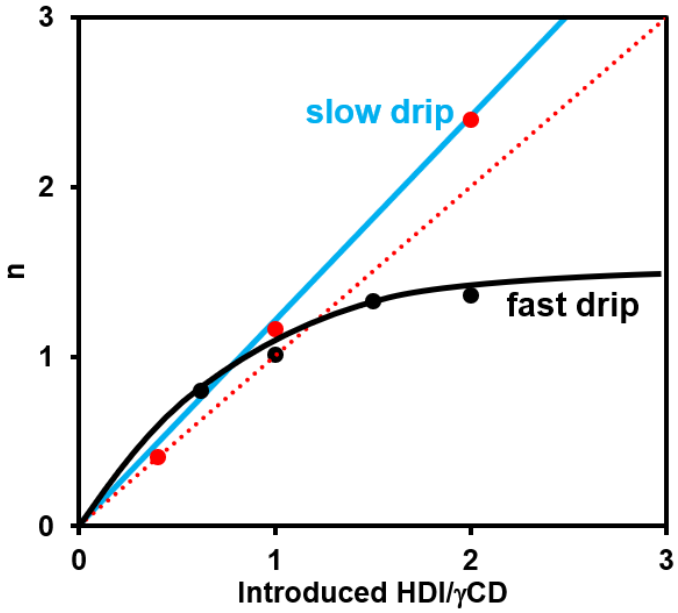


**Figure 3.4** *Evolution curves of n for γPOL$_n$ as a function of initial introduced HDI:γCD ratio using fast (1 drop per 1 s, black curve) or slow (1 drop 10 s, blue curve) addition of HDI during the synthesis. Red line is the reference diagonal, y = x, to guide the eyes.*

Solid-state NMR was also recorded to further characterize the polymeric products, especially those that are insoluble. The $^{13}$C CPMAS spectra of some selected γPOL with different HDI/CD ratio are shown in Figure 3.5 and signal assignments are shown according to solution NMR results (Figure 3.3B) and the literature.[42,43] The characteristic signals of the CD and HDI units in the polymeric precursors are well identified in the spectra, and by integrating the corresponding signals the HDI/CD ratio can be calculated from quantitative direct excitation $^{13}$C measurements (not shown). The resulting HDI/CD ratio are reported in Table 3-3 and compared to liquid $^{1}$H NMR data of soluble samples. We can show that the final HDI/CD ratio is similar, either obtained by liquid $^{1}$H NMR or solid $^{13}$C NMR, validating solid-state NMR as quantitate method to evaluate high HDI/CD ratios. The same trend observed previously, i.e., the final HDI/CD ratio in the solid product is higher than the initial ratio used in the synthesis, is still valid even for high HDI/CD ratios. From the overall results of solution and solid-state NMR (Tables 3-2 and 3-3), it appears clear that HDI/CD ratio exceeding 2 in the final product leads to insoluble polymers.

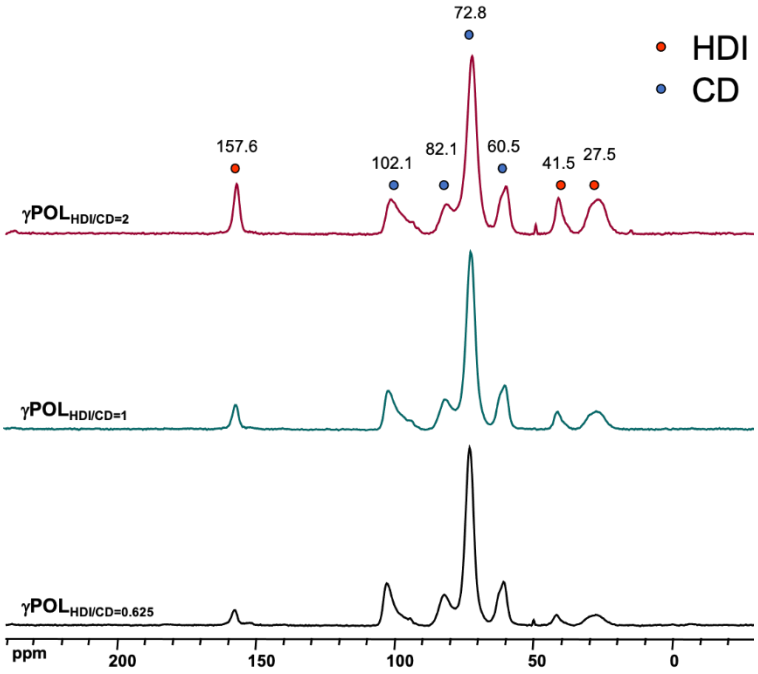


**Figure 3.5** *$^{13}C\{^{1}H\}$ 20 kHz CP-MAS NMR of solid polymeric precursors γPOL$_{HDI/CD=2}$, γPOL$_{HDI/CD=1}$, and γPOL$_{HDI/CD=0.625}$.*

**Table 3-3** *Initial and final HDI:γCD ratios in γPOLn synthesized from "slow additions" of HDI protocol as measured by $^{1}H$ solution and $^{13}C$ solid-state NMR.*

| Sample of γPOL$_{HDI/CD=n}$ | Initial introduced HDI/CD ratio | Final HDI/CD ratio from liquid $^{1}H$ NMR | Final HDI/CD ratio from solid $^{13}C$ NMR |
|---|---|---|---|
| γPOL$_{HDI/CD=0.625}$ | 0.625 | 0.86 | 0.66 |
| γPOL$_{HDI/CD=1}$ | 1 | 1.29 | 1.27 |
| γPOL$_{HDI/CD=2}$ | 2 | insoluble | 2.34 |

### 3.2.2.3 Mass spectrometry.

Mass spectrometry (MS) allows fine characterization of CD and its derivatives at the molecular level. MALDI and ESI soft ionization methods are proven to generate gas-phase ions from non-volatile compounds, allowing rapid characterization of molecular sample distribution and molecular weight. In fact, MS has been used to characterize β-CD derivatives.[44,45] Here, ESI MS was used to assess whether cyclodextrin and HDI were cross-linked in POL to produce aggregates and how they were distributed. It is clear that in negative mode of polymeric precursors γPOL$_{1.16}$ revealed small oligomeric fragments comprising up to four CD units (see Figure 3.6). Furthermore, Table 3-4 shows the distribution of oligomeric fragments, including 1-4 CD units.

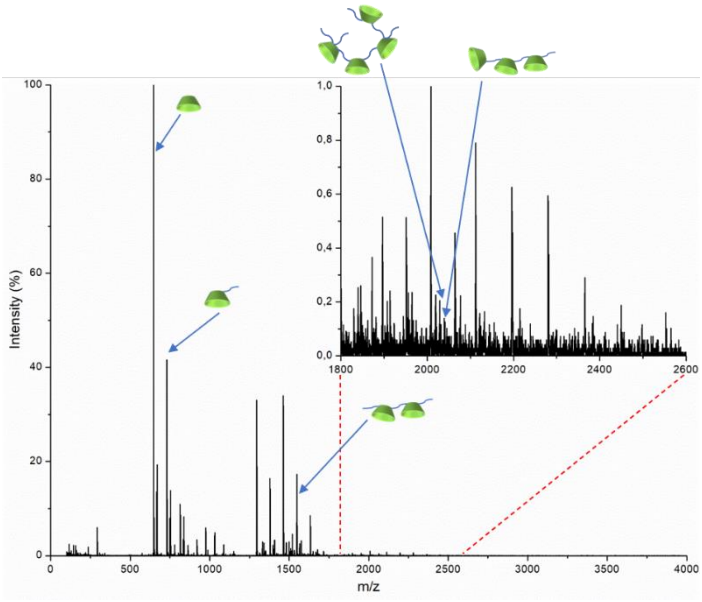


**Figure 3.6** *ESI-MS spectrum of γPOL$_{1.16}$.*

**Table 3-4** *ESI- mass spectrum of γPOL$_{1.16}$, (HDI)m(CD)n in negative ion linear mode. (HDI)**m**(CD)**n** represents the formula γPOL$_{1.16}$ (C$_8$H$_{12}$N$_2$O$_2$)$_m$(C$_{48}$H$_{80}$O$_{40}$)$_n$.*

| m/z | z | m (exp) | m (calc) | n | m |
|---|---|---|---|---|---|
| 2280 | 2 | 4560 | 4563 | 3 | 4 |
| 2196 | 2 | 4392 | 4395 | 3 | 3 |
| 2121 | 3 | 6363 | 6364 | 4 | 7 |
| 2113 | 2 | 4226 | 4227 | 3 | 2 |
| 2065 | 3 | 6195 | 6196 | 4 | 6 |
| 2009 | 3 | 6027 | 6028 | 4 | 5 |
| 1952 | 3 | 5856 | 5860 | 4 | 4 |
| 1896 | 3 | 5688 | 5692 | 4 | 3 |
| 1632 | 2 | 3264 | 3266 | 2 | 4 |
| 1548 | 2 | 3096 | 3098 | 2 | 3 |
| 1464 | 1 | 1464 | 1465 | 1 | 1 |
| 1380 | 2 | 2760 | 2762 | 2 | 1 |
| 1295 | 1 | 1295 | 1297 | 1 | 0 |
| 976 | 2 | 1952 | 1951 | 1 | 4 |
| 838 | 2 | 1676 | 1677 | 1 | 2 |
| 815 | 2 | 1630 | 1633 | 1 | 2 |
| 754 | 2 | 1508 | 1509 | 1 | 1 |
| 731 | 2 | 1462 | 1465 | 1 | 1 |
| 670 | 2 | 1340 | 1341 | 1 | 0 |
| 647 | 2 | 1294 | 1297 | 1 | 0 |

a) Calculated with minus 1 $H_2O$, b) Calculated with plus 1 $CO_2$

Furthermore, Maldi-TOF technique was also employed and the corresponding spectrum is shown in Figure 3.7. Three different matrices were tested, i.e., synaptic acid, alpha-cyano-4-hydroxycinnamic acid (CHCA) and 2,5-dihydroxybenzoic acid (DHB). DHB is retained for all analyses providing better sensitivity and resolution. All

measured masses are found to be monoisotopic. In addition, all analyses were performed with the addition of $CF_3COONa$ to increase sensitivity, and simplify spectral analysis (e.g., Na/K exchange). The largest molecular species was $(C_8H_{12}N_2O_2)_7(C_{48}H_{80}O_{40})_5$, $(HDI)_7(CD)_5$, *M/z* 7658.

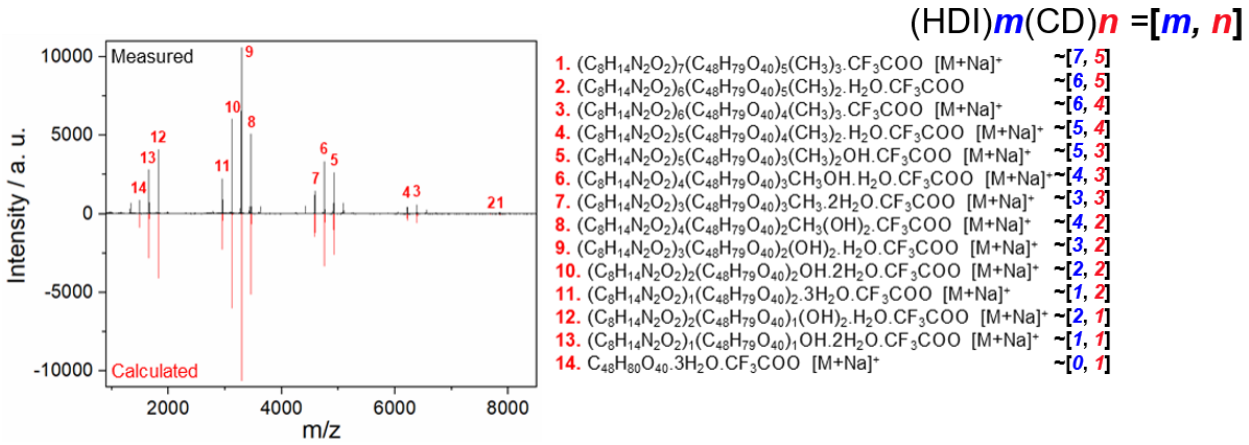


**Figure 3.7** *MALDI-TOF mass spectrum of γPOL1.16 in positive ion linear mode.*

Although the method is semi-quantitative, the nuclearity *n* of the reacted γCD in the $\gamma POL_{1.16}$ sample of composition $(HDI)_m(CD)_n$ showed a distribution with maximum intensity for oligomers containing 2 CD units (see Figure 3.8), which is consistent with the ESI measurement results. Overall, MS analyses indicate that the polymers in fact made up of small fragments of oligomeric species.

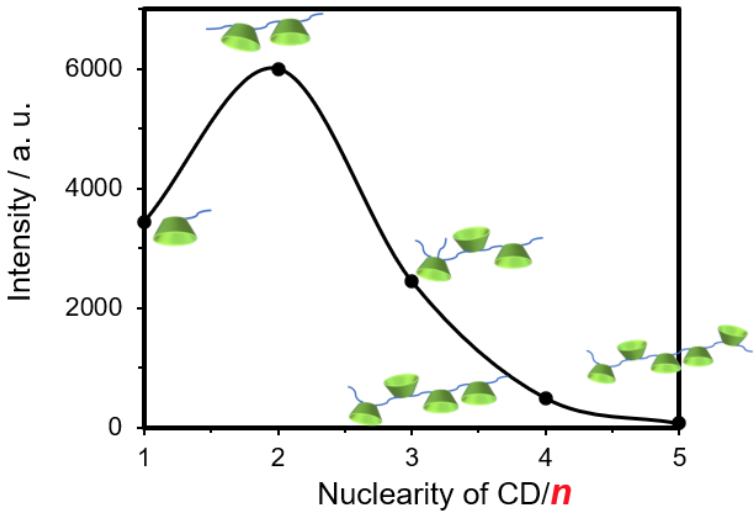


**Figure 3.8** *Distribution of oligomer components $(HDI)_m(CD)_n$ following their CD nuclearity n within $\gamma POL_{1.16}$ as measured by MALDI-TOF mass spectrometry.*

To conclude, we have successfully synthesized CD-containing polymeric precursors crosslinked with hexamethyl dicarbamate moieties. Most precursors are soluble in water for the $aPOL_n$ compounds with $n$ = HDI/CD < 2. Usually, the $n$ parameter is slightly higher than the initial HDI:CD ratio introduced in the synthesis when the HDI addition is fast, while controlled slow addition of reactant (HDI to CD) promotes mostly reticulation leading to high $n$ parameter. The typical precursor $\gamma POL_{1.16}$ was characterized by TGA, NMR, and mass-spectrometry, revealing it is composed of small oligomers where the number of linked CD does not exceed 4-5 motifs. The prominent species contain at most 2-3 CD units.

### 3.2.3 Experimental techniques

**Nuclear magnetic resonance (NMR).** All solution NMR spectra were measured in $D_2O$ or $CD_3Cl$ (in case of HDI) at 25 °C. $^1H$ NMR spectra were recorded on a Bruker Avance 400 spectrometer at a Larmor frequency of 400.1 MHz, using 5 mm standard NMR tubes. The $^1D$ $^1H$ spectra were recorded with one pulse sequence at 30° flip angle (pulse duration 2.7 µs), using 0.1 s recycle delay, 3 s acquisition time, and 8 number of scans. Translational diffusion measurements were performed using Bruker's “ledbpgs2s” stimulated echo DOSY pulse sequence including bipolar and spoil gradients. Apparent diffusion coefficients were obtained using an adapted algorithm based on the inverse Laplace transform stabilized by maximum entropy.[46] The $^{13}C$ spectra were obtained with standard power-gated decoupling pulse sequence, using typically 2 s recycle delay, 1.3 s acquisition time, and ca. 33000 number of scans. Solid-state NMR spectra were recorded on Bruker Avance NEO spectrometer equipped with a 11.7 T wide-bore superconducting magnet. Samples were packed into 2.5 mm zirconia rotors and rotated at the magic angle spinning (MAS) at at 10 KHz. $^{13}C$ NMR spectra were recorded using cross-polarization (CP) from $^1H$ with a spin lock pulse (ramped for $^1H$) of 1.5 ms. SPINAL-64 decoupling of $^1H$ ($\nu_1$ = 100 kHz) was applied during acquisition. Signal averaging was carried out for ca. 9000 transients with a repeat interval of 3.5 s. Direct polarization experiments with high-power decoupling (HPDec) were also recorded for quantitative measurements, using repetition delay of 75 s and ca. 1000 number of scans. Chemical shifts are reported relative to tetramethylsilane (TMS).

**Thermal gravimetric analysis (TGA)**. To determine water and organic contents, a Mettler Toledo TGA/DSC 1, STARe System apparatus was used under oxygen flow (50 $mL.min^{-1}$) at a heating rate of 5 $°C.min^{-1}$ up to 700 °C.

**MALDI-TOF mass spectrometry**. MALDI-TOF MS analyses were performed using an UltrafleXtreme mass spectrometer (Bruker Daltonics). The instrument is equipped with an Nd:YAG laser (operating at 355 nm wavelength of < 500 ps pulse and 200 Hz repetition rate). Acquisitions were performed in reflector ion mode. The laser intensity was set just above the ion generation threshold to obtain peaks with the highest possible signal-to-noise (S/N) ratio without significant peak broadening. 2,5-Dihydroxybenzoic acid (DHB) was used as the matrix for MALDI-TOF MS, and was of highest grade available from Sigma-Aldrich (used without further purification). The samples were first prepared at a concentration of 100 μM in $H_2O$. An aqueous solution of 6 mM matrix was used to prepare the MALDI sample by mixing the polymeric precursors solution with matrix solution at a volume ratio of 1:9. Finally, $CF_3COONa$ salt at 1 % was also added for a better S/N ratio.

**Viscometry**. A viscometer (LVDVNX cone & plate AMETEK Brookfield, Middleboro, MA, USA) was used to determine the absolute dynamic viscosity of aqueous solutions of POL, and POL containing POM (0.5:1 POM:γCD). The solutions were prepared and 0.6 mL of each sample was transferred to the viscometer. The temperature was controlled by a TC-150MX-230 AMETEK Brookfield circulator water bath, and used in the range 25-60 °C.

**Electrochemistry**. Cyclic voltammetric (CV) experiments were carried out with a Methrom Autolab PGSTAT230 driven by a computer using NOVA software. Measurements were performed at room temperature in a conventional single compartment cell. A glassy carbon (GC) electrode with a diameter of 5 mm was used as the working electrode. The auxiliary electrode was a Pt plate placed within a fritted-glass isolation chamber and potentials are quoted against an Ag/AgCl electrode. The solutions were deaerated thoroughly for at least 10 min with pure argon.

**Small Angle X-ray Scattering (SAXS)**. SAXS measurements using Mo radiation (λ = 0.071 nm) were performed on a bench built by XENOCS. The scattered beam was recorded using a large online scanner detector (diameter: 345 mm, from MAR

Research). A large q-range (0.2 to 40 $nm^{-1}$) was covered with an off-center detection. The collimation was applied using a 12:α multilayer Xenocs mirror (for Mo radiation) coupled to two sets of scatterless FORVIS slits providing a 0.8 x 0.8 mm X-ray beam at the sample position. Pre-analysis of the data was performed using FIT2D software. The scattered intensities are expressed versus the magnitude of scattering vector q = $[(4\pi)/\lambda]\sin(\theta/2)$, where λ is the wavelength of incident radiation and θ the scattering angle. 2 mm quartz capillaries were used as sample containers for the analyzed solutions. Usual corrections for background (empty cell and detector noise) and intensity normalization using a high-density polyethylene as a standard were applied. Experimental resolution was $\Delta q/q = 0.05$. The concentration of POM was fixed at 4 mM to get a reasonable signal from the laboratory SAXS camera.

## 3.3 POM@CD-polymers: stimuli-responsive polymer materials

### 3.3.1 Preparation of the POM@γPOL$_n$ gel

In a typical procedure, 300 mg γPOL$_n$ was dissolved in 0.5 ml $H_2O$. acid form or salt form of POM as a powder (ca. 360-380 mg, 0.5 eq./CD) was then added and the mixture was shaken for 5 min to ensure complete dissolution and homogenization at room temperature. We synthesized the classical POMs, $Na_3[PW_{12}O_{40}]\cdot 14H_2O$, $H_3[PW_{12}O_{40}]\cdot 9H_2O$, $H_4[SiW_{12}O_{40}]\cdot 17H_2O$, $K_5[BW_{12}O_{40}]\cdot 12H_2O$, $H_5[BW_{12}O_{40}]\cdot 9H_2O$, and $Rb_{4.5}Na_{1.5}[H_2W_{12}O_{40}]\cdot 11H_2O$ according to the reported procedures.[47–50] $Na_1K_3[PW_{11}V^{V}O_{40}]\bullet 7H_2O$, $K_4[SiW_{11}Mo^{VI}O_{40}]\bullet 5H_2O$, and $K_5[SiW_{11}V^{V}O_{40}]\bullet 7H_2O$ were synthesized and purified according to published procedures.[51–57] Depending on the nature of the Keggin ion, fluid homogenous solution or homogeneous gel result from the mixture at room temperature. The behavior of the various native Keggin-type anion in the presence of the γPOL$_{1.16}$ at room temperature is summarized in Table 3-5. As expected, the solution behavior appears strongly dependent on the charge of the POM. Thus, for the low anionic charge (less than 4-), a gelation process take place while for higher anionic charge (higher than 4-), the solution remains fluid. Such observations are fully consistent with the chaotropic effect of POMs described in chapter 2, which governs the recognition process between the ionic Keggin anion and the γ-CD unit. With the precursor γPOL$_{1.16,}$ the Keggin-type anion should act as reticulation nodes through the host-guest recognition process involving the γ-CD

units. Actually, such a hypothesis would allow to promote a gel-to-fluid phase transition through redox stimuli of the POM species. The gelation process is based on host-guest interaction between oligomers and POM. Aggregate formation is an increase in viscosity in solution resulting in a gel (see Figure 3.9).

**Table 3-5** *Solution behavior at room temperature of native Keggin-type anions in the presence of γPOL$_{1.16}$ aqueous solution.*

| **Anions** | no POM | $[PW_{12}O_{40}]^{3-}$ | $[PW_{11}VO_{40}]^{4-}$ | $[SiW_{12}O_{40}]^{4-}$ | $[SiW_{11}MoO_{40}]^{4-}$ | $[SiW_{11}VO_{40}]^{5-}$ | $[BW_{12}O_{40}]^{5-}$ | $[H_2W_{12}O_{40}]^{6-}$ |
|---|---|---|---|---|---|---|---|---|
| **Behavior** | solution | gel | gel | gel | gel | fluid solution | fluid solution | fluid solution |

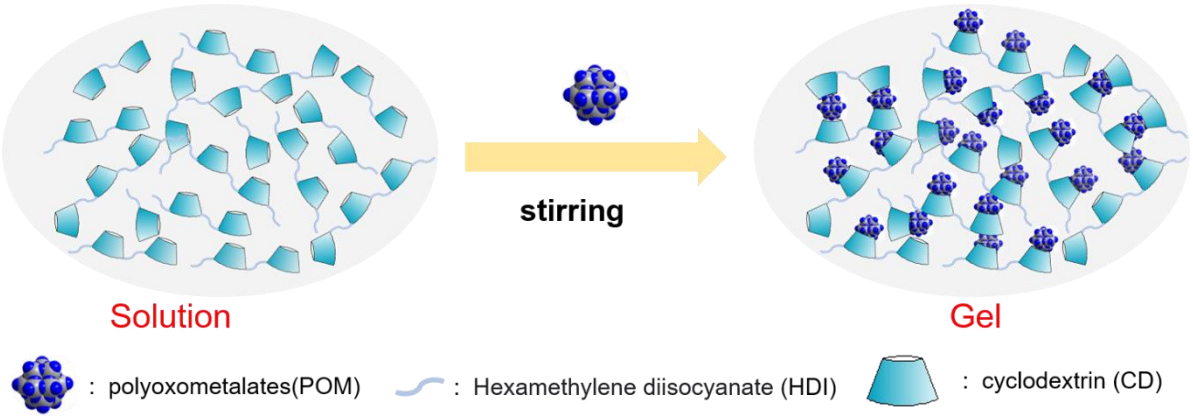


**Figure 3.9** *Schematic representation of formation of CD/POM hybrid hydrogel.*

Then, qualitative experiments have been carried out, by using sodium dithionite as reducing agent $Na_2S_2O_4$ and sodium peroxodisulfate $Na_2S_2O_8$ as oxidizing agent (see Figure 3.10). The chemical system $[PW_{12}O_{40}]^{3-}$-γPOL$_{1.16}$ behaves as a hydrogel. Addition of the reducing agent ($Na_2S_2O_4$, 5 mg) provokes a fast color change from colorless to dark blue but does not modify the situation of the solution, characterized by the preservation of the gelation properties. Conversely, the behavior appears quite different with the POM species $[PW_{11}VO_{40}]^{4-}$, $[SiW_{12}O_{40}]^{4-}$ and $[SiW_{11}MoO_{40}]^{4-}$. These native species give rise to the formation of hydrogel, but in the presence of sodium dithionite as reducing agent, a gel-to-fluid phase transition is observed. It should be worth mentioning that in this case, the reduction provokes also a color change to dark blue or violet, depending on the nature of the POM. Interestingly, the

phase transition appears fully reversible. In the presence of oxidizing agent (sodium peroxodisulfate), the discoloration of the solution, which is the fingerprint of the POM oxidation, is accompanied by a gelling process. The behavior of these hybrid POM-$\gamma POL_{1.16}$ aqueous solutions toward redox switch is illustrated in Figure 3.10. These experiments qualitatively reveal that the gel-fluid phase transition occurs specifically for the change in the anionic charge between 4- and 5- where the changes in host-guest interactions are large enough, but also not too strong, to cause either association or dissociation of the hybrid material.

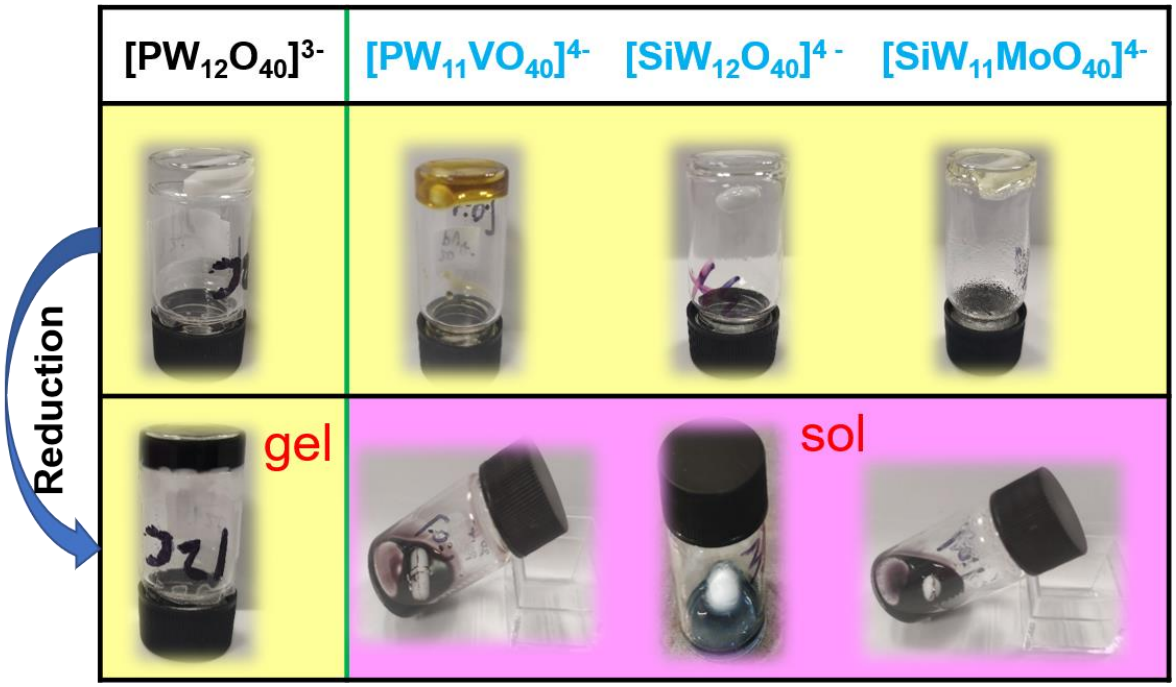


**Figure 3.10** *Pictures of hydrogelation between the $\gamma POL_{1.16}$ (467 mM CD) and different Keggin POMs (0.5 eq./CD), before, after addition of $Na_2S_2O_4$ as reducing agent, and subsequent addition of $Na_2S_2O_8$ as oxidizing agent.*

Such assembly-disassembly process can be expressed by the equation:

$POM^{4-}$-$\gamma POL_{1.16}$ + 1e- ⇄ $POM^{5-}$ + $\gamma POL_{1.16}$ (see Figure 3.11).

In the case of the anion $[PW_{12}O_{40}]^{3-}$, the charge change from 3- to 4- in our experimental conditions does not make it possible to decrease enough the strength of host-guest interaction to lead to the dissociation of the hybrid polymer. The resulting gel therefore persists along the redox stimuli. In contrast, for the POMs with higher charges, i.e., $[BW_{12}O_{40}]^{5-}$ and $[H_2W_{12}O_{40}]^{6-}$, no gelling process was observed and the solutions remains fluid whatever their oxidation state. In such a situation, the

strength of the host-guest interaction is too weak to promote the gelling effect. These qualitative observations correlate nicely with the quantitative study presented previously in chapter 2 in which the supramolecular properties between Keggin-type POMs and γ-CD were quantitatively dissected. Such a behavior can be explained by the chaotropic effect of Keggin-type POM that governs the strength of host-guest associations with the γ-CD moieties of the polymer. Furthermore, in these POM@γPOL$_{1.16}$ polymers, POM would act as cross-linking agent capable to interconnect oligomer fragments and thus cause gelation.

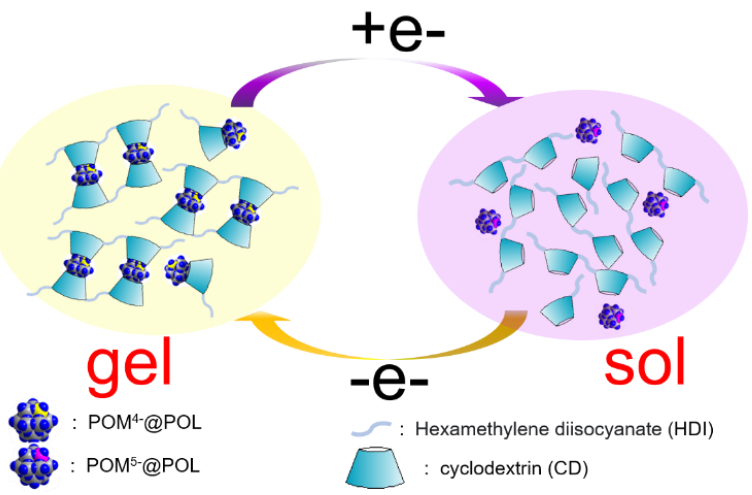


**Figure 3.11** *Schematic representation of the reversible redox-induced assembly-disassembly process.*

To further investigate the gelation process and to get more insight into POM@γPOL$_{1.16}$ complex, solution studies were carried out on dilute systems where the solution remains fluid (regime before phase transition). Titration experimentations and solution investigations were monitored by cyclic voltammetry, NMR spectroscopy and Small Angle X-ray Scattering (SAXS). In addition, the aggregation behavior at high concentrations was also evidenced quantitatively via viscosity measurements.

### 3.3.2 Viscosity properties

The viscosity of POM@γPOL$_{1.16}$ hydrogels is significantly dependent on concentration, whereas the viscosity of the POM-free γPOL$_{1.16}$ is only slightly affected when changing its concentration at room temperature (see Figure 3.12A).

The viscosity of polymer ($[SiW_{12}O_{40}]^{4-}$-γPOL$_{1.16}$) aqueous solutions at room temperature rises gradually with the concentration in the 125-300 mM range. From 375 mM, the viscosity change becomes abrupt up to 500 mM where the system becomes too much viscous preventing any viscosity measurement. Viscosity profile reveals the formation of higher-order aggregates of oligomers and polymers at room temperature, induced by the presence of the $[SiW_{12}O_{40}]^{4-}$ anion. The gel-to-fluid transition was analyzed by dynamic rheology. Macroscopic gelation at $T$ = 298 K was observed at a sample concentration of 490 mM. The thermal behavior of the transparent and homogenous gel has been investigated by heating/cooling cycles in the 25-60 °C temperature range in which the solution converts from gel to fluid. The viscosity of a concentrated hydrogel ([CD] = 417 mM) was measured from room temperature to 60 °C (Figure 3.12B), revealing that the gels become fully fluid around 40 °C ($T_{sol}$). In addition, hydrogels stored in sealed vials remained stable for over a month, indicating excellent long-term stability. Gentle heating of the hydrogels (up to 40 °C) followed by the addition of sodium dithionite (0.5 eq./POM) leads to the reduction of POM inducing a phase transition from gel to fluid, with a color change to blue for $[SiW_{12}O_{40}]^{5-}$, and to purple for $[SiW_{11}MoO_{40}]^{5-}$. Due to its rapid oxidation in air, the viscosity of the $[SiW_{12}O_{40}]^{5-}$γPOL$_{1.16}$ system could not be measured. Indeed, a gelling process occurs from the fluid solution after a few minutes in contact with air. However, the reduced state of the monosubstituted anion $[SiW_{11}MoO_{40}]^{5-}$ exhibits fair stability in the presence of oxygen allowing the viscosity measurements and a comparison of the polymer behavior in the presence of oxidized or reduced anion. At room temperature, the viscosity of the oxidized POM-γPOL$_{1.16}$ is about 165 cp while for its reduced counterpart, viscosity falls down to about 10 cp showing quantitatively the effect of the charge (see Figure 3.12B).

As a general trend, the heating of the POM-γPOL$_{1.16}$ leads to the decrease of the viscosity. At last, this redox-controlled phase transition is tuned by the Keggin global charge density that influences the host-guest binding constant $K_{1:1}$. For the oxidized $[SiW_{12}O_{40}]^{4-}$ or $[SiW_{11}MoO_{40}]^{4-}$ anions, the high binding constant values of $K_{1:1}$ = 17-18 $10^3$ $M^{-1}$ relate a strong interaction with the native γ-CD units (see Chapter 2). Similar strong host-guest interaction should take place between the POM species and the γ-CD unit of the polymer chains resulting in gel formation. Meanwhile, for the reduced $[SiW_{11}MoO_{40}]^{5-}$ anion, the modest value of $K_{1:1} \approx 0.5\ 10^3\ M^{-1}$ reflects a weak

interaction, insufficient to support aggregation phenomena between the γ-CD of the polymeric chains, which prevent any gelling process.

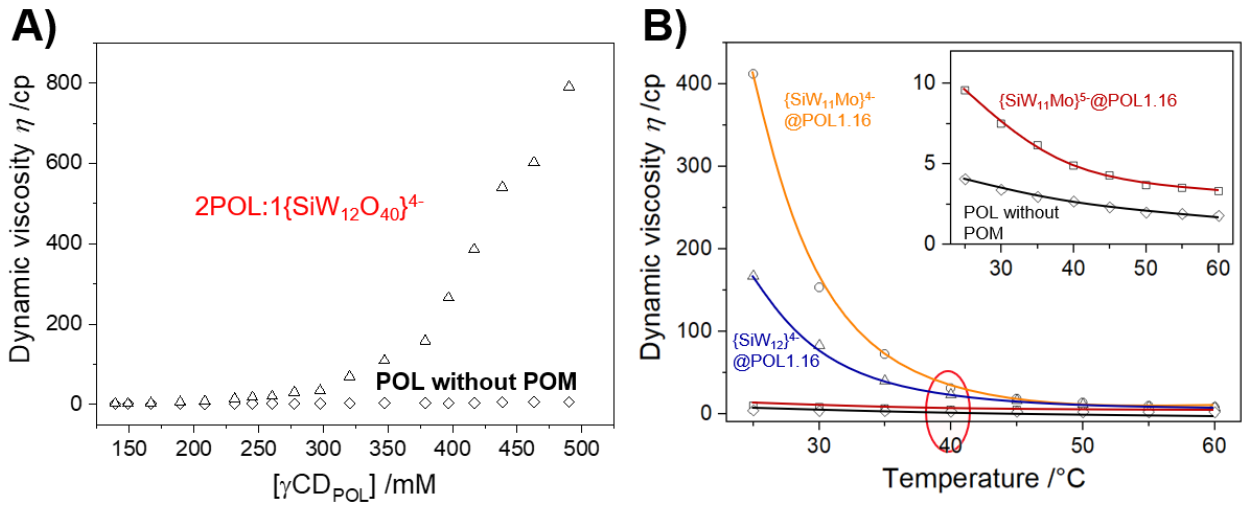


**Figure 3.12** *A) Plots of dynamic viscosity of (triangle) $\{SiW_{12}\}^{4-}$@γPOL$_{1.16}$ (0.5:1) and (rhombus) γPOL$_{1.16}$ as function of the γCD$_{POL}$ concentration in aqueous solution at 25 °C. B) Temperature-dependent dynamic viscosity of aqueous solution of γPOL$_{1.16}$ ([γCD$_{POL}$] = 417 mM), containing (circle) $\{SiW_{12}\}^{4-}$, (triangle) $\{SiW_{11}Mo\}^{4-}$, (square) $\{SiW_{11}Mo\}^{5-}$, and (rhombus) no POM.*

### 3.3.3 Electrochemistry

The electrochemical response of POM has found to be very sensitive to the supramolecular interaction with CD, even allowing a quantitative analysis capable of determining the host-guest stability constant between the oxidized and reduced species. In Chapter 2, we monitored the $[XW_{11}M]^{n-}$ anion interaction with native γ-CD in the presence of tori hosts through changes in the POM half-wave potential.[19] Such a previous study constitutes the basis for this present investigation of the CD-containing polymers and the POMs.

In the same way, the variation of their half-wave potentials allows to evidence the complexation process between the POM and the γ-CD tori within the γPOL$_{1.16}$. Cyclic voltammograms (CVs) of a 1 mM Keggin POMs ($[SiW_{12}O_{40}]^{4-}$ and $[SiW_{11}Mo]^{4-}$) in acidic aqueous solution were recorded with increasing γ-CD concentration up to 10 eq. as shown in Figure 3.13. As expected, similar CV patterns were obtained using oxidized or reduced form $[SiW_{11}Mo]^{4-/5-}$. In the presence of γ-POL$_{1.16}$, CVs show a

significant negative shifts potential of the first wave as γ-POL1.16 increases up to 10 eq. (about -100 mV for $[SiW_{12}O_{40}]^{4-/5-}$ and -105 mV for $[SiW_{11}MoO_{40}]^{4-/5-}$). Such a result indicates that the Keggin anions becomes more difficult to reduce in the polymer, meaning that the γ-CD within polymer interact much stronger with the oxidized species. Moreover, the quasi-similar variation of the half-wave potential values between both $[SiW_{12}O_{40}]^{4-}$ and $[SiW_{11}Mo]^{4-}$ anions confirms a comparable affinity for the γCD within the POL. This outcome is explained by the same global charge density bring by these anions which governs the solvent effect and the host-guest interaction strength as discussed in Chapter 2.

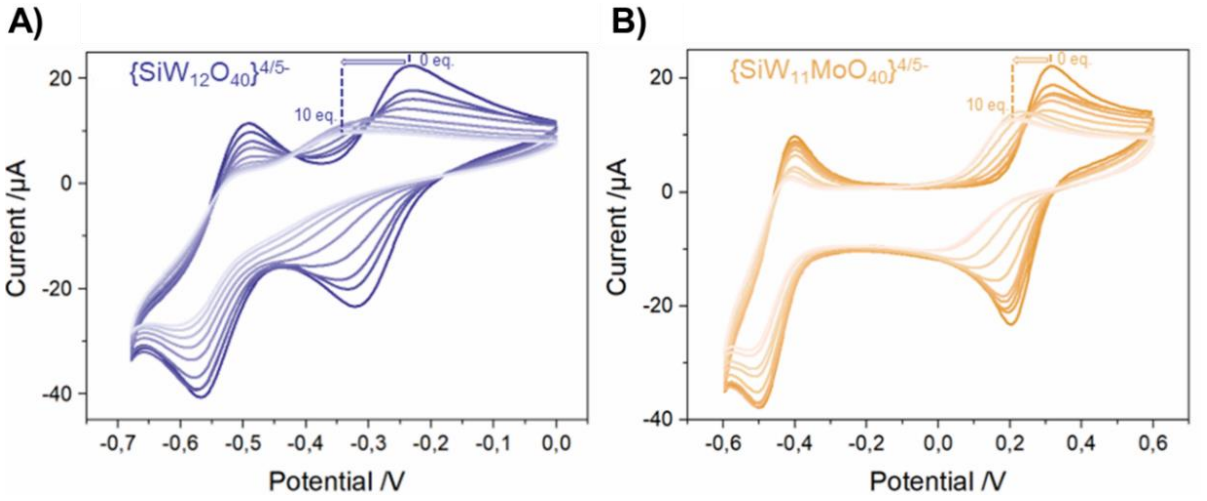


**Figure 3.13** *Cyclic voltammetry of A) $[SiW_{12}O_{40}]^{4-}$ and B) $[SiW_{11}Mo]^{4-}$ ([POM] = 1 mM, glassy carbon working electrode, Ag/AgCl reference electrode, and scan rate of 50 mV/s) in the presence of increasing amount of γCD within $\gamma POL_{1.16}$ (from 0 to 10 eq.). The experiments have been performed in 0.025 M $HClO_4$ aqueous solution.*

This phenomenon has already been observed in the case of the interaction with native γCD, and it should indicate the formation of host-guest complexes within the polymer. As shown in Figure 3.14, the half-wave potential changes in a similar way either in the presence of native γ-CD or γ-CD in $\gamma POL_{1.16}$. Besides, a severe decrease of the peak current density occurs upon the addition of the γCD. Interestingly, this decrease in current intensity is more pronounced with increasing amount of polymeric precursor compared to the system with native CD. This is an additional evidence of POM@$(\gamma CD)_n$ complexes formation within the POL that diffuse more slowly in the aqueous electrolyte than solvated Keggin anions. Thus,

the relative diffusion coefficient values estimated from the Randles-Sevick equation (see below) show a stronger decay in the presence of the γPOL$_{1.16}$ than the native γCD.

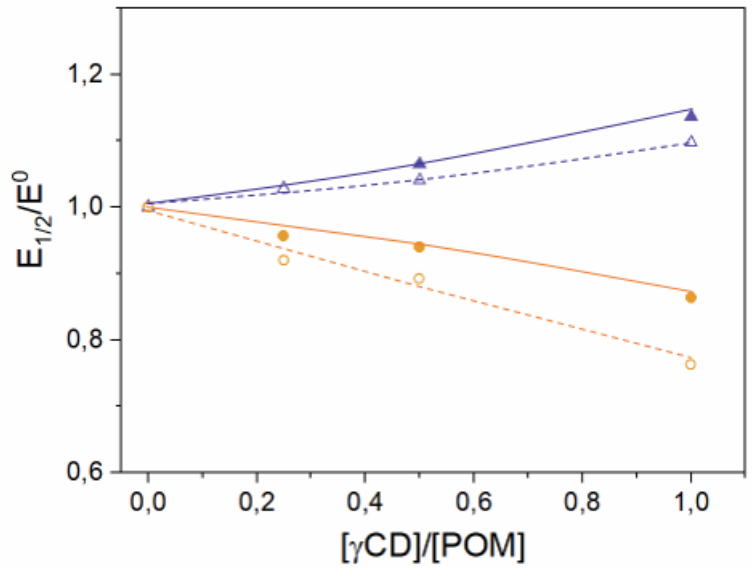


**Figure 3.14** *Relative variation of half-wave potentials of the couple [SiW$_{12}$O$_{40}$]$^{4/5-}$ and [SiW$_{11}$MoO$_{40}$]$^{4/5-}$ observed in CVs of 1 mM POM as a function of molar ratio γCD/POM. Filled symbols correspond to the native γCD while the unfilled one are related to the γCD within the POL, with (blue triangle) [SiW$_{12}$O$_{40}$]$^{4/5-}$, (orange circle) [SiW$_{11}$MoO$_{40}$]$^{4/5-}$.*

**Determination of diffusion coefficient *D* from Randles-Sevcik equation**. The cyclic voltammetry current maximum ($i_p$) is proportional to the square root of the analyte diffusion coefficient ($D$), as described by the Randles-Sevcik equation:

$$i_p = 0.4463n \cdot F \cdot A \cdot C \left(\frac{nF\nu D}{RT}\right)^{\frac{1}{2}} \qquad (3.7)$$

where $i_p$ is the current maximum (A), $n$ the number of electrons transferred in the redox process, here $n$ = 1, $F$ is the Faraday constant (96 485 C.mol$^{-1}$), $A$ the electrode area (cm$^2$), here $A$ = 0.2 cm$^2$, $C$ is the POM concentration (mol.cm$^{-3}$), here $C$ = 1.0 10$^{-6}$ mol.cm$^{-3}$, $v$ is the scan rate (V.s$^{-1}$), $D$ the diffusion coefficient (cm$^2$.s$^{-1}$), $R$ the gas constant (8.314 J.K$^{-1}$.mol$^{-1}$), and $T$ the temperature (K), here $T$ = 298 K.

For our study, we assume that [SiW$_{11}$MO$_{40}$]$^{4-/5-}$ (where M = W$^{V/VI}$ or Mo$^{V/VI}$) diffusion coefficients are similar. Thus, we determine the POM diffusion coefficient by recording the corresponding cyclic voltammogram over a range of scan rates from 10 to 100 mV.s$^{-1}$. Then, the POM diffusion coefficient can be calculated graphically

from the slope of the linear plot of the reduction current ($i_p$) versus the square root of the scan rate ($v^{½}$), as shown in Figure 3.15.

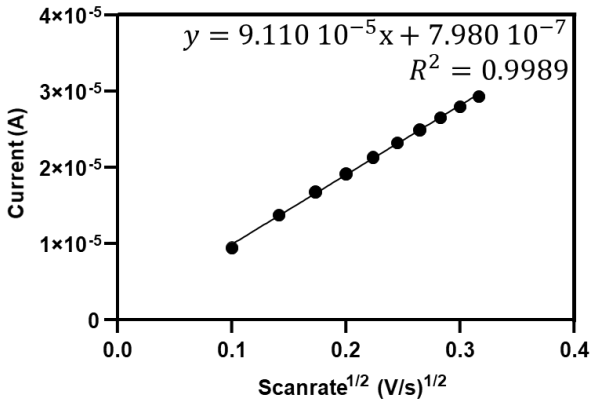


**Figure 3.15** *Plot of $[SiW_{12}O_{40}]^{4-}$ reduction current ($i_p$) versus the square root of the scan rate ($v^{½}$).*

Indeed, the current density according to Equation (3.7) is a linear function (Equation 3.8) where the slope defined in Equation (3.9) is a function of *D*.

$$i_p = f\left(v^{\frac{1}{2}}\right) \qquad (3.8)$$

$$slope = 0.4463nFAC\left(\frac{nFD}{RT}\right)^{\frac{1}{2}} \qquad (3.9)$$

$$D = \frac{RT}{nF}\left(\frac{slope}{0.4463nFAC}\right)^2 \qquad (3.10)$$

Then the calculated value for POM from Equation (3.10) was found $\boldsymbol{D = 280\ \mu m^2.s^{-1}}$ that appears similar to reported values in the literature.[59,60]

It is worth mentioning that the complexity of the POM-γCD and POM-γ$POL_{1.16}$ should include several POM-CD adducts and take into account their behavior toward redox processes. The method described above is therefore not suitable for determining the diffusion coefficient of the POM within its supramolecular assembly. Actually, the POM reduction leads to a dissociation phenomenon that change the distribution of the host-guest species at the electrode interface. Thus, we propose an estimation of the diffusion coefficient in these systems related to that of the solvated POM in solution as follows:

$$i_p \propto D^{\frac{1}{2}} \quad (3.11)$$

$$D \propto {i_p}^2 \quad (3.12)$$

Related to the solvated diffusion coefficient of the free POM, notated $D_0$, and the corresponding initial current maximum ($i_{p0}$), the POM diffusion coefficient interacting with CD notated *D'* can be estimated as:

$$\frac{D'}{D_0} = \left(\frac{i'_p}{i_{p0}}\right)^2 \quad (3.13)$$

$$D' = D_0 \left(\frac{i'_p}{i_{p0}}\right)^2 \quad (3.14)$$

with $i_p$' is the maximum current in the presence of CD. Thus, Equation (3.14) allows to calculate the average diffusion coefficient of the POM along the complexation process either by γCD or γPOL. The calculation of D' upon the POM complexation is graphically shown in Figure 3.16. The diffusion coefficient *D*' decreases continuously with increasing CD content in solution as a result POM-CD complexation. However, this effect appears more pronounced with $POL_{1.16}$ precursor than with native γCD, indicating that the POM embedded within polymerized γCD has a slower diffusion rate, forming aggregates of larger sizes. This again indicates probably the cross-linking role of the POM associating several oligomer fragments through host-guest supramolecular complexation. Besides, it is worth mentioning that the viscosity of the electrolyte does not change significantly upon the addition of CD in these dilute systems confirming that the observed changes in diffusion rates are mainly due to the aggregation phenomenon. Furthermore, the Stokes-Einstein relation, Equation (3.15), can give an estimation of the average size of the aggregates. As the diffusion coefficients approach the limit values of 50-30 $\mu m^2.s^{-1}$ at large excess of $\gamma POL_{1.16}$, these aggregates, approximated as spheroidal are estimated to reach 4.4-8 nm in diameter.

$$D = \frac{K_B T}{6\pi\eta R_h} \quad (3.15)$$

where $D$ is the observed diffusion coefficient ($m^2.s^{-1}$), $k_B$ the Boltzmann constant ($1.38\ 10^{-23}\ J.K^{-1}$), $T$ is the temperature (K), here $T$ = 298 K, $r$ is the particle radius (m), and $\eta$ is the dynamic viscosity ($kg\ .m^{-1}.s^{-1}$), here $\eta = 8.90*10^{-4}\ kg\ .m^{-1}.s^{-1}$.

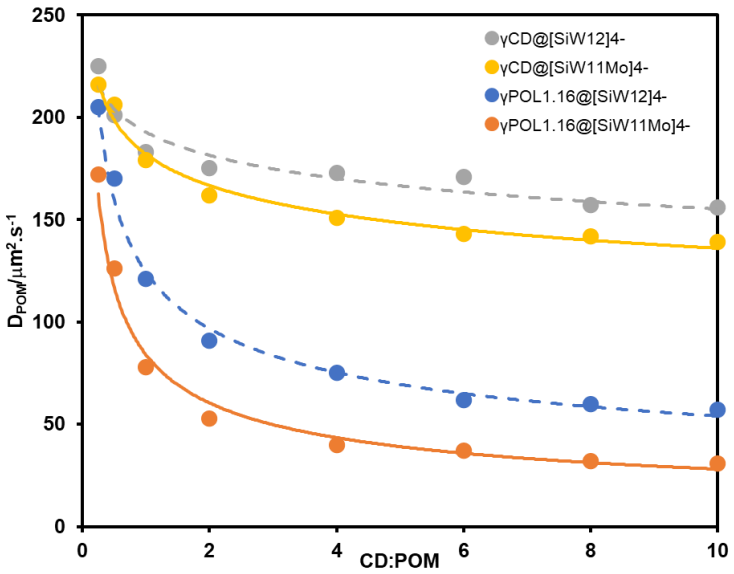


**Figure 3.16** *Variation of the average diffusion coefficients of POM as a function of the CD:POM molar ratio, measured from CV of 1 mM of $[SiW_{12}O_{40}]^{4-}$ and $[SiW_{11}MoO_{40}]^{4-}$ with native γCD or γCD within $\gamma POL_{1.16}$.*

### 3.3.4 NMR titration studies in solution

#### 3.3.4.1 Interaction of $aPOL_n$ with $[XM_{12}O_{40}]^{n-}$

The formation and stability of Keggin POM complexes with $\gamma POL_n$ were further investigated by $^1H$ NMR spectroscopy in $D_2O$. Herein, we observe the CD supramolecular behavior in the presence of POMs. Therefore, an aqueous solution of 2 mM $\alpha POL_{1,86}$, $\beta POL_{1,41}$, or $\gamma POL_{1,16}$ is systematically titrated with $[PW_{12}O_{40}]^{3-}$ from 0 to 16 equivalents. In the range of 3.4 to 4.2 ppm chemical shifts, the $^1H$ NMR spectra (see Figure 3.17) correspond to the protons of the internal cavity (the most sensitive to host-guest complexation), where H3 and H5 are located inside the cavity and H6 at the top of the primary rim (see Figure 3.3 for proton numbering scheme). The NMR signals are broad due to the restricted molecular motion and the polydispersity of local environment in CD-based $POL_n$. Depending on the cavity size of the three types of CD, the spectra showed contrasted alteration in relationship with the CD-specific recognition process as previously reported in Chapter 2. With the polymers containing smaller CD cavities in $\alpha POL_{1.86}$ and $\beta POL_{1.41}$, the most affected $^1H$ NMR signal corresponds to that of H6 present on the primary rim of the CD. The situation differs for $\gamma POL_{1.16}$ showing a significant downfield shift for the proton H3 in accordance with formation of strong host-guest complexes.

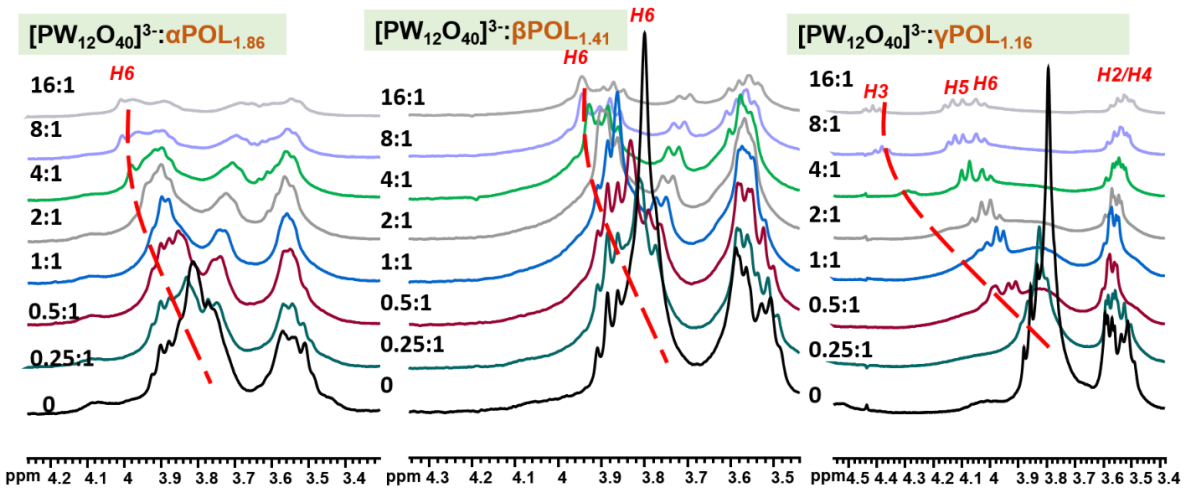


**Figure 3.17** *$^{1}$H NMR spectra in the 3.3-4.2 ppm range resulting from the titration of 2 mmol.L$^{-1}$ aqueous solution of CD within POL$_n$ by $[PW_{12}O_{40}]^{3-}$: (left) $[PW_{12}O_{40}]^{3-}$@ αPOL$_{1.86}$, (middle) $[PW_{12}O_{40}]^{3-}$@ βPOL$_{1.41}$, and (right) $[PW_{12}O_{40}]^{3-}$@γPOL$_{1.16}$.*

The extent of chemical shift variations observed for H6 appears mainly related to the nature of CD included within the polymer (see Figure 3.17). When the $[PW_{12}O_{40}]^{3-}$ ion was added to the β-CD-based POL$_{1.41}$ solution, the H6 signal undergoes a maximal variation of 0.14 ppm, whereas the change of this chemical shift appears significantly larger with αPOL$_{1.86}$ and γPOL$_{1.16}$ (0.20 and 0.25 ppm, respectively), consistent with stronger interactions. These results suggest that the significant supramolecular contact in solution occurs preferentially on the primary face of the CDs. However, the shift of proton H3 in αPOL$_{1.86}$ and βPOL$_{1.41}$ remains nearly unchanged, indicating that $[PW_{12}O_{40}]^{3-}$ has no interaction with the internal cavity of these CDs. Notably, much larger effects were observed in the case of γPOL$_{1.16}$, where variations up to 0.55 and 0.36 ppm downfield shifts were observed for inner protons H3 and H5, respectively (see Figure 3.18). These changes may also indicate the involvement of the secondary face of the γ-CD in the interaction with $[PW_{12}O_{40}]^{3-}$ because the H3 protons are closer to the secondary rim than to the primary face.

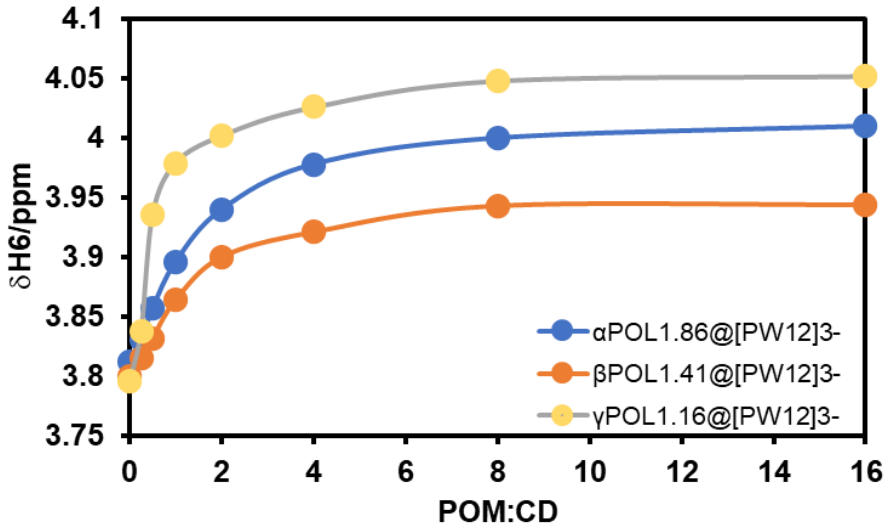


**Figure 3.18** *Variation of the $^{1}$H NMR chemical shifts of H6 as a function of POM/CD molar ratio (conditions: 2 mM CD-containing aPOL$_n$.*

Besides, the interaction of other Keggin POMs with γPOL$_{1.16}$ was also investigated by $^{1}$H NMR titration. Here, we conducted a comparative titration study of 2 mM aqueous in γPOL$_{1.16}$ with the three Keggin-types anions, $[XW_{12}O_{40}]^{n-}$ (X = $P^{5+}$, $Si^{4+}$, $B^{3+}$; n = 3-5). The resulting $^{1}$H-NMR spectra are presented in Figure 3.19. As expected, the H6 (and also H5) signal evolves much more significantly with increasing $[SiW_{12}O_{40}]^{4-}$ amount compared to $[BW_{12}O_{40}]^{5-}$ although the final chemical shift at the highest ratio is the same. As previously observed with native CDs (see section 2.3, Chapter 2), the signal of the H6 protons keeps its initial appearance of singlet with $[BW_{12}O_{40}]^{5-}$ containing solutions, whereas it splits into two unresolved doublets with the other POMs. We can see that the interaction strengths in POM@γPOL$_{1.16}$ are similar to those involving native γ-CD because they induce similar effects on the NMR chemical shifts of the probed protons (see Figure 3.20). At last, the recognition process does not seem to be altered by the linking of the γ-CD in the CD-based polymer γ-POL$_{1.16}$.

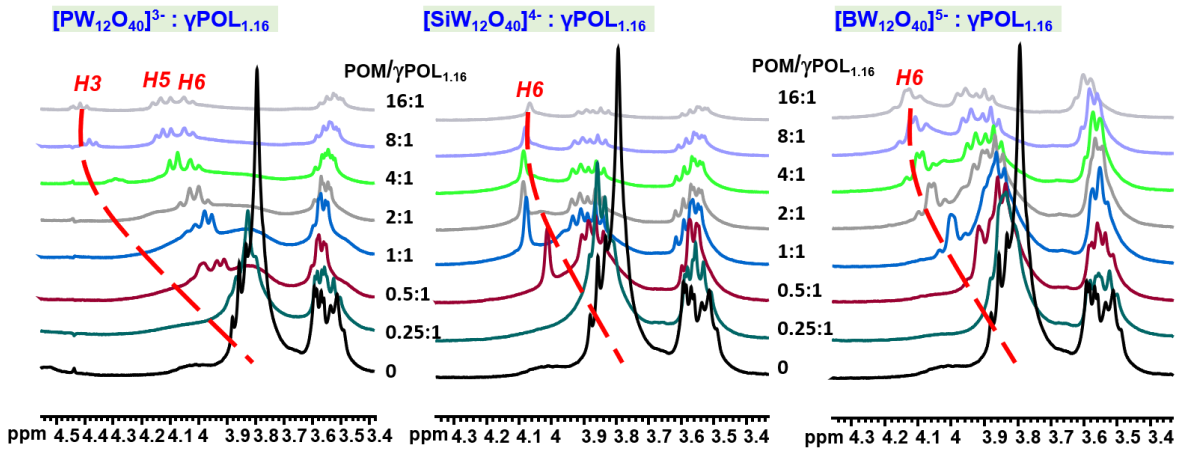


**Figure 3.19** *Selected $^{1}H$ NMR spectra resulting from the titration of 2 mmol.L$^{-1}$ aqueous solution of γPOL$_{1.16}$ by $[PW_{12}O_{40}]^{3-}$, $[SiW_{12}O_{40}]^{4-}$ and $[BW_{12}O_{40}]^{5-}$.*

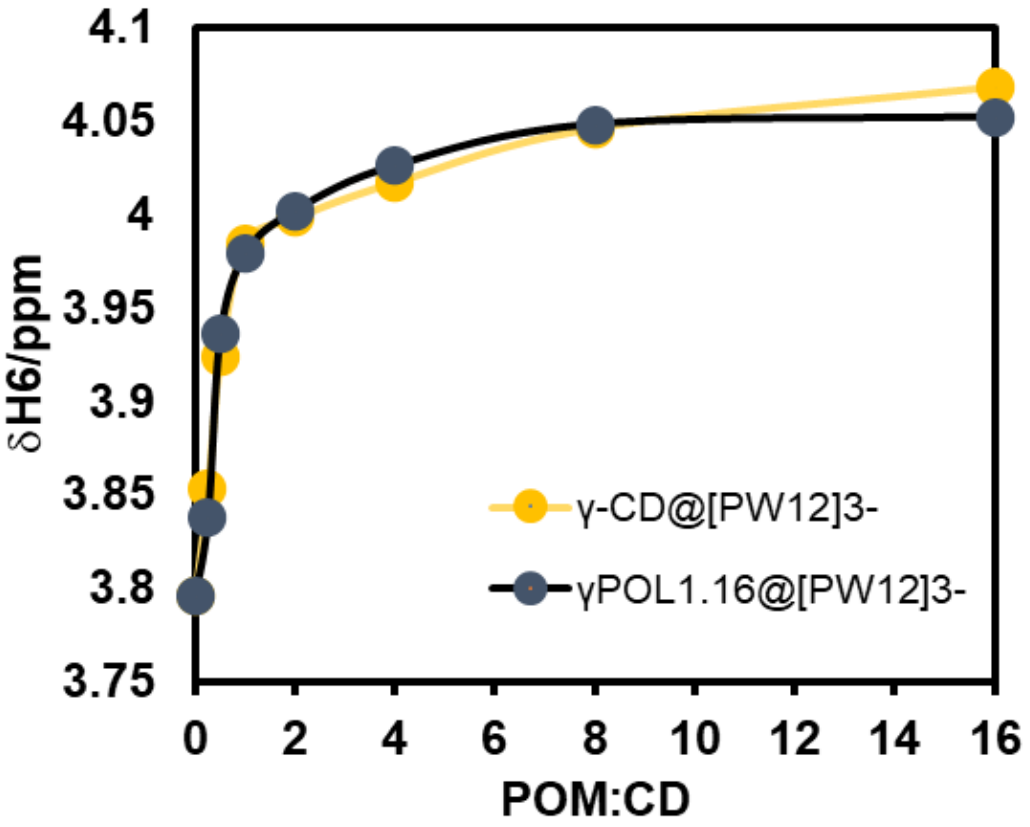


**Figure 3.20** *Comparison of the evolution of the γ-CD proton H6 NMR shift as a function of the POM/CD molar ratio during titration of 2 mM γ-CD as a native compound or in γPOL$_{1.16}$ with $[PW_{12}O_{40}]^{3-}$.*

Further quantitative investigations were also carried out using DOSY NMR. Since the viscosity changes significantly with increasing CD concentration, especially in polymeric form, all measurements were performed with a constant CD concentration

of 2 mM. In the concentration range studied, the dynamic viscosity remains constant at 1 cp in the presence of 0-16 equivalents POM. Variation of the diffusion coefficient *D* as a function of $[PW_{12}O_{40}]^{3-}$ concentration is shown in Figure 3.21A using 2 mM native γ-CD, $\gamma POL_{0.8}$ or $\gamma POL_{1.16}$. The initial *D* values measured from POM free aqueous solutions corresponded to 254, 195, and 182 $\mu m^2.s^{-1}$ for native γ-CD, $\gamma POL_{0.8}$, and $\gamma POL_{1.16}$, respectively. The difference in the *D* values is consistent with the increase of the average molecular size when the ratio linker/CD increases within the precursor. The drop of the *D* value in the presence of POM translates the aggregation phenomenon based on the host-guest process between the POM and the CD moieties. A plateau for a large excess in $[PW_{12}O_{40}]^{3-}$ ion is observed probably due to the saturation of the γ-CD receptor sites. Interestingly, the presence of a minimum *D* value observed for a molar ratio POM/CD = 0.5 should be consistent with the formation of larger intermediates in the solution. This minimum of *D* values observed for the three compounds at *D*(γCD) = 205 $\mu m^2.s^{-1}$, *D*($\gamma POL_{0.8}$) = 161 $\mu m^2.s^{-1}$, and *D*($\gamma POL_{1.16}$) = 119 $\mu m^2.s^{-1}$, should correspond to aggregated species combining two CDs per POM to form sandwich host-guest assemblies. It should be worth noting that the existence of the POM@2γCD “sandwich”-type host-guest supramolecular complex was demonstrated with native γ-CD in the previous Chapter 2.3. Therefore, larger aggregated species formed in $\gamma POL_{0.8}$ and $\gamma POL_{1.16}$, should be considered as interconnected fragments where POM acts as reticulating nodes. Besides, depending on the characteristics of the Keggin-type anions, which differ by their anionic charge, the observed diffusion coefficients *D* as a function of the POM@-CD molar ratio exhibit various profiles (see Figure 3.21B). The aggregation phenomenon was found to be less effective with more negatively charged POMs, which is quite consistent with the complexation induced by the chaotropic effect.

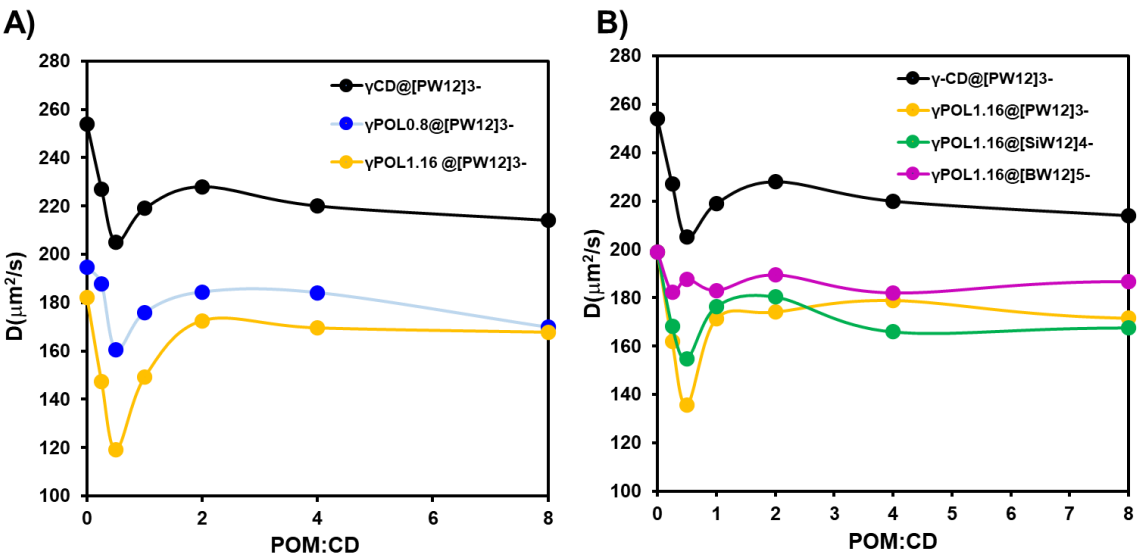


**Figure 3.21** *A) Diffusion coefficients of CD as a function of POM:CD molar ratio, measured from $^1$H DOSY NMR of 2 mM-CD solution of γ-CD, γPOL$_{0.8}$, or γPOL$_{1.16}$ in presence of various amounts of [PW$_{12}$O$_{40}$]$^{3-}$. B) Diffusion coefficients of CD as a function of POM:CD molar ratio, measured from $^1$H DOSY NMR of 2 mM-CD solution of γ-CD or γPOL$_{1.16}$ in presence of various amounts of [PW$_{12}$O$_{40}$]$^{3-}$, [SiW$_{12}$O$_{40}$]$^{4-}$ or [BW$_{12}$O$_{40}$]$^{5-}$.*

In summary, the NMR analysis provided a clear insight about the local interactions between the POM and γPOL, allowing a clear correlation between the gelation effect and the supramolecular host-guest interaction, where the POM species behave as crosslinking agents. At last, the common denominator of these supramolecular systems arises from the chaotropic effect which provides the main driving force for the assembling processes.

### 3.3.4.2 Interaction of γPOL$_{1.16}$ with mixed-metal Keggin POM [XMW$_{11}$O$_{40}$]$^{n-}$

The behavior of monosubstituted Keggin POM complexes containing Mo or V with γPOL$_{1.16}$ were also investigated by $^1$H NMR spectroscopy in D$_2$O. $^1$H NMR spectra shown in Figure 3.22, were measured for a fixed concentration of γPOL$_{1.16}$ (2 mM γCD) in the presence of the oxidized Keggin anions [SiW$_{12}$O$_{40}$]$^{4-}$ and [SiW$_{11}$MoO$_{40}$]$^{4-}$, and the reduced [SiW$_{11}$MoO$_{40}$]$^{5-}$.

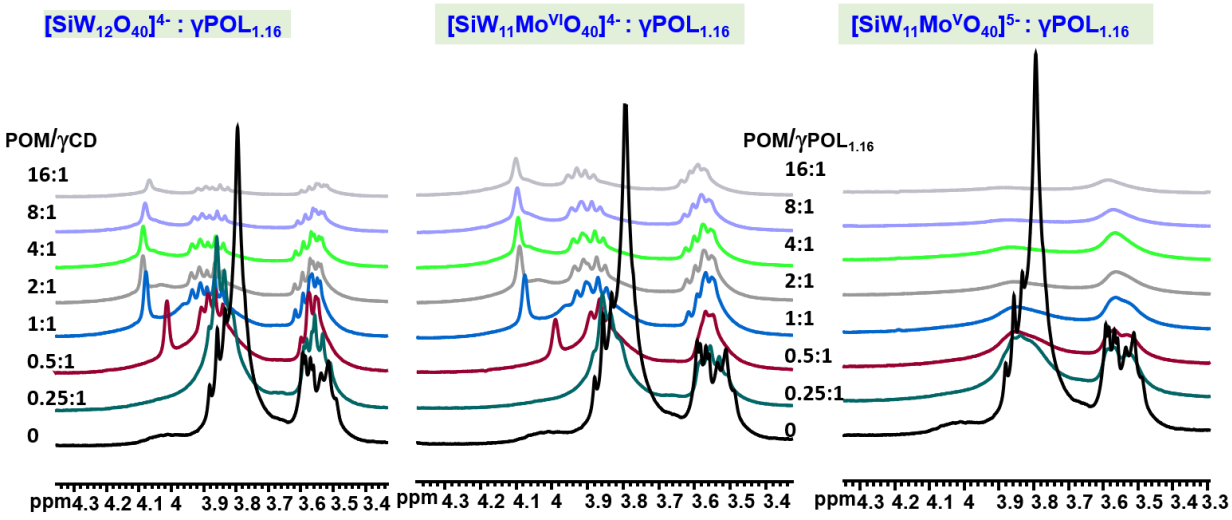


**Figure 3.22** *Selected $^1$H NMR spectra resulting of the titration of 2 mmol.L$^{-1}$ aqueous solution of CD in γPOL$_{1.16}$ by [SiW$_{12}$O$_{40}$]$^{4-}$, [SiW$_{11}$MoO$_{40}$]$^{4-}$, and [SiW$_{11}$MoO$_{40}$]$^{5-}$anions.*

For diamagnetic $[SiW_{12}O_{40}]^{4-}$ and $[SiW_{11}Mo]^{4-}$ anions, a significant line broadening is observed for the H3, H5, and H6 NMR resonances in relationship with the aggregation processes. These NMR spectra have been previously interpreted as the predominant interaction of the POM with the primary rim of the γCD. However, the titration with the paramagnetic $[SiW_{11}MoO_{40}]^{5-}$ POM results in an abrupt and substantial line broadening of all the resonances due to the very efficient relaxation processes arising from the nuclear spin-electron spin dipolar interactions. Likewise, the binding modes in the hybrid polymers $[SiW_{12}O_{40}]^{4-}$@γPOL$_{1.16}$, $[SiW_{12}O_{40}]^{4-}$@γPOL$_{1.16}$, and $[SiW_{11}MoO_{40}]^{4-}$@γPOL$_{1.16}$ are almost the same by comparing the shifts of H6 signal (see Figure 3.23A). Diffusion-ordered $^1$H-NMR spectroscopy (DOSY) was also carried out to investigate the supramolecular aggregation of the diamagnetic $[SiW_{12}O_{40}]^{4-}$ and $[SiW_{11}MoO_{40}]^{4-}$ Keggin anions with γPOL$_{1.16}$. Because the γCD is trapped within the polymeric precursor unit, it diffuses more slowly ($D_{POL}$ = 198 µm$^2$.s$^{-1}$) compared to the native γCD ($D_{\gamma CD}$ = 254 µm$^2$.s$^{-1}$) at the same concentration (see Figure 3.23B). In the presence of POMs, the average *D* value of the polymers drops down rapidly as a result of supramolecular host-guest complexation between the POM and the CD of the γPOL$_{1.16}$. The comparison of the observed DOSY diffusion coefficient curves as a function of added POM recorded with the native γCD, and the γPOL$_{1.16}$ emphasized the formation of much bigger aggregates in the case of the polymerized γPOL$_{1.16}$ (see Figure 3.23B). As a general feature primarily governed by the anionic charge density of the POM, the mixed-

metal $[SiW_{11}MoO_{40}]^{4-}$ Keggin behaves similarly to the $[SiW_{12}O_{40}]^{4-}$ Keggin anion, whose behavior toward $\gamma POL_{1.16}$ has been fully described in the previous section (see Figure 3.22).

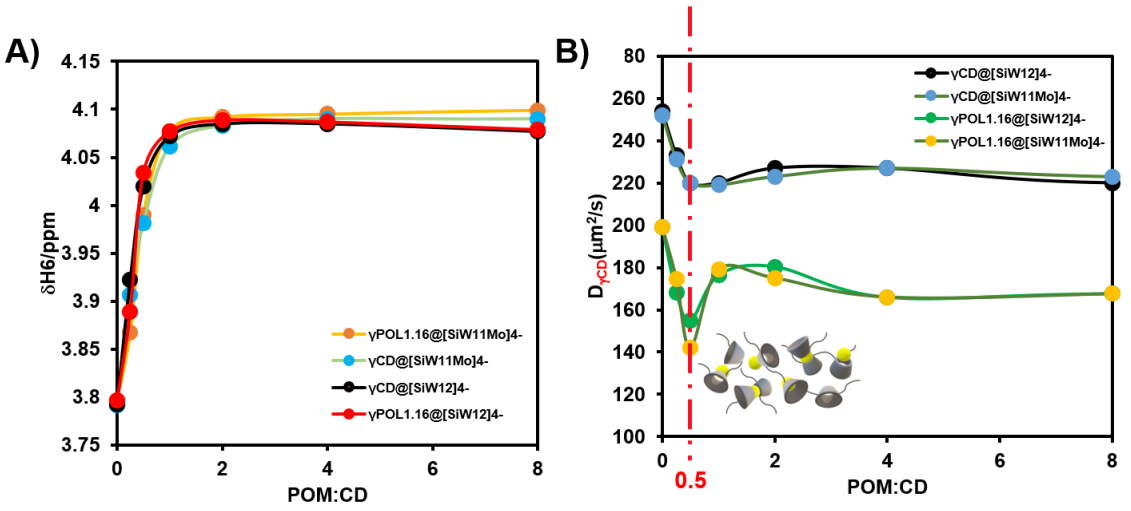


**Figure 3.23** *A) Comparison of evolution of γ-CD proton H6 shift as a function of POM/CD molar ratio during titration 2 mM-CD solution of γ-CD and γPOL$_{1.16}$ with $[SiW_{11}MoO_{40}]^{4-}$ and $[SiW_{12}O_{40}]^{4-}$, B) Diffusion coefficients of CD as a function of POM:CD molar ratio, measured from $^{1}$H DOSY NMR during titration of 2 mM-CD solution of γ-CD, and γPOL$_{1.16}$ with $[SiW_{12}O_{40}]^{4-}$ and $[SiW_{11}MoO_{40}]^{4-}$.*

As already observed for the $[SiW_{12}O_{40}]^{4-}$ anion, the *D* value reaches a minimum for 0.5 equivalents of POM due to cross-linking effect of the POM since, at this chemical composition, the inclusion sandwich complexes are most favored. The minimum *D* values exhibits large difference between native γCD and polymerized γPOL, i.e., $D_{\gamma POL}$ = 155 µm$^2$.s$^{-1}$ *vs* $D_{\gamma CD}$ = 220 µm$^2$.s$^{-1}$ with $[SiW_{12}]^{4-}$, and $D_{\gamma POL}$ = 142 µm$^2$.s$^{-1}$ *vs* $D_{\gamma CD}$ = 220 µm$^2$.s$^{-1}$ with $[SiW_{11}MoO_{40}]^{4-}$. This cross-linking effect has been associated to the formation of host-guest POM@2γCD "sandwich" adduct,[37] at the origin of the gelation phenomena.

Similar NMR features were also observed with the vanadium-monosubstituted Keggin-type $[PW_{11}VO_{40}]^{4-}$ (see Figure 3.24), which further demonstrated that the ionic charge determines the thermodynamic stability of the POM•••γCD supramolecular aggregates. Globally, all mixed Keggin $[POM]^{4-}$ showed comparable and reproducible results as long as they have the same overall ionic charge. Besides, it should also worth mentioning that in the presence of the paramagnetic species

$[PW_{11}VO_{40}]^{5-}$ containing the vanadyl group $\{V^{IV}O\}$, the NMR resonances of the γ-CD undergo a strong line-broadening which hides any clear observation of aggregation phenomenon (see Figure 3.24).

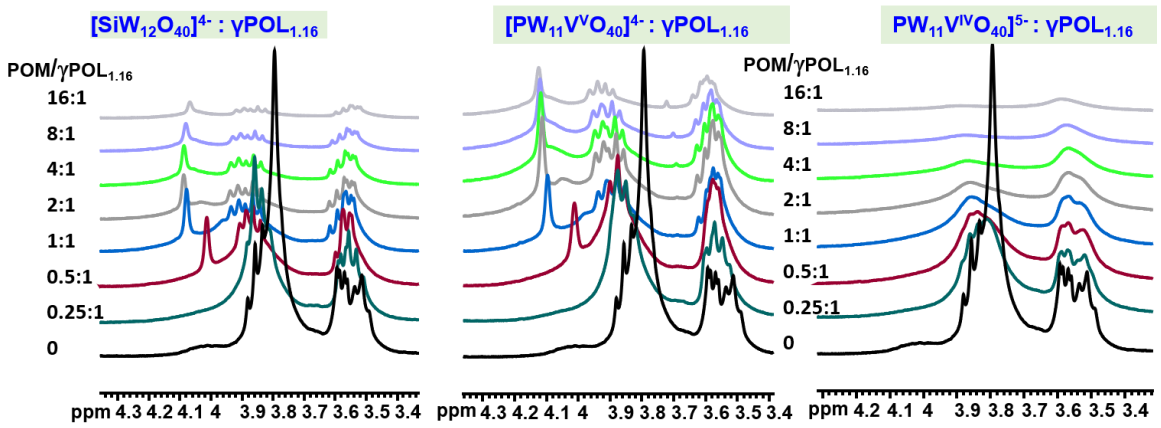


**Figure 3.24** *Selected $^{1}H$ NMR spectra resulting from the titration of 2 mmol.L$^{-1}$ CD of aqueous solution present in γPOL$_{1.16}$ with $[SiW_{12}O_{40}]^{4-}$, $[PW_{11}VO_{40}]^{4-}$, and $[PW_{11}VO_{40}]^{5-}$anions.*

### 3.3.4.3 Monitoring POM-CD host-guest assembling-disassembling in POM@POL by variable-temperature $^{1}$HNMR

Yan et al. reported that oligoethylene glycol-modified (OEG) cyclodextrin was highly soluble in water at low temperature, but its solution became cloudy after heating to a certain temperature.[61] This temperature-responsive property results from the hydrophilic/hydrophobic balance achieved by the dehydration of the OEG unit which leads to a demixing process. Such a phenomenon is similar to that called the Cloud-Point-Temperature which corresponds to the demixing of the $C_8E_4$ polymer from aqueous solutions. However, aqueous solutions of polymer γPOL$_{1.16}$ herein exhibit a perfect thermal stability without phase transition. Variable-temperature $^{1}$H NMR experiments from 28 to 80 °C of a concentrated aqueous solution of γPOL$_{1.16}$ (208 mM CD) reveals a continuous line-narrowing as the temperature increases up to 80°C (see Figure 3.25). Such a phenomenon is fully reversible that results of a restauration of the initial NMR spectrum as the temperature is returned to RT. We infer that, in addition to the effect of the temperature on the molecular dynamics, the polymer adopts instead an unfolded conformation at high temperature that increase the degrees of freedom of the building unit within the polymer and a folded mode at

room temperature.[62] In the presence of POM, different behaviors are observed depending on the nature of the POM used, in acid form or an alkali salt. When using the acid form $H_4[SiW_{12}O_{40}]$, an irreversible transformation of the polymer can be noticed during the cooling process, while the potassium salt $K_4[SiW_{11}MoO_{40}]$ leads to a fully reversible behavior change. It seems that the high acidity combined with the high temperature destroy the polymer structure. Therefore, we avoided using POMs in their acidic forms in the following studies with polymeric CDs. Interestingly, the gel formed from $\gamma POL_{1.16}$ material in concentrated condition solution ([CD] = 208 mM) and $K_4[SiW_{11}MoO_{40}]$ showed also thermally reversible phenomena comparable to POM-free system. However, note the much broader NMR lines in the presence of POM, indicating lower molecular dynamics due to the cross-linking effect of POM.

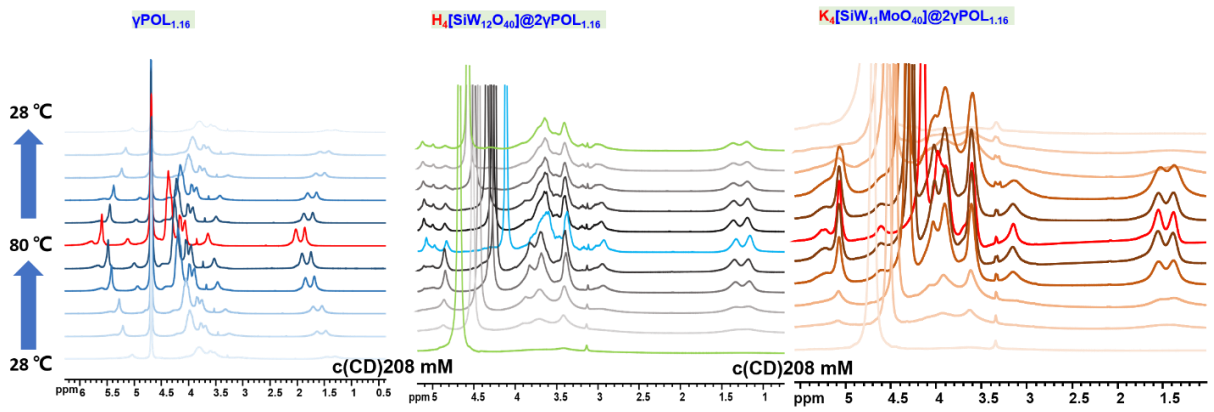


**Figure 3.25** *Variable-temperature (VT) $^1H$ NMR spectra of 208 mM-CD aqueous solution of γ-POL1.16, $H_4[SiW_{12}O_{40}]$@2γ-POL1.16, and $K_4[SiW_{11}MoO_{40}]$@2γ-POL1.16, respectively (from left to right).*

The thermal behavior of POM@$\gamma POL_{1.16}$ in dilute solution was also investigated by $^1H$ NMR spectroscopy in the temperature range 28-80 °C (see Figure 3.25). Herein, we studied three types of 2 mM-CD solutions, i.e., $[SiW_{12}O_{40}]^{4-}$@$\gamma POL_{1.16}$, and for comparison, the starting $\gamma POL_{1.16}$ without POM and the $[SiW_{12}O_{40}]^{4-}$@2γ-CD with native CD. No significant changes are observed in the NMR spectra of the POM-free $\gamma POL_{1.16}$ material in dilute conditions. A contrasted situation is observed in the presence of POM, highlighted by the evolution of the H6 proton NMR signal, used as probe of the supramolecular host-guest association. Increasing temperature resulted

in a high-field shift from ca. 4.00 ppm at RT to ca. 3.85 ppm at 80 °C, corresponding to a nearly POM-free CD (see Figures 3.26B & 3.26C). This means that increasing temperature tends to dissociate the host-guest CD-POM assembly, as expected because the encapsulation process corresponds to an exothermic process ($\Delta_r H^* < 0$). Furthermore, this thermal behavior proved to be perfectly reversible process while cooling restored the initial NMR spectra (see Figure. 3.26). Besides, no polymer degradation was detected.

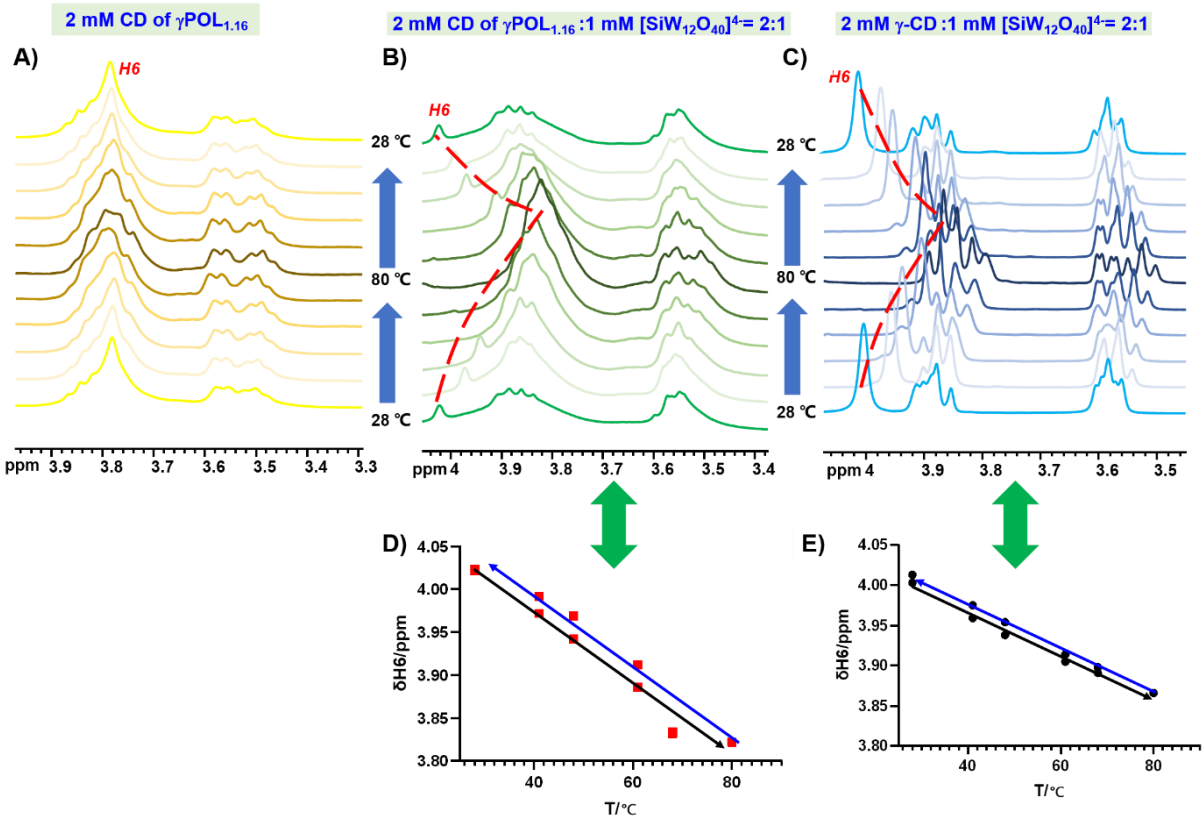


**Figure 3.26** *VT $^1$H NMR of 2 mM-CD solutions of A) γPOL1.16, B) $[SiW_{12}O_{40}]^{4-}$@γPOL1.16, and C) $[SiW_{12}O_{40}]^{4-}$@2γ-CD, during one temperature cycle from 28 to 80 to 28 °C. A plot of γ-CD proton H6 shift as a function of temperature in the system D) $[SiW_{12}O_{40}]^{4-}$@γPOL1.16 and E) $[SiW_{12}O_{40}]^{4-}$@2γ-CD are also shown. Black line: increase temperature; Blue line: decrease temperature.*

### 3.3.5 SAXS analysis

Small-angle X-ray scattering (SAXS) is an effective technique to provide information on the size, shape, conformation, and aggregation of nanoparticles, but also on interactions between clusters, distribution of polymers, and morphological changes in the solution.[63] SAXS can be used to obtain low-resolution structural information,

which is practical for analyzing large molecules that do not crystallize easily.[64] This technique has been mainly used to identify folding or unfolding of macromolecular proteins.[65] In recent years, many researchers have also used these methods to demonstrate the formation and self-assembly of organic-inorganic hybrid molecular modules.[26,66] In collaboration with Pierre Bauduin's research group at the Institut de Chimie Séparative de Marcoule, SAXS measurements have been performed on some representative samples of POM@POL.

The SAXS spectra have been measured at room temperature from homogeneous aqueous solutions containing 4 mM POMs ($H_3PW_{12}O_{40}$, $H_4SiW_{12}O_{40}$, or $H_5BW_{12}O_{40}$) in the presence of various amounts of CD-oligomeric $POL_{1.16}$. The superchaotropic character of the Keggin POMs is elucidated in Chapter 2. As shown in Figure 3.27, the SAXS spectra of the POM@POL polymer appear to be dominated primarily by the POM anions as the heaviest well-defined component of the solution. The black curves of three free Keggin anions ($PW_{12}O_{40}^{3-}$, $SiW_{12}O_{40}^{4-}$, and $BW_{12}O_{40}^{5-}$) show similar features that should be typical of spherical shaped objects. For $[PW_{12}O_{40}]^{3-}$ in the presence of oligomer POL results in a shift of a maxima to low $q$ values, demonstrating the complex formed by cyclodextrin within the oligomeric backbone and $[PW_{12}O_4]^{3-}$ ions (Figure 3.27A). Furthermore, the aggregate size continued to increase and reach the maximum of 11.6 nm until $q$ = 0.54 $nm^{-1}$ upon addition of 4 equivalents CD of oligomer POL (according to the Equation, $d = 2\pi/q$). Simultaneously, the system with $[SiW_{12}O_4]^{4-}$ shows a similar trend in the presence of oligomer POL to that with $[PW_{12}O_4]^{3-}$, while with $[BW_{12}O_{40}]^{5-}$, we see almost no shift in the maximum. For $[SiW_{12}O_4]^{4-}$ ions, the size of the aggregates reaches 10 nm after adding 8 equivalents CD in oligomer POL and then become smaller for larger CD excess (Figure 3.27B). The possible reason is the disassembly of the aggregates due to addition of large excess of free oligomers that disturb the polymer structure. It's worth mentioning that the SAXS size estimation of aggregates agrees well with those obtained from electrochemical data, approximated as spheroidal to 4-8 nm, in c(POM) = 1 mM system (see section 3.3.3). Previous work demonstrated that cyclodextrins have a weak affinity for $[BW_{12}O_{40}]^{5-}$ because of its high charge densitiy.[37] In this case, comparatively more equivalents of CDs are needed to form aggregates and the polymer structure remains weak (Figure 3.26C). Finally, the spectra in the very low $q$ range revealed increasing important interparticle repulsions

with the increase of polymer in the system containing $[PW_{12}O_{40}]^{3-}$, while this phenomenon is less pronounced with $[SiW_{12}O_{40}]^{4-}$, and even absent with $[BW_{12}O_{40}]^{5-}$. This is counterintuitive observation because of the well-established tendency of the charge drop (here from 5- to 3-) to increase electrostatic repulsion. Probably, the more chaotropic P-Keggin anion induces well-defined and more separated cross-linking nodes in the polymer compared to the B-type Keggin system.

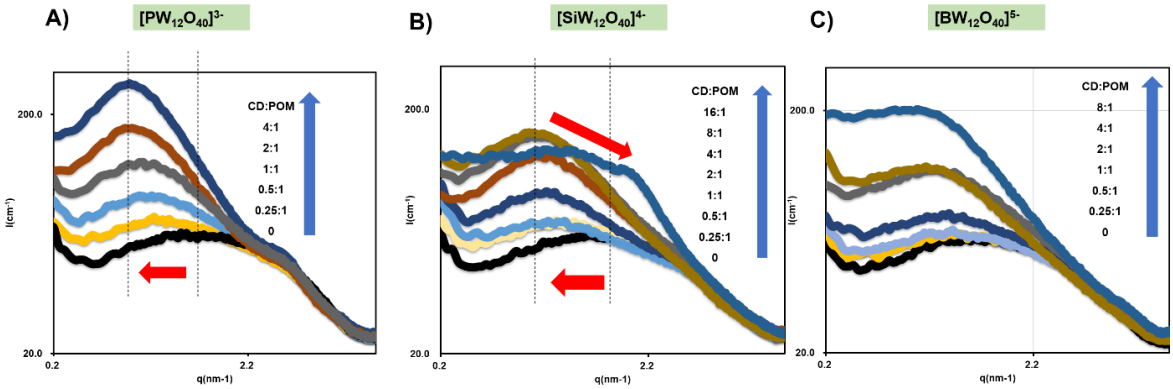


**Figure 3.27** *A) SAXS-spectra of 4 mM B) $H_3PW_{12}O_{40}$, B) $H_4SiW_{12}O_{40}$ and C) $H_5BW_{12}O_{40}$ solution in the presence of variable amounts CD-oligomeric γPOL$_{1.16}$ (from 0 to up 16 equivalents).*

### 3.3.6 Conclusion

In conclusion, we described a redox- and thermo-responsive supramolecular polymeric hydrogel schematically described in Figure 3.27. The host-guest interaction between γPOL$_n$ and Keggin-type POMs was observed and studied both in the macroscopic sol-gel state and in an aqueous solution.

Importantly, the supramolecular gelling process and related properties of the material are directly dependent on the POM's chaotropic character, which is related to its global charge density. The gelation capacity of γPOL by Keggin-type anions $[XW_{12}O_{40}]^{n-}$ can be tuned by reversible electron transfer. The 3-/4- charged POMs showed strong interactions with γ-POL to produce gels, while supramolecular interactions remain too weak with the 5-/6- charged anions to form gels even for high concentrations.

In this context, such a system could behave as switchable redox platform where one-electron transfer could alter significantly the supramolecular interaction to promote a

gel-to-fluid phase transition. Our attention focused on the monosubstituted anion $[SiW_{11}MoO_{40}]^{4-/5-}$ which exhibits two air-stable redox states, easily available by using sodium dithionite as reducing agent or sodium peroxydisulfate as oxidizing agent. The host-guest binding strength between γCD in POL and oxidized $[SiW_{11}MoO_{40}]^{4-}$ anion is high enough to ensure cross-linking between oligomeric chains, leading to the hydrogel formation. As the POM is one-electron reduced, the binding constant decreases strongly and the host-guest dissociation occurs with consequence to promote a gel-to-fluid phase transition. It should be worth noting that the $K_{1:1}$ binding constant between POM and native γ-CD decreases dramatically from 17700 to about 500 $M^{-1}$ when the $[SiW_{11}MoO_{40}]^{4-}$ anion is one-electron reduced into $[SiW_{11}MoO_{40}]^{5-}$ anion. Such a quantitative result constitutes a rational basis to understand this striking gel-to-fluid phase transition. Furthermore, such a supramolecular dissociation which promotes gel-to-fluid transition is also observed by temperature change in the 28-80 °C range. These systems offer a promising class of molecular materials for designing new hybrid supramolecular materials responsive by redox or thermal stimuli, useful for optic detection or catalyze application.[67,68]

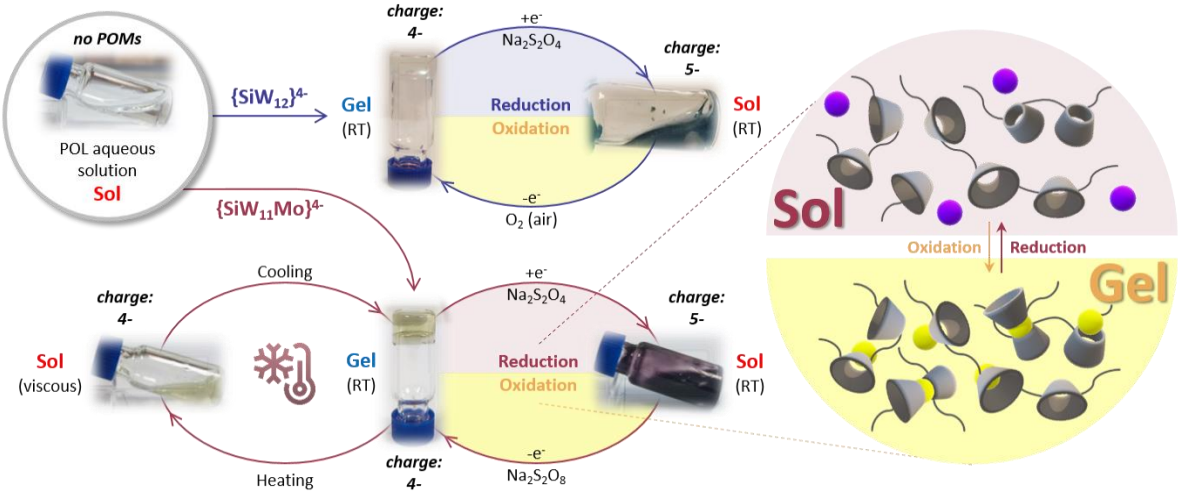


**Figure 3.28** *Reversible gel-sol transitions of hydrogel containing $[SiW_{12}O_{40}]^{4-}$ or $[SiW_{11}MoO_{40}]^{4-}$ upon reduction/oxidation and heating/cooling. Inset: Representation of the host-guest supramolecular interaction between POMs and the γCD-based polymeric chains (POL) in the sol/gel phase.*

# Bibliography


1. Lehn, J.-M. Perspectives in Supramolecular Chemistry—From Molecular Recognition towards Molecular Information Processing and Self-Organization. *Angew. Chem. Int. Ed. Engl.* **29**, 1304–1319 (1990).
2. Sun, Y., Chen, C. & Stang, P. J. Soft Materials with Diverse Suprastructures via the Self-Assembly of Metal–Organic Complexes. *Acc. Chem. Res.* **52**, 802–817 (2019).
3. Chakrabarty, R., Mukherjee, P. S. & Stang, P. J. Supramolecular Coordination: Self-Assembly of Finite Two- and Three-Dimensional Ensembles. *Chem. Rev.* **111**, 6810–6918 (2011).
4. Norioka, C., Inamoto, Y., Hajime, C., Kawamura, A. & Miyata, T. A universal method to easily design tough and stretchable hydrogels. *NPG Asia Mater.* **13**, 1–10 (2021).
5. Liu, X., Zhao, L., Liu, F., Astruc, D. & Gu, H. Supramolecular redox-responsive ferrocene hydrogels and microgels. *Coord. Chem. Rev.* **419**, 213406 (2020).
6. Deng, Z., Guo, Y., Zhao, X., Ma, P. X. & Guo, B. Multifunctional Stimuli-Responsive Hydrogels with Self-Healing, High Conductivity, and Rapid Recovery through Host–Guest Interactions. *Chem. Mater.* **30**, 1729–1742 (2018).
7. Silva, O. F., Fernández, M. A., Pennie, S. L., Gil, R. R. & de Rossi, R. H. Synthesis and Characterization of an Amphiphilic Cyclodextrin, a Micelle with Two Recognition Sites. *Langmuir* **24**, 3718–3726 (2008).
8. Karoyo, A. H. & Wilson, L. D. Preparation and Characterization of a Polymer-Based “Molecular Accordion”. *Langmuir* **32**, 3066–3078 (2016).
9. Chen, G. & Jiang, M. Cyclodextrin-based inclusion complexation bridging supramolecular chemistry and macromolecular self-assembly. *Chem. Soc. Rev.* **40**, 2254–2266 (2011).
10. Zhu, X., Quaranta, A., Bensasson, R. V., Sollogoub, M. & Zhang, Y. Secondary-Rim γ-Cyclodextrin Functionalization to Conjugate with C60: Improved Efficacy as a Photosensitizer. *Chem. – Eur. J.* **23**, 9462–9466 (2017).
11. Harada, A., Li, J. & Kamachi, M. The molecular necklace: a rotaxane containing many threaded α-cyclodextrins. *Nature* **356**, 325–327 (1992).
12. Miyamae, K., Nakahata, M., Takashima, Y. & Harada, A. Self-Healing, Expansion–Contraction, and Shape-Memory Properties of a Preorganized Supramolecular Hydrogel through Host–Guest Interactions. *Angew. Chem. Int. Ed.* **54**, 8984–8987 (2015).
13. Harada, A., Kobayashi, R., Takashima, Y., Hashidzume, A. & Yamaguchi, H. Macroscopic self-assembly through molecular recognition. *Nat. Chem.* **3**, 34–37 (2011).
14. Alsbaiee, A. *et al.* Rapid removal of organic micropollutants from water by a porous beta-cyclodextrin polymer. *Nature* **529**, 190–4 (2016).
15. Baroudi, I. *et al.* Supramolecular Assembly of Gelatin and Inorganic Polyanions: Fine-Tuning the Mechanical Properties of Nanocomposites by Varying Their Composition and Microstructure. *Chem. Mater.* **27**, 1452–1464 (2015).
16. Moussawi, M. A. *et al.* Polyoxometalate, Cationic Cluster, and γ-Cyclodextrin: From Primary Interactions to Supramolecular Hybrid Materials. *J. Am. Chem. Soc.* **139**, 12793–12803 (2017).
17. Moussawi, M. A. *et al.* Nonconventional Three-Component Hierarchical Host–Guest Assembly Based on Mo-Blue Ring-Shaped Giant Anion, γ-Cyclodextrin, and Dawson-type Polyoxometalate. *J. Am. Chem. Soc.* **139**, 14376–14379 (2017).
18. Buchecker, T. *et al.* Polyoxometalates in the Hofmeister series. *Chem. Commun.* **54**, 1833–1836 (2018).
19. Yao, S. *et al.* Redox-Responsive Host–Guest Association between γ-Cyclodextrin and Mixed-Metal Keggin-Type Polyoxometalates. *Inorg. Chem.* **60**, 7433–7441 (2021).
20. Wankar, J. *et al.* Recent Advances in Host–Guest Self-Assembled Cyclodextrin Carriers: Implications for Responsive Drug Delivery and Biomedical Engineering. *Adv. Funct. Mater.* **30**, 1909049 (2020).
21. Assaf, K. I., Gabel, D., Zimmermann, W. & Nau, W. M. High-affinity host-guest chemistry of large-ring cyclodextrins. *Org. Biomol. Chem.* **14**, 7702–7706 (2016).
22. Assaf, K. I. *et al.* Hierarchical host-guest assemblies formed on dodecaborate-coated gold nanoparticles. *Chem. Commun.* **53**, 4616–4619 (2017).
23. Su, P., Smith, A. J., Warneke, J. & Laskin, J. Gas-Phase Fragmentation of Host-Guest Complexes of Cyclodextrins and Polyoxometalates. *J. Am. Soc. Mass Spectrom.* **30**, 1934–1945 (2019).
24. Ivanov, A. A. *et al.* Host–Guest Binding Hierarchy within Redox- and Luminescence-Responsive Supramolecular Self-Assembly Based on Chalcogenide Clusters and γ-Cyclodextrin. *Chem. – Eur. J.* **24**, 13467–13478 (2018).
25. Fa Bamba, I. *et al.* Host-Guest Complexation Between Cyclodextrins and Hybrid Hexavanadates: What are the Driving Forces? *Chem. – Eur. J.* **27**, 15516–15527 (2021).
26. Falaise, C. *et al.* ‘Host in Host’ Supramolecular Core-Shell Type Systems Based on Giant Ring-Shaped Polyoxometalates. *Angew. Chem. Int. Ed. Engl.* **60**, 14146–14153 (2021).
27. Ivanov, A. A. *et al.* Size-Exclusion Mechanism Driving Host–Guest Interactions between Octahedral Rhenium Clusters and Cyclodextrins. *Inorg. Chem.* **58**, 13184–13194 (2019).
28. Abramov, P. A. *et al.* Supramolecular Adduct of γ-Cyclodextrin and $[\{Re_6Q_8\}(H_2O)_6]^{2+}$ (Q=S, Se). *J. Clust. Sci.* **29**, 9–13 (2018).
29. Ivanov, A. A. *et al.* Stabilization of Octahedral Metal Halide Clusters by Host–Guest Complexation with γ-Cyclodextrin: Toward Nontoxic Luminescent Compounds. *Inorg. Chem.* **61**, 14462-14469 (2022).

30. Chen, J.-J. *et al.* Effective Storage of Electrons in Water by the Formation of Highly Reduced Polyoxometalate Clusters. *J. Am. Chem. Soc.* **144**, 8951–8960 (2022).
31. Himeno S., Takamoto M., Santo R. & Ichimura A. Redox Properties and Basicity of Keggin-Type Polyoxometalate Complexes. *Bull. Chem. Soc. Jpn.* **78**, 95-100 (2005).
32. Wang, S.-S. & Yang, G.-Y. Recent Advances in Polyoxometalate-Catalyzed Reactions. *Chem. Rev.* **115**, 4893–4962 (2015).
33. Blazevic, A. & Rompel, A. The Anderson–Evans Polyoxometalate: From Inorganic Building Blocks via Hybrid Organic–Inorganic Structures to Tomorrows "Bio-POM". *Coord. Chem. Rev.* **307**, 42–64 (2016).
34. Van Rompuy, L. S. & Parac-Vogt, T. N. Interactions between polyoxometalates and biological systems: from drug design to artificial enzymes. *Curr. Opin. Biotechnol.* **58**, 92–99 (2019).
35. Wang, S.-M., Hwang, J. & Kim, E. Polyoxometalates as promising materials for electrochromic devices. *J. Mater. Chem. C* **7**, 7828–7850 (2019).
36. Martinetto, Y., Pégot, B., Roch-Marchal, C., Cottyn-Boitte, B. & Floquet, S. Designing Functional Polyoxometalate-Based Ionic Liquid Crystals and Ionic Liquids. *Eur. J. Inorg. Chem.* **2020**, 228–247 (2020).
37. Yao, S. *et al.* Hofmeister effect in the Keggin-type polyoxotungstate series. *Inorg. Chem. Front.* **8**, 12–25 (2021).
38. Solé-Daura, A., Poblet, J. M. & Carbó, J. J. Structure–Activity Relationships for the Affinity of Chaotropic Polyoxometalate Anions towards Proteins. *Chem. – Eur. J.* **26**, 5799–5809 (2020).
39. Karoyo, A. H., & Wilson, L. D. Preparation and Characterization of a polymer-based "Molecular Accordion". *Langmuir*, **32**, 3066-3078 (2016).
40. Gao, B., Li, B. & Wu, L. Layered supramolecular network of cyclodextrin triplets with azobenzene-grafting polyoxometalate for dye degradation and partner-enhancement. *Chem. Commun.* **57**, 10512–10515 (2021).
41. Zou, C., Zhao, P., Ge, J., Qin, Y. & Luo, P. Oxidation/adsorption Desulfurization of Natural Gas by Bridged Cyclodextrins Dimer Encapsulating Polyoxometalate. *Fuel* **104**, 635–640 (2013).
42. Gerbaud, G., Hediger, S., Gadelle, A. & Bardet, M. Synthesis and solid-state NMR Study of Chromium Complexes of Per(3,6-anhydro)-α-cyclodextrin Based Polymers. *Carbohydr. Polym.* **73**, 64–73 (2008).
43. Ferro, M. *et al.* Dynamics and Interactions Of Ibuprofen in Cyclodextrin Nanosponges by Solid-State NMR Spectroscopy. *Beilstein J. Org. Chem.* **13**, 182–194 (2017).
44. Harabagiu, V. *et al.* Synthesis and Characterization of Persilylated Cyclodextrins. *Carbohydr. Polym.* **56**, 301–311 (2004).
45. Mercier, J. Ph., Debrun, J. L., Dreux, M., Elfakir, C. & Hakim, B. Mass Spectrometric Study of Randomly Methylated B-Cyclodextrins Using Ionspray, Atmospheric Pressure Chemical Ionization and Matrix-Assisted Laser Desorption/Ionization. *Rapid Commun. Mass Spectrom.* **14**, 68–70 (2000).
46. Dumoulin, C. L. & Levy, G. C. Spectroscopic Data Processing. NMRI Software and Its Applications in Chemistry and Biophysics. *J. Mol. Struct.* **113**, 299–310 (1984).
47. Rocchiccioli-Deltcheff, C., Fournier, M., Franck, R. & Thouvenot, R. Vibrational Investigations of Polyoxometalates. 2. Evidence for Anion-Anion Interactions in Molybdenum(VI) and Tungsten(VI) Compounds Related to The Keggin Structure. *Inorg. Chem.* **22**, 207–216 (1983).
48. Fletcher, H., Allen, C. C., Burns, R. C. & Craig, D. C. Pentapotassium Dodecatungsto-borate(III) Hexadecahydrate. *Acta Crystallogr. C* **57**, 505–507 (2001).
49. Hervé, G. & A, T. Study of Alpha - and Beta -Enneatungstosilicates and -germanates. *Inorg. Chem.* 16, 2115-2117 (1977).
50. Wu, H. Contribution to the Chemistry of Phosphomolybdic Acids, Phosphotungstic Acids, and Allied Substances. *J. Biol. Chem.* **43**, 189–220 (1920).
51. Rusu, D., *et al.* Synthesis and Characterization of the Potassium 11-Tungstovanado (IV) Phosphate. Rev. Roum. Chim, **55**, 843-850 (2010).
52. Grigoriev, V. A., Cheng, D., Hill, C. L. & Weinstock, I. A. Role of Alkali Metal Cation Size in the Energy and Rate of Electron Transfer to Solvent-Separated 1:1 [(M+)(Acceptor)] (M+ = Li+, Na+, K+) Ion Pairs. *J. Am. Chem. Soc.* **123**, 5292–5307 (2001).
53. de Paiva Floro Bonfim, R. *et al.* Synthesis and Structural Characterization of a New Nanoporous-like Keggin Heteropolyanion Salt: $K_3(H_2O)_4[H_2SiVW_{11}O_{40}](H_2O)8+x$. *Inorg. Chem.* **46**, 7371–7377 (2007).
54. Li, C., Sun, M., Xu, L., Wang, Y. & Huang, J. The First Heteropoly Blue-Embedded Metal–Organic Framework: Crystal Structure, Magnetic Property and Proton Conductivity. *CrystEngComm* **18**, 596–600 (2016).
55. Sanchez, C., Livage, J., Launay, J. P., Fournier, M. & Jeannin, Y. Electron Delocalization in Mixed-Valence Molybdenum Polyanions. *J. Am. Chem. Soc.* **104**, 3194–3202 (1982).
56. Leparulo-Loftus, M. A. & Pope, M. T. Vanadium-51 NMR Spectroscopy of Tungstovanadate Polyanions. Chemical Shift and Line-Width Patterns for The Identification of Stereoisomers. *Inorg. Chem.* **26**, 2112–2120 (1987).
57. Domaille, P. J. The 1- and 2-dimensional Tungsten-183 and Vanadium-51 NMR Characterization of Isopolymetalates and Heteropolymetalates. *J. Am. Chem. Soc.* **106**, 7677–7687 (1984).
58. Sadakane, M. & Steckhan, E. Electrochemical Properties of Polyoxometalates as Electrocatalysts. *Chem. Rev.* **98**, 219–238 (1998).
59. Friedl, J. *et al.* Asymmetric Polyoxometalate Electrolytes for Advanced Redox Flow Batteries. *Energy Environ. Sci.* **11**, 3010–3018 (2018).
60. Fay, N. *et al.* Structural, Electrochemical, and Spectroscopic Characterization of a Redox Pair of Sulfite-Based Polyoxotungstates: α-$[W_{18}O_{54}(SO_3)_2]^{4-}$ and α-$[W_{18}O_{54}(SO_3)_2]^{5-}$. *Inorg. Chem.* **46**, 3502–3510 (2007).

61. Yan, J. *et al.* Thermoresponsive Cyclodextrins with Switchable Inclusion Abilities. *J. Mater. Chem.* **22**, 17424–17428 (2012).
62. Wilson, L. D. & Verrall, R. E. A $^{1}$H NMR Study of Cyclodextrin - hydrocarbon Surfactant Inclusion Complexes in Qqueous Solutions. *Can. J. Chem.* **76**, 25–34 (1998).
63. Nyman, M. Small-angle X-ray Scattering to Determine Solution Speciation of Metal-Oxo Clusters. *Coord. Chem. Rev.* **352**, 461–472 (2017).
64. Dede, F., Dinler, G. & Sayers, Z. 3D Macromolecular Structure Analyses: Applications in Plant Proteins. *Brilliant Light in Life and Material Sciences*. 141–151 (2007).
65. Putnam, C. D., Hammel, M., Hura, G. L. & Tainer, J. A. X-ray Solution Scattering (SAXS) Combined with Crystallography and Computation: Defining Accurate Macromolecular Structures, Conformations and Assemblies in Solution. *Q. Rev. Biophys.* **40**, 191–285 (2007).
66. Schmid, P. *et al.* Polymeric Surfactant P84/Polyoxometalate α-PW12O403-—A Model System to Investigate the Interplay Between Chaotropic and Hydrophobic Effects. *Colloids Interfaces* **6**, 16 (2022).
67. Bagheri, A. R. *et al.* Polyoxometalate-based Materials in Extraction, and Electrochemical and Optical Detection Methods: A review. *Anal. Chim. Acta* **1209**, 339509 (2022).
68. Yaqub, A. *et al.* Organic–Inorganic Hybrid Films of the Sulfate Dawson Polyoxometalate, $[S_2W_{18}O_{62}]^{4-}$, and Polypyrrole for Iodate Electrocatalysis. *ACS Omega* **7**, 43381–43389 (2022).

# Chapter 4 Conclusion & Perspective

Polyoxometalate (POM) chemistry has experienced explosive growth due to its remarkable physical and chemical properties. It is a crucial factor in developing complex materials for various scientific fields such as catalysis, biology, and environmental science or data storage. From classical methodologies of synthesis to modern breakthrough methods of controlling and adjusting compositions, topologies, and hierarchical assemblies in complex structures, it is possible to design unique POM-based multifunctional materials with diverse and versatile physical-chemical applications. In recent years, introducing POMs into supramolecular chemistry has resulted in striking hybrid materials by combining the properties of complementary components, such as organic, complexes, clusters, and POMs. The broad structural flexibility of these emerging systems enables the rational design of hybrid architectures, which ensures a better control of the inter-component interactions generating synergistic phenomena of fundamental interest in different domains. The work presented in this thesis shows that the archetypal Keggin-type heteropolyanion is capable of forming stepwise inclusion complexes with cyclic γ-cyclodextrin (γ-CD) in aqueous solution, which can be exploited to design POM-based smart soft-materials.

We demonstrated in **Chapter 2** how the affinity between γ-CD and Keggin-type polyoxometalate $[XW_{12}O_{40}]^{n-}$ anions can vary with the overall ionic charge density of the nanosized polyanion in solution. The results of the comparative study demonstrate that the binding ability of the POMs towards γ-CD can be tuned by the global charge of the POM. Single crystal X-ray diffraction analysis showed distinct organizations of the POMs with γ-CD in the solid-state, depending on the nature of the POM. While the moderately chaotropic $[BW_{12}O_{40}]^{5-}$ interacts with the outer wall of the γ-CD, on the other side of the series, $[PW_{12}O_{40}]^{3-}$ penetrates deeply into the γ-CD cavity through its secondary rim with an optimal contact surface. Moreover, such a study has been expanded to other systems using a series of molybdenum and vanadium monosubstituted anions, confirming that the ionic charge corresponds to the main parameter governing the host-guest process rather than the composition. Moreover, POM/CD association driven by the chaotropic effect has dramatic consequences on the redox properties of POMs. The affinity between Keggin-type

POMs and γ-CD can be finely tuned over a wide range of stability constants of three orders of magnitude. These interactions were quantified by titration experiments using complementary techniques such as ITC, DOSY NMR, and electrochemistry. In conclusion, the formation of CD and Keggin POM complexes can be understood with the thermodynamic features of the hydration shell around POM, which is directly related to the chaotropic nature of POM. POM presents highly disordered solvated water on its surface, which makes its binding to neutral hydrophobic surfaces energetically very favorable ($\Delta H<0$). At the same time, the results of ITC show that the entropy cost shifts from disordered systems to ordered ones($\Delta S<0$). Furthermore, CDs have the ability to improve the stability domain of low charged Keggin $[PM_{12}O_{40}]^{3-}$ species by 2-3 higher pH units for due to formation of CD-protecting shell against the nucleophilic attacks of the hydroxide ions. Besides, the distribution of transient species produced by the degradation of Keggin-type anions can be strongly altered by the presence of the CD.

In **Chapter 3**, these specific interactions are extended to CD-based polymers to produce hydrogels responsive to external stimuli. We successfully prepared CD-containing oligomers (γPOL) from the addition reaction of γ-CD with 1,6-hexamethylene diisocyanate (HDI), which were characterized in solution by $^{1}H$ NMR spectroscopy and MALDI-TOF mass spectrometry. Soluble oligomers were obtained for molar ratio HDI:CD < 1.5 in the synthesis mixture, and the oligomers consisted of short linear chains of only a few CD units, ranging from 1 to 5 CDs with prominent species containing 2-3 CD units. Gelation of the solution occurs through the addition of Keggin POMs which behave as supramolecular guest crosslinkers due to their high binding constant with γ-CD. Additionally, a fast reversible redox process occurs in the presence of a reducing agent, which is manifested by a pronounced color change from yellow to purple and a phase transition from gel-to-fluid. These phenomena were fully reversible during cyclic thermal treatment or redox process. Insoluble polymers were obtained for higher HDI:CD molar ratio (> 1.5), but probably due to the short chains of the HDI linker the polymeric solids were found to be too dense for absorption of Keggin POMs. These physicochemical properties are expected to pave the way for the design of innovative smart hybrid functional materials in various fields such as catalysis, optics, energy, and biology, using the remarkable properties of the water molecules as sovant.[1–3]

As a Perspective, these results open new perspectives for the design of new various POM-based hierarchical materials for promising and creative applications in different fields. For example, the chaotropic approach can be explored and extended to other classes of cavitand molecules such as calixarene, pillarene, resorcinarene, cucurbituril, and other organocages.[4,5] The host-guest encapsulation capability should strongly depend on geometrical considerations of the host such as its cavity size and shape, which obviously restricts the selection of POMs not only on the basis of their charge but also their nuclearity and symmetry.[6,7] This allows the use of other POM structures than the classical Keggin, including smaller like the Lindqvist or Anderson, and larger like the Dawson or Preyssler (see Figure 4.1A~B).[8]

To expand the scope of this thesis relevant perspectives can be proposed in relationship with these results. For instance, we can be varied the nature of the cyclodextrin-based polymers, by including polyethylene glycol unit (PEG) as co-crosslinking agent of HDI. Preliminary results inspired from literature lead to the formation of CD-(HDI-PEG) polymers which reveal highly insoluble in water.[9–11] Furthermore, this CD-(HDI-PEG) solid polymers showed a strong affinity for POMs when contacted with POM aqueous solutions. In the future, this class of CD-based polymers have to be considered as immobilizing matrix of polyoxometalates. There are several types of CD polymers with many functional groups and synthetic designs, including linear CD chains, cross-linked CD networks, and star-shaped CD polymers.[12,13] Furthermore, Many polymers such as sodium alginate, poly(propylene alcohol), and poly(N-isopropylacrylamide) have been adopted as linear components in the synthesis of 1D- or 2D-CD polymers.[14–16] Among the most studied 3D condensed polymeric CD networks are CD-epichlorohydrin (EP) polymers which yield fully water-insoluble materials useful for absorption and surface science (see Figure 4.1C).[17] Finally, functionalization of a single CD molecule with polymeric moieties leading to dendrimer (or star) CD polymers would constitute interesting strategy to extent our approach toward giant POMs such as Keplerate $\{Mo_{132}\}$ and blue wheel $\{Mo_{154}\}$ (see Figure 4.1D).[18]

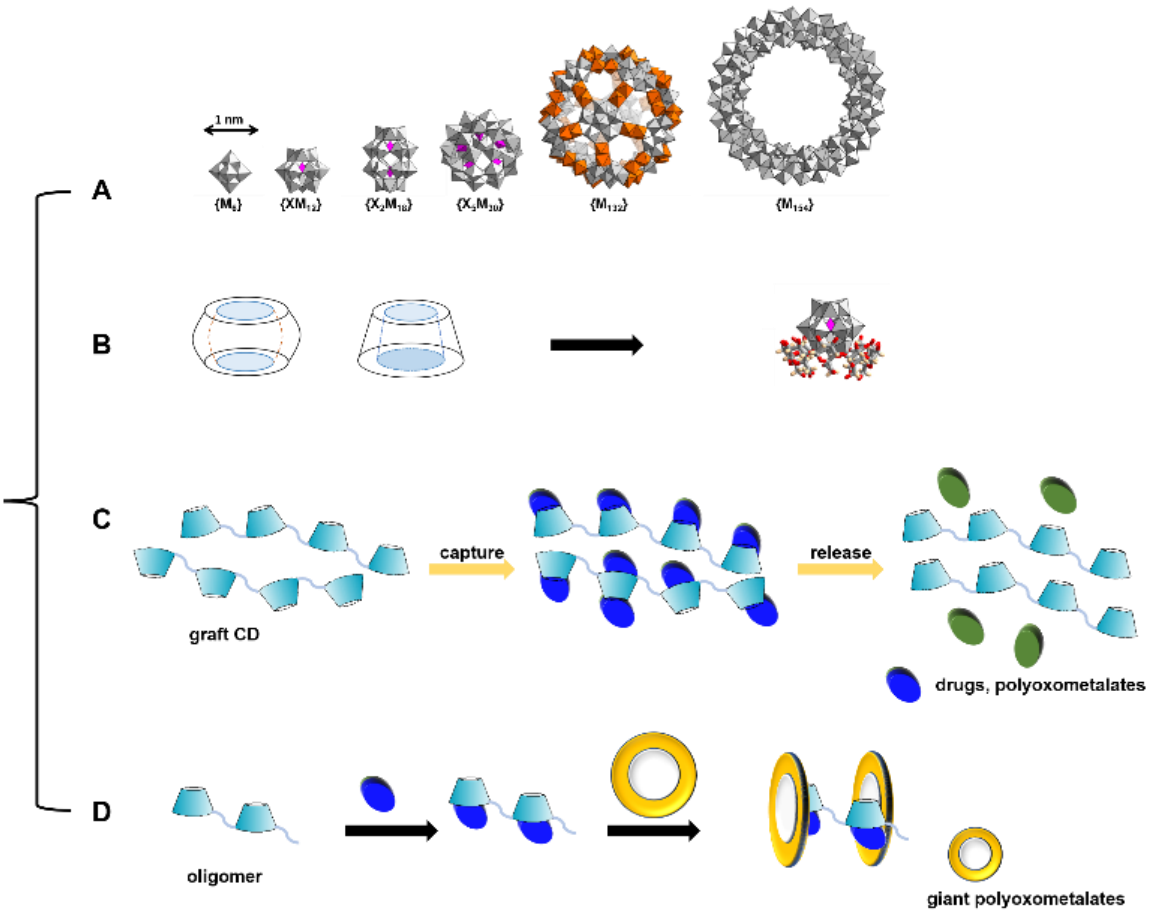


**Figure 4.1** *General scheme showing potential perspective for design functional materials with different A) POM types, B) cavitand molecules, and C) polymeric or D) oligomeric CDs.*

# Bibliography


1. Bijelic, A., Aureliano, M. & Rompel, A. Polyoxometalates as Potential Next-Generation Metallodrugs in the Combat Against Cancer. *Angew. Chem. Int. Ed.* **58**, 2980–2999 (2019).
2. Fabre, B., Falaise, C. & Cadot, E. Polyoxometalates-Functionalized Electrodes for (Photo)Electrocatalytic Applications: Recent Advances and Prospects. *ACS Catal.* **12**, 12055–12091 (2022)
3. Liu, Y., Zhang, J., Lu, S. & Xiang, Y. Polyoxometalate-based Electrolyte Materials in Redox Flow Batteries: Current Trends and Mmerging Opportunities. *Mater. Rep. Energy* **2**, 100094 (2022).
4. Giri, A., Sahoo, A., Dutta, T. K. & Patra, A. Cavitand and Molecular Cage-Based Porous Organic Polymers. *ACS Omega* **5**, 28413–28424 (2020).
5. Chen, Y., Zhang, Y.-M. & Liu, Y. Molecular Selective Binding and Nanofabrication of Cucurbituril/Cyclodextrin Pairs. *Isr. J. Chem.* **51**, 515–524 (2011).
6. Hampson, E. *et al.* Asymmetric Hybrid Polyoxometalates: A Platform for Multifunctional Redox-Active Nanomaterials. *Angew. Chem. Int. Ed.* **58**, 18281–18285 (2019).
7. Ivanov, A. A. *et al.* Size-Exclusion Mechanism Driving Host–Guest Interactions between Octahedral Rhenium Clusters and Cyclodextrins. *Inorg. Chem.* **58**, 13184–13194 (2019).
8. Leclerc, N. *et al.* Supramolecular Association between γ-Cyclodextrin and Preyssler-Type Polyoxotungstate. *Molecules* **26**, 5126 (2021).
9. Du, X. *et al.* Reverse Micelles Based on β-cyclodextrin-incorporated Amphiphilic Polyurethane Copolymers for Protein Delivery. *Polym. Chem.* **5**, 5300–5309 (2014).
10. Liu, D.-E., Chen, Q., Long, Y.-B., Ma, J. & Gao, H. A Thermo-responsive Polyurethane Organogel for Norfloxacin Delivery. *Polym. Chem.* **9**, 228–235 (2017).
11. Swiech, O., Majdecki, M. & Bilewicz, R. PEGylated Network Nanostructured by Gold Nanoparticles for Electrochemical Sensing of Aromatic Redox and Nonredox Analytes. *ACS Appl. Polym. Mater.* **5**, 214-222 (2022)
12. Liu, Z., Ye, L., Xi, J., Wang, J. & Feng, Z. Cyclodextrin polymers: Structure, Synthesis, and Use as Drug Carriers. *Prog. Polym. Sci.* **118**, 101408 (2021).
13. Crini, G. Cyclodextrin–epichlorohydrin Polymers Synthesis, Characterization and Applications to Wastewater Treatment: a review. *Environ. Chem. Lett.* **19**, 2383–2403 (2021).
14. Xue, K. *et al.* In Vitro Degradation and Multi-antibacterial Mechanisms of β-cyclodextrin@curcumin Embodied $Mg(OH)_2$/MAO Coating on AZ31 Magnesium Alloy. *J. Mater. Sci. Technol.* **132**, 179–192 (2023).
15. Higueras, L., López-Carballo, G., Gavara, R. & Hernández-Muñoz, P. Effect of Hydroxypropyl-β-cyclodextrin and Coadjuvants on the Sorption Capacity of Hydrophilic Polymer Films for Monoterpene Alcohols. *Carbohydr. Polym.* **151**, 1193–1202 (2016).
16. Fawaz, F. *et al.* Bioavailability of Norfloxacin from PEG 6000 Solid Dispersion and Cyclodextrin Inclusion Complexes in Rabbits. *Int. J. Pharm.* **132**, 271–275 (1996).
17. Moya-Ortega, M. D. *et al.* Drug Loading in Cyclodextrin Polymers: Dexamethasone Model Drug. *J. Incl. Phenom. Macrocycl. Chem.* **69**, 377–382 (2011).
18. Moussawi, M. A. *et al.* Nonconventional Three-Component Hierarchical Host–Guest Assembly Based on Mo-Blue Ring-Shaped Giant Anion, γ-Cyclodextrin, and Dawson-type Polyoxometalate. *J. Am. Chem. Soc.* **139**, 14376–14379 (2017).